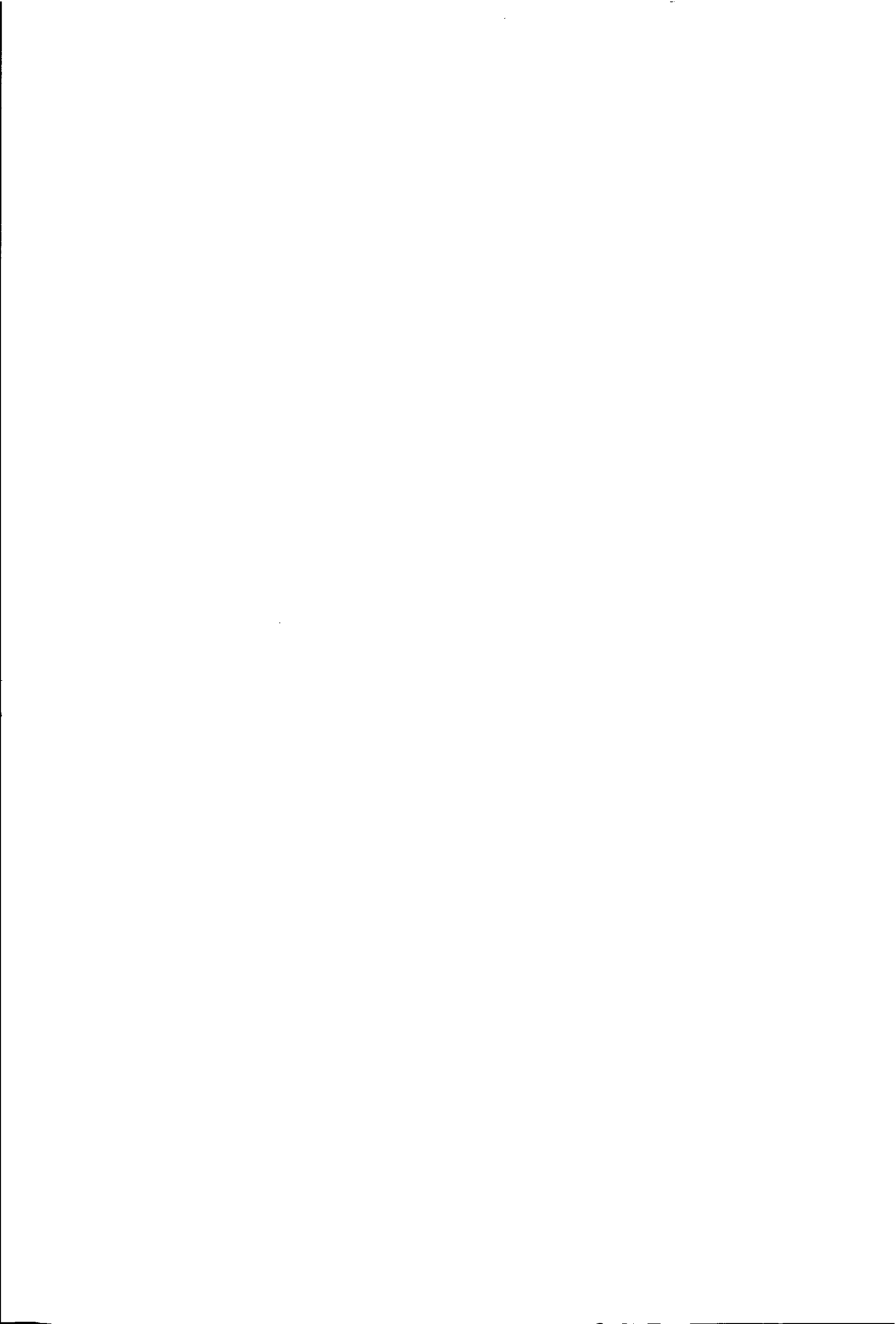


The Physical Behaviour of Shear Connections in Composite Slabs



R.G. Schuurman



TR 3718 S

Stellingen

behorende bij het proefschrift

Physical Behaviour of Shear Connections in Composite Slabs

Remco Schuurman

juni 2001



Stellingen

1. Als in een staalplaat-betonvloer slip optreedt in de verbinding tussen een van deuken voorziene staalplaat en het beton, worden de deuken uit het beton gedrukt. Hierdoor vervormt en verplaatst de staalplaat. De verhouding tussen vervormen en verplaatsen is een maat voor de schuifweerstand van de verbinding.
2. Een eenvoudig model kan het complexe gedrag van een staalplaat-betonvloer niet beschrijven of voorspellen, maar is zeer geschikt voor het verkrijgen van inzicht en kan daardoor van groot belang zijn tijdens de ontwikkeling en het gebruik van complexere modellen.
3. Bij trapeziumvormige staalplaten verzorgen de indeukingen naast schuifweerstand ook de weerstand tegen verticaal separatie. Hierdoor is de geometrie van de plaat en de geometrie en de locatie van de indeukingen belangrijker dan bij zwaluwstaartvormige platen.
4. Een hogere betonsterkte vergroot de sterkte en stijfheid en reduceert de vervormingscapaciteit van de verbinding tussen de staalplaat en het beton. Hierdoor zal de ontwerpsterkte van een staalplaat-betonvloer vaker af- dan toenemen.
5. Het is verleidelijk, maar fysisch niet correct, de invloed van de oplegreactie op de schuifweerstand in staalplaat-betonvloeren te associëren met droge wrijving.
6. Detailproeven kunnen een alternatief zijn voor ware grootte proeven als de uitvoering ervan eenvoudig is, de randvoorwaarden representatief zijn voor het werkelijke gedrag van de vloer en een rekenmodel beschikbaar is om de resultaten toe te passen bij de analyse van volledige vloeren.
7. Fundamenteel onderzoek is moeilijk te plannen.
8. De toename van het aantal onderzoekers en promoties in het huidige A.I.O.-stelsel doet onderzoekers van eerdere generaties, al dan niet gepromoveerd, te kort.
9. Het unieke van een A.I.O.-aanstelling is, dat de duur van de aanstelling niet gerelateerd is aan de te verrichten werkzaamheden.
10. Als je van je hobby je werk maakt, is het tijd voor een nieuwe hobby.
11. Als doorgaan niets meer is dan het uitstellen van stoppen, is het beter te stoppen.
12. Later is al lang begonnen. (*H. Jekkers / K. Meinderts - 1984*)



372415

757735

2009907

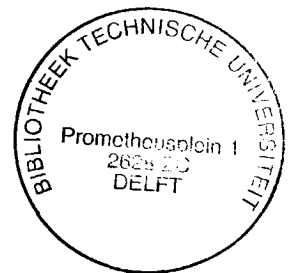
TR3718

The Physical Behaviour of Shear Connections in Composite Slabs

Remco Schuurman



The Physical Behaviour of Shear Connections in Composite Slabs



Proefschrift

ter verkrijging van de graad van doctor
aan de Technische Universiteit Delft,
op gezag van de Rector Magnificus prof. ir. K.F. Wakker,
voorzitter van het College van Promoties,
in het openbaar te verdedigen op maandag 25 juni 2001 om 13.30 uur

door
Remco Gerben SCHUURMAN

civiel ingenieur
geboren te Utrecht

Dit proefschrift is goedgekeurd door de promotor:

Prof. ir. J.W.B. Stark

Samenstelling promotiecommissie:

Rector Magnificus,	voorzitter
Prof. ir. J.W.B. Stark,	Technische Universiteit Delft, promotor
Prof. ir. H.H. Snijder,	Technische Universiteit Eindhoven
Prof. ir. F.S.K. Bijlaard,	Technische Universiteit Delft
Prof. dr. ir. J.C. Walraven,	Technische Universiteit Delft
Prof. dr. ir. J. Wardenier,	Technische Universiteit Delft
Dr. R.M. Lawson,	The Steel Construction Institute

Published and distributed by: DUP Science

DUP Science is an imprint of
Delft University Press
P.O. Box 98
2600 MG Delft
The Netherlands
Telephone: +31 15 2785678
Telefax: +31 15 2785706
E-mail: DUP@Library.TUdelft.NL

ISBN 90-407-2199-8

Keywords: Steel-concrete composite slabs; Shear connection; Indentations

Copyright © 2001 by Remco Schuurman

All rights reserved. No part of the material protected by this copyright notice may be reproduced or utilized in any form or by any means, electronic or mechanical, including photocopying, recording or by any information storage and retrieval system, without written permission from the publisher: Delft Univeristy Press.

Printed in the Netherlands

SUMMARY

This thesis focusses on the shear connection between profiled sheeting and concrete in composite slabs, in which resistance is provided by indentations in the sheeting. The aim of the project was to obtain an understanding of the physical behaviour of the shear connection. Existing design methods are empirical, which prevents application of existing profiles outside the tested range of parameters and development of new types of profiles. Both these items are important in the current European market.

By describing the mechanisms providing shear resistance a greater understanding of the physical behaviour of connections is obtained. Distinction is made between deformation and displacement of the sheeting. The displacement of the sheeting consists of vertical separation between the sheeting and the concrete. Vertical separation reduces the level of deformation of the sheeting and therefore reduces the level of shear resistance.

A method for analysing shear connections is developed. The approach is also valid for other means of shear resistance as long as the mechanisms providing resistance can be described. For simple shear connections a *Visual Solution Method* is developed which provides optimum transparency into various aspects and parameters of shear connections. For more complicated configurations Simplified Frame models (*SF-models*) are developed. Finite Element models (*FE-models*) are used to consider all nonlinear phenomena. Since FE-models are less transparent, recognition of mechanisms determining the behaviour of connections is more difficult. The combination of simple, transparent models and more accurate and complex models provides a powerful tool for performing parametric studies and application during product development.

Based on the performed series of experiments and understanding of the behaviour, requirements for small-scale experiments are listed. It appears that current small-scale test arrangements can be simplified, although more experimental data are required.

The phenomenon of vertical separation is most important for trapezoidal profiles. The shape of re-entrant profiles provides sufficient resistance to vertical

Summary

separation. In Europe material efficiency of both steel and concrete is required to obtain competitive flooring systems. Trapezoidal profiles, which achieve limited resistance to vertical separation, are and have been developed. For these profiles, the shear resistance between the sheeting and the concrete, understanding of the physical behaviour of connections and the influence of the behaviour of the connection on the behaviour of the slab is very important.

TABLE OF CONTENTS

1. INTRODUCTION	
1.1 Scope	1.1
1.2 Aims	1.4
1.3 Outline Thesis	1.4
2. QUALITATIVE DESCRIPTION OF PHYSICAL BEHAVIOUR	
2.0 Introduction	2.1
2.1 General behaviour Composite Member	2.1
2.2 General behaviour of Shear Connections in Composite Slabs	2.3
.1 Strength of the Shear Connection	2.4
.2 Stiffness of the Shear Connection	2.5
.3 Deformation Capacity of the Shear Connection	2.9
2.3 Failure Mechanisms of Composite Slabs	2.13
2.4 General Behaviour of Composite Slabs	2.15
2.5 Existing Design Methods	2.20
.1 'm-k' Method	2.20
.2 Partial Shear Connection Method	2.22
.3 Proposed adjustments to the PSC Method	2.23
2.6 Overview of Research into Composite Slabs	2.25
2.7 Conclusions for Chapter 2	2.26
3. PHYSICAL BEHAVIOUR SHEAR CONNECTION	
3.0 Introduction	3.1
3.1 Shear Connection in Composite Slabs	3.1
3.2 Hypothesis	3.4
3.3 Qualitative Description Shear Connection	3.6
3.4 Method for Analysing Shear Connections in Composite Slabs	3.7
3.5 Example	3.11
.1 Determination Characteristics Basic Configuration	3.12
.2 Parametric Study Example	3.16
3.6 Conclusions for Chapter 3	3.18
4. NUMERICAL MODELS	
4.0 Introduction	4.1
4.1 Justification of Numerical Models	4.1
4.2 Cross-sectional Analysis	4.2
4.3 Simplified Frame Models	4.4
.1 Solution Technique	4.4
.2 Possible Degrees of Freedom	4.5
.3 Description ACTION part	4.7

Table of Contents

.4 Description REACTION part	4.10
4.4 Finite Element Models	4.12
4.5 Example	4.14
.1 Example SF-Model	4.14
.2 Example FE-Model	4.23
.3 Evaluation Assumptions SF-Model	4.25
4.6 Conclusions for Chapter 4	4.29
5. EXPERIMENTS	
5.0 Introduction	5.1
5.1 Series I: Validation Hypothesis	5.1
.1 Objective of Series I	5.2
.2 Specimen of Series I	5.3
.3 Test Arrangement of Series I	5.4
.4 Results of Series I	5.6
5.2 Series II: Simplified Shear Connection (Level 1)	5.10
.1 Objective of Series II	5.10
.2 Specimen of Series II	5.10
.3 Test Arrangement of Series II	5.15
.4 Results of Series II	5.19
.5 Friction Tests	5.29
5.3 Series III: Realistic Shear Connection (Level 2)	5.31
.1 Objective of Series III	5.32
.2 Specimen of Series III	5.32
.3 Test Arrangement of Series III	5.34
.4 Results of Series III	5.36
5.4 Conclusions for Chapter 5	5.40
5.5 Photographs	5.42
6. VALIDATION	
6.0 Introduction	6.1
6.1 Series I: Validation Hypothesis	6.1
.1 Comparable Shear Connection: Concrete Crack subjected to Shear	6.2
.2 Comparison Connection Concrete Crack Model versus Composite Slabs	6.3
.3 Actual Validation Series I	6.4
.4 Comparison Experimental, Theoretical and Numerical Results	6.5
6.2 Series II: Validation Simplified Shear Connections (Level 1)	6.7
.1 Validation of FE-Models	6.7
.2 Validation of SF-Models	6.14
6.3 Series III: Validation Realistic Shear Connections	6.22
6.4 Conclusions for Chapter 6	6.31

7. PARAMETRIC STUDY	
7.0 Introduction 7.1
7.1 Parametric Study Example Chapters 3 & 4 7.1
7.2 Parametric Study Series II 7.5
7.3 Parametric Study Series III 7.10
7.4 Conclusions for Chapter 7 7.17
8. FULL-SCALE SLAB ANALYSIS	
8.0 Introduction 8.1
8.1 General Model Full-scale Composite Slab - Level 3 8.1
8.2 General Model Shear Connection - Level 1 8.5
8.3 Partial Shear Connection method 8.8
8.4 Small-scale Experiments 8.10
8.5 Product Development 8.13
8.6 Conclusions for Chapter 8 8.15
9. GENERAL CONCLUSIONS & RECOMMENDATIONS	
REFERENCES I
NOTATIONS V
TERMINOLOGY VII
SAMENVATTING IX
ACKNOWLEDGMENTS XI
CURRICULUM VITAE XII

1. INTRODUCTION

1.1 Scope

A steel-concrete composite slab consists of profiled steel sheeting and concrete. During construction the sheeting is brought into the structure in bundles, and put in place by hand. The sheeting acts as a safe working platform and formwork for concrete. Usually no propping is required, which is favourable for fast erection.

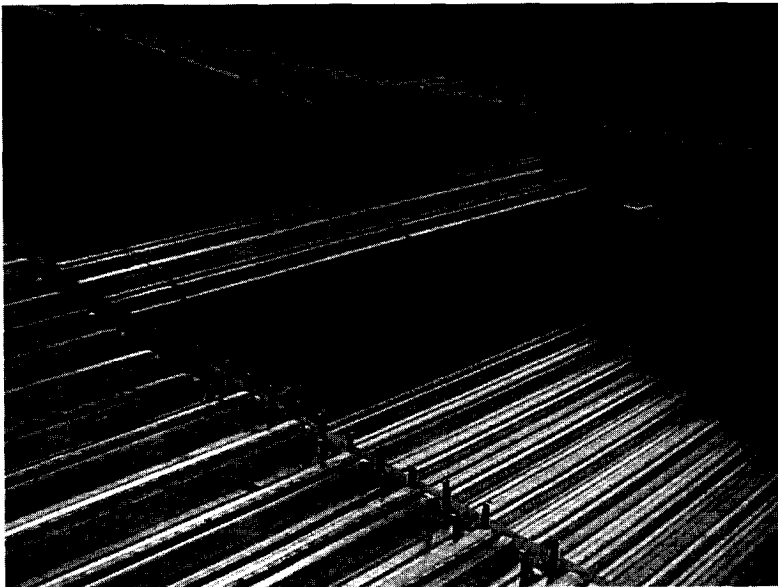


Figure 1.1: Composite slab under construction

Early composite slabs were either designed as concrete or steel slabs. Profiled sheeting was used as lost formwork for reinforced concrete slabs, or concrete was used to create a flat surface for steel decking. If a connection between the sheeting and concrete is established, the sheeting acts as reinforcement for the slab and the most favourable material properties of both steel and concrete are used. Nowadays, in order to achieve competitive flooring systems, interaction between sheeting and concrete is inevitable.

Profiled sheeting is made by a cold roll-forming process. Figure 1.2 illustrates the process for cold-formed sections. A roll-former consists of a series of rolls, which

stepwise deform flat sheeting into cold-formed elements. In order to obtain interaction between sheeting and concrete in composite slabs, similar to the interaction between reinforcement bars and concrete in reinforced concrete, indentations are added to the sheeting.

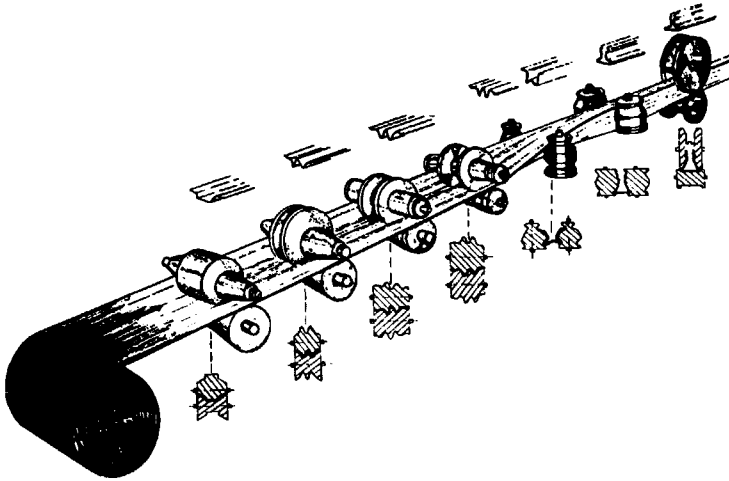


Figure 1.2: Roll-former used for making profiled sheeting.

Based on the height of the profiled sheeting, distinction can be made between three fields of application: short, regular and long span. Table 1.1 contains average dimensions for the three fields of application. With regard to the geometry of profiled sheeting, distinction can be made between trapezoidal and re-entrant shaped profiles. As illustrated in Fig. 1.3 profiled sheeting can be either trapezoidal, re-entrant or a combination of both basic shapes.

Table 1.1: Dimensions of existing profiles used for composite slabs

	Short Span	Regular Span	Long Span
<i>Sheeting</i>			
Height	15-35 mm	40-80 mm	200-225 mm
Thickness	0.50-0.70 mm	0.70-1.00 mm	1.00-1.50 mm
<i>Composite Slab</i>			
Slab depth	40-100 mm	100-200 mm	280-340 mm
Span	0.60-1.50 m	2.0-6.0 m	4.0-9.0 m

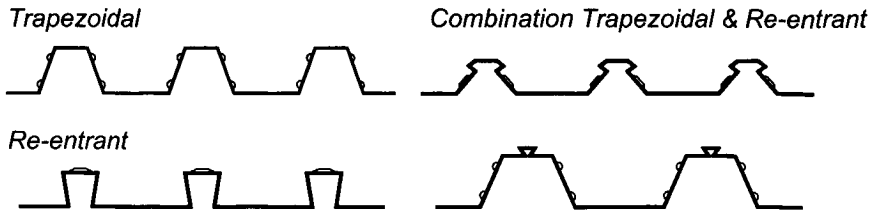


Figure 1.3: Profiled sheeting used for composite slabs

The analogy between shear connections in composite and reinforced concrete slabs is illustrated in Fig. 1.4. The main difference is that the ribbed reinforcement bars are embedded in concrete, where the sheeting can be pushed along and separated from the concrete. Therefore, although the physical behaviour of both connections is similar, the strength and stiffness of the shear connection in composite slabs is usually only 10 to 20% of values found for connections in reinforced concrete. In reinforced concrete the appearance of slip or failure of the connection is caused by deformation (cracking) of concrete. Due to the more flexible character of the shear connection in composite slabs, deformation and displacements of the sheeting determine the behaviour of the connection. The analysis of the shear connection therefore focuses on steel sheeting rather than concrete.

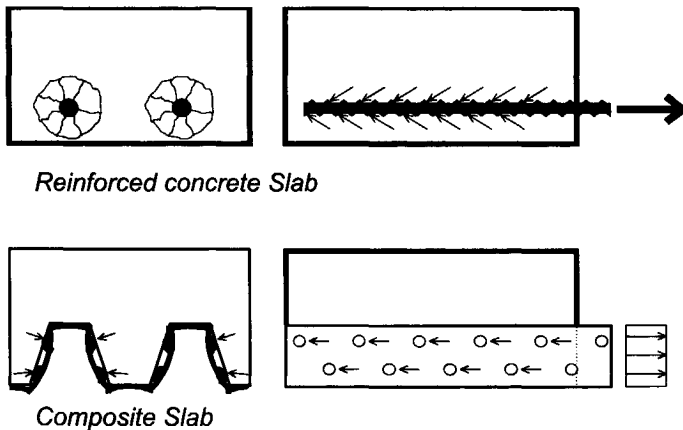


Figure 1.4: Analogy between reinforced concrete and composite slabs.

Lack of insight into the physical behaviour of shear connections between profiled sheeting and concrete causes that existing design methods for composite slabs are (semi-)empirical. The empirical character of the methods prevents the

application of composite slabs outside the range of tested parameters. New applications require expensive and time consuming tests. Due to historically based differences in building practice between different countries, international exchange of products is difficult. Apart from the application of profiled sheeting outside its original field of application, understanding of the behaviour of the shear connection is important during the development of new types of sheeting. The optimum geometry has to be determined before the roll-forming equipment is made, since adjustments to the equipment are expensive.

1.2 Aims

The aim of this study was to obtain insight into the physical behaviour of longitudinal shear connections in composite slabs. Based on understanding of the behaviour mechanisms are described. By implementing the mechanisms into calculation models, tools are developed to analyse the properties of the connections.

Due to the diversity of existing and recently developed types of sheeting, a general model for shear connections in composite slabs is not feasible, nor desirable. Developments outside the scope of any general model require adjustments to the model. Therefore a general model does not provide the required flexibility. This study focuses on the development of a transparent method for analysing the physical behaviour of a connection.

1.3 Outline thesis

The outline of the thesis is shown in Fig. 1.5. First, a general introduction into composite action between concrete and sheeting is given in Chapter 2. In Chapter 3 a hypothesis concerning the physical behaviour of shear connections in composite slabs is presented. Based on the physical behaviour of the shear connection, a method for analysing shear connections is developed. Two types of numerical models are discussed in Chapter 4. Both the hypothesis and the numerical models are validated by experiments. Three series of experiments are discussed in Chapter 5. The validation of the hypothesis and the numerical models is discussed in Chapter 6. In Chapter 7 the results of a parametric study

are presented. In Chapter 8 the results of the analysis of the shear connection between the sheeting and the concrete are related to the behaviour of full-scale composite slabs. The conclusions and recommendations are discussed in Chapter 9.

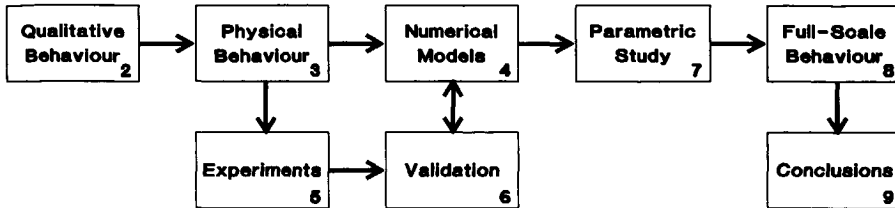


Figure 1.5: Outline thesis with reference to corresponding chapters

2. QUALITATIVE DESCRIPTION OF PHYSICAL BEHAVIOUR

2.0 Introduction

The behaviour of composite slabs depends on the behaviour of concrete, profiled sheeting and the connection between them. Lack of insight concerning the behaviour of composite slabs focuses on the shear connection. Prior to the discussion of shear connections in composite slabs (§ 2.4), a general introduction into composite members (§ 2.1), the general characteristics of shear connections (§ 2.2) and the failure mechanisms of composite slabs (§ 2.3) are discussed. Existing design methods with regard to composite slabs are discussed (§ 2.5) and the relation between the contents of this thesis, existing research and existing design methods is illustrated (§ 2.6).

2.1 General behaviour Composite Member

Figure 2.1 shows a composite slab represented by a 2-D composite beam member, consisting of two separate elements. The lower element represents the sheeting and the upper element represents the concrete.

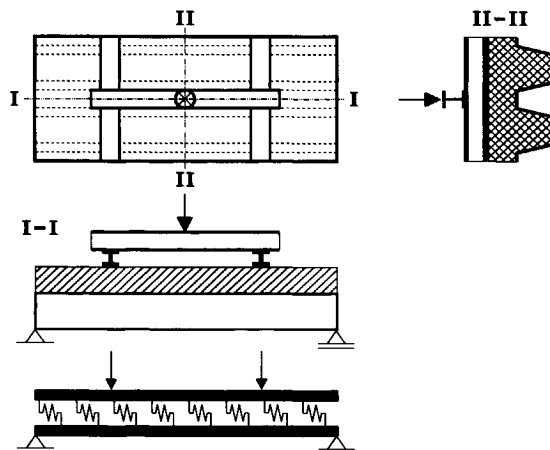


Figure 2.1: Composite slab represented as composite beam member

The behaviour of the composite beam is determined by the behaviour of the separate elements, and by the connection between them. In Fig. 2.1 the connection is represented by horizontal springs. The phenomenon in which properties of a composite beam are improved by the presence of a shear connection is referred to as composite action. Composite action is illustrated using a simplified composite beam, consisting of two identical homogeneous elements, as shown in Fig. 2.2. Both elements exhibit elasto-plastic behaviour.

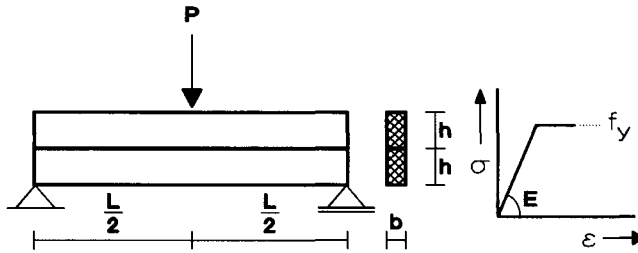


Figure 2.2: Configuration simplified composite beam

Extreme situations of composite action are no interaction and full interaction. In case of no interaction, the properties of the 'composite' beam are a summation of the properties of the separate elements, with dimensions $b \cdot h$. In case of full interaction, the properties correspond to properties of a homogeneous beam with dimensions $b \cdot 2h$.

No Interaction

$$A_{ni} = 2 \cdot A = 2 \cdot bh$$

$$I_{ni} = 2 \cdot I = 2 \cdot \frac{bh^3}{12} = \frac{1}{6} \cdot bh^3$$

$$W_{p;ni} = 2 \cdot W_p = 2 \cdot \frac{bh^2}{4} = \frac{1}{2} \cdot bh^2$$

Full Interaction

$$A_{fi} = b \cdot (2h) = 2 \cdot bh = A_{ni}$$

$$I_{fi} = \frac{b(2h)^3}{12} = \frac{2}{3} \cdot bh^3 = 4 \cdot I_{ni}$$

$$W_{p;fi} = \frac{b(2h)^2}{4} = bh^2 = 2 \cdot W_{p;ni}$$

Figure 2.3 shows composite beams with no and full interaction. The deformed beam and longitudinal slip are shown. Longitudinal slip is the difference between horizontal displacements of the separate elements in the connection. For the cross-section at mid span, normal and shear stresses are shown. In agreement with the given cross-sectional properties, the deflection and maximum normal stresses reduce if full interaction is compared to no interaction.

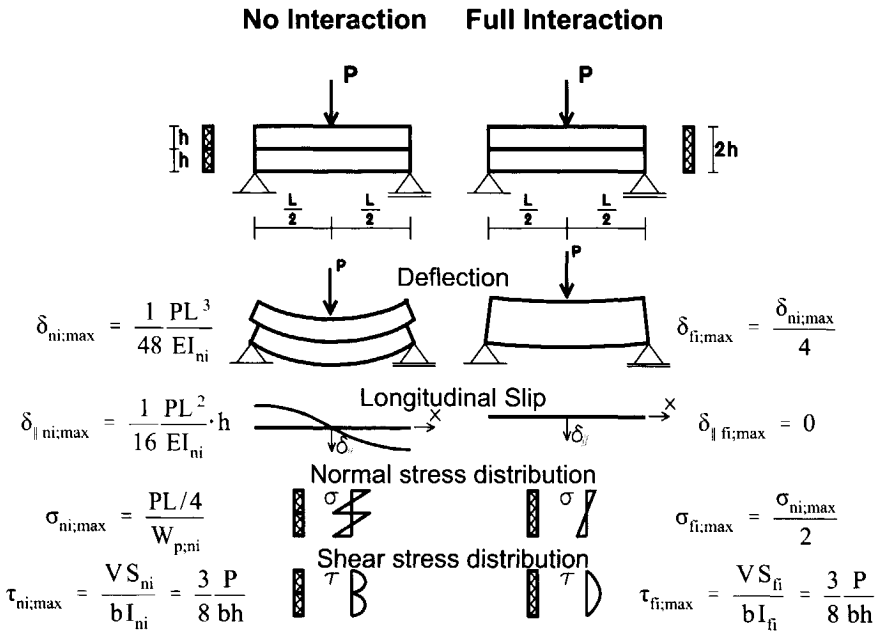


Figure 2.3: Composite beams with no and full interaction

2.2 General Behaviour of Shear Connections in Composite Slabs

Figure 2.4 shows a qualitative presentation of a shear connection. The shear stress is related to the longitudinal slip. Three independent characteristics of the connection can be distinguished: strength, stiffness and deformation capacity (ductility). No and full interaction correspond to the axes of the diagram. In case of no interaction, the shear stress is zero for all values of slip. In case of full interaction no slip occurs, while both the stiffness and strength are infinite. All situations between no and full interaction are referred to as partial interaction.

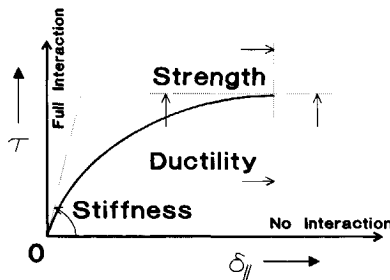


Figure 2.4: Qualitative representation behaviour shear connection

The influence of the strength, stiffness and deformation capacity of a connection to the behaviour of a composite beam is illustrated in this paragraph by the simplified beam shown in Fig. 2.2.

2.2.1 Strength of the Shear Connection

Figure 2.5 shows the relation between the resultant shear force (T) and the normal forces acting in the separate elements ($N_{1/2}$). In each cross-section the normal force in the separate elements equals the resultant shear force between the considered cross-section and the supports.

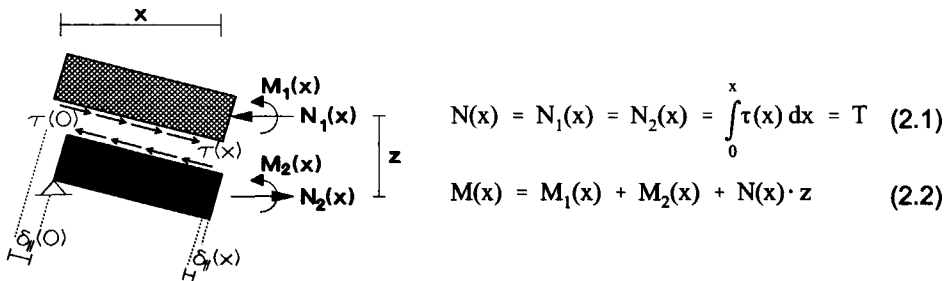


Figure 2.5: Cross-sectional forces in separate members

The internal bending moment of the composite cross-section consists of a contribution of normal forces and bending moments in the separate elements. The bending resistance of the separate elements (M_p) is reduced due to the presence of the normal forces. For a homogeneous cross-section, with elasto-plastic material behaviour, the relation between the reduced bending moment (M_p^*) and the normal force (N) is given by eq. (2.3), illustrated in Fig. 2.6.

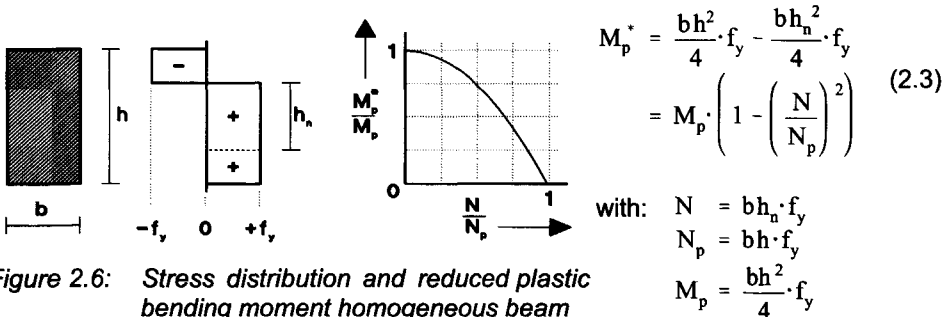


Figure 2.6: Stress distribution and reduced plastic bending moment homogeneous beam

Combining eqs. (2.1) to (2.3) returns eq. (2.4), describing the bending resistance of the cross-section as a function of the resultant shear force (T).

$$M_u = N \cdot z + 2 \cdot M_p^* = N \cdot h + 2 \cdot M_p^* = 4 \cdot M_p \cdot \frac{N}{N_p} + 2 \cdot M_p \cdot \left(1 - \left(\frac{N}{N_p} \right)^2 \right) \quad (2.4)$$

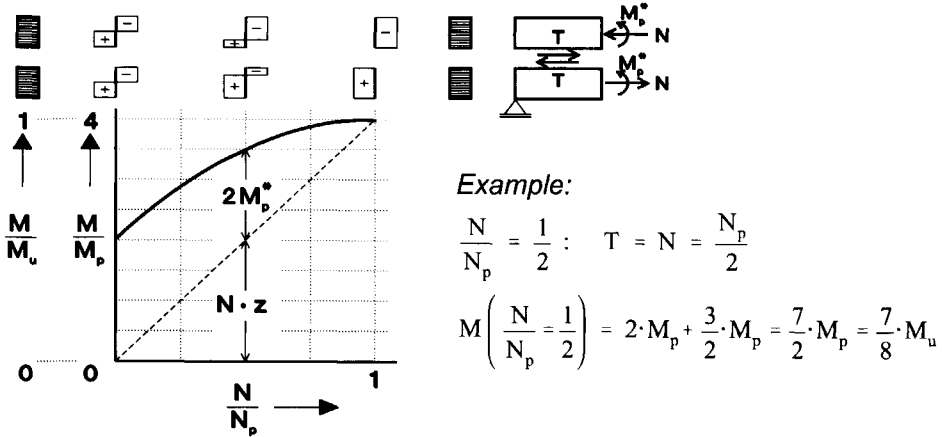


Figure 2.7: Relation between the resultant normal force and the bending resistance of a cross-section

Equation (2.4) and Fig. 2.7 illustrate the influence of the strength of the connection on the behaviour of a composite beam. If the shear stress in the connection ($\tau(x)$) increases the shear force T, and therefore the bending resistance, increases. Equation (2.1) and Fig. 2.5 show that the distance x, which is required to reach the ultimate capacity of the cross-section (M_u), reduces if the strength of a connection increases. The example in Fig. 2.7 shows that 87.5 % of the ultimate capacity is present if only 50 % of the maximum shear force is activated.

2.2.2 Stiffness of the Shear Connection

Figure 2.8 relates the vertical shear stresses in a cross-section ($\tau_{xz}(x,z)$) to the longitudinal shear stress ($\tau(x)=\tau_{zx}(x,z)$). By definition $\tau_{xz}(x,z)$ equals $\tau_{zx}(x,z)$, which means that the vertical shear stress at the interface equals the longitudinal shear stress in the connection. The vertical shear stress in a homogeneous cross-section is given by eq. (2.5).

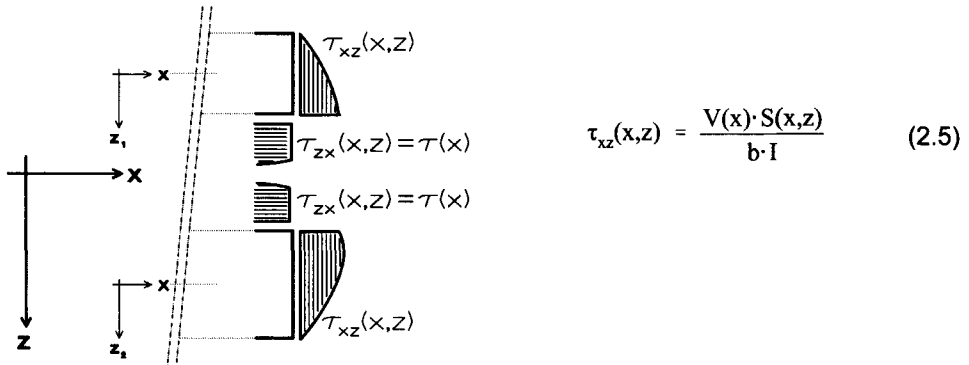


Figure 2.8: Relation vertical - longitudinal shear stress

In case of no interaction, eq. (2.5) is applicable for the separate elements. The shear stresses refer to the local coordinate systems (x, z_1) and (x, z_2) . In case of full interaction the composite cross-section can be considered as a homogeneous cross-section. The vertical shear stress distribution for no and full interaction is given in eqs. (2.6) and (2.7), and presented in Fig. 2.3.

No interaction:

$$-\frac{h}{2} \leq z_{1/2} \leq \frac{h}{2}: \quad \tau_{xz}(x, z_{1/2}) = \frac{V_{1/2}(x) \cdot \frac{b}{2} \cdot \left(\left(\frac{h}{2} \right)^2 - z_{1/2}^2 \right)}{b \cdot \frac{bh^3}{12}} = \frac{3 \left(\frac{P}{4} \right)}{2 bh} \left(1 - \left(\frac{z_{1/2}}{(h/2)} \right)^2 \right) \quad (2.6)$$

Full Interaction:

$$-h \leq z \leq h: \quad \tau_{xz}(x, z) = \frac{V(x) \cdot \frac{b}{2} \cdot (h^2 - z^2)}{b \cdot \frac{b(2h)^3}{12}} = \frac{3 \left(\frac{P}{2} \right)}{2 b(2h)} \left(1 - \left(\frac{z}{h} \right)^2 \right) \quad (2.7)$$

Maximum values for τ_{xz} are equal for no and full interaction:

$$\tau_{xz}(x, z_{1,2}=0) = \tau_{xz}(x, z=0) = \frac{3 P}{8 bh} \quad (2.8)$$

For full interaction the longitudinal shear stress $\tau(x)$ can be derived from eq. (2.7).

$$\tau(x) = \tau_{xz}(x, z=0) = \frac{3}{8} \frac{P}{bh} \quad (2.9)$$

If the strength of a shear connection is infinite, and the stiffness increases from nil to infinity, the behaviour of the composite beam changes from no to full interaction. The vertical shear stress distribution in each cross-section changes from eq. (6) to (7) and the cross-sectional properties change from values found for no to full interaction. Figure 2.9 shows the vertical shear stress distribution of a cross-section qualitatively. Three contributions can be distinguished:

- A Quadratic contribution caused by the vertical shear forces ($V_{1/2}$).
- B Linear contribution caused by the shear stress (τ_0) in the connection.
- C Quadratic contribution caused by the eccentricity of τ_0 .

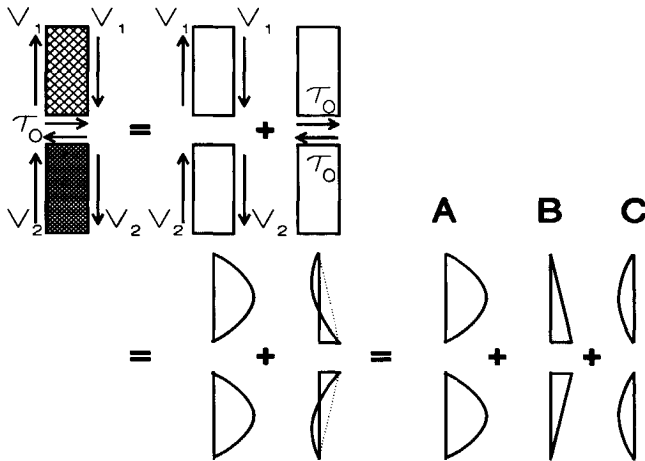


Figure 2.9: Vertical shear stress distribution partial interaction

Shear pattern A corresponds to the stress distribution of no interaction. Shear patterns B & C introduce the influence of the shear connection. The total area enclosed by the vertical shear stress distribution is independent of shear connection, since it represents the vertical shear force. Therefore the sum of the enclosed areas B & C is zero. If the stiffness of the shear connection increases, τ_0 increases. With τ_0 , the enclosed area of pattern C increases. The sum of the patterns A & C is proportional to the curvature in the cross-section. In eq. (2.10), the vertical shear stress distribution is evaluated for the upper element.

$$\begin{aligned} \tau_{xz}(x, z_1) &= \tau_A(x, z_1) + \tau_B(x, z_1) + \tau_C(x, z_1) \\ &= \frac{3}{8} \frac{P}{bh} \cdot \left(1 - \left(\frac{z_1}{h/2} \right)^2 \right) + \frac{\tau_0}{2} \cdot \left(1 + \frac{z_1}{h/2} \right) - \frac{3}{4} \tau_0 \cdot \left(1 - \left(\frac{z_1}{h/2} \right)^2 \right) \end{aligned} \quad (2.10)$$

Figure 2.9 and eq. (2.10) show, that vertical shear stresses can occur in composite beams, even if no vertical shear force is present ($\tau = \tau_B + \tau_C$). If eq. (2.10) is integrated over the cross-section, the different shear patterns can be distinguished, as shown in eq. (2.11).

$$\begin{aligned} V_1(x) &= \int_{-h/2}^{h/2} b \cdot \tau_A \, dz + \int_{-h/2}^{h/2} b \cdot \tau_B \, dz + \int_{-h/2}^{h/2} b \cdot \tau_C \, dz \\ &= \frac{3}{8} \frac{P}{bh} \cdot \frac{2}{3} bh + \frac{\tau_0}{2} \cdot bh - \frac{3}{4} \tau_0 \cdot \frac{2}{3} bh \\ &= \frac{P}{4} + \tau_0 \cdot \frac{bh}{2} - \tau_0 \cdot \frac{bh}{2} \end{aligned} \quad (2.11)$$

If the longitudinal shear stress is increased in three equal steps from zero to its maximum value ($\tau_{0,max}$), the stiffness of the connection increases from zero to infinity, corresponding to no and full interaction. For all steps, the enclosed areas of patterns A, B & C are calculated using eq. (2.11). The corresponding stress distribution is given in Fig. 2.10. It shows that from no to full interaction, pattern C increases from 0 to 75 % of the constant pattern A. This implies that the sum of the quadratic patterns, and therefore the curvature, reduces by a factor 4, which means that, in agreement with the derived properties for no and full interaction, the bending stiffness increases by a factor 4.

The evaluation of vertical shear stresses illustrates that the presence of longitudinal shear stresses in the connection reduces the curvature, and therefore increases the bending stiffness of the composite beam. The stiffness of a shear connection does not influence the strength of the composite beam. However, if the stiffness of a connection reduces, the deformation of the composite member corresponding to the ultimate resistance is larger, so the required deformation capacity of the separate elements and the connection is higher.

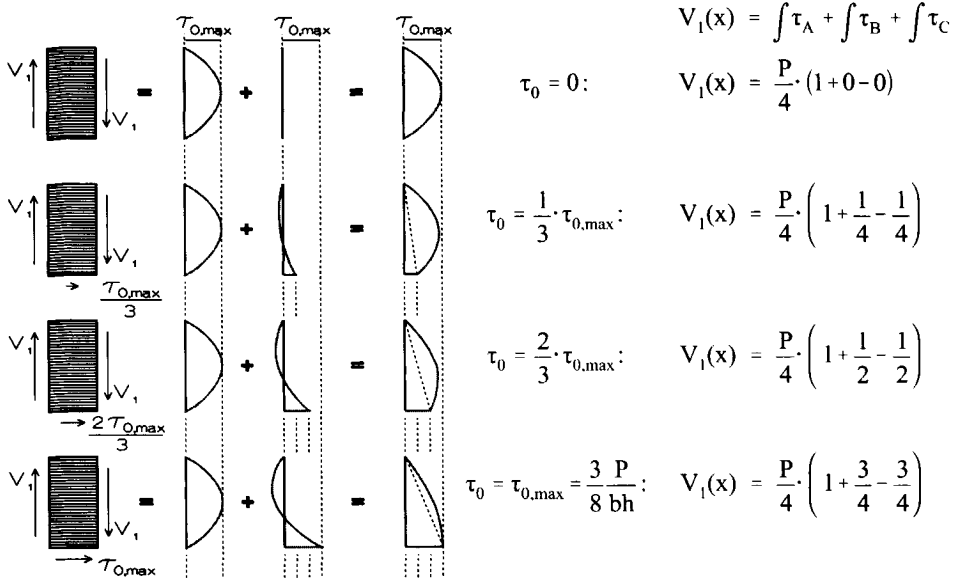


Figure 2.10: Vertical shear stress distribution partial interaction

2.2.3 Deformation Capacity of the Shear Connection

A shear connection can be seen as the third element in a composite cross-section. Lack of deformation capacity (ductility) of the shear connection can introduce (brittle) failure of the connection and the composite beam. In order to illustrate the influence on the deformation capacity of the shear connection on the behaviour of a composite beam, the concentrated load (P) is replaced by a uniformly distributed load (q), as shown in Fig. 2.11. The material behaviour of the separate elements is linear elastic instead of elasto-plastic. The influence of the deformation capacity is illustrated by three different shear connections. Connection A has a high stiffness and no deformation capacity. Connection B combines a high stiffness with ductile behaviour. Connection C combines a finite stiffness with ductile behaviour. The behaviour of the corresponding composite beams A to C is presented in Fig. 2.15.

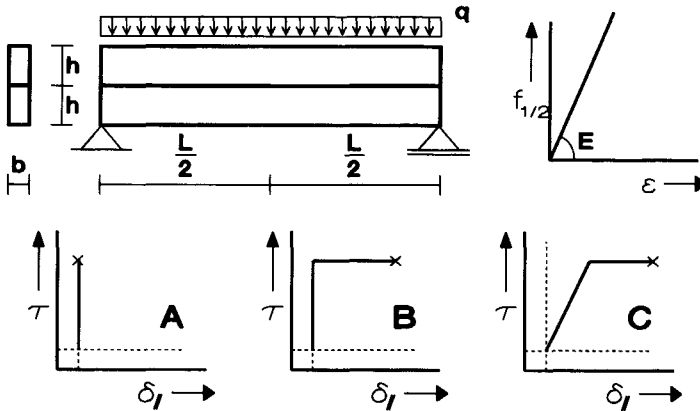


Figure 2.11: Simplified composite beam with different shear connections

Connection A

Figure 2.12 shows the behaviour of composite beam A. Until first failure of the connection full interaction is present. The longitudinal shear stress is proportional to the vertical shear force. No slip occurs.

$$-\frac{L}{2} \leq x \leq \frac{L}{2}; \quad \tau(x) = \tau_{xz}(x,z) = \tau_{xz}(x,0) = \frac{V(x) \cdot \frac{b}{2} \cdot (h^2 - z^2)}{b \cdot \frac{b(2h)^3}{12}} = \frac{3 q \cdot x}{4 bh} \quad (2.12)$$

Once the ultimate shear stress in the connection (τ_u) is reached at the support, the connection will fail rapidly like a zipper. Equation (2.13) determines the load ($q_{u,fi}$), at which initiation of failure of the connection occurs (A1).

$$\tau(\pm L/2) = \pm \frac{3 q \cdot L}{8 bh} = \tau_u \Rightarrow q_{u,fi} = \frac{8 bh}{3 L} \cdot \tau_u \quad (2.13)$$

Figure 2.12 shows the longitudinal shear stress distribution ($\tau(x)$) and the bending stiffness (EI^*) for composite beam A. At point A1 first failure of the connection occurs at both supports. Failure of the connection propagates from the supports to mid span. From A1 to A2 slip arises, and the behaviour changes from full to no interaction. According to the cross-sectional properties, the stiffness after point A2 is decreased by a factor 4 with regard to the stiffness between 0 and A1.

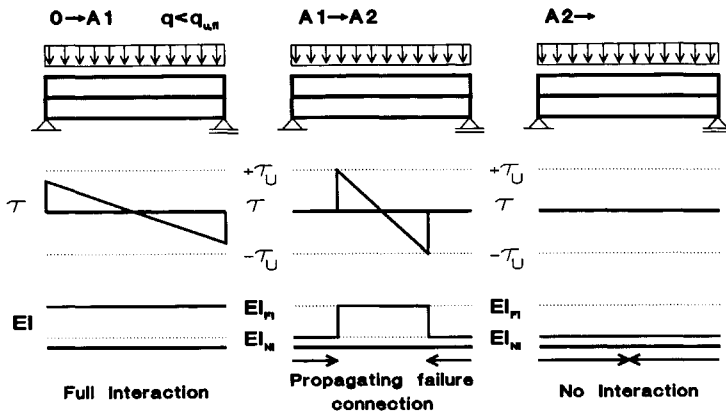


Figure 2.12: Behaviour of composite beam A

Connection B

Figure 2.13 shows the behaviour of composite beam B. Until $q_{u,fi}$ beam B behaves similar to beam A. When $q_{u,fi}$ is reached (B1) longitudinal slip occurs. Propagation of slip occurs, instead of brittle failure (B1-B2). Due to the ductile behaviour, the ultimate shear strength (τ_u) can be developed over the connection. With the appearance of longitudinal slip, the bending stiffness reduces, and lies between values found for no and full interaction. From B1 to B2 the stiffness reduces by a factor 4. After B2, the resultant shear force no longer increases and additional loading is carried by the separate elements.

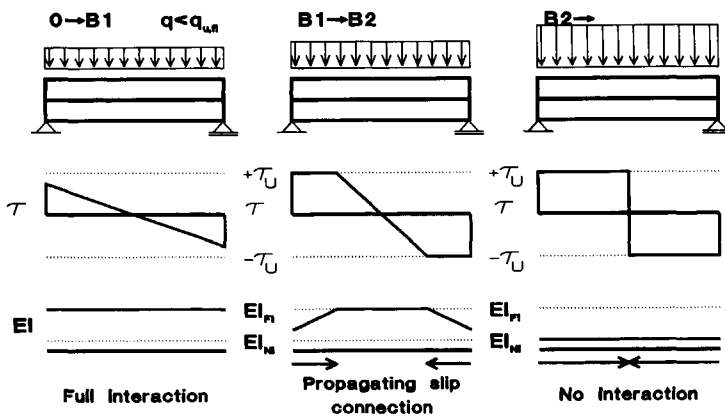


Figure 2.13: Behaviour of composite beam B

Connection C

Figure 2.14 shows the behaviour of composite beam C. Compared to beam B, beam C shows longitudinal slip before τ_u is reached. The initial bending stiffness of the composite beam is smaller than found for connections A and B. Due to the appearance of slip, the distribution of the longitudinal shear stress over the connection is no longer proportional to the vertical shear force. The enclosed area underneath the longitudinal shear stress diagram found for connection C is larger than found for A and B, and therefore the resultant shear force is larger. According to Fig. 2.7, the capacity of the composite beam is higher when τ_u is first reached at the supports ($q_{C1} > q_{A1} = q_{B1}$). Once τ_u is developed over the full length of the shear connection, the corresponding capacity equals the capacity of connection B ($q_{C2} = q_{B2}$). However, in order to reach the same capacity, the required deformation capacity is higher, since the level of slip is higher.

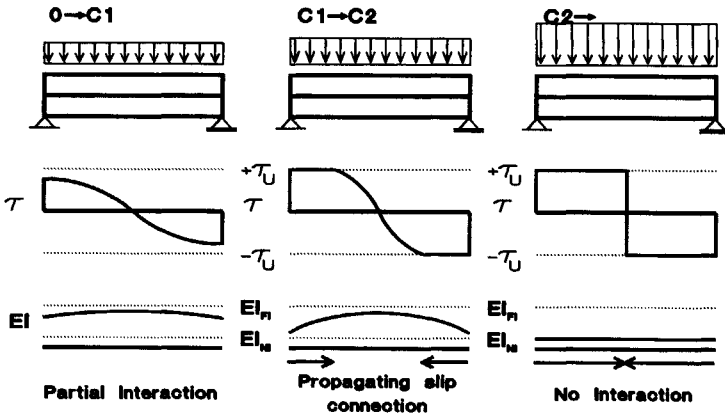


Figure 2.14: Behaviour of composite beam C

The behaviour of the composite beams A, B & C is illustrated in Fig. 2.15. The characteristic points in the load and longitudinal slip versus deflection diagrams are given. Eventually, for all beams, the bending stiffness reduces to the bending stiffness corresponding to no interaction. For beam A, the connection has failed completely, whereas for beams B and C the connection is fully active. Due to the linear material behaviour of the separate elements no ultimate capacity is found.

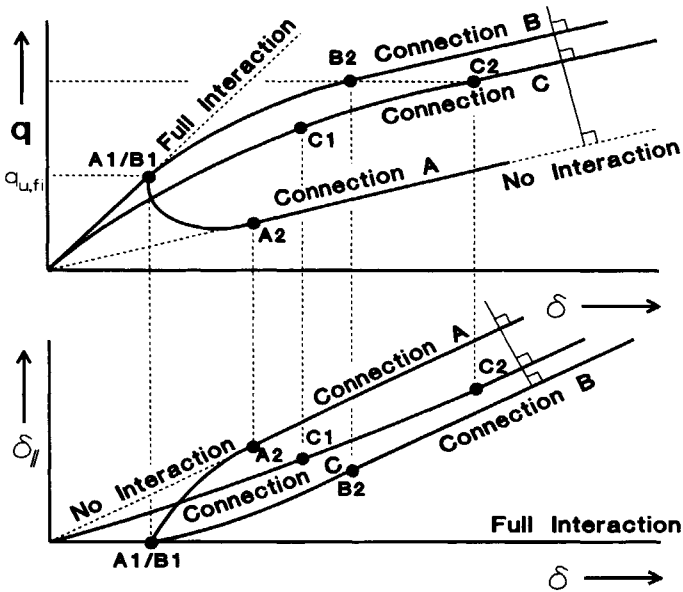


Figure 2.15: Load versus deflection for composite beams A to C

Ductile behaviour enables the development of the ultimate cross-sectional strength of the connection (τ_u) over a larger part of the connection. In case of a uniformly distributed load, the resultant shear force (T) for a ductile connection can be doubled with regard to a brittle connection.

2.3 Failure Mechanisms of Composite Slabs

For a composite beam member, three failure mechanisms can occur: flexural (I), longitudinal shear (II) and vertical shear or shear tension failure (III). The corresponding critical cross-sections are shown in Fig. 2.16. *Flexural failure* occurs when the ultimate capacity of the composite cross-section is reached. *Longitudinal shear failure* occurs if the capacity of the slab is limited by the capacity of the shear connection. *Vertical shear or shear tension failure* only occurs if deep slabs and short spans lead to large vertical shear forces, which does not occur in commonly used composite slabs, and should be avoided because of its brittle character.

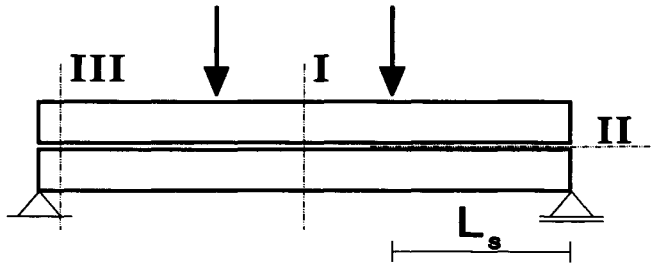


Figure 2.16: Failure mechanisms of a composite beam member

Eurocode 4 [1] uses the shear span (L_s) as the length of the shear connection between the support and the critical cross-section. For the composite slab as shown in Fig. 2.2, the shear span is $L/2$. For a uniformly distributed load, as shown in Fig. 2.11, EC4 uses $L/4$.

Figure 2.17 shows the possible failure mechanisms as a function of the shear span (L_s). The capacity of the slab is represented by the support reaction (V_i). If L_s is short, vertical shear or shear tension failure occurs (0-I). If L_s is large, flexural failure occurs (II-), since, due the length of the shear span, the shear connection is not critical. If the shear connection is critical, longitudinal shear failure occurs (I-II).

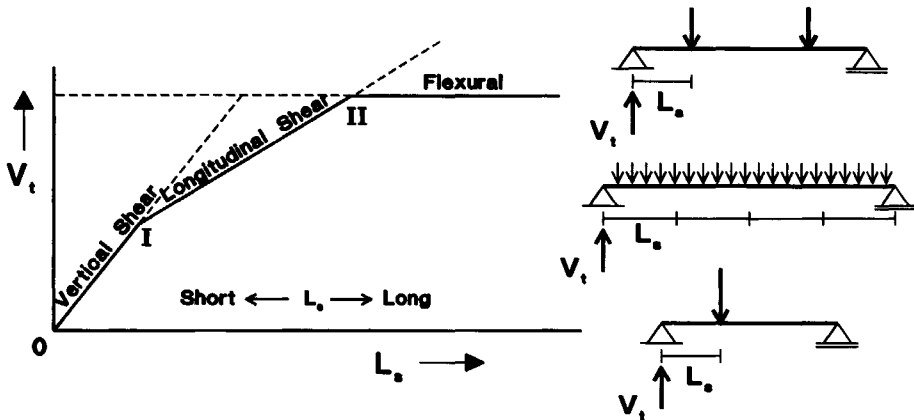


Figure 2.17: Failure Mechanisms as a function of the shear span (L_s)

2.4 General Behaviour of Composite Slabs

In order to relate the behaviour of composite beam members to composite slabs, a simplified case is considered, as shown in Fig. 2.18. The simplifications do not violate the characteristic phenomena of composite slabs. The dimensions of the slab are realistic. The sheeting is a symmetrical trapezoidal profile. The stress-strain relations of both steel and concrete and the shear stress-slip relation of the connection are bi-linear. Tensile stresses in the concrete are neglected.

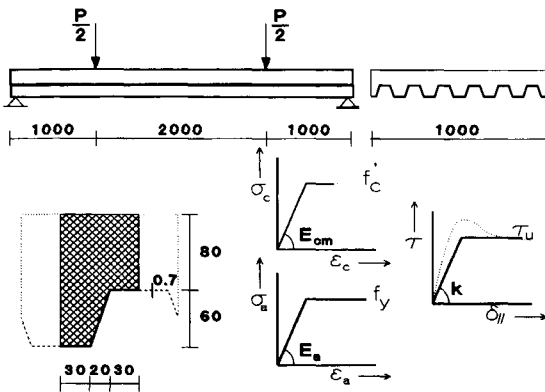


Table 2.1: Properties Slab

Concrete	
f_c	= 16.7 N/mm ²
E_{cm}	= 29.000 N/mm ²
Sheeting	
f_y	= 235 N/mm ²
E_a	= 210.000 N/mm ²
A_a	= 1078 mm ² /m
I_a	= 638.5 · 10 ³ mm ⁴ /m
W_{ea}	= 21.28 · 10 ³ mm ³ /m
W_{pa}	= 24.05 · 10 ³ mm ³ /m
$N_{pa} = A_a \cdot f_y$	= 253.0 · 10 ³ N/m
$M_{pa} = W_{pa} \cdot f_y$	= 6.20 · 10 ⁶ Nmm/m
Connection	
T_u	= 0.20 N/mm ²
	= 200 N/mm/m
k_1	= 0.20 N/mm ³

Figure 2.18: Simplified behaviour of composite slab

The ultimate capacity of the cross-section ($M_{p,Rd}$) is reached when N_{pa} is reached in the sheeting, as illustrated in Fig. 2.19. The stress distribution in the concrete is simplified in order to simplify the determination of the lever arm z .

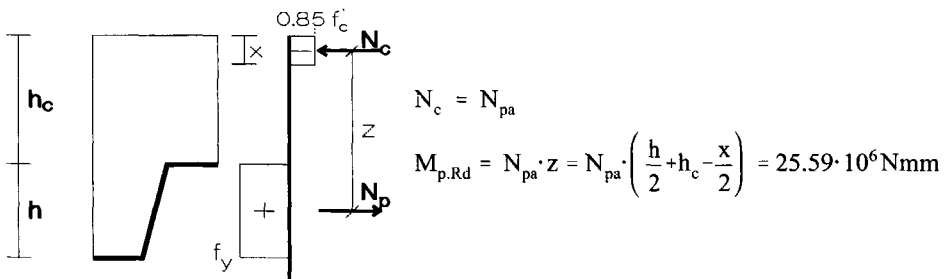


Figure 2.19: Ultimate capacity of a composite cross-section

Figure 2.20 relates the bending resistance of a cross-section to the resultant normal force, similar to Fig. 2.7. If no normal force is present, the bending resistance corresponds to the plastic bending moment of the sheeting (M_{pa}), since no tensile stresses occur in the concrete. For composite slabs, compared to composite beams, the ratio between M_{pa} and $M_{p,Rd}$ is small, which means that the presence and properties of the shear connection are more important.

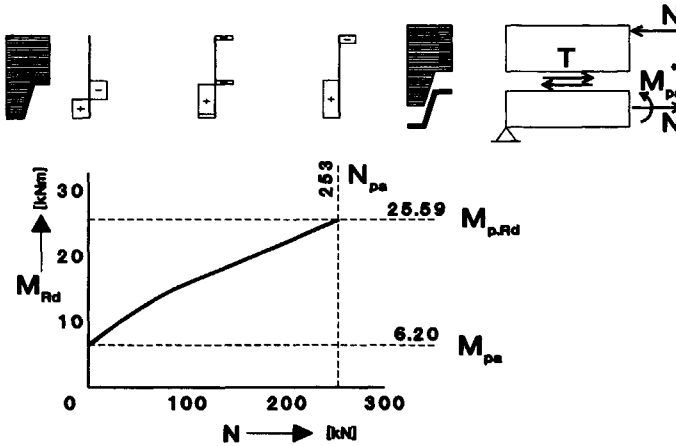


Figure 2.20: Bending resistance versus resultant shear force for a simplified composite slab

The characteristics of shear connections in composite slabs depend on the geometry of the sheeting and indentations. The resultant shear force (T), developed over a certain length of the shear connection (L_x), is given by eq. (2.14) and represents the enclosed area, as illustrated in Fig. 2.21.

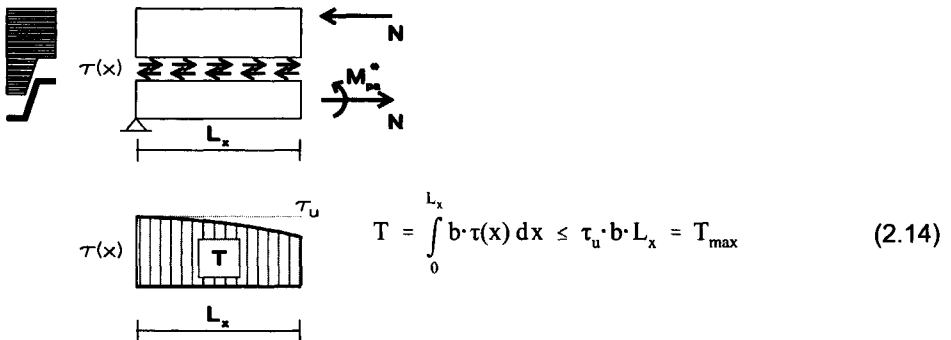


Figure 2.21: Resultant shear force T transferred over the length L_x

The resultant shear force (T) equals the resultant normal forces (N) and is related to the length of the connection (L_x). Fig. 2.20 can be transferred to Fig. 2.22, relating the bending resistance (M_{Rd}) to the length of the shear connection (L_x). The diagram is referred to as the partial interaction diagram. The ultimate capacity of a cross-section ($M_{p,Rd}$) is developed at a distance L_{SF} from the supports. The capacity of the cross-section does not increase if $L_x > L_{SF}$.

$$L_{SF} = \frac{N_{pa}}{b \cdot \tau_u} = \frac{253000}{1000 \cdot 0.2} = 1265 \text{ mm} \quad (2.15)$$

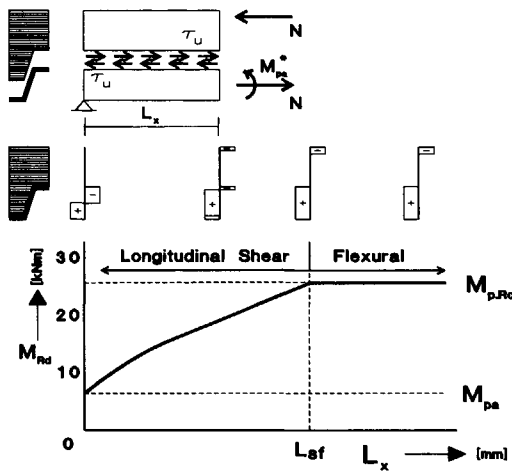


Figure 2.22: Partial Interaction diagram for a simplified composite slab

The external bending moments (M_{sd}) can be added to the partial interaction diagram, as illustrated in Fig. 2.23. In each cross-section the capacity (M_{Rd}) should be larger than the external bending moment ($M_{Rd} \geq M_{sd}$). The cross-section in which M_{Rd} equals M_{sd} is the critical cross-section. The location of the critical cross-section with regard to L_{SF} , determines the failure mode. If $L_S > L_{SF}$ flexural failure occurs, which implies that the ultimate capacity ($M_{p,Rd}$) is reached. If $L_S < L_{SF}$ longitudinal shear failure occurs. The shear connection fails and reduces the bending resistance. Figure 2.23 shows that, for the configuration of Fig. 2.18, longitudinal shear failure occurs. The load at failure can be derived from Fig. 2.23.

$$\begin{aligned}
 M_{Rd}(L_x=1000) &= M_{Sd}(L_x=1000) = \frac{P \cdot L}{2 \cdot 4} \\
 \Rightarrow P_u &\approx \frac{8 \cdot 21.47 \cdot 10^6}{4000} = 42.9 \text{ kN} \\
 \Rightarrow q_u &\approx \frac{P_u}{B} L = \frac{42.9}{1.0 \cdot 4.0} = 10.7 \text{ kN/m}^2
 \end{aligned}
 \tag{2.16}$$

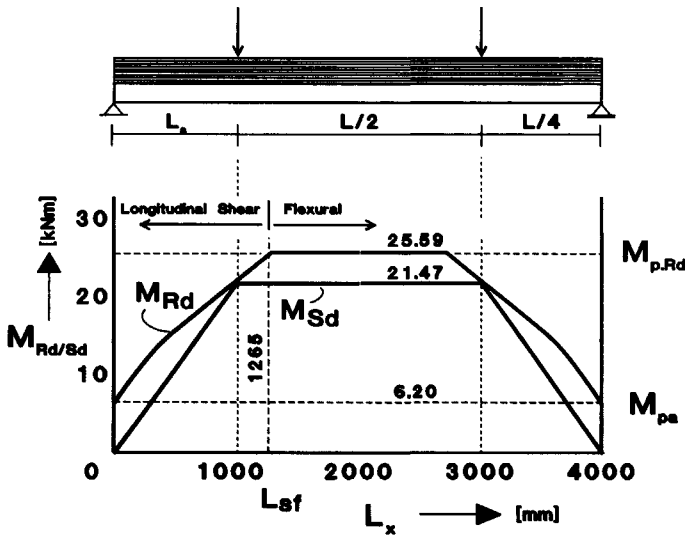


Figure 2.23: Partial interaction diagram simplified composite slab

With respect to the deformation capacity of the connection § 2.2.2 and 2.2.3 illustrate that the stiffness of the connection or a lack of deformation capacity can lead to a reduction of the capacity of the slab. A general impression concerning the required deformation capacity can be derived from the properties of the shear connection. In order to ensure the development of the ultimate shear strength over the considered shear span, the longitudinal slip should exceed 1.0 mm over the complete shear span. The required deformation capacity to reach the ultimate bending capacity is at least 2 mm. The deformation capacity required to assure ductile slab behaviour is at least 3 times larger. In general, the required deformation capacity increases if the stiffness of the connection (k_1) decreases.

To increase understanding of composite action in composite slabs, two variations of the basic configuration are considered. The influence of both

variations is illustrated by adjusting the partial interaction diagram. Figure 2.24 shows the basic and adjusted configurations and the corresponding partial interaction diagrams.

Variation 1: Reduced strength, stiffness or ductility shear connection

Reduction of the strength (A) of the shear connection leads to a reduction of the resultant shear force (T) in every cross-section. L_{SF} increases and the partial interaction diagram is expanded horizontally. The ultimate capacity of the cross-section ($M_{p,Rd}$) does not change since it is a cross-sectional parameter, which is not influenced by the strength of the shear connection. The failure mechanism might shift from flexural to longitudinal shear failure, due to the increased value of L_{SF} . Reduction of the stiffness (B) increases the required deformation capacity. Lack of deformation capacity (C) leads to early (brittle) failure of the slab.

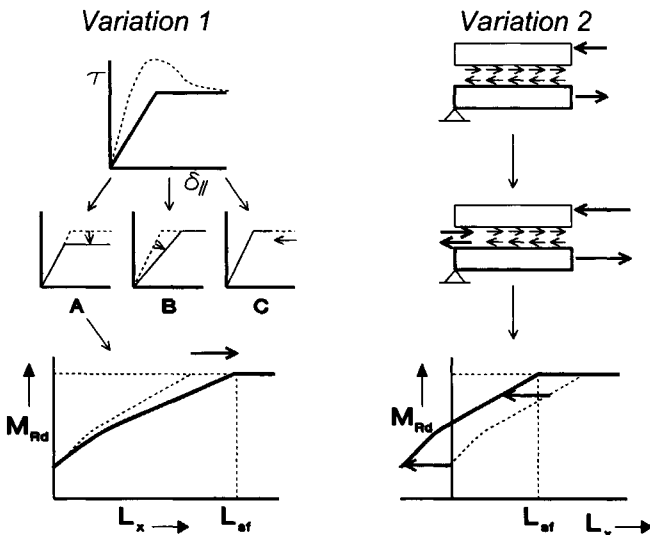


Figure 2.24: Influence of variations to partial interaction diagram

Variation 2: Improved characteristics at supports

Due to the presence of the support reaction, the characteristics of the shear connection at the supports are improved with respect to the characteristics found between the supports. Further improvement can be obtained by deforming the sheeting or shear devices at the supports. The contribution to the shear resistance can be taken into account by a concentrated shear force at the supports. The partial interaction diagram shifts to the left. L_{SF} reduces and the

capacity of all cross-sections increases. Again, the ultimate capacity of the cross-section ($M_{p,Rd}$) does not change. The failure mechanism might shift from longitudinal shear to flexural failure, due to the reduction of L_{SF} .

2.5 Existing Design Methods

Eurocode 4 [1] offers two methods for the design of composite slabs: the 'm-k' method and the Partial Shear Connection (PSC) method. Both methods are based on the results of full-scale experiments. Depending on the test results the behaviour of a slab is classified as brittle or ductile. The 'm-k' method may be used for all profiles. The PSC method may be used only for ductile profiles. Both methods are discussed in § 2.5.1 and 2.5.2. In § 2.5.3 two proposals for adjustments to the PSC method are discussed.

2.5.1 'm-k' Method

The 'm-k' method uses full-scale experiments to determine the capacity of a composite slab. The 'm-k' method derives a design line for longitudinal shear failure. The load corresponding to flexural failure is based on the calculation model, as illustrated in Fig. 2.19. The results of the 'm-k' method are presented in a diagram which relates the ultimate support reaction (V_t) to the shear span (L_s), as shown in Fig. 2.25. Compared to the presentation of Fig. 2.17, the reciprocal value of the shear span L_s is plotted on the horizontal axes. Other parameters at the axes of Figs. 2.25 and 2.26 represent the width of the slab (b), the distance between the neutral axis of the sheeting and the top of the slab (d_p) and the steel area in the cross-section (A_p).

A typical result of the 'm-k' method is shown in Fig. 2.26. Two series of at least three experiments are required. Series A & B represent respectively a relative long and short shear span. The values at the horizontal axis should be chosen close to points II & I, as given in Fig. 2.25, in order to represent longitudinal shear failure. A design line can be drawn based on the results of each group.

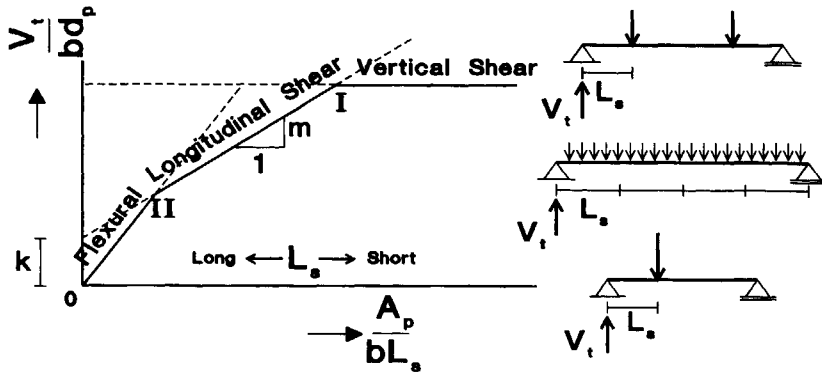


Figure 2.25: Base diagram of the 'm-k' method

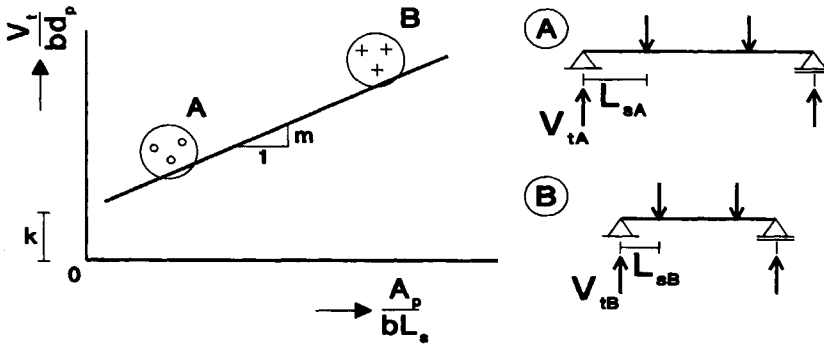


Figure 2.26: Typical results 'm-k' method

The derived design line may only be used for the tested configuration or for configurations in which the changed parameters are known to have a positive effect on the capacity of the slab. Since this positive effect may not be taken into account, the usage of the 'm-k' method outside the tested range of parameters is either not permitted or conservative. Furthermore, the boundaries of longitudinal shear failure (I & II), can only be estimated well, if a general impression about the performance of the shear connection is available.

2.5.2 Partial Shear Connection Method

The Partial Shear Connection method uses a partial interaction diagram to relate the bending resistance M_{Rd} to the applied bending moments M_{Sd} , as shown in Fig. 2.23. The partial interaction diagram is based on the ultimate shear stress τ_u , or $\tau_{u\mu}$ in case friction at the supports is considered [2]. Values for τ_u and $\tau_{u\mu}$ are derived from full-scale experiments, as shown in Fig. 2.27. The original PSC method as implemented in previous versions of Eurocode 4 [3] did not take into account friction at the supports. The adjusted PSC method as implemented in the current Eurocode 4 [1] allows for friction to be taken into account.

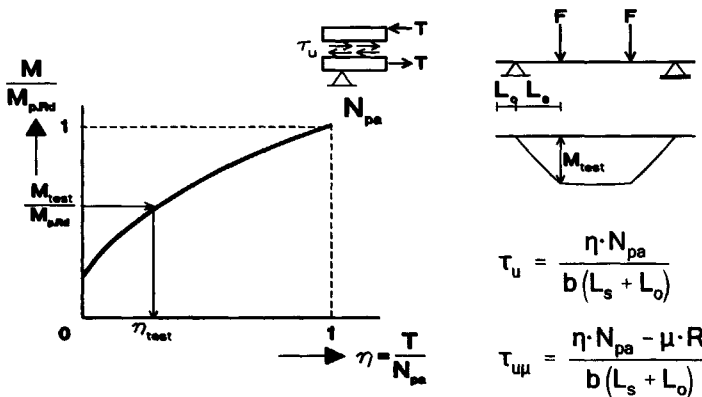


Figure 2.27: Determination of τ_u using full-scale experiments

If friction at the supports is not considered, the design partial interaction diagram can be derived by using the ultimate shear stress τ_u , as shown in Fig. 2.28. Similar to Fig. 2.23, the design bending moments M_{Sd} can be added to determine the critical cross-section and the ultimate capacity of the slab. Three different configurations are considered in Fig. 2.28. If friction at the supports is taken into account, the partial interaction diagram shifts to the left due to the frictional force at the supports ($\mu \cdot R$) and expands due to the reduced ultimate shear stress ($\tau_u > \tau_{u\mu}$) as illustrated in Fig. 2.24.

With regard to the 'm-k' method, the PSC method can be used for a wider range of parameters, since the effect of cross-sectional parameters can be taken into account. With regard to the tested configuration, parameters influencing the ultimate shear stress $\tau_{u/\mu}$ may not be varied. The fact that only ductile profiles

can be evaluated is not a disadvantage, since application of brittle profiles is not desirable.

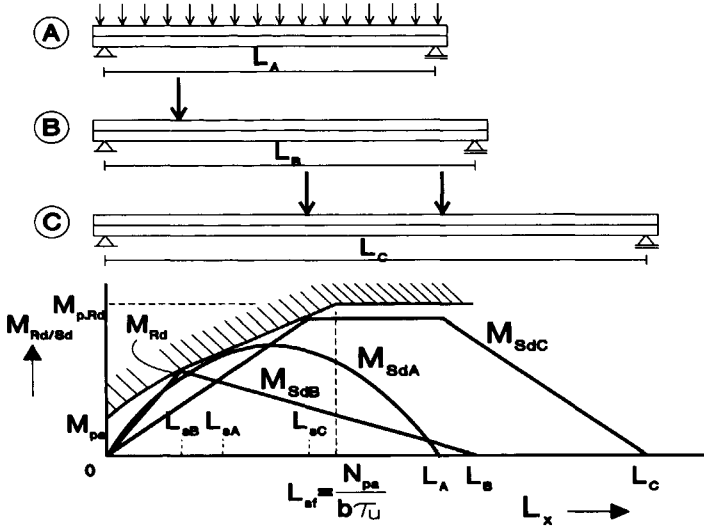


Figure 2.28: Design partial interaction diagram

The PSC method is based on a calculation model with a physical background, as illustrated in Fig. 2.22. The model assumes a uniform distribution of the shear stress $\tau_{u/uy}$ over the considered shear span. In this thesis, it is stated that the ultimate shear stress of cross-sections varies over the considered shear span. Together with the issue of shear stress development as discussed in § 8.3, a nonuniform shear stress distribution at the ultimate limit state is possible, and for some profiles more likely than an uniform distribution. This implies that the derived values for the ultimate shear stress $\tau_{u/uy}$ are average values of the shear stress at failure. Application of the calculation model of Fig. 2.22 suggests a physical background, which is only correct for configurations which have an uniform distribution of shear stresses in the connection at failure.

2.5.3 Proposed adjustments to the Partial Shear Connection Method

Two design methods are developed, based on the original PSC method. The *New Partial Shear Connection Method* [4,5], which is already implemented in the

Australian standards, and the *Three Parameter Partial Shear Connection Method* (3P PSCM) [6]. The background of both methods is discussed briefly.

Both methods propose the usage of small- instead of full-scale tests for the derivation of the characteristics of a shear connection. Instead of the indirect derivation of the strength τ_u , the strength, stiffness and deformation capacity are obtained from small-scale tests. Three different types of small-scale tests are schematically shown in Fig. 2.29. Disadvantage of small-scale experiments is the fact that boundary conditions of specimen are not in all aspects consistent with conditions in a full-scale specimen. For instance curvature of the slab and cracking of concrete is not considered in a small-scale specimen. In general boundary conditions influence the behaviour of the specimen. Due to the limited size of the specimen the boundary conditions can dominate the behaviour of small-scale specimen.

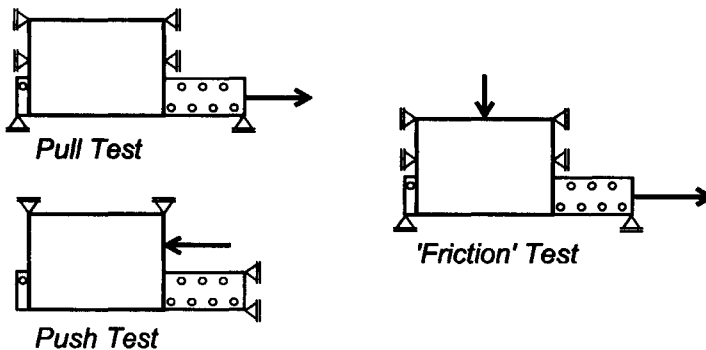


Figure 2.29: Small-scale test arrangements

Both methods recognize the appearance of friction at the supports. Two different types of small-scale tests are performed. One represents the behaviour between the supports, which implies that no or only a limited force is present perpendicular to the shear connection (*Pull/Push Tests*). The second represents the behaviour at the supports (*'Friction' Test*). A lateral force is applied to represent the support reaction.

Within both methods, the second series of experiments is referred to as *Friction Tests*, which is physically not correct if dry friction is considered. Since profiled sheeting with indentations is considered the ratio between longitudinal shear forces and lateral forces, acting perpendicular to the slab, can be larger than 1,

as illustrated for a simple configuration in Figs. 5.1 and 5.27. For profiled sheeting with indentations the contribution to the longitudinal shear resistance at the supports should not be referred to as dry friction. The derived 'coefficient of friction' from the *Friction Tests* might differ considerably from the coefficient of friction found for an interface with flat sheeting and concrete.

The 3P PSC method includes an additional parameter, and a corresponding small-scale test. Apart from a *Push* and '*Friction*' Test, the behaviour of the connection with tensile strains is considered (*Tension-Push Test*). It is stated that the presence of large tensile strains influences the behaviour of the shear connection.

The proposed small-scale tests [6,7,8] are very complex. Further improvement of test arrangements and design methods requires understanding of the physical behaviour of the shear connection. The mechanisms which determine the behaviour of shear connections might lead to simplified test arrangements and a reduction of the required number of tests. With the approach discussed in this thesis, the improved behaviour at the supports as well as the influence of tensile strains can be investigated, since the phenomena are part of the mechanisms which determine the physical behaviour of the shear connection.

2.6 Overview of Research into Composite Slabs

Different levels of research can be distinguished with regard to composite slabs. The work presented in this thesis can be related to both the existing design methods and these levels of research, as shown in Fig. 2.30.

Level 3: Macro. Level 3 deals with full-scale composite slabs. The existing design methods are level 3 design methods. In spite of the size of full-scale specimen, experiments on level 3 are relatively easy to perform.

Level 2: Meso. Level 2 deals with sections of composite slabs, comparable to the size of specimen commonly used in small-scale tests [4, 5 & 6]. This implies the presence of approximately 20 to 60 indentations, depending on the type of sheeting. A modified Partial Shear Connection method might start on this level by determining the characteristics of the shear connection based on small-

instead of full-scale experiments. Compared to full-scale experiments, performing small-scale experiments is usually more complicated.

Level 1: Micro. Level 1 deals with analysis on the level of indentations, or slices of sheeting with a limited number of indentations. The approach presented in this thesis is based on the physical description of a shear connection at Level 1. The characteristics of the shear connection are determined based on a cross-sectional analysis. Results can be used in Level 2 or 3 composite slab analysis.

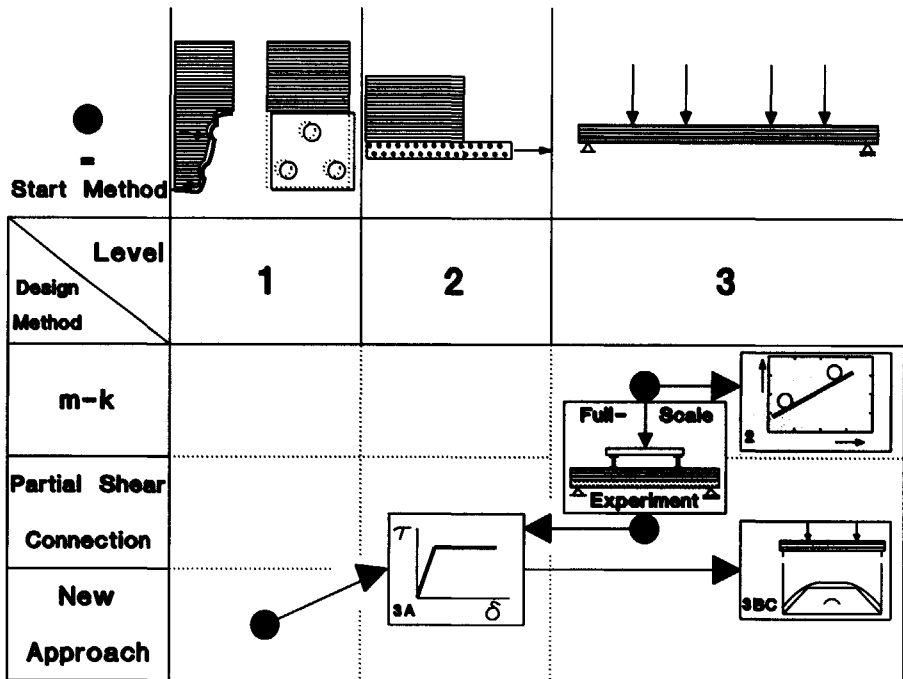


Figure 2.30: Three levels of research for analyzing composite slabs

2.7 Conclusions for Chapter 2

- # For a better understanding of the physical behaviour of shear connections it is important to distinguish the independent characteristics: strength, stiffness and deformation capacity. (§ 2.2)

- # The advantages of the 'm-k' method is the simplicity of the full-scale experiments, the fact that these experiments represent the actual behaviour of slabs and the fact that the method may be used for both brittle and 'ductile' profiles. The disadvantage is the limited applicability of test results. (§ 2.5.1)
- # The advantage of the PSC method is the applicability of test results over a wider range of parameters and the fact that the method is based on a physical model. The disadvantages are that the method may only be used for 'ductile' profiles and the fact that the physical model is not correct for profiles which do not exhibit a constant shear stress over the shear span at failure. (§ 2.5.2)
- # The term *Friction Tests* for small-scale tests which are subject to lateral forces is misleading. Applying the principles of dry friction to profiled sheeting with indentations might lead to 'coefficients of friction' which are considerably higher than coefficients found for a flat surface. (§ 2.5.3)
- # Performing small-scale instead of full-scale experiments for the derivation of characteristics of a shear connection supplies more information about the connection, which is favourable for analytical and numerical analysis of composite slabs. However, performing small-scale experiments is more complicated, which has lead to complex test arrangements. (§ 2.5.3)
- # Further improvement of test arrangements and design methods requires understanding of the physical behaviour of the shear connection. (§ 2.5)
- # Analysing the cross-sectional behaviour and the description of mechanisms is a fundamental and innovative approach for obtaining understanding of the physical behaviour of a shear connection in composite slab. (§ 2.6)

3. PHYSICAL BEHAVIOUR SHEAR CONNECTION

3.0 Introduction

In this chapter, a hypothesis is presented, which forms the basis for a method for analysing mechanisms, which determine the behaviour of shear connections in composite slabs. Prior to the hypothesis (§ 3.2), the forms of shear connection in composite slabs are discussed (§ 3.1). Prior to the discussion of the method for analysing shear connections (§ 3.4), a qualitative description of the behaviour is given (§ 3.3). Finally, the method is illustrated by an example and a parametric study (§ 3.5).

3.1 Shear Connection in Composite Slabs

Analogy exists between the behaviour of composite and reinforced concrete slabs. Loaded in positive bending, steel is subjected to tension and concrete to compression, due to the presence of a shear connection. Figure 3.1 illustrates the connection between steel and concrete for both reinforced concrete and composite slabs. Reinforcement in concrete slabs is embedded in concrete, and therefore the connection acts very stiff and strong. In composite slabs the sheeting is not embedded in concrete. Due to the limited thickness of profiled sheeting, the capacity of sheeting to resist forces acting perpendicular to the indentations is limited. The sheeting can be separated from the concrete.

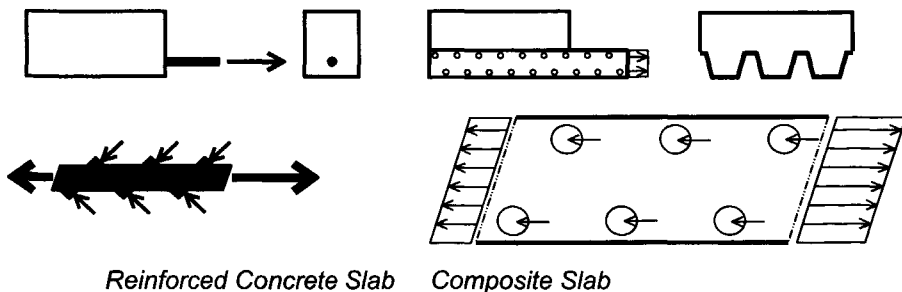


Figure 3.1: Comparison of shear connections in reinforced concrete and composite slabs

Due to the strength and stiffness of shear connections in concrete slabs, longitudinal slip between reinforcement bars and concrete only occurs if cracks arise in the concrete. Shear stresses in connections between profiled sheeting and the concrete are smaller. Due to its flexibility, the sheeting tends to separate from the concrete. If separation is prevented, the sheeting deforms. The occurrence of slip in composite slabs is caused by deformation and displacement of the sheeting. The fact that the sheeting deforms and separates from the concrete causes mechanisms, determining the behaviour of the connection, to be different than found for reinforced concrete slabs.

Eurocode 4 [1] distinguishes 5 different mechanisms for the development of shear resistance between profiled sheeting and concrete, of which 4 are illustrated in Fig. 3.2.

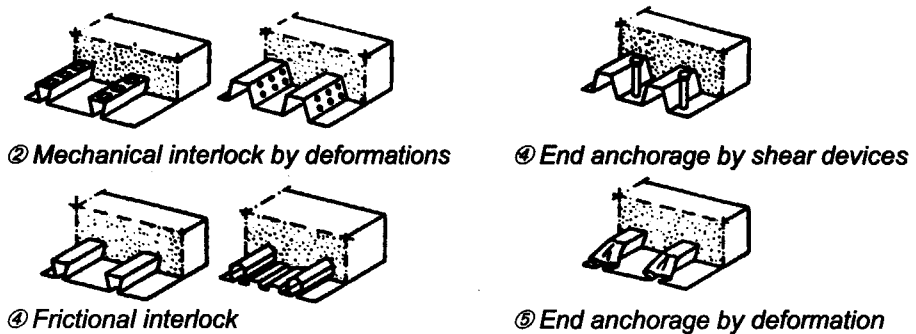


Figure 3.2: Different means for development of shear resistance in composite slabs

- ① *Pure or chemical bond*
Chemical bond arises during hardening of concrete. Although shear stresses due to chemical bond can be significant, EC4 does not allow addition of this contribution to the shear resistance, due to its brittle failure mechanism.
- ② *Mechanical interlock provided by deformations in the profile*
Almost all existing types of sheeting have indentations or deliberately applied deformations in the sheeting in order to develop shear resistance.
- ③ *Frictional interlock*
Profiles might contribute to the shear resistance by friction. Even without the presence of indentations, contact forces arise if a slab deforms. Contact forces give rise to frictional forces, which contribute to the shear resistance.

④ *End anchorage provided by external shear devices*

End anchorage improves the shear resistance at the supports. End anchorage can be obtained by welded studs or other types of shear devices, which are connected to the supporting beam through the profiled sheeting.

⑤ *End anchorage by deformation of the ribs at the supports*

End anchorage can be obtained by deliberately deforming the ribs at the supports (Hammer-dübel).

This thesis focuses on mechanical interlock, since it is characteristic for composite slabs. Different mechanisms are required for the description of the behaviour of shear connections, as currently available for other types of connections or shear devices. For different reasons the other contributions to the shear resistance are not considered in this thesis.

① Due to the high stiffness of chemical bond, a slab shows full interaction as long as bond is intact. Since in design reliance on chemical bond is not permitted, it is important that other means of shear resistance are able to prevent brittle failure of the slab after the breakdown of bond.

③ Limited application is found for re-entrant profiles without indentations, relying only on frictional interlock. Although these profiles, due to the absence of indentations, lie outside the scope of the thesis, the behaviour can be analysed with the developed method. If the mechanisms which provide shear resistance can be described, the behaviour of any shear connection can be analysed.

④/⑤ Mechanisms describing the behaviour of end anchorage are essentially different from mechanisms describing mechanical interlock. Since end anchorage devices are embedded in concrete the behaviour lies closer to the behaviour of reinforced concrete, with corresponding concrete-related failure mechanisms. The contribution of end anchorage can be determined separately and added to other forms of interlock.

Although the following hypothesis deals with mechanical interlock by indentations, all existing profiles can be analysed, using the method based on the hypothesis.

3.2 Hypothesis

The hypothesis concerning the behaviour of shear connections in composite slabs focuses on indentations, which provide shear resistance via mechanical interlock. Due to the limited thickness of sheeting (0.7 to 1.25 mm) the bending stiffness of the webs and flanges is limited. This allows for deformation of the cross-section of the sheeting, if contact forces are present between indentations and concrete. Figure 3.3 shows two circular indentations. If longitudinal slip occurs, indentations will be separated from the concrete. Between the indentations and concrete interaction forces occur (F_i), which can be separated in longitudinal shear forces (F_{\parallel}), which contribute to the shear resistance, and forces perpendicular to the sheeting (F_{\perp}), which deform the cross-section of the sheeting.

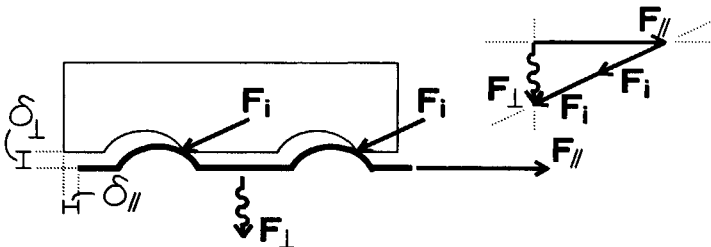


Figure 3.3: Indentations over-riding the concrete

In order to develop shear resistance, the sheeting should be able to resist the forces acting perpendicular to the surface of the sheeting (F_{\perp}). If these forces cannot be resisted, no equilibrium of forces is possible, hence no shear resistance is developed. This implies that a suitable form of shear connection should be able to resist forces which tend to separate indentations from the concrete.

The hypothesis concerning the behaviour of the shear connection in composite slabs is based on Fig. 3.3 and its implications. The hypothesis consists of two parts. Figure 3.3 shows the ACTION part. The required response of the sheeting to the forces tending to separate the indentations from the concrete is the REACTION part:

ACTION: *Over-riding of indentations by the concrete after longitudinal slip has occurred*

REACTION: *Response of the sheeting to the over-riding of indentations*

The response of the sheeting is a combination of deformation and displacement. The behaviour of shear connections in composite slabs depends on the ratio between the deformation and displacement. Figure 3.4 shows three identical top flanges of a re-entrant profile. The ACTION part is the same for all profiles, since the displacement of the indentation with respect to the concrete is the same. The response of the flanges shows different levels of vertical displacement. It shows that the deformation decreases if vertical separation increases. The deformation is a measure for the resistance of the sheeting to the over-riding of the concrete by the indentations. Therefore the shear resistance of the connections decreases from A to C.

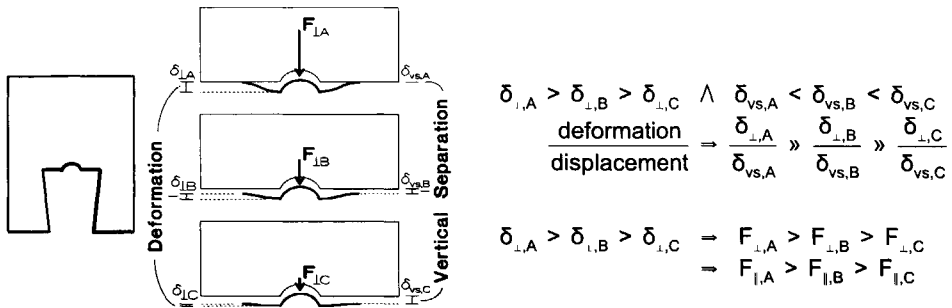


Figure 3.4: Ratio of deformation and displacement in response sheeting

Hypothesis:

The longitudinal shear resistance of a connection between concrete and sheeting in composite slabs depends on the response of sheeting to forces tending to separate the indentations from the concrete, after longitudinal slip has occurred. The response is a combination of deformation and displacement. The ratio between deformation and displacement determines the characteristics of the shear connection.

The two parts of the hypothesis, referred to as ACTION and REACTION part, can be considered separately. In order to clarify the implications of the hypothesis a qualitative description of the two basic shapes of profiled sheeting used for composite slabs is given (§ 3.3). A method for analysing shear connections, based on the hypothesis, is presented and illustrated by two examples and a parametric study (§ 3.4 & 3.5).

3.3 Qualitative Description Shear Connection

With regard to the geometry of profiled sheeting used in composite slabs, two basic shapes can be distinguished: re-entrant and trapezoidal. All existing profiles are derived from these basic shapes, or a combination of both, as shown in Fig. 1.3. The response of the basic shapes to over-riding of indentations is essentially different.

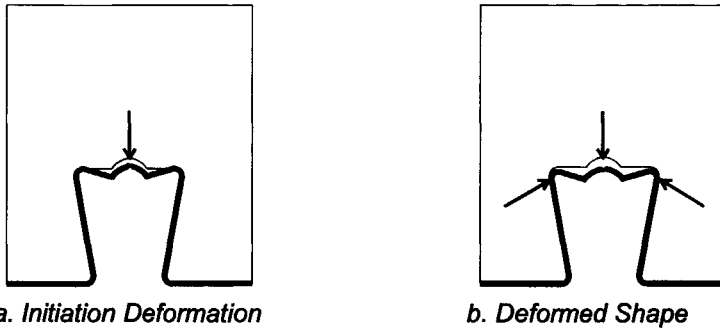


Figure 3.5: Response of re-entrant profiles

Re-entrant profiles usually have indentations in the top flange. Once slip has occurred, the indentations are separated from the concrete and the top flange is pushed down. The rib is pushed into the wedge of concrete, as shown in Fig. 3.5a. Due to the wedge of concrete re-entrant profiles are able to resist vertical separation. Large contact stresses between the sheeting and concrete occur, as shown in Fig. 3.5b. Via friction these contact stresses contribute to the shear resistance.

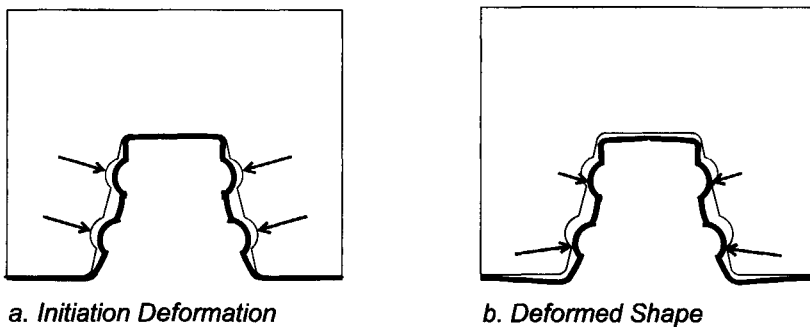


Figure 3.6: Response of trapezoidal profiles

Trapezoidal profiles usually have indentations in the web. After slip has occurred

the vertical component of the interaction forces tends to separate the sheeting from the concrete vertically, as shown in Fig 3.6a. If the sheeting is not able to resist vertical separation, the indentations are separated from the concrete without developing shear resistance. For trapezoidal profiles, the geometry of the rib itself does not provide resistance to the vertical separation. Depending on the slope of the web and the geometry and location of the indentations, the indentations resist both to longitudinal slip and vertical separation. Vertical separation occurs, as shown in Fig. 3.6b, changing the direction of the forces acting on the indentations until equilibrium of vertical forces is obtained. For trapezoidal profiles, the presence of longitudinal slip implies the presence of vertical separation. As illustrated in Fig. 3.4, the appearance of separation reduces the level of deformation and therefore reduces the shear resistance. The geometry of the sheeting and the geometry and location of the indentations, is more important for trapezoidal profiles than for re-entrant profiles.

The qualitative analysis shows, that for trapezoidal profiles indentations should be located in the web. If indentations are located in the flanges, the tendency of separation is larger, while no resistance to vertical separation is present. For re-entrant profiles, indentations can be located in both flanges and webs. If indentations are located in the web, the vertical component of the interaction forces acts upwards, so no tendency of vertical separation is present.

The analysis of the cross sectional behaviour shows that distinction can be made between ACTION, over-riding of the concrete by the indentations (Fig. 3.3), and REACTION, deformation and displacement of the sheeting (Figs. 3.5 and 3.6).

3.4 Method for analysing Shear Connections in Composite Slabs

Based on the hypothesis (§ 3.2), a method for analysing shear connections in composite slabs is developed. In order to focus on the method itself, the connection used to clarify the method is simplified, as shown in Fig. 3.7. Although simplified, it contains all aspects of a realistic connection. The indentation is pyramid shaped. The sheeting is flat, supported vertically and horizontally along the sides. A shear force is applied to the sheeting. A similar configuration is used in a series of experiments (§ 5.1).

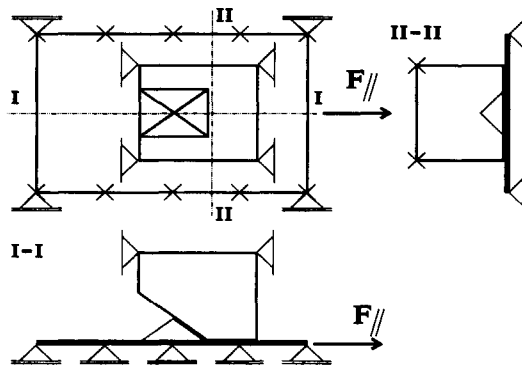


Figure 3.7: Simplified shear connection

The rotation of the indentation, causing different vertical displacements of the front and back toe of the indentation, is neglected. Therefore the displacement of the indentation with respect to the concrete has only two degrees of freedom: longitudinal slip (δ_1) and vertical displacement (δ_\perp). If the concrete and the indentation do not deform, the relation between δ_1 and δ_\perp depends on the geometry of the indentation, as shown in Fig. 3.8. Equation (3.1) describes the ACTION-part of the analysis.

$$\delta_\perp = \frac{H}{D/2} \cdot \delta_1 \tag{3.1}$$

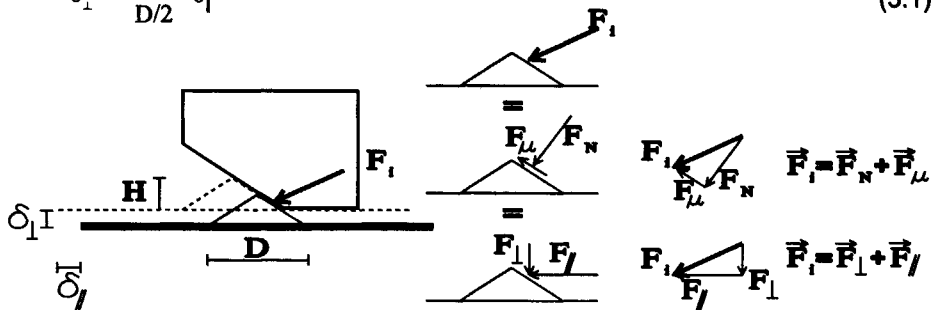


Figure 3.8: Displacement indentation and interaction force between concrete and indentation

If the indentation is separated from the concrete, interaction forces occur between the indentation and the concrete. An assumption has been made concerning the direction of interaction forces. The assumption is validated by experiments (§ 5.1 & 6.1). It is assumed that the interaction force is a summation of a normal (F_N) and a frictional force (F_μ). The normal force acts perpendicular to the area of contact on the indentation. The frictional force acts perpendicular

to the normal force, and its direction depends on the incremental displacement between the indentation and concrete. The interaction force can be decomposed into a shear force (F_{\parallel}), and a force which tends to separate the indentation from the concrete (F_{\perp}), as illustrated in Figs. 3.3 and 3.8.

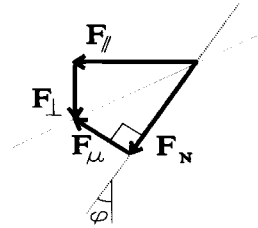
$$F_{\parallel} = F_N \sin\varphi + F_{\mu} \cos\varphi \quad (3.2)$$

$$F_{\perp} = F_N \cos\varphi - F_{\mu} \sin\varphi \quad (3.3)$$

$$\text{with: } \tan\varphi = \frac{H}{D/2} \quad (3.4)$$

$$F_{\mu} = \mu \cdot F_N \quad (3.5)$$

$$\mu = f(F_N) \quad (3.6)$$



The ratio between F_{\parallel} and F_{\perp} can be derived from eqs. (3.2) to (3.6). Equation (3.7) also deals with the ACTION part of the analysis.

$$\frac{F_{\parallel}}{F_{\perp}} = \frac{\sin\varphi + \mu \cdot \cos\varphi}{\cos\varphi - \mu \cdot \sin\varphi} = \frac{\tan\varphi + \mu}{1 - \mu \cdot \tan\varphi} = \frac{2 \cdot H + \mu \cdot D}{D - 2 \cdot \mu \cdot H} \quad (3.7)$$

The REACTION part determines the response of the sheeting to the force tending to separate the indentation from the concrete (F_{\perp}). The response can be given as a stiffness (k_{\perp}). Depending on the simplicity of the response, the stiffness can be determined analytically, experimentally or numerically.

$$k_{\perp} = \frac{F_{\perp}}{\delta_{\perp}} \quad (3.8)$$

For the simplified shear connection, the ACTION and REACTION parts of the analysis are now completed. Results can be combined to relate the shear force (F_{\parallel}) to the longitudinal slip (δ_{\parallel}). Equations derived for the separate parts of the analysis are linked in eq. (3.9):

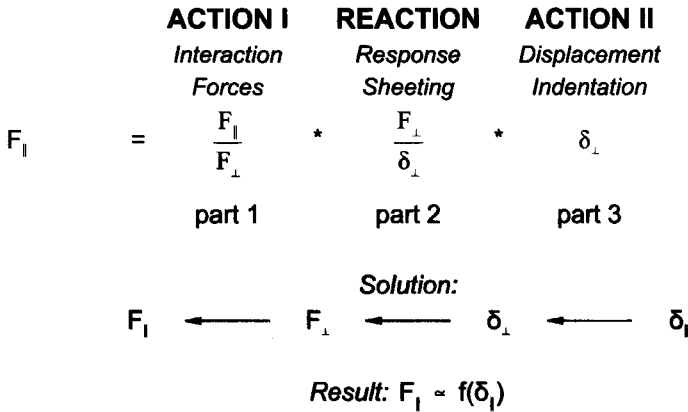
$$F_{\parallel} = \frac{F_{\parallel}}{F_{\perp}} \cdot \frac{F_{\perp}}{\delta_{\perp}} \cdot \delta_{\perp} \quad (3.9)$$

$$\begin{aligned}
 F_I &= \frac{F_I}{F_{\perp}} * \frac{F_{\perp}}{\delta_{\perp}} * \delta_{\perp} \\
 &= \frac{2 \cdot H + \mu \cdot D}{D - 2 \cdot \mu \cdot H} * k_{\perp} * \frac{H}{D/2} \cdot \delta_I = k_I \cdot \delta_I
 \end{aligned}
 \tag{3.10}$$

eq. (3.7) eq. (3.8) eq. (3.1)

The solution technique consists of back substitution of δ_I into the described relations for the ACTION and REACTION parts:

Solution Technique Simple Shear Connections



Equation (3.10) is visualized by a set of diagrams in Fig. 3.9. Results from the separate parts (eqs. (3.7), (3.8) and (3.1)) are presented in separate diagrams. The resistance of the connection for a certain level of slip can be found by following the line marked by the numbers ① to ⑤:

- ① Considered level of longitudinal slip δ_I .
- ② The vertical displacement δ_{\perp} is related to δ_I by eq. (3.1).
- ③ The force perpendicular to the indentation F_{\perp} is related to δ_{\perp} by eq. (3.8).
- ④ The shear force F_I is related to F_{\perp} by eq. (3.7).
- ⑤ The shear force corresponding to the considered level of slip is plotted in a diagram, which relates F_I to δ_I .

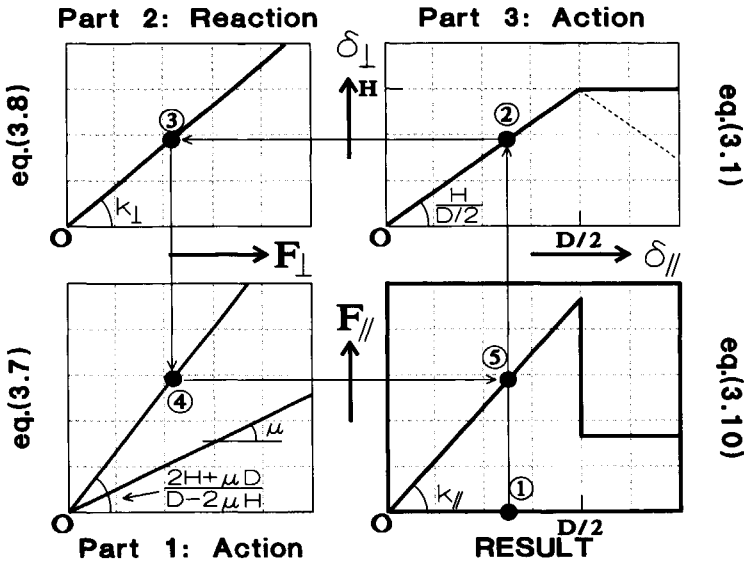


Figure 3.9: Visualization Method based on hypothesis

In this case, all relations are linear, so the final result is linear. If slip reaches $D/2$, the indentation is pushed completely out of the concrete. The displacement (Part 3) and the lateral force (Part 2) remain constant. The normal direction of the interaction force changes (Part 1), which reduces the shear resistance to a level corresponding to friction.

Equation (3.10) and Fig. 3.9 show that the analysis of the behaviour of a shear connection can be divided into an ACTION and a REACTION part. Combination of separate parts leads to the behaviour of the shear connection.

3.5 Example

In order to illustrate the possibilities of the method for analysing more realistic shear connections, an example is evaluated. The characteristics of the connection are determined and a parametric study is performed.

3.5.1 Determination Characteristics Basic Configuration

The configuration of the example is shown in Fig. 3.10. The webs of the sheeting are vertical. A circular indentation is located in the centre of the webs. The widths of the top and bottom flanges are equal. The concrete on top of both flanges is removed, which means that the flanges can deform freely, without touching the concrete. Due to symmetry, no vertical separation occurs since no vertical forces arise if the indentation is separated from the concrete. In § 4.5 the example is evaluated again, taking contact between flanges and concrete into account.

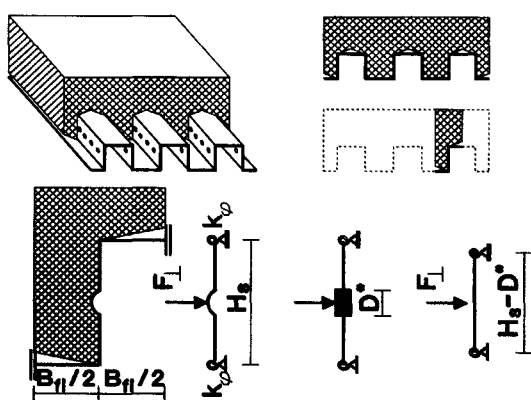


Table 3.1: Dimensions Example

Height sheeting	H_s	60 mm
Thickness sheeting	t	0.70 mm
Width flanges	B_n	60 mm
Considered length	L	40 mm
Diameter indentation	D	12 mm
Height indentation	H	3.0 mm
Radius indentation	R	7.5 mm

Figure 3.10: Configuration Example § 3.5

Within the mechanical model of the sheeting, the flanges are replaced by rotational springs. The presence of the indentation increases the bending stiffness of the web. The improvement of the bending resistance can be taken into account by assuming the bending stiffness to be infinite over a certain distance D^* . The fictitious value for D^* , should be based on the geometry of the indentation and the distance between the indentations. Upper and lower boundary values for D^* are 0 and D .

The three separate parts of eq. (3.9) are evaluated in reverse order for the configuration of Fig. 3.10, similar to the back substitution in the solution technique.

Part 3: *Relation between the longitudinal slip and the displacement of the indentation perpendicular to the web: $\delta_{\parallel} \sim \delta_{\perp}$*

In this case, due to symmetry, the indentation does not rotate around the longitudinal axes. Since the distance between indentations in the longitudinal direction is small, the deformation of the web is assumed to be cylindrical. Rotation around the vertical axes is neglected. Figure 3.11 shows the displacement of the indentation and the interaction force between the indentation and concrete. The relation between the longitudinal slip δ_{\parallel} and the displacement of the indentation perpendicular to the web δ_{\perp} can be derived from Fig. 3.11. Equation (3.11) represents the third part of eq. (3.9).

$$\left[\frac{D}{2} - \delta_{\parallel}\right]^2 + [R - h + \delta_{\perp}]^2 = R^2 \tag{3.11}$$

$$\delta_{\perp} = -(R-h) + \sqrt{(R-h)^2 - \delta_{\parallel}(\delta_{\parallel} - D)}$$

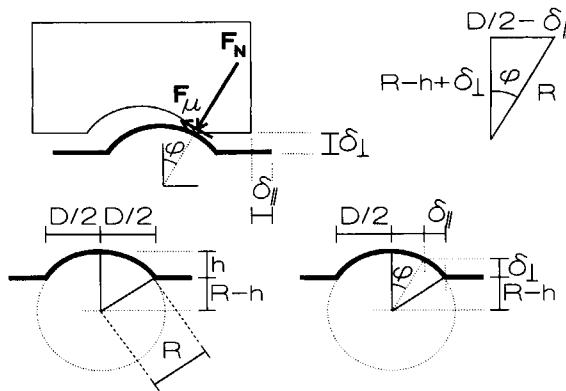


Figure 3.11. Assumption interaction forces

Part 2: *Relation between the displacement of the indentation perpendicular to the web and the force perpendicular to the web: $\delta_{\perp} \sim F_{\perp}$*

To relate the component of the interaction force acting perpendicular to the web F_{\perp} to the displacement δ_{\perp} , the mechanical model of the sheeting shown in Fig. 3.10 can be established. The stiffness of the rotational springs is k_{ϕ} .

$$k_{\phi} = \frac{2EI}{B_{fl}} \quad (3.12)$$

Without giving the full derivation, the results of the mechanical model are given below. The bending moments in the edges $M_{flange-web}$ and the displacement of the indentation (δ_{\perp}) can be calculated as a function of F_{\perp} .

$$M_{flange-web} = \frac{F_{\perp} \cdot (H_s - D^*)}{4} \cdot \left[\frac{1}{4EI / (k_{\phi} \cdot (H_s - D^*)) + 2} \right] \quad (3.13)$$

$$\delta_{\perp} = \frac{F_{\perp} \cdot (H_s - D^*)^3}{48EI} \cdot \left[\frac{\frac{4EI}{k_{\phi} \cdot (H_s - D^*)} + \frac{1}{2}}{\frac{4EI}{k_{\phi} \cdot (H_s - D^*)} + 2} \right] \quad (3.14)$$

Similar to eq. (3.8), the response of the sheeting can be given as a stiffness k_{\perp} :

$$k_{\perp} = \frac{F_{\perp}}{\delta_{\perp}} = \frac{48EI}{(H_s - D^*)^3} \cdot \left[\frac{\frac{4EI}{k_{\phi} \cdot (H_s - D^*)} + 2}{\frac{4EI}{k_{\phi} \cdot (H_s - D^*)} + \frac{1}{2}} \right] \quad (3.15)$$

Substitution of eq. (3.12) leads to the second part of eq. (3.9):

$$k_{\perp} = \frac{48EI}{(H_s - D^*)^3} \cdot \left[\frac{4 \cdot B_{fl} + 4 \cdot (H_s - D^*)}{4 \cdot B_{fl} + (H_s - D^*)} \right] \quad (3.16)$$

Part 1: Relation between the shear force and the force perpendicular to the web: $F_{\perp} \sim F_l$

Figure 3.11 shows the interaction forces between the indentation and the concrete. The shear force (F_l) and the force perpendicular to the web, separating the indentation from the concrete (F_{\perp}), are derived similar to the derivation given in eq. (3.7). For the circular indentation $\tan\phi$ is no longer constant, but a function of the longitudinal slip. The coefficient of friction μ is assumed to be constant. The ratio between F_l and F_{\perp} is the first part of eq. (3.9):

$$\frac{F_{\parallel}}{F_{\perp}} = \frac{\sin\varphi + \mu \cdot \cos\varphi}{\cos\varphi - \mu \cdot \sin\varphi} = \frac{\tan\varphi + \mu}{1 - \mu \cdot \tan\varphi} \quad (3.17)$$

with: $\tan\varphi = \frac{D/2 - \delta_{\perp}}{R - h + \delta_{\perp}}$ (3.18)

Similar to the diagrams of Fig. 3.9 the results of the three separate parts are plotted in Fig. 3.12. Since eq. (3.17) is a function of δ_{\perp} , the diagram presenting Part 1 consists of several lines representing different levels of slip. Similar to eq. (3.7) the ratio between F_{\parallel} and F_{\perp} can be derived. For the circular indentation $\tan\varphi$ is no longer constant. Therefore the ratio between F_{\parallel} and F_{\perp} is a function of the considered level of slip. The ratio between F_{\parallel} and F_{\perp} can be taken at point ④, since the level of slip is known.

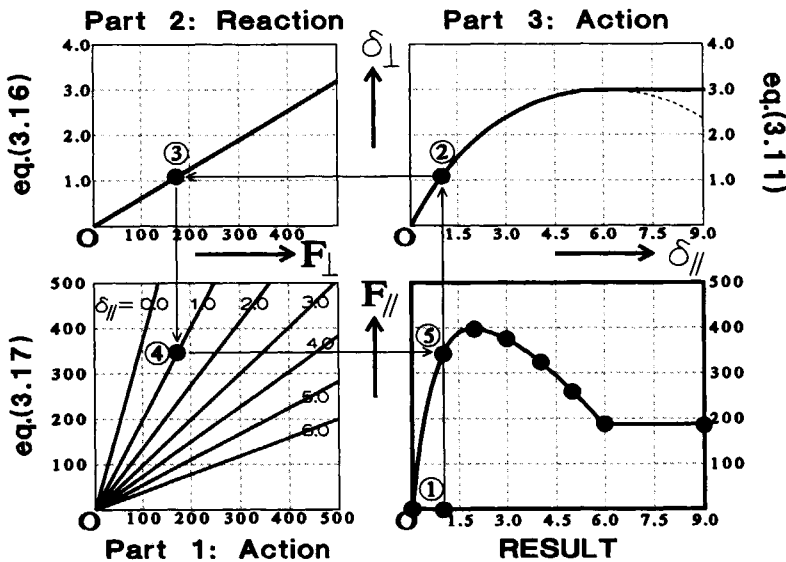


Figure 3.12: Derivation shear resistance example 3.5

Compared to commonly available profiles, the number of ribs in this configuration is higher, since the width of the bottom flange is reduced in order to create a symmetrical profile. More ribs imply more indentations, which improves the shear characteristic. The location of the indentation, in the centre of the web, minimizes the stiffness k_{\perp} . The calculated ultimate shear stress τ_u for the simplified connection leads to a reasonable value.

$$\tau_u = \frac{F_{I\text{MAX}}}{A} = \frac{F_{I\text{MAX}}}{L \cdot B_{fl}} \approx \frac{400}{40 \cdot 60} \approx 0.17 \text{ N/mm}^2 \quad (3.19)$$

3.5.2 Parametric Study Example

To illustrate the use of the method, 4 variations to the basic configuration are considered. The effect of the variations to the shear resistance is shown in a set of diagrams similar to Fig. 3.12.

Plasticity

Plasticity of the sheeting influences the response of the sheeting (Part 2). Figure 3.13 shows the adjusted response of the sheeting. For the mechanical model of Fig. 3.10, first yielding occurs at the indentation, which reduces the stiffness k_{\perp} . A plastic mechanism occurs if the plastic bending moments appear in the rotational springs. Part 2 is no longer linear, but tri-linear. In this case, the plastic mechanism is not developed within the considered range of parameters. Due to the adjustment of Part 2, the strength of the connection decreases and the connection behaves more brittle.

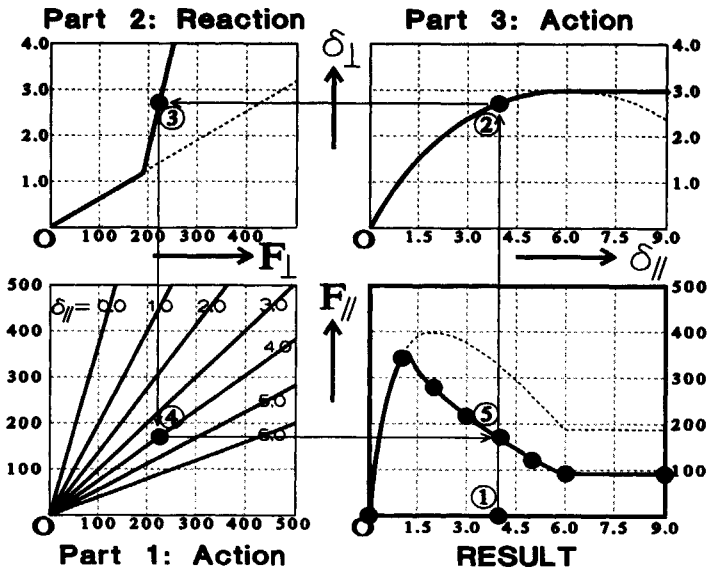


Figure 3.13: Parametric Study: Plasticity sheeting

Geometry indentation

The height of the indentation is reduced, which changes both Part 1 and 3. Figure 3.14 shows the adjusted diagrams. Part 3 shows the adjusted geometry. In Part 1, the ratio between F_{\perp} and F_{\parallel} for different levels of slip reduces, due to the reduced inclination of the indentation. The adjustments to Part 1 and 3 both have a negative effect on the strength and stiffness of the shear connection.

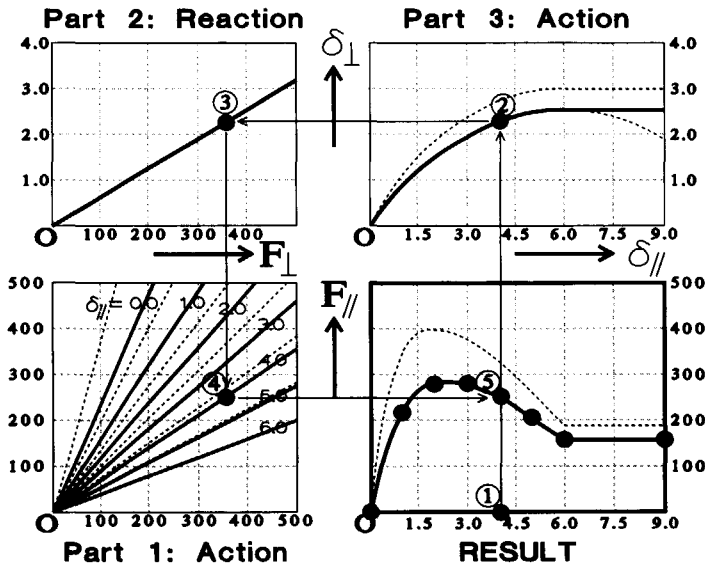


Figure 3.14: Parametric Study: Geometry indentation

Thickness of sheeting and width of flanges

Variation of the thickness of the sheeting (t) and the width of the flanges (B_f) influence the response of the sheeting (Part 2). If the thickness increases, the bending stiffness also increases. If the width of the flanges increases, the stiffness of the rotational springs (k_{ϕ}) decreases, and therefore k_{\perp} decreases. Due to the adjustment of k_{\perp} , the stiffness of the connection respectively increase and decrease for the variations of t and B_f . Figure 3.15 shows the effect of both variations. The line ①-⑤ is drawn for the variation of B_f .

The diagrams for the basic and adjusted configurations, shown in Figs. 3.12 to 3.15, illustrate that the distinction of the separate parts of the analysis increases the understanding of the behaviour of the shear connection. Although the strict distinction is no longer possible for complex shear connections, the numerical

tools, as discussed in chapter 4, are also based on this distinction.

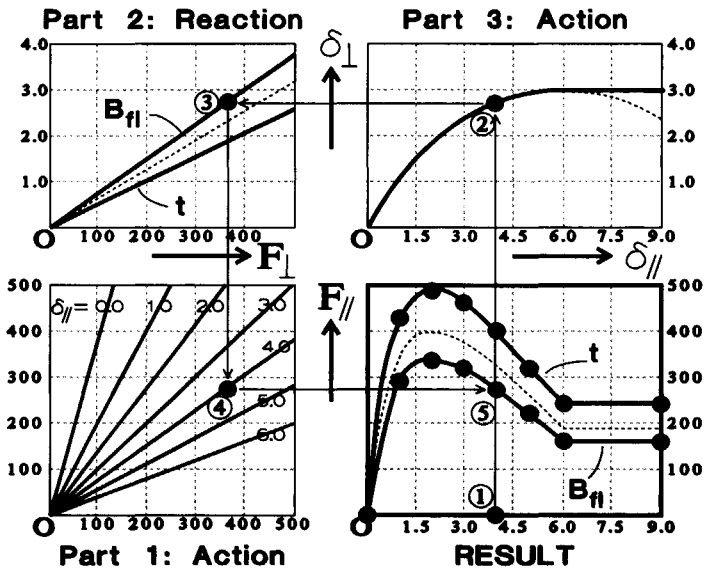


Figure 3.15: Parametric Study: thickness sheeting & width flanges

3.6 Conclusions for Chapter 3

Although analogy exists between shear connections in reinforced concrete and composite slabs, the mechanisms determining the behaviour of the connections are essentially different. Since in composite slabs the sheeting is not embedded in concrete and behaves flexible, due to its limited thickness, mechanisms consist of deformation and displacement of sheeting rather than cracking or crushing of concrete. (§ 3.1)

Hypothesis concerning the behaviour of shear connections in composite slabs:

The longitudinal shear resistance of a connection between concrete and sheeting in composite slabs depends on the response of sheeting to forces tending to separate the indentations from the concrete, after longitudinal slip has occurred. The response is a combination of

deformation and displacement. The ratio between deformation and displacement determines the characteristics of the shear connection.

The hypothesis consists of two parts. The ACTION part describes the behaviour of the indentations, which are separated from the concrete after longitudinal slip has occurred. The REACTION part describes the response of the sheeting to forces tending to separate the indentations from the concrete. (§ 3.2)

- # Both basic shapes of sheeting, re-entrant and trapezoidal, tend to separate from the concrete after slip has occurred. The response of the basic shapes to the over-riding is essentially different. Re-entrant profiles are able to develop high resistance to vertical separation. For trapezoidal profiles, indentations resist both longitudinal slip and vertical separation. In that case, the presence of slip implies the presence of vertical separation. The presence of separation reduces the level of deformation and therefore reduces the shear resistance. (§ 3.3)
- # The geometry of the sheeting and the geometry and location of the indentations is more important for trapezoidal profiles than for re-entrant profiles. (§ 3.3)
- # The method for analysing shear connections in composite slabs shows that the ACTION and the REACTION part of the analysis can be considered separately. Combining of the results of the separate parts leads to the behaviour of the shear connection. (§ 3.4)
- # The visual solution method leads to an ultimate level of transparency by showing different parts of the connection, the relations between them and the influence of each part on the overall behaviour of the connection. The various examples show that the method is effective. (§ 3.4 & 3.5)



4. NUMERICAL MODELS

4.0 Introduction

The hypothesis concerning the behaviour of shear connections in composite slabs is implemented in two types of numerical models. Prior to the discussion of the numerical models (§ 4.3 and 4.4), the development of numerical models is justified (§ 4.1). Similar to the hypothesis, both models perform a cross-sectional analysis (§ 4.2). Possibilities and limitations of both models are illustrated by an example (§ 4.5).

4.1 Justification of Numerical Models

Within shear connections in composite slabs several nonlinear phenomena occur:

- # Plasticity of the steel sheeting
- # Cracking or deformation of concrete
- # Contact between steel and concrete, including friction
- # Geometrical nonlinear behaviour

The nonlinear phenomena justify the usage of sophisticated Finite Element models, referred to as FE-models. Modelling the smallest possible repeating section of a shear connection leads to relatively large FE-models. With the size of FE-models, computing time increases, transparency reduces, and interpretation of results and recognition of mechanisms becomes more difficult.

Alternative for sophisticated FE-models are models, based on the hypothesis as discussed in chapter 3. The solution technique, which implements the hypothesis, is extended in order to deal with realistic shear connections. The models are referred to as Simplified Frame Models, which refers to the simple frame analysis used to describe the response of the sheeting.

SF-models do not include non-linear phenomena. Therefore SF-models alone, are not suitable for determination of the behaviour of shear connections.

However, the approach is based upon the belief that simple models may not be very accurate, but allow for obtaining understanding of the physical behaviour. Based upon obtained understanding more sophisticated analyses can be performed. The other way around, sophisticated FE-analyses can be used to investigate mechanisms, which can be implemented in SF-models. Due to their transparency and the limited computing time, SF-models are very suitable for performing parametric studies.

Considering advantages and disadvantages of both simple SF- and sophisticated FE-models shows that a combination of both types of models produces a powerful tool for obtaining understanding and performing parametric studies. FE-models are suitable for the determination of the behaviour of a basic configuration and for investigation of mechanisms, while SF-models are suitable for performing parametric studies.

4.2 Cross-sectional Analysis

For both SF- and FE models the number of indentations, and therefore the length of the considered shear connections is limited to the smallest repeating section, as illustrated in Fig. 4.1.

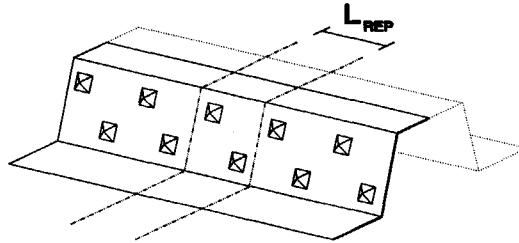


Figure 4.1: *Smallest repeating section shear connection*

SF-models are restricted by the solution technique, which is not suitable for large numbers of degrees of freedom. FE-models are restricted by the size of the model which mainly depends on the considered number of indentations. For common profiles the smallest repeating section is usually smaller than 50 mm. Therefore, both models concern analysis of a cross-section, since only a slice of the composite element is considered. The analysis is either 2-D or semi 3-D.

The behaviour of both full- and small-scale experiments differs from cross-sectional analysis, since within the specimen different slices show different behaviour. With regard to the full-scale specimen, two areas and a transition area can be recognized, as illustrated in Fig. 4.2. The support reaction improves the characteristics of the shear connection over the supports by pushing the sheeting towards the concrete and therefore reducing vertical separation (Area I). Between the supports, no lateral force is present (Area II). Both areas can be analysed using cross-sectional analysis. The length of the transition area between Area I and II depends on the geometry of the sheeting. The behaviour of full-scale specimen cannot be determined directly using cross-sectional analysis. The areas I and II can be analysed separately and results can be combined to derive the behaviour of the shear connection.

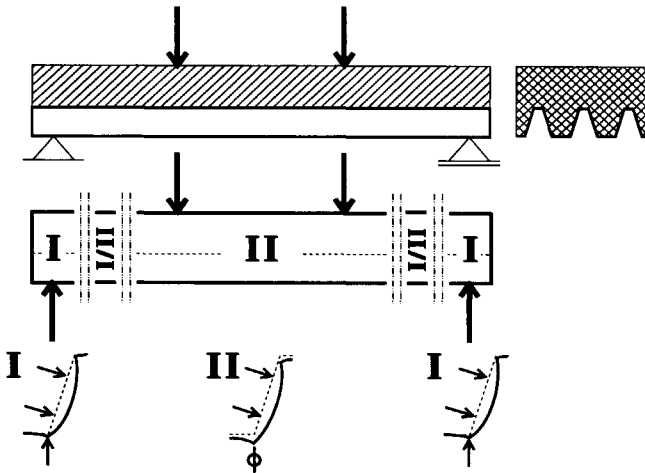


Figure 4.2: Limited applicability cross-sectional approach for full- and small-scale specimen

In order to control the behaviour of the small-scale specimen in a test arrangement, boundary conditions are applied to the specimen, which also affect the behaviour of the connection, and often cause the separation between concrete and sheeting to be restricted or variable over the specimen. This implies that different slices may exhibit different behaviour, and therefore direct determination of the behaviour is not possible using cross-sectional analysis.

Although direct determination of the behaviour of shear connections is not

possible using cross-sectional analyses, the considered models are valuable. Firstly, by using different analyses for different areas of the shear connection the behaviour of the connection can be determined by combining the results of the different areas. Secondly, the approach is useful for increasing understanding and performing parametric studies. If variations to a basic configuration are considered, determination of the behaviour of the basic configuration itself is not necessary to investigate the effect of variations.

4.3 Simplified Frame Models

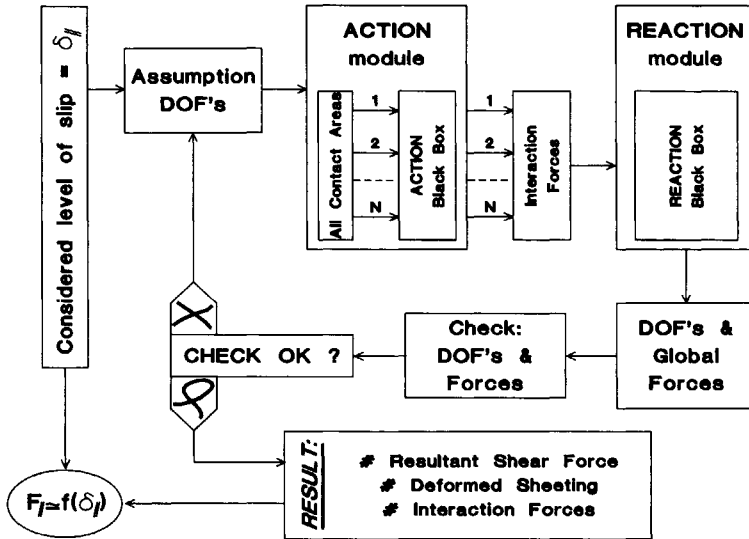
Similar to the hypothesis, SF-models are based on distinction between the ACTION and the REACTION parts of the analysis. In this paragraph a general solution technique, possible degrees of freedom and the ACTION and REACTION parts are discussed.

4.3.1 Solution Technique

For the simple shear connections, illustrated in § 3.4 and 3.5, description of the ACTION and REACTION parts was possible. Due to the limited number of degrees of freedom and the simple geometry, it was possible to combine both parts in order to relate the shear force in the connection F_1 to the longitudinal slip δ_1 . For common shear connections in composite slabs, more degrees of freedom are active and the geometry of the sheeting is more complex. In this case, description of the ACTION and REACTION parts is still possible, but combining both parts in order to derive a formula for the shear resistance is no longer possible.

For the shear connections considered in chapter 3, apart from the applied slip δ_1 , only one degree of freedom was present: δ_2 . The solution technique consists of back substitution of δ_1 into the described relations for the ACTION and REACTION parts. If more degrees of freedom are considered, relating the ACTION and REACTION part becomes more difficult, and the simple solution technique is no longer applicable. A general solution technique for shear connections is developed, which uses an iterative procedure to relate the ACTION and REACTION parts.

General Solution Technique Shear Connections in Simplified Frame Models:



Within the ACTION part, interaction forces at and displacements of the indentations are described for each contact area. The direction of interaction forces is determined, similar to the ACTION I module in the solution technique for simple shear connections (§ 3.4). Description of the displacements relates all considered degrees of freedom at the indentation to the applied slip δ_1 , similar to the ACTION II module. Both modules are implemented in the ACTION-Black Box. The REACTION module contains a REACTION-Black Box, describing the response of the sheeting, which relates the interaction forces from the ACTION module to values for all considered degrees of freedom. As long as the derived values do not match the assumed values, the iterative procedure continues. The iterative procedure of the general solution technique is suitable for implementation in computer programs.

4.3.2 Possible Degrees of Freedom

Contact areas are defined as areas at which contact might occur between concrete and sheeting, once longitudinal slip occurs. Apart from indentations,

contact areas occur at locations where sheeting is pushed towards the concrete once the sheeting deforms, contributing to the shear resistance via friction. Figure 4.3 shows a trapezoidal type of sheeting with pyramid shaped indentations in the web. Reflections concerning the degrees of freedom (DOFs) are also valid for other types of sheeting and indentations.

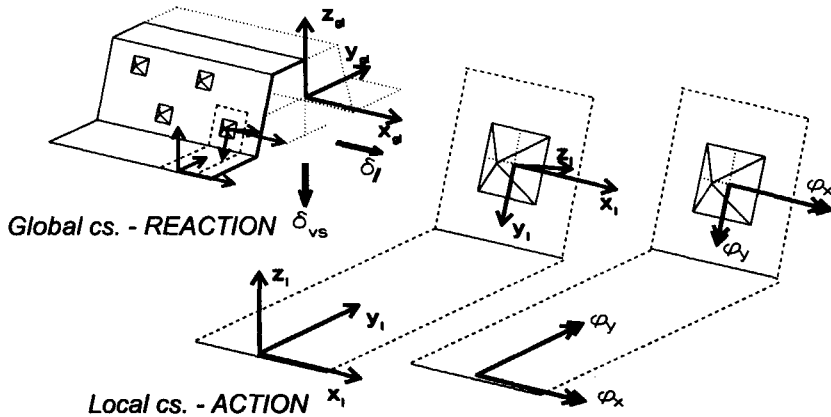


Figure 4.3: Coordinate systems used within SF-models

The ACTION part focuses on contact areas and refers to local coordinate systems. Each contact area has 5 possible DOFs:

- ① x_l : Local x-axis; coincides with direction of longitudinal slip ($\sim \delta_l$).
 - ② y_l : Local y-axis; x_l - y_l describes plane of contact area.
 - ③ z_l : Local z-axis; coincides with δ_{\perp} .
 - ④ φ_x : Rotation around the x_l -axis occurs if the sheeting deforms or is caused by eccentricities of the interaction forces acting on indentations.
 - ⑤ φ_y : Rotation around the y_l -axis is caused by eccentricities of the interaction forces acting on indentations. φ_y results in different values in the z_l -direction (δ_{\perp}) for the front and back toe of indentations.
- φ_z : Rotation around z_l -axis is prevented by in plane stiffness of sheeting.

The REACTION part relates contact areas to global displacements of the sheeting (δ_l and δ_{vs}) and refers to local and global coordinate systems.

- ① x_{gl} : Global x-axis; coincides with x_l and δ_l
- ② y_{gl} : Global y-axis

③ z_{gl} : Global z-axis; coincides with the direction of vertical separation ($\sim -\delta_{vs}$).

For the shear connection, illustrated in § 3.4, the local and global coordinate systems coincide. Rotation of the indentation was neglected ($\varphi_x = \varphi_y = 0$). In plane displacement of the sheeting perpendicular to the applied slip was prevented ($y_{gl} = y_l = 0$). Two DOFs were considered:

- ① $x_{gl} = x_l \approx \delta_l$
- ② $z_{gl} = -z_l \approx -\delta_{\perp}$
- $y_{gl} = y_l = \varphi_x = \varphi_y = 0$

For the example illustrated in § 3.5, the local and global coordinate systems do not coincide. Due to the absence of concrete at the flanges, vertical separation does not occur ($\delta_{vs} \approx z_{gl} = 0$). Due to symmetry and the neglecting of eccentricities of the interaction force, no rotation occurred ($\varphi_x = \varphi_y = 0$). Again two DOFs were considered:

- ① $x_{gl} = x_l \approx \delta_l$
- ② $y_{gl} = z_l \approx \delta_{\perp}$
- $z_{gl} = -y_l \approx \delta_{vs} = \varphi_x = \varphi_y = 0$

If the number of contact areas increases, the number of DOFs increase. If more DOFs are active, the solution technique for simple shear connections is no longer applicable. The general solution technique becomes more complicated, but is still applicable.

4.3.3 Description ACTION part

A general approach is used to describe the ACTION part. The approach is illustrated for a spherical indentation, but valid for all types of indentations. Figure 4.4 shows a contact area containing an indentation. Considering contact between indentations and concrete, the concrete can be seen as a fictitious indentation, which covers the indentation in the sheeting. The five DOFs (x_l , y_l , z_l , φ_x and φ_y) displace the indentation with respect to the fictitious concrete indentation. If a contact area does not contain an indentation, the procedure is simplified.

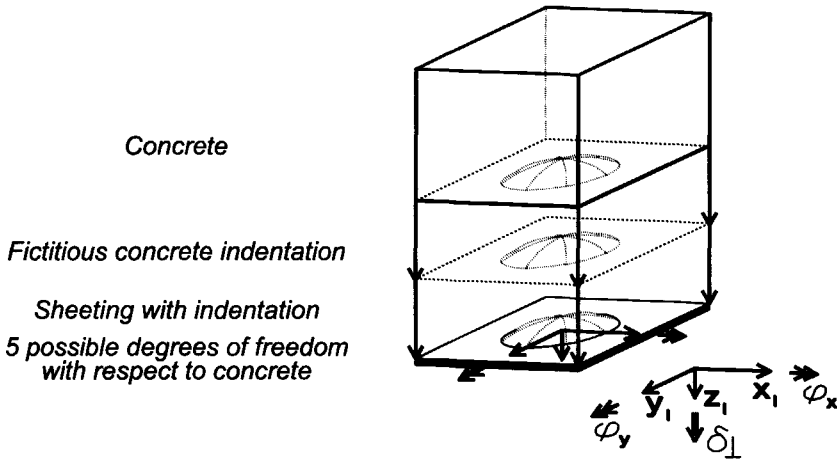
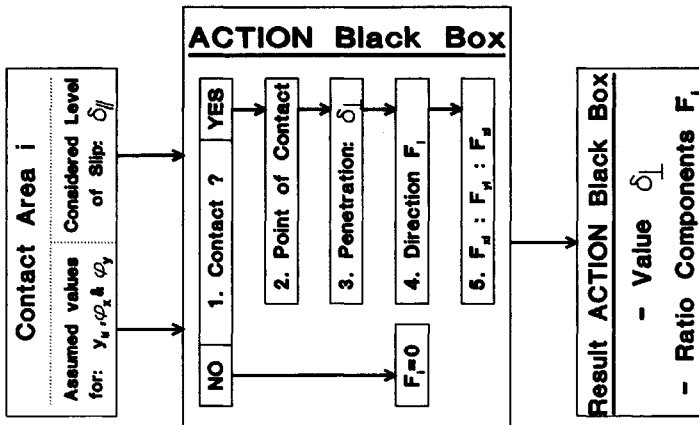


Figure 4.4: Visualisation of a contact area

The Black Box in the ACTION module determines a possible point of contact and corresponding direction of interaction forces for each contact area.

ACTION Black Box:



0. Degrees of freedom

The level of slip is known ($x_i \approx \delta_i$). A value for δ_{\perp} in the z_i -direction is derived within the black box. For the remaining DOFs (y_i , ϕ_x and ϕ_y), values are set outside the ACTION Black Box.

1. *Determination of penetration indentation in the concrete*

Figure 4.5 shows all possible DOFs of the indentation (x_i , y_i , φ_x and φ_y), which might lead to penetration of the indentation into the concrete ($\delta_{\perp} < 0$). If no penetration occurs, there is no contact, so no interaction force (F_i) occurs.

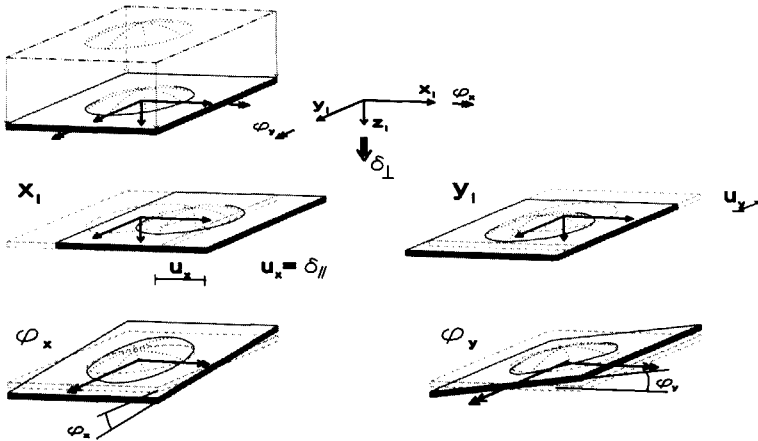


Figure 4.5: *Determination penetration indentation in concrete*

2. *Determination of the point of contact*

The point of contact between the indentation and the concrete is found at the location where penetration of the indentation into the concrete is maximum.

3. *Determination of the value DOF in z_i-direction (δ_{\perp})*

The maximum penetration equals δ_{\perp} . The indentation is pushed away from the concrete with a value δ_{\perp} .

4. *Determination of the direction of the interaction force*

The interaction force is a summation of a normal and a frictional force: $\vec{F}_i = \vec{F}_N + \vec{F}_{\mu}$. F_N acts perpendicular to the surface of the indentation at the point of contact. F_{μ} acts perpendicular to F_N and its direction depends on the incremental displacement of the indentation with respect to the concrete.

5. *Determination of the ratio of local forces on the indentation*

The interaction force can be separated into three components, according to the local coordinate system: $\vec{F}_i = \vec{F}_{x_i} + \vec{F}_{y_i} + \vec{F}_{z_i}$. Figure 4.6 illustrates the decomposition for a given point of contact.

$$F_{x_i} : F_{y_i} : F_{z_i} = \cos\beta \cdot \frac{\tan\varphi + \mu}{1 - \mu \cdot \tan\varphi} : \sin\beta \cdot \frac{\tan\varphi + \mu}{1 - \mu \cdot \tan\varphi} : 1 \quad (4.1)$$

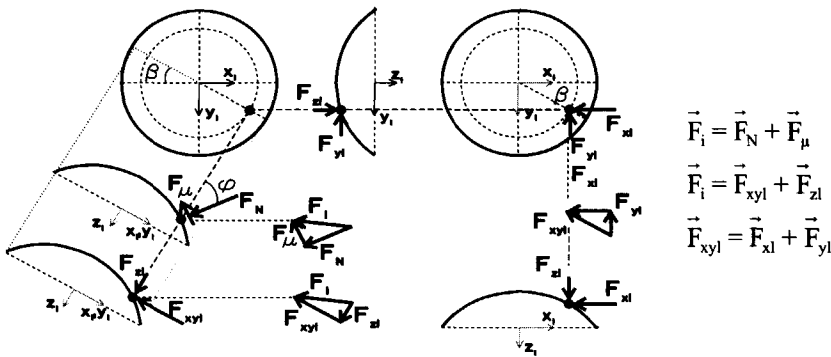


Figure 4.6: Decomposition interaction force

$$F_{xyl} = F_N \cdot \sin\phi + F_\mu \cdot \cos\phi \quad (4.2)$$

$$F_{z_l} = F_N \cdot \cos\phi - F_\mu \cdot \sin\phi \quad (4.3)$$

$$F_{x_l} = F_{xyl} \cdot \cos\beta \quad (4.4)$$

$$F_{y_l} = F_{xyl} \cdot \sin\beta \quad (4.5)$$

The illustrated procedure determines displacements and the direction of the interaction force for a considered contact area, based on values for the considered DOFs. Using the general solution technique, the behaviour of all contact areas is considered in the iterative procedure.

The described procedure is suitable for implementation in a computer program. In some cases the ACTION part can be described analytically. In all cases the procedure should supply the point of contact, a value for δ_\perp and the ratio between the components of the interaction force with respect to a local coordinate system.

4.3.4 Description REACTION part

Within the REACTION module, the response of the sheeting is described using a mechanical model, containing all considered DOFs, and loaded by the forces derived in the ACTION module. For all DOFs new values are derived, which can be compared to the assumed values. Within the iterative procedure the final solution is determined, using the boundary equations to satisfy compatibility and

equilibrium. The mechanical model can be a simplified 2-D frame model or a sophisticated 3-D FE-model. Figure 4.7 shows part of the trapezoidal sheeting of Fig. 4.3, with forces corresponding to the considered DOFs.

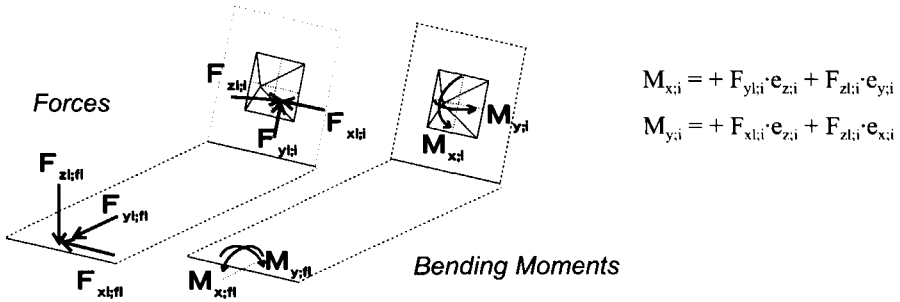


Figure 4.7: Forces corresponding to possible DOFs in contact areas

The response of the sheeting is presented as a stiffness matrix $[A]$ which relates forces $[F]$ to the considered DOFs $[u]$.

$$[A_{j,k}] \cdot [F_j] = [u_j] \tag{4.6}$$

If a shear connection contains n contact areas, $[A]$ leads to the matrix:

$$\begin{bmatrix}
 A_{1,1} & \dots & A_{1,5} & \dots & A_{1,5n-4} & \dots & A_{1,5n} \\
 \cdot & \cdot & \cdot & \cdot & \cdot & \cdot & \cdot \\
 \cdot & \cdot & \cdot & \cdot & \cdot & \cdot & \cdot \\
 A_{5,1} & \dots & A_{5,5} & \dots & \cdot & \dots & \cdot \\
 \cdot & \cdot & \cdot & \cdot & \cdot & \cdot & \cdot \\
 A_{5n-4,1} & \dots & \dots & \dots & A_{5n-4,5n-4} & \dots & A_{5n-4,5n} \\
 \cdot & \cdot & \cdot & \cdot & \cdot & \cdot & \cdot \\
 \cdot & \cdot & \cdot & \cdot & \cdot & \cdot & \cdot \\
 A_{5n,1} & \dots & \dots & \dots & A_{5n,5n-4} & \dots & A_{5n,5n}
 \end{bmatrix} \cdot \begin{bmatrix} F_{x1;1} \\ F_{y1;1} \\ F_{z1;1} \\ M_{x;1} \\ M_{y;1} \\ \cdot \\ \cdot \\ F_{x1;n} \\ F_{y1;n} \\ F_{z1;n} \\ M_{x;n} \\ M_{y;n} \end{bmatrix} = \begin{bmatrix} u_{x1;1} \\ u_{y1;1} \\ u_{z1;1} \\ \phi_{x;1} \\ \phi_{y;1} \\ \cdot \\ \cdot \\ u_{x1;n} \\ u_{y1;n} \\ u_{z1;n} \\ \phi_{x;n} \\ \phi_{y;n} \end{bmatrix} \tag{4.7}$$

All entries $A_{j,k}$ of the stiffness matrix $[A]$ are determined by applying unified forces F_j to the mechanical model, which results in values for all DOFs u_j . Usually not all DOFs are active, which reduces the size of the stiffness matrix. For the shear connections, illustrated in § 3.4 & 3.5, the size of the stiffness matrices was reduced to $[1 \times 1]$, since there was only one contact area, which contained only one active DOF: δ_{\perp} . The second DOF, the applied slip δ_{\parallel} , is known and therefore eliminated from the matrix.

$$\text{§ 3.4:} \quad [A] \cdot [F] = [u] \Rightarrow [A_{1,1}] [F_{z1}] = [u_{z1}] \Rightarrow [1/k_{\perp}] [F_{\perp}] = [\delta_{\perp}] \quad (4.8)$$

$$\text{§ 3.5:} \quad [A] \cdot [F] = [u] \Rightarrow [A_{1,1}] [F_{z1}] = [u_{z1}]$$

$$\rightarrow \left[\begin{array}{c} (H_s - D^*)^3 \\ 48EI \end{array} \cdot \frac{4 \cdot B_{fl} + (H_s - D^*)}{4 \cdot B_{fl} + 4 \cdot (H_s - D^*)} \right] \cdot [F_{\perp}] = [\delta_{\perp}] \quad (4.9)$$

The matrix $[A]$ for the evaluated example in § 4.5 is reduced to $[4 \times 4]$, which already requires the general solution technique. If description of the ACTION and REACTION module in parameters is possible, both modules can be implemented in computer programs containing the iterative procedure of the general solution technique, which reduces the computing time considerably.

Due to simplifications, the SF-models remain transparent. Even if the simplifications affect the behaviour of the shear connection, SF-models can be used effectively for parameter investigations. If the effect of simplifications can be quantified, for instance by using sophisticated FE-models, SF-models are powerful tools for investigating shear connections in composite slabs.

4.4 Finite Element Models

Although FE-models are not based on the strict distinction between ACTION and REACTION, the physical background of the hypothesis can be implemented. FE-models of shear connections should model the 4 components of shear connections: sheeting, indentations, concrete and the interface between concrete and sheeting.

① *Sheeting*

- # Within the hypothesis, displacement and deformation of the sheeting is important, so the sheeting has to be modelled accurately. Due to the limited thickness of the sheeting ($t \leq 1.25$ mm), the sheeting is modelled using beam elements (2-D) or plate bending elements (semi 3-D).
- # Plasticity of sheeting can be implemented. Large strains can occur at contact areas and at the edges between web and flanges. If plasticity is considered, the element distribution should not affect the development of plastic mechanisms.
- # Geometrical non-linear behaviour should be considered, due to the large deformation of the cross-section.
- # Profiled sheeting is made by repeated deformation of flat sheeting, which influences the yield stress and thickness of the sheeting. Variations of yield stress and thickness can be implemented.

② *Indentations*

- # Since the normal direction to the contact surface at the indentation determines the direction of the interaction forces, an accurate description of the indentation is crucial.
- # The element distribution at the indentations should allow for deformation or instability of the indentation itself.
- # Indentations are added to the profiled sheeting by plastic deformation. Similar to profiled sheeting, possible variation of properties can be implemented.

③ *Concrete*

- # The outer layer of concrete, which is in contact with the sheeting, is cement paste rather than structural concrete. The deformation of the concrete is therefore caused by deformation of the paste. The strength and stiffness of the paste is smaller than found for structural concrete. The indentations dig "channels" through the paste, which should be taken into account by the solid concrete elements.
- # Due to the number of indentations and the flexibility of the sheeting interaction forces between concrete and sheeting remain relatively small. Usually no cracking of the concrete occurs.
- # Concrete is modelled at all possible contact areas. Within FE-models, the point of contact is a result of the analysis, whereas within the mechanical model of SF-models the location of contact is predestinated.

In full-scale experiments, cracking of concrete occurs due to curvature of the cross-section. The presence of these cracks influences the behaviour of the shear connection. Due to the cross-sectional approach these effects are not taken into account.

④ *Interface between the concrete and the sheeting*

Contact elements consist of two parts which are connected to different parts of the FE-model which might contact during loading. One of these parts determines the direction of the interaction forces. Since the assumption with regard to the direction of the interaction force is based on the geometry of the sheeting or indentation at the point of contact, this part of the contact elements is connected to the sheeting. If contact occurs, contact elements return an interaction force which prevents penetration. Similar to the hypothesis, the interaction force consists of a normal and an (optional) frictional force.

Friction can be implemented in contact elements. Different types of friction are available. Rigid Coulomb Friction is used. This type of friction ensures occurrence of the maximum coefficient of friction if slip occurs.

4.5 Example

The example of § 3.5 is considered again taking into account the concrete at the flanges, as shown in Fig. 4.8. If contact arises between flanges and concrete, interaction forces tend to separate the sheeting from the concrete, which can only be resisted by the indentation. The example is evaluated using SF- and FE-models.

4.5.1 Example SF-model

All 6 elements of the general solution technique are discussed:

- 1 - *Determination of active degrees of freedom (§ 4.5.1a)*
- 2 - *Iterative procedure (§ 4.5.1b)*
- 3 - *ACTION module (§ 4.5.1c)*
- 4 - *REACTION module (§ 4.5.1d)*
- 5 - *Checks in iterative procedure (§ 4.5.1e)*

6 - Results of analysis (§ 4.5.1f)

Simplifications within the SF-model are marked in the text (Ass. X). All assumptions are reconsidered in § 4.5.3 using the FE-results.

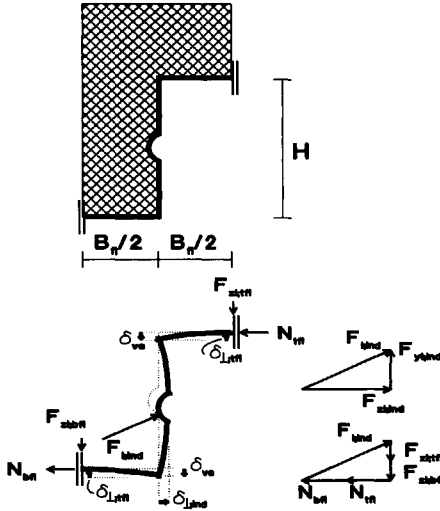


Table 4.1: Dimensions Example § 4.5

Height sheeting	H	60 mm
Thickness sheeting	t	0.70 mm
Width flanges	B _n	60 mm
Considered length	L	40 mm
Diameter indentation	D	12 mm
Height indentation	h	3.0 mm
Radius indentation	R	7.5 mm

$$\vec{F}_{i;ind} = \vec{F}_{y;ind} + \vec{F}_{z;ind}$$

$$\vec{F}_{i;ind} = \vec{F}_{z;tfl} + \vec{F}_{z;bfl} + \vec{N}_{tfl} + \vec{N}_{bfl}$$

$$\Rightarrow F_{y;ind} - F_{z;tfl} - F_{z;bfl} = 0$$

Figure 4.8: Configuration Example § 4.5

4.5.1a Determination active degrees of freedom

There are 3 possible contact areas: the indentation (*ind*) and both flanges (*tfl/bfl*). Each area has five possible DOFs. It is assumed that the longitudinal displacement of all areas equals the applied slip (Ass. 1: $u_{xgl}=u_{x;bfl}=u_{x;ind}=u_{x;tfl}=\delta_1$).

Sheeting

Due to the large deformation of the web, the edges between web and flanges do not have the same vertical displacement: $\delta_{vs;web/bfl} < \delta_{vs;ind} < \delta_{vs;web/tfl}$. This effect increases the interaction force at the bottom flange ($F_{i;bfl}$) and reduces the force at the top flange ($F_{i;tfl}$). This effect is neglected (Ass. 2: $\delta_{vs;web/bfl} = \delta_{vs;ind} = \delta_{vs;web/tfl}$).

Flanges

Contact between flanges and concrete is assumed to be located in the centre of the flanges (Ass. 3). Due to the boundary conditions at the flange, only $u_{z;tfl}$ is

active.

Indentation

Eccentricities of the interaction force with respect to the indentation are neglected (Ass. 4). Due to assumption 2 and the equal width of both flanges ($B_{bfl}=B_{tfl}$), the cross-section remains symmetrical. Therefore, both rotations of the indentation are zero ($\varphi_{x;ind}=\varphi_{y;ind}=0$). Two DOFs are active: $u_{y;ind}$ & $u_{z;ind}$. Due to the vertical web, $u_{y;ind}$ coincides with the direction of vertical separation ($u_{y;ind}=\delta_{vs}$). $u_{z;ind}$ coincides with $\delta_{\perp;ind}$, which represents the fictitious penetration, derived in the ACTION module.

Five DOFs are active within the ACTION and/or REACTION module. Each DOF has a corresponding force:

<i>Sheeting</i>	①	$u_{xgl}=u_{xl;bfl}=u_{xl;ind}=u_{xl;tfl} \sim \delta_l$	\rightarrow	$F_{xl;bfl}+F_{xl;ind}+F_{xl;tfl} = F_l$
<i>Bottom flange</i>	②	$u_{zl;bfl} \sim \delta_{\perp;bfl}$	\rightarrow	$F_{zl;bfl}$
<i>Indentation</i>	③	$u_{y;ind} \sim \delta_{vs}$	\rightarrow	$F_{y;ind}$
	④	$u_{z;ind} \sim \delta_{\perp;ind}$	\rightarrow	$F_{z;ind}$
<i>Top flange</i>	⑤	$u_{zl;tfl} \sim \delta_{\perp;tfl}$	\rightarrow	$F_{zl;tfl}$

4.5.1b Iterative procedure

The general solution technique requires assumptions for DOFs which are not derived within the ACTION and REACTION modules. Since the applied slip δ_l is known and $\delta_{\perp;ind}$ is derived within the ACTION module, the remaining DOFs are unknown and assumptions are required to start the iterative procedure. Each assumption requires an equation which checks the assumed values once the ACTION and REACTION modules are performed. In this case, three equations are required.

<i>Active DOF</i>	<i>DOF</i>	<i>Assumed value</i>	<i>Check</i>
1	$u_{zl;bfl}$	0	Contact at bottom flange: $F_{i;bfl} > 0$
2	$u_{y;ind}$	δ_{vs}	Resultant lateral force $F_{\perp} = F_{zl;bfl}+F_{y;ind}+F_{zl;tfl} = 0$
3	$u_{zl;tfl}$	0	Contact at top flange: $F_{i;tfl} > 0$

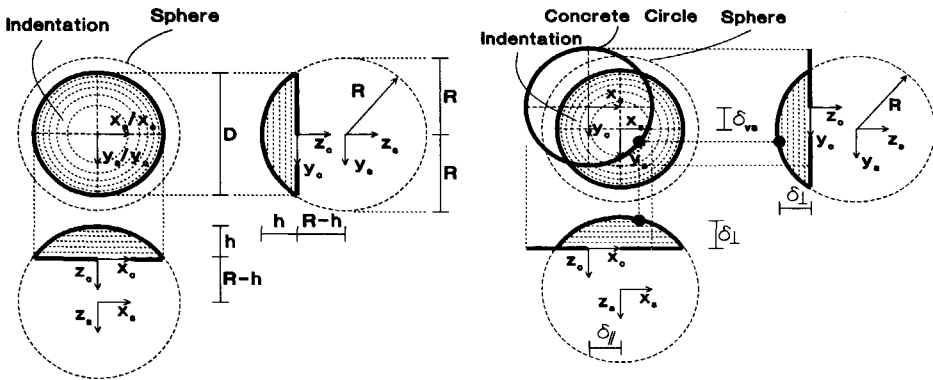
The mechanical model used within the REACTION module assumes contact

between the flanges and the concrete. This implies a zero displacement for $u_{z;l;bff}$ and $u_{z;l;ttf}$. The check corresponding to the assumption is the sign of the interaction forces at the flanges ($F_{i;bff}$ & $F_{i;ttf}$). These forces should be positive. If one of these forces becomes negative, the corresponding contact area should be eliminated from the mechanical model.

The REACTION module determines values for all forces acting on the cross-section. The resultant force in the global z-direction should be zero, since no external lateral force is present: $F_{zgl} = F_i = F_{z;l;bff} + F_{y;l;ind} + F_{z;l;ttf} = 0$. If $F_{z;l}$ is not zero, the assumed value for the vertical separation δ_{vs} should be adjusted.

4.5.1c ACTION module

The ACTION module is described in parameters. The spherical indentation can be described as part of a sphere, as shown in Fig. 4.9a. Displacements of the indentation ($u_{x;l;i} = \delta_i$ and $u_{y;l;i} = \delta_{vs}$) can be translated to a displacement of the fictitious sphere with respect to the concrete, as shown in Fig. 4.9b. The displacements δ_i and δ_{vs} lead to penetration of the fictitious steel sphere into the concrete, δ_{fp} . If deformation of the indentation and concrete is neglected (Ass. 5), the point of contact lies on the circle describing the toe of the concrete indentation.



a. Description indentation as part of sphere

b. Displacement sphere with respect to concrete circle

Figure 4.9: Description indentation as part of fictitious sphere

The indentation and the concrete are described by a sphere and a circle:

$$\text{Steel Sphere: } x_s^2 + y_s^2 + z_s^2 = R^2 \quad (4.10)$$

$$\text{Concrete Circle: } x_c^2 + y_c^2 = \left(\frac{D}{2}\right)^2 \quad (4.11)$$

$$\begin{aligned} \text{with: } x_s &= x_c - \delta_l \\ y_s &= y_c - \delta_{vs} \\ z_s &= -(R-h) - \delta_{fp} \end{aligned}$$

The origin of the local coordinate system for the concrete circle lies at the centre of the circle. The origin of the local coordinate system of the sphere lies at the centre of the sphere. Each possible point of contact (x_c, y_c) at the concrete circle might penetrate into the steel sphere $\delta_{fp}(x_c, y_c)$. Equation (4.10) can be rewritten as:

$$\text{Steel Sphere: } (x_c - \delta_l)^2 + (y_c - \delta_{vs})^2 + (-\delta_{fp} - (R-h))^2 = R^2 \quad (4.12)$$

The concrete circle can be described using polar coordinates:

$$0 < \beta < 2 \cdot \pi: \quad x_c = \frac{D}{2} \cdot \cos\beta; \quad y_c = \frac{D}{2} \cdot \sin\beta$$

For all possible points of contact at the concrete circle, a value for $\delta_{fp}(x_c, y_c)$ can be determined. If δ_{fp} is negative, no contact occurs. If δ_{fp} is positive, (x_c, y_c) is a possible point of contact. The maximum value of δ_{fp} represents the maximum penetration of the indentation into the concrete which equals $\delta_{\perp, ind}$. Equation (4.12) can be rewritten:

$$\left(\frac{D}{2} \cdot \cos\beta - \delta_l\right)^2 + \left(\frac{D}{2} \cdot \sin\beta - \delta_{vs}\right)^2 + (-\delta_{fp} - (R-h))^2 = R^2 \quad (4.13)$$

$$\Rightarrow (-D \cdot \cos\beta \cdot \delta_l + \delta_l^2) + (-D \cdot \sin\beta \cdot \delta_{vs} + \delta_{vs}^2) + (\delta_{fp}^2 + 2 \cdot \delta_{fp} \cdot (R-h)) = 0$$

$$\text{with: } (R-h)^2 + \left(\frac{D}{2}\right)^2 = R^2$$

Resulting in δ_{fp} as a function of β :

$$\delta_{fp}^2 + 2 \cdot \delta_{fp} \cdot (R - h) + \left[\delta_l \cdot (\delta_l - D \cdot \cos\beta) + \delta_{vs} \cdot (\delta_{vs} - D \cdot \sin\beta) \right] = 0 \quad (4.14)$$

$$\Rightarrow \delta_{fp} = -(R - h) + \sqrt{(R - h)^2 - \delta_l \cdot (\delta_l - D \cdot \cos\beta) - \delta_{vs} \cdot (\delta_{vs} - D \cdot \sin\beta)}$$

Differentiation of δ_{fp} to β determines the location of the maximum value of δ_{fp} :

$$\frac{\partial \delta_{fp}}{\partial \beta} = \frac{1}{2} \cdot \frac{-\delta_l \cdot D \cdot \sin\beta + \delta_{vs} \cdot D \cdot \cos\beta}{\sqrt{(R - h)^2 - \delta_l \cdot (\delta_l - D \cdot \cos\beta) - \delta_{vs} \cdot (\delta_{vs} - D \cdot \sin\beta)}} = 0 \quad (4.15)$$

$$\Rightarrow \delta_l \cdot \sin\beta = \delta_{vs} \cdot \cos\beta \quad \Rightarrow \tan\beta = \frac{\delta_{vs}}{\delta_l}$$

The fictitious penetration of the indentation into the circle of concrete at point (x_c, y_c) equals $\delta_{\perp, ind}$:

$$\delta_{\perp, ind} = \delta_{fp}(x, y) = -(R - h) + \sqrt{(R - h)^2 - \delta_l \cdot \left(\delta_l - \frac{D \cdot \delta_l}{\sqrt{\delta_l^2 + \delta_{vs}^2}} \right) - \delta_{vs} \cdot \left(\delta_{vs} - \frac{D \cdot \delta_{vs}}{\sqrt{\delta_l^2 + \delta_{vs}^2}} \right)} \quad (4.16)$$

$$\text{at: } (x_c, y_c) = \left(\frac{D}{2} \cdot \cos\beta, \frac{D}{2} \cdot \sin\beta \right) = \left(\frac{D}{2} \cdot \frac{\delta_l}{\sqrt{\delta_l^2 + \delta_{vs}^2}}, \frac{D}{2} \cdot \frac{\delta_{vs}}{\sqrt{\delta_l^2 + \delta_{vs}^2}} \right)$$

Figure 4.10 shows the function of δ_{fp} for three different combinations of slip and separation, for values of β from $-\pi/2$ to $\pi/2$, corresponding to the front half of the concrete circle.

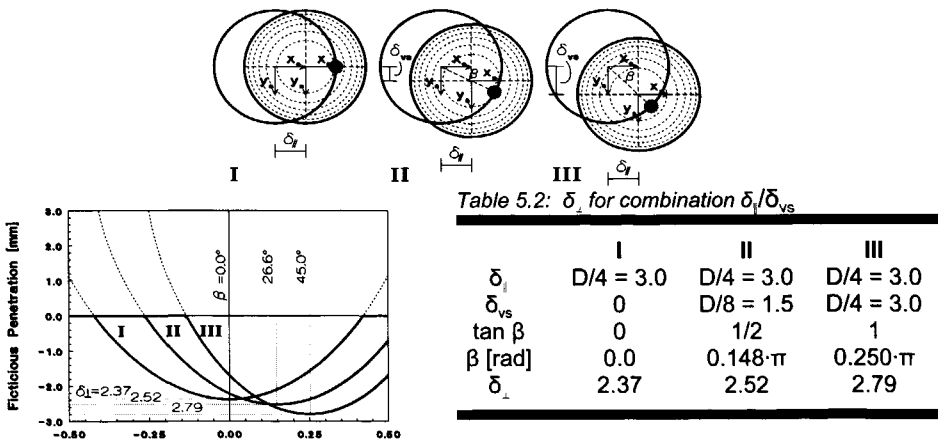


Figure 4.10: Result ACTION module for combinations of δ_l and δ_{vs}

The inclination of the indentation at the point of contact (x_s, y_s) determines the normal direction at the indentation, and therefore the direction of $F_{N;ind}$. The frictional force $F_{\mu;ind}$ acts perpendicular to $F_{N;ind}$ and depends on the incremental displacement of the indentation, which represents the movement of the indentation with respect to the concrete at the considered level of slip. In this case, no previous levels of slip are considered. The direction of $F_{\mu;ind}$ is based on the displacement of the indentation with respect to the undeformed geometry (Ass. 6). Similar to Fig. 4.6, the interaction force $F_{i;ind}$, which is a summation of $F_{N;ind}$ and $F_{\mu;ind}$, can be decomposed with respect to the local coordinate system, resulting in a ratio between local forces. For the given values of δ_1 and δ_{vs} the ratio between the local forces can be determined.

$$\vec{F}_{i;ind} = \vec{F}_{N;ind} + \vec{F}_{\mu;ind} = \vec{F}_{x;ind} + \vec{F}_{y;ind} + \vec{F}_{z;ind} \Rightarrow F_{x;ind} : F_{y;ind} : F_{z;ind} \quad (4.17)$$

For the contact areas between flanges and concrete, the ratio between the local forces is determined by the coefficient of friction.

$$F_{x;bf/tf} : F_{y;bf/tf} : F_{z;bf/tf} = F_{\mu;bf/tf} : 0 : F_{N;bf/tf} = \mu \cdot F_{N;bf/tf} : 0 : F_{N;bf/tf} = \mu : 0 : 1 \quad (4.18)$$

The location of the point of contact, a value for δ_1 and the ratio between local forces at each contact area are a result of the ACTION module. Rotation of the indentation ($\phi_{x;ind} \neq 0 \wedge \phi_{y;ind} \neq 0$) can be implemented by a displacement of the centre of the steel sphere.

4.5.1d REACTION module

The response of the sheeting consists of displacement and deformation of the sheeting. The mechanical model of Fig. 4.11 describes the deformation of the sheeting. The model relates active DOFs ($u_{z;bf}$, $u_{z;ind}$ and $u_{z;tf}$) to corresponding forces ($F_{z;bf}$, $F_{z;i}$ and $F_{z;tf}$). The deformed shape of the sheeting is a summation of vertical separation and deformation, as shown in Figs. 4.11b & 4.11c. In order to maintain contact between the centre of the flanges and the concrete, the vertical separation should equal the deformation of the flanges.

$$u_{z;bf/tf} = \delta_{vs} + \delta_{\perp;bf/tf} = 0 \Rightarrow \delta_{\perp;bf/tf} = -\delta_{vs} \quad (4.19)$$

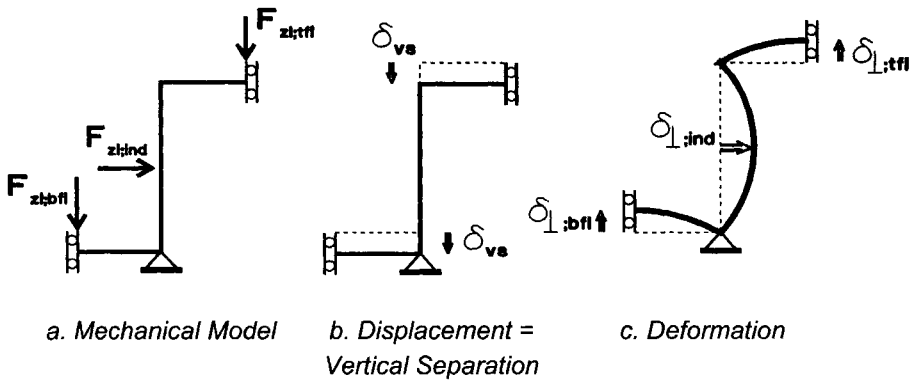


Figure 4.11: Mechanical model SF-model

The influence of the indentation to the bending stiffness of the web is neglected (Ass. 7: $D^* = 0$). The mechanical model is a 2-D frame model, which neglects variation of deformation along the x-axis (Ass. 8). The stiffness matrix for the given mechanical model, assuming contact at both flanges, can be evaluated:

$$[A] \cdot [F] = [u] \Rightarrow \begin{bmatrix} A_{1,1} & A_{1,2} & A_{1,3} \\ A_{2,1} & A_{2,2} & A_{2,3} \\ A_{3,1} & A_{3,2} & A_{3,3} \end{bmatrix} \cdot \begin{bmatrix} F_{zl;bff} \\ F_{zl;ind} \\ F_{zl;tff} \end{bmatrix} = \begin{bmatrix} u_{zl;bff} \\ u_{zl;ind} \\ u_{zl;tff} \end{bmatrix} = \begin{bmatrix} \delta_{\perp;bff} \\ \delta_{\perp;ind} \\ \delta_{\perp;tff} \end{bmatrix} = \begin{bmatrix} -\delta_{vs} \\ \delta_{\perp;ind} \\ -\delta_{vs} \end{bmatrix} \quad (4.20)$$

Values for the DOFs in $[u]$ are available. $\delta_{\perp;bff}$ and $\delta_{\perp;tff}$ result from the assumption that contact is present ($\delta_{\perp;bff/tff} = -\delta_{vs}$). $\delta_{\perp;ind}$ results from the ACTION module. The forces acting on the cross-section can be derived:

$$[F] = [A]^{-1} \cdot [u] \quad (4.21)$$

Result of the REACTION module are values for all forces corresponding to the active DOFs ($F_{zl;bff}$, $F_{zl;ind}$ and $F_{zl;tff}$).

In this case, a simple 2-D frame model is used within the REACTION module. It is also possible to consider more DOFs and use more sophisticated tools, for instance FE-models, to determine the response of the sheeting. If the response is not determined in parameters, each configuration requires determination of a stiffness matrix $[A]$.

4.5.1e Iterative procedure general solution technique

From the ACTION module, a ratio between local components of the interaction force in each contact area is found (eq. (4.17)). From the REACTION module, values for forces corresponding to active DOFs are found (eq. (4.21)), which implies that all components in each contact area are determined. All local components can be transferred to the global coordinate system. Summation of all global forces results in a resultant shear force (F_{\parallel}) in the x-direction and a resultant lateral force (F_{\perp}):

$$F_{\parallel} = F_{x1;bfl} + F_{x1;ind} + F_{x1;tfl} = \mu \cdot F_{z1;bfl} + \left[\frac{F_{x1;ind}}{F_{z1;ind}} \right]^{ACTION} \cdot F_{z1;ind} + \mu \cdot F_{z1;tfl} \quad (4.22)$$

$$F_{\perp} = -F_{z1;bfl} + F_{y1;ind} - F_{z1;tfl} = -F_{z1;bfl} + \left[\frac{F_{y1;ind}}{F_{z1;ind}} \right]^{ACTION} \cdot F_{z1;ind} - F_{z1;tfl} \quad (4.23)$$

The checks, listed in § 4.5.1b, can be performed. When all checks are satisfied, the solution is found. If one or more checks fail, corresponding assumptions have to be adjusted. If the first or third check fails ($F_{z1;bfl} < 0$ and/or $F_{z1;tfl} < 0$), the mechanical model in the REACTION module should be adjusted: $F_{z1;bfl}$ and/or $F_{z1;tfl}$ should be taken out of the model. If the second check fails ($F_{\perp} \neq 0$) the level of vertical separation should be adjusted. If an external force is applied to the cross-section, for instance by a support reaction, equilibrium should be obtained between the external and internal forces ($F_{\perp} = F_{z1;ext}$).

4.5.1f Results

Figure 4.12 shows the results of the SF-model. The solid line represents the applied shear force (F_{\parallel}) versus longitudinal slip (δ_{\parallel}) to the left axis. The dashed line underneath the solid line represents the contribution of the indentation to the applied shear force. The dotted line represents the result as found in § 3.5.

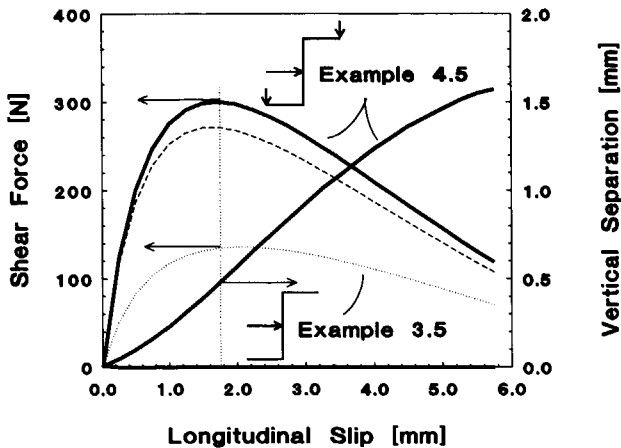


Figure 4.12: Results SF-Model

Contact between flanges and concrete doubles the contribution of the indentation to the shear force. This is caused by the increased rotational stiffness of the edges between the flanges and the web. The total capacity is further increased by the contribution of friction between the flanges and concrete. To the right axis the vertical separation (δ_{vs}) is plotted versus δ_l . The ratio between δ_{vs} and δ_l is almost constant. It can be recognized that the ratio increases until the maximum shear stress is reached, and decreases once the shear resistance drops. For large values of separation, the difference between the examples of § 3.5 and 4.5 reduces due to the decreasing contact forces between the flanges and concrete.

4.5.2 Example FE-model

An FE-model with linear elastic behaviour is considered in order to evaluate the assumptions of the SF-model. The sheeting is modelled accurately using shell elements. For all contact areas all relevant DOFs are active. Concrete at the flanges is modelled using solids. Concrete at the indentation is modelled by half a cylinder, placed in front of the indentation.

Since only linear contact elements are available, the contact surface at the indentation is described by flat surfaces. Figure 4.13 shows the effect to the applied shear force, caused by the angle between the contact elements. The

vertical component of the interaction force F_{\perp} does not change when an edge is passed, since the displacements of the indentation are continuous. Equilibrium of forces at both sides of the edge determines the reduction of the applied shear force. The effect can be reduced by increasing the number of elements, which reduces the angle between the contact elements.

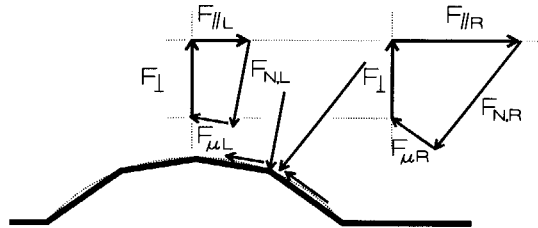


Figure 4.13. Discontinuity applied shear force caused by linear contact elements on spherical indentations

Figure 4.14 shows results of both the SF- and FE-model. The shear resistance of the FE-model is higher and the vertical separation smaller. Differences between the SF- and FE-results are attributed to the influence of the indentation to the bending stiffness of the web. This effect is investigated in § 4.5.3-7.

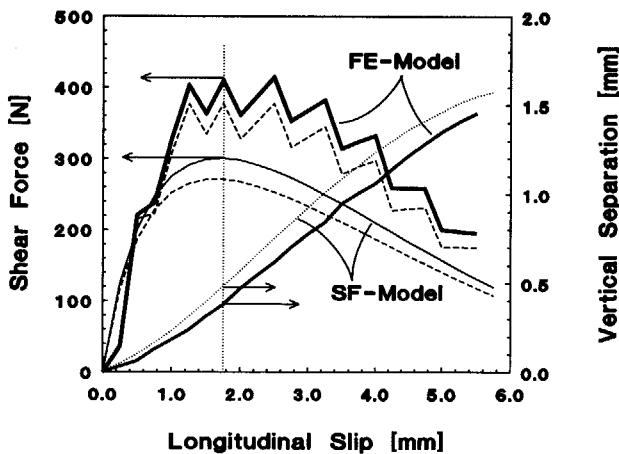


Figure 4.14: Results FE-Model

4.5.3 Evaluation Assumptions SF-model

The assumptions used within the SF-model are evaluated using the FE-results.

Assumption 1: $u_{xgl} = u_{xl;bfl} = u_{xl;ind} = u_{xl;tfl} = \delta_{||}$

Longitudinal displacements of all contact areas are presented in Table 5.3 for three levels of slip. The assumption shows to be reasonable.

Table 5.3: Displacement contact areas in x-direction

Applied slip = δ_j	1.500	3.000	4.500
$u_{xl;bottom\ flange}$	1.512	3.005	4.497
$u_{xl;indentation\ front\ toe}$	1.500	2.996	4.495
$u_{xl;indentation\ back\ toe}$	1.508	3.004	4.500
$u_{xl;top\ flange}$	1.512	3.005	4.497

Assumption 2: $\delta_{vs;web/bfl} = \delta_{vs;ind} = \delta_{vs;web/tfl}$

Due to the large deformation of the web, the assumption is not correct. Table 5.4 shows values for the vertical displacement of the edges between flanges and web. As expected $\delta_{vs;web/bfl} < \delta_{vs;web/tfl}$ and

Table 5.4: Vertical separation

Applied slip = δ_j	1.500	3.000	4.500
$\delta_{vs;bfl-web}$	0.365	0.777	1.105
$\delta_{vs;tfl-web}$	0.438	0.981	1.399
$F_{zl;bfl}$	39.4	40.9	30.9
$F_{zl;tfl}$	36.3	36.1	24.6

therefore $F_{zl;bfl} > F_{zl;tfl}$. Figure 4.12 shows that the interaction forces at the flanges are small compared to the interaction force at the indentation. Table 5.4 shows that the variation between the forces at the flanges is small, and therefore the assumption is reasonable.

Assumption 3: Contact area at flanges located at the centre of flanges
 In general, if flanges are wide, the point of contact does not lie at the centre, but shifts towards the edges. If flanges are small, contact is lost once vertical separation arises. Results of the mechanical model show that for the considered configuration the assumption is reasonable.

Assumption 4: Neglecting of eccentricities of the forces at the indentation
 Eccentricities of the interaction force with respect to the indentation result in a tendency of the indentation to

Table 5.5: Rotation of the indentation

Applied slip = δ_j	1.500	3.000	4.500
$\varphi_{x;ind} \cdot 10^{-3}$	-0.108	+5.308	+5.708
$\varphi_{y;ind} \cdot 10^{-3}$	-3.958	-2.492	-0.250

rotate. Rotations of the indentation within the FE-model are presented in Table 5.5. Rotations are derived from the displacement of the front, back, upper and lower toe of the indentation in the local z-direction. Rotations remain small compared to the maximum rotation of the edges for large values of slip, which approaches $200 \cdot 10^{-3}$.

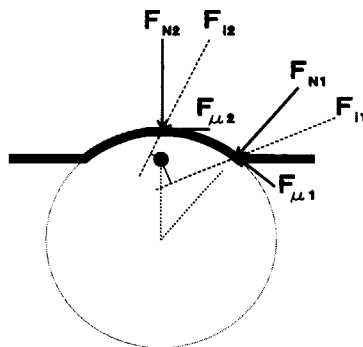


Figure 4.15: Rotation indentation due to eccentricity interaction force

Table 5.5 shows that disturbance of the symmetrical behaviour as discussed at Ass. 2, results in rotation of the indentation around the longitudinal axis (φ_x). With respect to the shear resistance, rotation around the local y-axis (φ_y) is more important. φ_y is negative for small values of slip and increases if slip increases. This effect is illustrated in Fig. 4.15. For small values of slip the interaction force points underneath the centre of the indentation. For large values of slip, the interaction force points over the centre of the indentation. Results show that due to the presence of friction the eccentricities around the local y-axis (φ_y) remain small.

φ_y affects the shear resistance in two ways. A negative value for φ_y results in a smaller value for $\delta_{L,ind}$, since the average displacement of the indentation reduces, which reduces the shear resistance. However, a negative value for φ_y increases the inclination of the indentation at the contact area, which improves the shear resistance. The overall influence of φ_y on the shear resistance depends on the geometry of the indentation and the sheeting. In this case, the level of rotation allows for neglecting of eccentricities of the interaction force within the SF-model.

Assumption 5: Neglecting of deformation of the indentation and the concrete
 Results of the FE-analysis show that high stress values arise at the indentation.

The maximum equivalent stress in the indentation is reached when the ultimate shear capacity is reached ($\sigma_{\text{aq}} \approx 700 \text{ N/mm}^2$). In general, stresses in the indentation remain smaller than stresses in the web, which implies that no large plastic strains are expected in the indentation if plasticity is considered. Even for the large stresses, found in the elastic analysis, deformation of the indentation is limited, since the spherical indentation is very stiff.

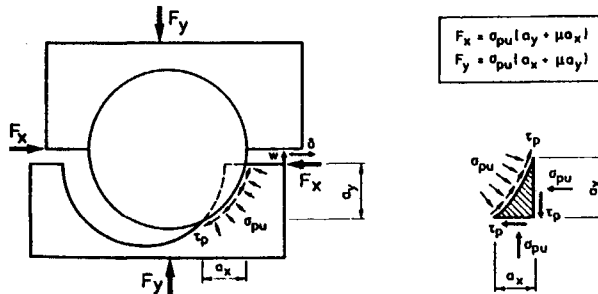


Figure 4.16: Contact mechanism shear displacement

When the shear capacity is reached, the maximum force acting at the concrete is approximately 360 N. This force acts at paste rather than at structural concrete. In [9] a concrete crack model is presented based on crushing of cement paste, as illustrated in Fig. 4.16. Compared to the concrete model interaction forces in composite slabs are relatively small. Nevertheless, neglecting the deformation of concrete requires a more thorough analysis. Similar to the deformation of the indentation, plasticity of sheeting reduces the interaction forces, and therefore the deformation of the concrete paste. Neglecting the deformation leads to over-estimation of the shear strength. The influence of the deformation of both steel and concrete can be taken into account in both SF- as FE-models.

Assumption 6: Direction of $F_{\mu,i}$ based on undeformed geometry

The direction of the frictional forces $F_{\mu,i}$ should be based on the incremental displacement of the contact areas. This implies that a stepwise analysis should be performed. In the SF-model, the direction of the interaction force is determined with respect to the undeformed geometry. The almost linear relation between δ_{vs} and δ_{l1} , as shown in Fig. 4.12, proves that the assumption is reasonable.

Assumption 7: Neglecting the influence of the indentation on the bending stiffness of the web

Since in the SF-model the influence of the indentation on the bending stiffness of the web is neglected ($D^*=0$), the shear capacity is under-estimated. Figure 4.17 shows the results of the FE-model and three SF-models, with different values for D^* . The bending stiffness of the web is taken infinite over a distance D^* , therefore $0 < D^* < D$. Figure 4.17 shows results for $D^*=0$, $0.56 \cdot D$ and D . $D^*=0.56 \cdot D$ is determined using a FE-model of the web with an indentation.

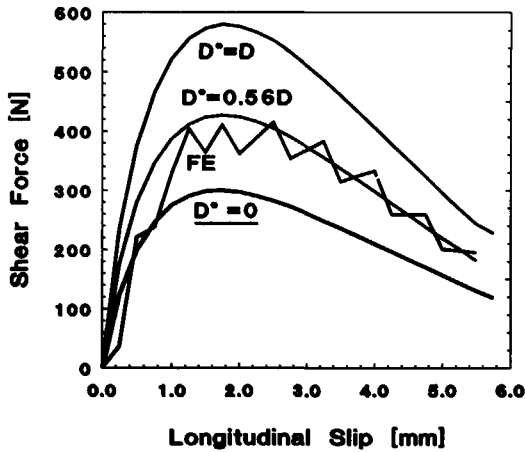


Figure 4.17: Results FE-Model and SF-model for $D^*=0/0.56 \cdot D/D$

Figure 4.17 shows the under-estimated result for $D^*=0$, the over-estimated result for $D^*=D$ and the result for $D^*=0.56 \cdot D$, which shows reasonable agreement with the FE-results.

Assumption 8: Neglecting the variation of deformation along the x-axis

In Table 5.6, displacements perpendicular to the web (u_{z1}) along the x-axis are presented. It shows that the displacement of the

Table 5.6: Displacement along x-axis

Applied slip = δ_x	1.500	3.000	4.500
$u_{z1,front-z=0}$	1.352	2.282	2.765
$u_{z1,indentation-z=0}$	1.392	2.351	2.801

indentation is only 2.5 % larger than the displacement at the front and rear section. This implies that neglecting the variation of displacements along the x-axis in the 2-D approach is reasonable for the assumed configuration.

The power of the SF-models lies in the simplicity and transparency of the solution technique. Although several simplifications were used within the SF-model the results show good agreement with FE-results. In § 7.1, a parametric study is performed using this example as the basic configuration.

4.6 Conclusions for Chapter 4

- # SF-models are based on the strict distinction between ACTION and REACTION as presented in the hypothesis. The modules are analysed separately, with tools matching the specific configuration. Possible tools are analytical solutions, simple frame analyses and simple or sophisticated FE-analyses. A general solution technique relates the modules in order to determine the behaviour of a connection. Transparency of the model and the modules is an important feature for obtaining understanding. Since nonlinear phenomena are not included, derivation of the actual behaviour of shear connections is not possible. The influence of variations of parameters on basic configurations can be investigated. (§ 4.3)
- # All nonlinear phenomena of shear connections in composite slabs can be implemented in FE-models. Due to the progressively increasing model size for increasing number of indentations, only 2-D or semi 3-D cross-sectional analyses can be performed (status: 1997). FE-models are not as transparent as SF-models. (§ 4.4)
- # With SF- and FE-models cross-sectional analyses are performed. Results are not suitable for direct implementation in small- or full-scale specimens. Recognition of areas with similar cross-sectional behaviour and combination of results for different areas is possible. (§ 4.2)
- # Combining SF- and FE-models creates a powerful tool for investigating shear connections in composite slabs. (§ 4.3-5)
- # Developments of FE-analysis allow for sophisticated parametric investigation. Understanding of the physical behaviour is essential for the development of proper FE-models and for checking FE-results.



5. EXPERIMENTS

5.0 Introduction

Three series of experiments were performed in order to validate the hypothesis and the numerical models:

Series I Validation Hypothesis (Level 1)

Series II Validation Numerical Models: Simplified shear connection (Level 1)

Series III Validation Numerical Models: Realistic shear connection (Level 2)

In § 2.6, three different levels of research are distinguished. Series I and II are Level 1 experiments. The shear connection contains only one indentation. Series III are Level 2 experiments. The connection contains about 50 indentations. The objective, the form of the specimen, the test arrangement, and the results are discussed for all Series. At the end of this chapter photographs of all series are shown.

5.1 Series I: Validation Hypothesis

Within the hypothesis, an assumption is made concerning the direction of the interaction force between indentations and concrete, first discussed in § 3.4 and illustrated in Fig. 5.1 for a circular indentation.

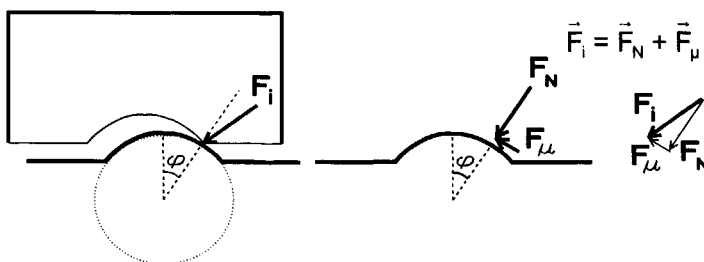


Figure 5.1: Assumption for the direction of the interaction force

It is assumed that the interaction force F_i is a summation of a normal and a

frictional component, F_N and F_μ . The normal force acts perpendicular to the surface of the indentation at the contact area. The frictional force acts perpendicular to the normal force and its direction depends on the incremental displacement of the indentation with respect to the concrete.

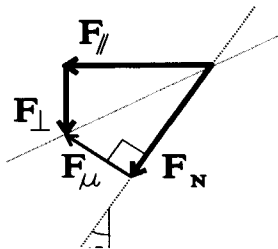
5.1.1 Objective of Series I

"Validation of the assumption concerning the direction of interaction forces between indentations and concrete, as implemented in the hypothesis"

In order to investigate the direction of the interaction force, all aspects of the shear connection, that are not directly related to the interaction force are either eliminated or simplified. The specimen corresponds to the fictitious shear connection, considered in § 3.4. With respect to the shear resistance, distinction can be made between three parts, which together determine the behaviour of the shear connection.

ACTION I	REACTION	ACTION II
<i>Interaction Forces</i>	<i>Response Sheeting</i>	<i>Displacement Indentation</i>
F_I	$= \frac{F_I}{F_\perp}$	$* \frac{F_\perp}{\delta_\perp} * \delta_\perp$

The ACTION I part deals with the direction of the interaction force. The REACTION and the ACTION II parts are simplified, as illustrated in § 5.1.2. Based on the assumption, the ACTION I part can be written as:



$$\frac{F_I}{F_\perp} = \frac{F_N \sin\phi + F_\mu \cos\phi}{F_N \cos\phi - F_\mu \sin\phi} = \frac{\tan\phi + \mu}{1 - \mu \tan\phi} \tag{5.1}$$

with: $F_\mu = \mu \cdot F_N$ (5.2)

$\mu = f(F_N)$ (5.3)

Equation (5.1) shows that the direction of the interaction force depends on the inclination of the contact area at the indentation ($\tan \phi$) and the coefficient of friction μ , which depends on the surface conditions and can be a function of F_N .

5.1.2 Specimen of Series I

Figure 5.2 shows a specimen of Series I. The appearance and dimensions of the sheeting, indentations and concrete are discussed.

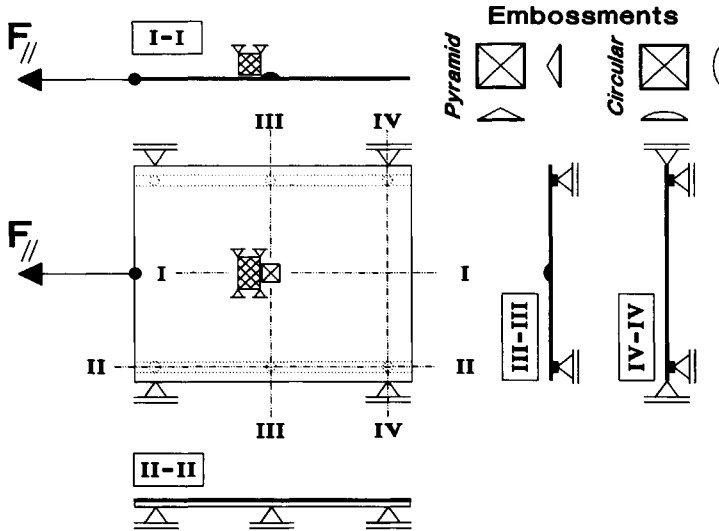


Figure 5.2: Appearance specimen Series I

Sheeting

- Flat sheeting instead of profiled sheeting was used, in order to simplify the response of the sheeting (REACTION part).
- Along both sides, hinged supports are present, using three roller-bearings. In order to prevent different vertical displacements over the bearings, prismatic beams ($b \cdot h = 10 \cdot 5$ mm) were placed between the sheeting and the bearings.
- In order to obtain reproducible experiments, linear elastic material behaviour is ensured by scaling up the dimensions of the specimen. Two pieces of sheeting were used, with a thickness of 0.75 and 1.00 mm, referred to as 075 and 100. To ensure elastic behaviour, the width of both pieces is different: $L \cdot B \cdot t = 600 \cdot 360 \cdot 0.75$ & $600 \cdot 440 \cdot 1.00$ mm
- Due to the dimensions of the specimen, rotation of the indentations during the experiments can be neglected. This eliminates two possible degrees of freedom ($\varphi_x = \varphi_y = 0$), which simplifies both the REACTION and the ACTION II part.

"Indentations"

- Only one indentation was used, in order to avoid the issue of distribution of forces over indentations.
- Pyramid and circular shaped indentations are used. The different geometry of the indentations enables investigation of the coefficient of friction.
- The indentations are made of solid steel, referred to as 'embossments', which eliminates deformation of the indentations during loading.
- Since rotation and deformation of the embossments can be neglected, the ACTION II part simplifies, and can be derived from the undeformed geometry of the embossment.
- In the specimen, the embossments are bolted to the sheeting. With 2 pieces of sheeting and 2 embossments a total of 4 specimens are achieved. Specimens containing circular embossments can be used for several experiments by adjusting the initial gap between the 'concrete' and the sheeting.

"Concrete" and Contact surface

- The concrete is replaced by a solid steel block. If concrete would have been used, the condition of the interface between the concrete and the embossment changes every time the test arrangement is used. Even small interaction forces, either smooth or rough the interfaces, which influences the coefficient of friction.

5.1.3 Test Arrangement of Series I

Figure 5.3 shows the loading and measurement arrangements.

Loading arrangement

The longitudinal shear force is applied by dead weight ($F_1=G$).

Measurements

Longitudinal slip is measured at both sides of the specimen. Vertical displacement of the sheeting is measured at four points around the embossment.

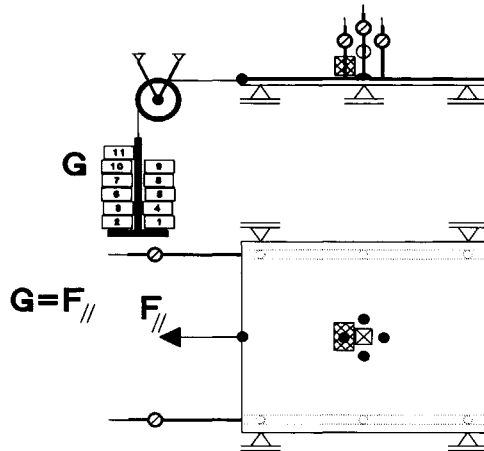


Figure 5.3: Test arrangement of specimen Series I

Prior to the actual experiment, the response of the sheeting is determined by a preliminary experiment. A vertical force (F_{\perp}) is applied directly to the embossment. A relation is obtained between the vertical force at the embossment and the vertical displacement of the sheeting ($\delta_{\perp,front}$, $\delta_{\perp,left}$, $\delta_{\perp,right}$ and $\delta_{\perp,back}$).

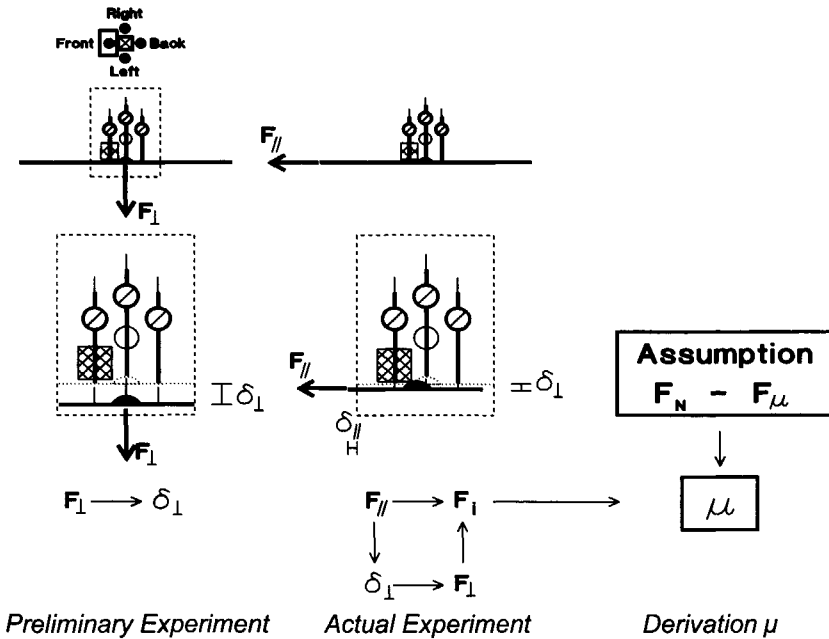


Figure 5.4: Preliminary and actual experiment and adopted procedure

After the actual experiment, the vertical component of the interaction force can be derived from the vertical displacements of the sheeting by using the results of the preliminary experiment. Once the horizontal (F_{\parallel}) and vertical component (F_{\perp}) of the interaction force (F_i) are known, the coefficient of friction can be derived from eq. (5.1), using the assumption. By performing various experiments, the assumption can be validated. The preliminary and actual experiment as well as the procedure are illustrated in Fig 5.4.

5.1.4 Results of Series I

For the two different pieces of sheeting (075 & 100), the results of the preliminary experiments (V075 & V100) are shown in Figs. 5.5 and 5.6. The vertical displacement at the front and rear of the embossment is larger than the displacement at the sides.

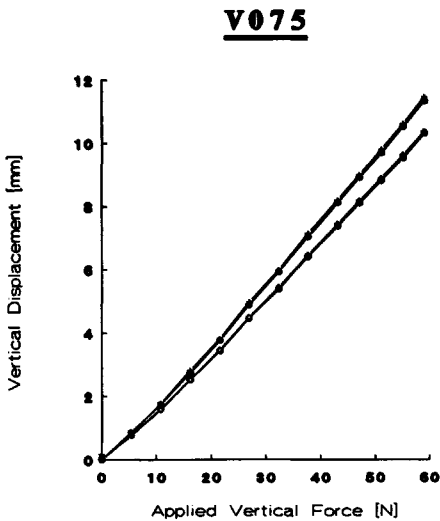


Figure 5.5: Results V075

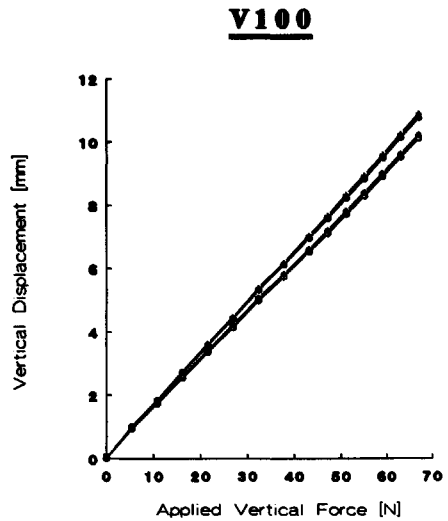


Figure 5.6: Results V100

As mentioned in § 5.1.2, various experiments can be performed with specimen containing circular embossments by adjusting the initial gap between the sheeting and the 'concrete', as illustrated in Fig. 5.7.

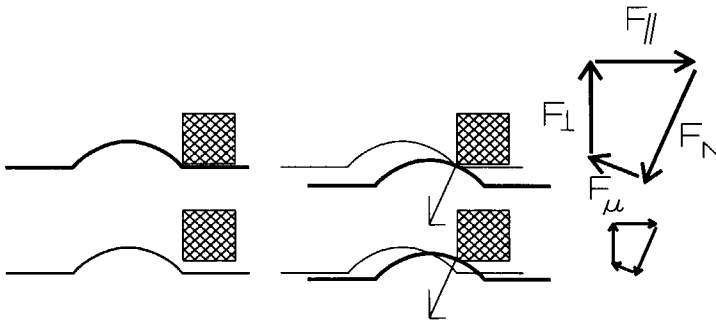


Figure 5.7: Influence of the initial gap

The influence of the initial gap on the shear resistance is illustrated in Fig. 5.8, using the visual solution method. The dotted lines in the *Part 3* and *RESULT* diagram correspond to a zero initial gap. Once longitudinal slip occurs, the embossment is pushed down immediately. The solid lines correspond to a situation with an initial gap, which is half the height of the embossment ($\delta_{\perp,0}=H/2$).

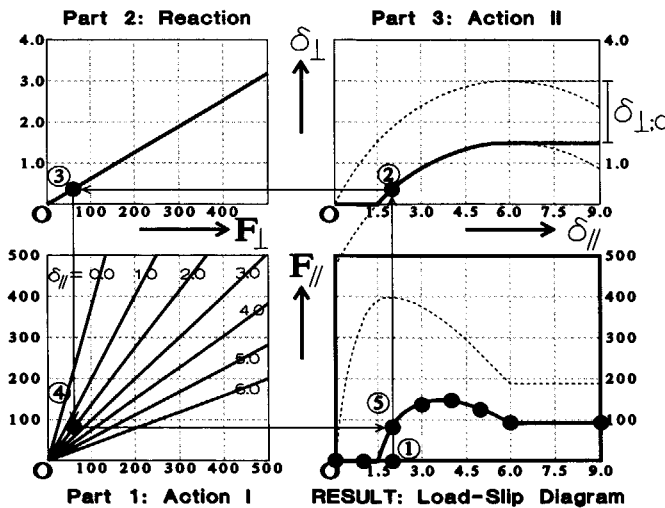


Figure 5.8: Influence initial gap on shear resistance

If a horizontal load is applied, the specimen displaces without any resistance until contact between the embossment and the 'concrete' occurs ($\delta_{\perp,0}$). The maximum vertical displacement of the embossment is reduced by the initial gap.

The inclination of the embossment at each level of slip remains the same, which implies that *Part 1* does not change. The response of the sheeting is independent of the initial gap, which implies that *Part 2* does not change. The behaviour of the shear connection with an initial gap can be determined by following the line from 1 to 5 again.

Specimen with pyramid embossments (P-Series) were released after loading. The difference between loading and reversed loading lies in the direction of the frictional force. The sign of μ in eq. (5.1) changes. For the P-Series, a value for μ is derived both for loading and unloading, referred to as a positive and negative value. Specimen with circular embossments (C-Series) were used with three different initial gaps. Results of all experiments are shown in Figs. 5.9 to 5.12 and presented in Table 5.1. The upper part of each graph, shows the applied shear force F_1 versus longitudinal slip δ_1 . A value for the coefficient of friction μ is derived at each load level and plotted in the lower part of each graph. It shows that within each experiment the coefficient of friction is consistent.

Table 5.1: Results of Series I

Experiment	Loading Direction	Dimensions of Sheeting [mm]	Type of Embossment	Initial Gap [mm]	$F_{1,MAX}$ [N]	Average μ [-]
V075	Vertical	360*600*0.75	Pyramid	-		-
P075	Shear + Shear -	360*600*0.75	Pyramid	2.584		+0.355 -0.247
C075-I	Shear	360*600*0.75	Circular	0.500	23.9	0.157
C075-II	Shear	360*600*0.75	Circular	1.382	19.9	0.130
C075-III	Shear	360*600*0.75	Circular	2.329	19.9	0.185
V100	Vertical	440*600*1.00	Pyramid	-		-
P100	Shear + Shear -	440*600*1.00	Pyramid	1.488		+0.186 -0.126
C100-I	Shear	440*600*1.00	Circular	0.703	28.7	0.137
C100-II	Shear	440*600*1.00	Circular	1.710	24.7	0.134
C100-III	Shear	440*600*1.00	Circular	4.883	12.0	0.166

P075

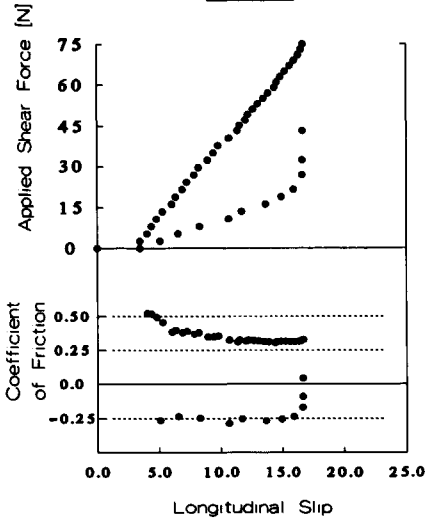


Figure 5.9: Results of P075

C075

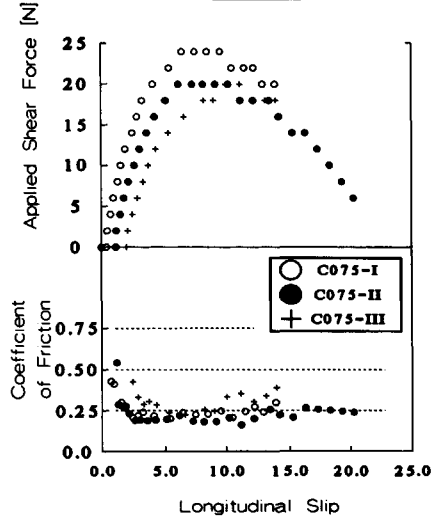


Figure 5.10: Results of C075

P100

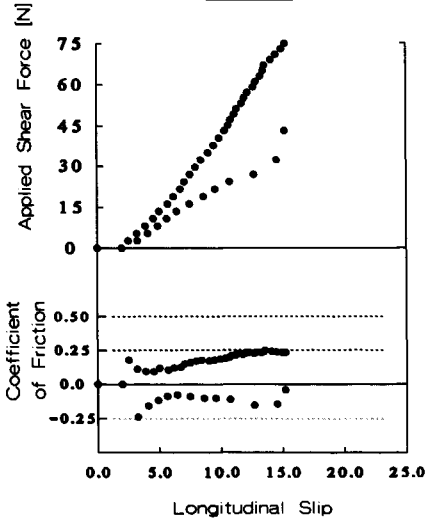


Figure 5.11: Results of P100

C100

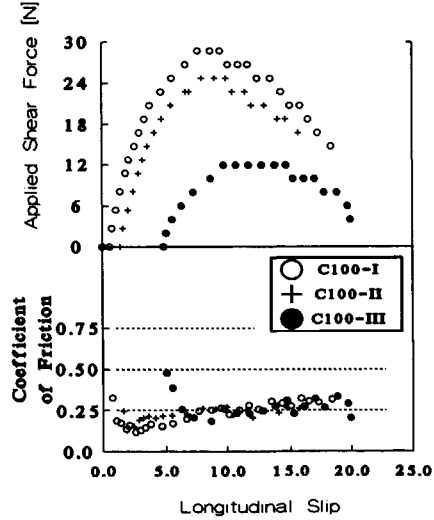


Figure 5.12: Results of C100

5.2 Series II: Simplified Shear Connection (Level 1)

The hypothesis concerning the behaviour of shear connections is based on the distinction of an ACTION and a REACTION part. The response of the sheeting to the over-riding of indentations by the concrete is a combination of vertical separation between sheeting and concrete and deformation of sheeting, as shown in Fig. 5.13 for two trapezoidal profiles. The ratio between separation and deformation determines the characteristics of the connection.

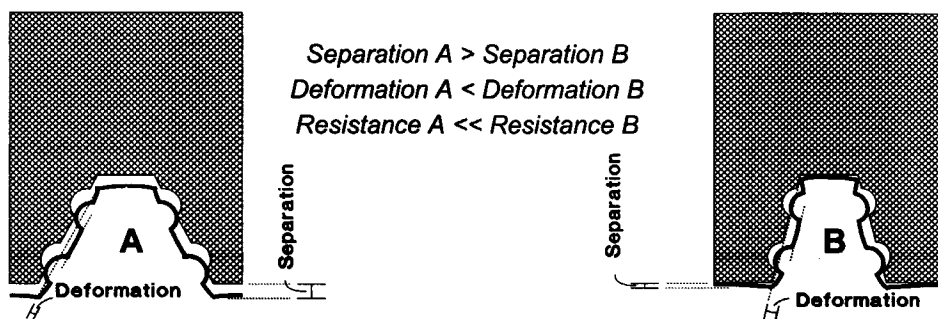


Figure 5.13: Response of the sheeting: Vertical Separation and Deformation

5.2.1 Objective of Series II

" Providing experimental data for a simplified shear connection, in order to support and validate both the hypothesis and the numerical models. "

Both existing design methods require full-scale experiments (Level 3). With this Series, the possibilities and limitations of Level 1 experiments are evaluated. A simplified connection is considered in order to investigate phenomena of shear connections in composite slabs, displacement and deformation of sheeting separately, which is not possible if realistic shear connections are considered.

5.2.2 Specimen of Series II

Figure 5.14 shows a specimen of Series II. Similar to Series I, the form and dimensions of the sheeting, indentation and concrete are discussed.

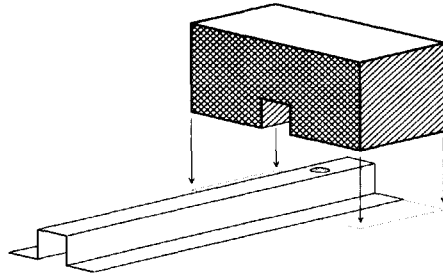


Figure 5.14: Appearance specimen of Series II

Sheeting

Figure 5.15 shows the geometry and dimensions of the profiled sheeting. Due to the vertical webs and the location of the indentation in the top flange, there is no resistance to vertical separation within the cross-section of specimen II. Vertical separation is prevented by external supports at the bottom flange. The support reactions are measured. By avoiding internal balancing of vertical forces, the vertical component of the interaction force at the indentation can be measured. Equilibrium of forces in the cross-sections of trapezoidal and re-entrant profiles and the considered specimen is illustrated in Fig. 5.16.

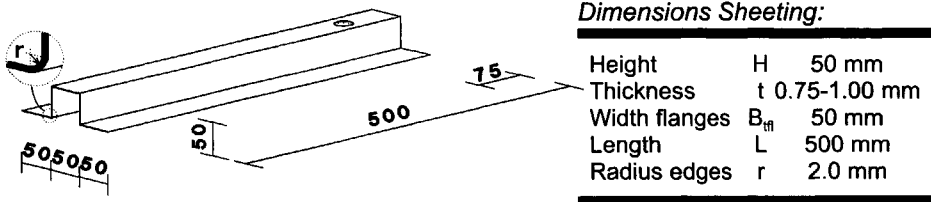


Figure 5.15: Dimensions sheeting

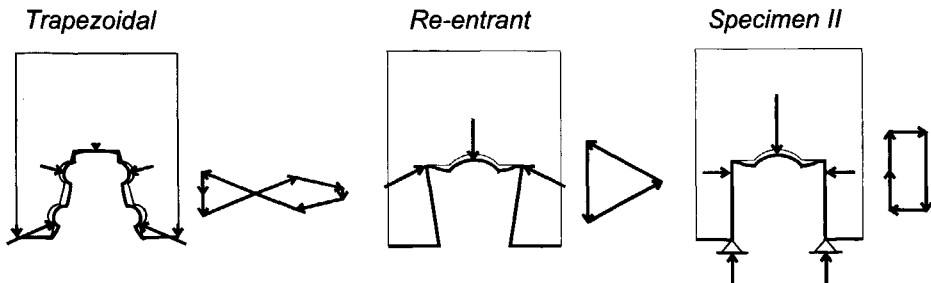


Figure 5.16: Equilibrium of forces in the cross-section of the sheeting

The thickness of the sheeting was varied: 0.75 and 1.00 mm. Two specimens of each thickness were available. The length of the sheeting is large compared to the cross-sectional parameters, in order to avoid affecting of the stress distribution at the indentation by the applied load. The load is applied to the top flange. The interaction force between the concrete and the sheeting also acts in the plane of the top flange. The eccentricity of these forces cause bending moments in the sheeting. Since only one indentation is present, axial stresses remain small.

Material properties are determined in two directions: parallel and perpendicular to the longitudinal direction of the sheeting in the specimen. Material properties are presented in Table 5.2. The properties referred to as 'perpendicular' correspond to the main direction of the coil of the sheeting.

Table 5.2: Material Properties of Series II: Sheeting

Thickness <i>s</i> [mm]	Direction [-]	E-modulus [N/mm ²]	Yield stress f_{yd} [N/mm ²]	Ultimate stress f_u [N/mm ²]
0.75	Parallel	213.969	341.0	376.4
	Perpendicular	193.218	315.5	378.2
1.00	Parallel	224.202	384.6	404.6
	Perpendicular	203.594	370.0	410.4

Indentations

Similar to Series I, only one indentation is present, in order to avoid the issue of distribution of forces over indentations. The circular indentation was added to the sheeting before it was folded to its final shape, using a set-up as shown in Fig. 5.17. A vertical force F_V is applied to a massive steel ball, which is guided vertically and centred above a steel ring. The sheeting is placed between the ball and the ring. The dimensions of the indentations are determined by the radius of the ball, the shape of the ring and the elastic relief of the indentation after unloading. For each thickness, the required vertical force is determined by trial and error ($F_{V,0.75}$ & $F_{V,1.00}$).

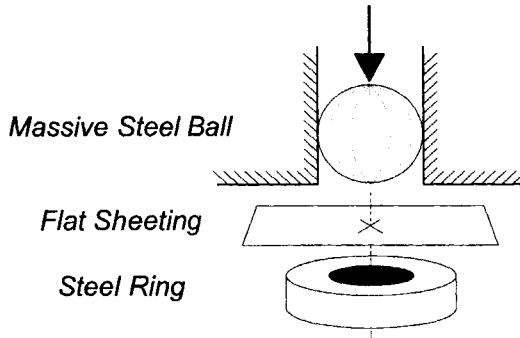


Figure 5.17: Set-up for applying indentations to the sheeting

The dimensions of the indentations are given in Fig. 5.18. The method of applying indentations to flat sheeting is checked by an FE-model. The elastic relief after unloading is less than 1 % for both types of sheeting. The empirically derived vertical forces agree with the FE-results. FE-results and visual inspection of the indentations confirm that sheeting is pushed into the ring as shown in Fig. 5.18. The inclination of the inner edge of the ring corresponds to the inclination of the indentation at the toe ($\tan \varphi_0$). Therefore, the diameter of the indentation corresponds to D_{Ring} . The height of the indentation is determined by the radius of the ball R_{Ball} and D_{Ring} . Elastic relief is included by increasing R_{Ball} with 1 %.

$$\left(R_{Ball} - H\right)^2 + \left(\frac{D_{Ring}}{2}\right)^2 = R_{Ball}^2 \Rightarrow H = R_{Ball} - \sqrt{R_{Ball}^2 - \frac{D_{Ring}^2}{4}} \quad (5.4)$$

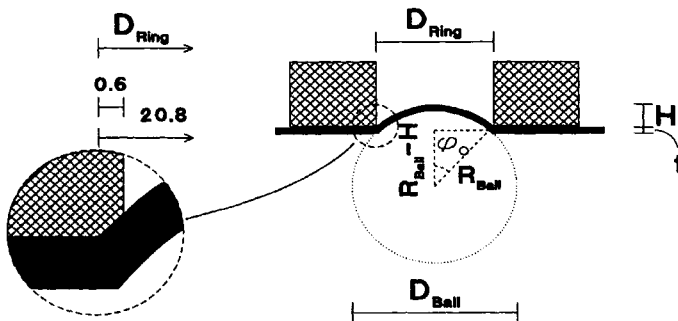


Figure 5.18: Dimensions indentations

Dimensions of the sheeting, ball and ring

Thickness	t	$= 0.75/1.00$ mm
Radius Ball	R_{ball}	$= 15.0$ mm
Diameter Ring	D_{Ring}	$= 20.8$ mm
	R_{Ring}	$= D_{ring}/2$
		$= 10.4$ mm
Applied Force	$F_{V,075/100}$	$= 10.0/18.0$ kN

Dimensions of the indentation

Diameter	D	$= D_{Ring} = 20.8$ mm
Radius	R	$= 101\% * R_{Ball}$
		$= 15.15$ mm
Height	H	$= 4.134$ mm
Inclination toe	$\tan \varphi_0$	$= R_{Ring}/(R_{Ball}-H)$
		$= 0.944$ -

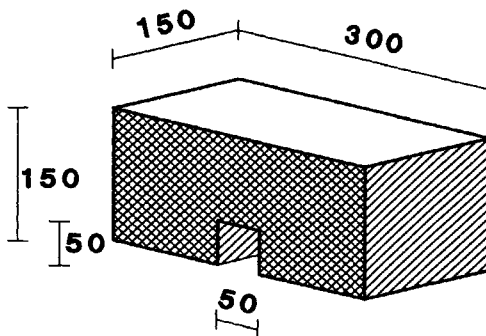
Indentations are applied by plastic deformation of the sheeting. If no material is pulled over the edges of the ring, the thickness of the sheeting in the indentation is reduced corresponding to the increased surface area of the indentation with respect to the flat sheeting.

$$\frac{A_{\text{Indentaion}}}{A_{\text{Sheeting}}} = \frac{2\pi RH}{\pi R_{Ring}^2} = \frac{393.5}{339.8} = 1.158 \Rightarrow t_{\text{Indentation}} = \frac{t_{\text{Sheeting}}}{1.158} \quad (5.5)$$

In general, the yield stress of sheeting increases due to plastic deformation. Due to severe plastic deformation, the yield stress is increased at the toe of the indentations. At the indentation itself the yield stress is hardly influenced, due to the large ratio between the radius and thickness of the indentation [10].

Concrete and Contact Surface

In order to minimize deformation of the concrete, high strength concrete was used. The dimensions of the concrete block are dictated by practical boundary conditions. Dimensions and material properties of the concrete are given in Fig. 5.19.



Dimensions Concrete Block

Length	L_c	$= 150$ mm
Width	B_c	$= 300$ mm
Height	H_c	$= 150$ mm

Material properties after 28 days

Strength	f_c	$= 74.66$ N/mm ²
E-modulus	E_c	$= 41.333$ N/mm ²

Figure 5.19: Dimensions Concrete Block

The specimen are loaded until the indentation is pushed out of the concrete

completely. Reversed loading returns the sheeting to its original position. Unlike Series I, the contact surface changes during the experiment. Deformation of concrete occurs. The condition of the concrete and steel surface, and therefore the condition of the contact surface changes, which implies that values of the coefficient of friction found for loading and reversed loading are not necessarily equal.

5.2.3 Test Arrangement of Series II

The specimen is placed vertically to enable visual inspection of the top flange and to improve the accessibility of the top flange for the measurement arrangement. Successively the boundary conditions, the loading arrangement and the measurements are discussed.

Boundary Conditions

Boundary conditions are applied to the specimen at the loading end, the bottom flange and the concrete. All boundary conditions are illustrated in Fig. 5.20. The load is applied at the top flange of the sheeting. Apart from the applied slip, the lateral displacements is prevented.

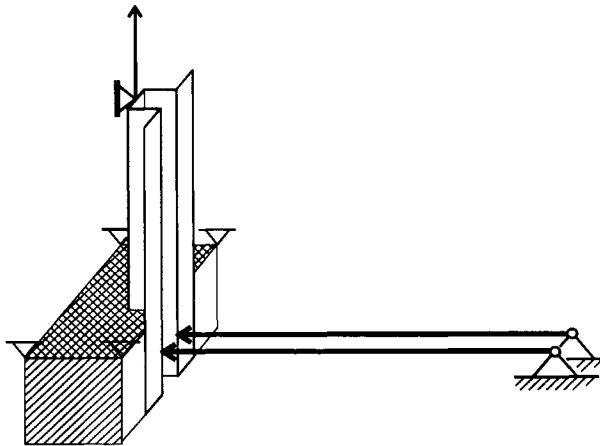


Figure 5.20: Boundary conditions Specimen II

Due to the absence of resistance to vertical separation in the cross-section, lateral supports are required, as justified in § 5.2.2. Lateral supports can be

displacement or force controlled, or a combination of both, respectively by using sliders, dead weight or springs. The objective of the lateral supports is to measure the support reaction and to control both the displacements and forces at the bottom flanges of the sheeting. The lateral supports are carried out as alternative sliders, as shown in Fig. 5.21.

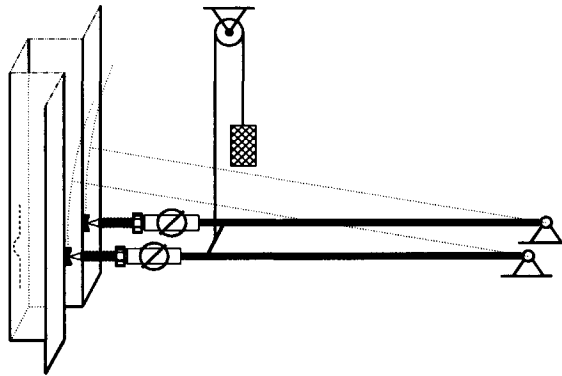


Figure 5.21: Lateral supports bottom flange

Regular sliders have two disadvantages: friction introduces longitudinal forces and measurement of the support reaction is difficult. The alternative sliders avoid these problems. The beams with hinges at both ends do not prevent the lateral displacement of the bottom flanges over the full range of slip. However, the lateral displacement caused by the described circles is known and minimized by using long beams. Dead weight of the beams is balanced. The beams contain load cells and threaded bars which makes it possible to apply prestress to the beams. At the start of experiments, each beam is prestressed by a force of 250 N. This force ensures contact between the sheeting and the concrete. The contact forces, caused by the prestressing force contribute to the shear resistance via friction.

The concrete block is fixed to the testing frame by two sets of U-beams and threaded bars, as shown in Fig. 5.22. The concrete was protected by thin layers of rubber, in order to prevent splitting of the concrete due to the clamping forces. The fixation of the concrete appeared to be unsatisfactory. In § 5.2.4 it is shown that separation occurred between the concrete and the sheeting, caused by displacement of the concrete block with respect to the testing frame.

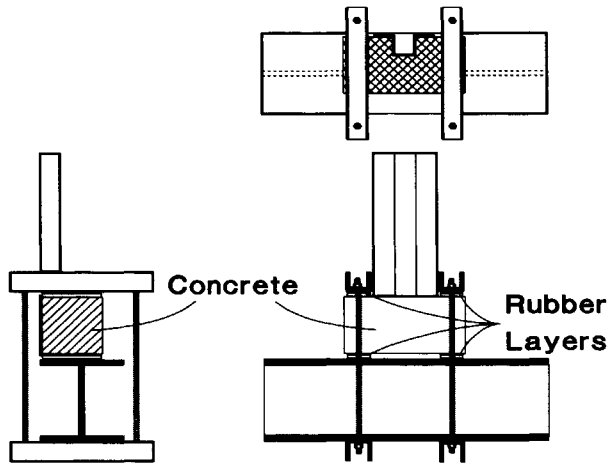


Figure 5.22: Fixation concrete block to testing frame

Loading Arrangement

The load is applied displacement controlled by hand. The loading arrangement is shown in Fig. 5.23. A threaded bar with a fine pitch is placed between the testing frame and a load cell, which is connected to the sheeting. The bar is guided by a steel plate, which provides the boundary conditions at the loading end of the sheeting. By using two nuts, the sheeting can either be pulled up or pushed down. The loading arrangement is simple and appeared to be satisfactory. Friction between the nuts and the bar could cause rotation of the sheeting. This effect can be avoided by minimizing friction or by placing a rotational weak element between the loading arrangement and the sheeting.

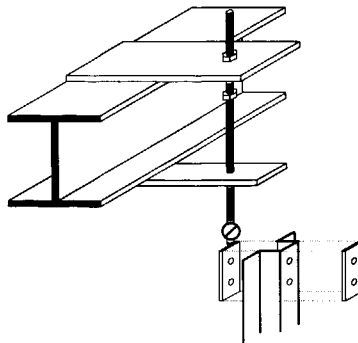


Figure 5.23: Loading arrangement

Measurements

Eleven measurements are taken from the specimen. All measurements but 10 & 11 are recorded electronically. Figure 5.24 shows half of the specimen. The missing measurements 3, 5 & 11 are taken from the other half of the specimen.

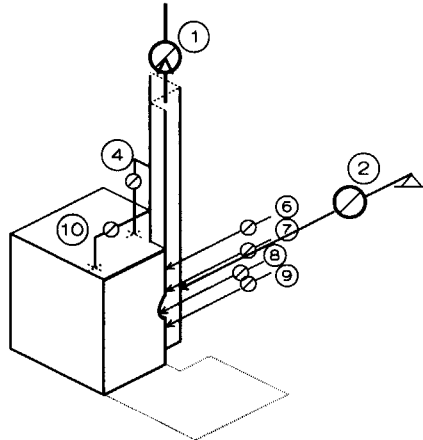


Figure 5.24: Measurements Specimen II

- 1 Applied Load; A load cell is placed between the threaded bar and the sheeting.
- 2 & 3 Lateral Support Reaction; Load cells are placed in both lateral support beams.
- 4 & 5 Longitudinal Slip; In both corners of the top flange slip between the concrete and the sheeting is measured just above the concrete block.
- 6 to 9 Lateral displacement; The displacement of the centerline of the top flange is measured at four locations. The appearance of the measurement arrangement for 6 to 9 is similar to the appearance of the lateral support beams. Since access to the top flange is limited, transducers are placed 750 mm away from the flange. Screws are glued to the sheeting and connected to the transducers via thin beams and fork heads. These beams also describe circles. The results are corrected according to the recorded level of slip.
- 10 & 11 Unexpected separation between concrete and sheeting occurred. The separation exceeds the separation caused by the described circles of the support beams. The last three experiments contained analogue measurements to record the separation.

5.2.4 Results of Series II

Results of all experiments (075-I, 075-II, 100-I, 100-II) are presented in graphs which contain two figures to clarify the contents. The upper figure shows the considered specimen schematically. The lower figure shows the measurements.

General Results

Figures 5.25 and 5.26 show the applied shear force and the lateral support reaction of all specimen.

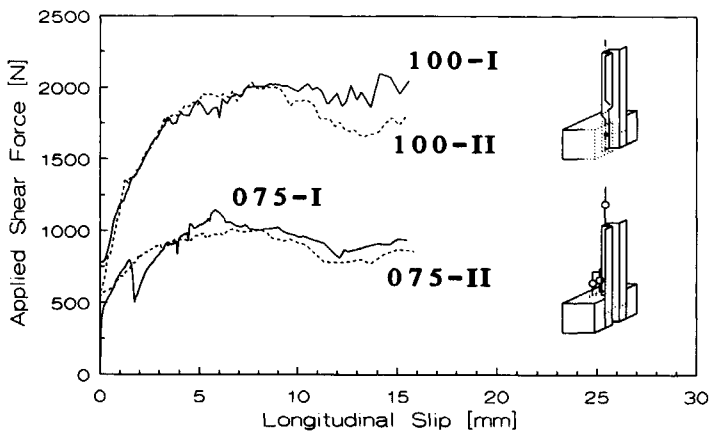


Figure 5.25: General Results: Applied shear force

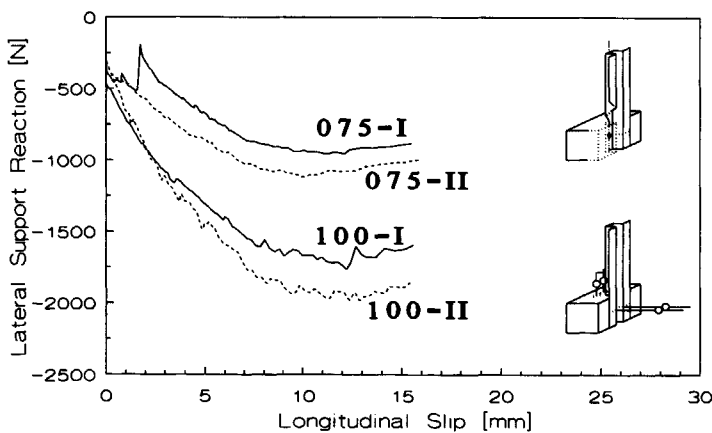


Figure 5.26: General Results: Lateral support reaction

During the first experiment (075-I), unexpected separation between the sheeting and concrete occurred. The experiment was stopped temporarily, which caused relaxation of the applied shear force and the lateral support reaction. For the remaining specimen the separation was measured. The separation was caused by a displacement of the concrete block with respect to the sheeting.

Specimen 075-I, 075-II, 100-I & 100-II

Results of all specimen are plotted in Figs. 5.28 to 5.31, each consisting of 3 graphs. Graphs *a* show the applied shear force and the lateral support reaction. Graphs *b* show the displacement of the top flange ($\delta_{\perp;F}$, $\delta_{\perp;FT}$, $\delta_{\perp;C}$ & $\delta_{\perp;B}$). Four measurements are taken, since the indentation rotates during the experiments. For specimen 075-II, 100-I and 100-II graphs *c* show the separation and the lateral support reaction.

Graphs 5.28a to 5.31a

- 1 - The applied slip ensures that indentations are pushed out of the concrete completely: $\delta_{I;MAX} \approx 20.0 \text{ mm} > D/2 = 10.4 \text{ mm}$.
- 2 - The lateral support reaction for loading and reversed loading is different, which implies that plastic deformation occurred during loading.
- 3 - For large values of slip ($\delta_1 > D/2$) the ratio between F_1 and F_{\perp} is almost 1, which can not be explained by dry friction. Due to the deformation of concrete, the indentations are not completely pushed out of the concrete. Furthermore, frictional forces between the webs and the concrete contribute to the shear resistance.
- 4 - If the sheeting is pushed back, the direction of frictional forces changes. Apart from the coefficient of friction, which is influenced by the surface conditions, the shear resistance for reversed loading equals the resistance for loading until the indentation re-enters the concrete. This phenomenon is checked by changing the direction of the slip several times before the indentation re-enters the concrete. Figures 5.30a & 5.31a show that the resistance slightly increases when the direction of the slip is changed. This implies that the contact surface becomes more rough, hence the coefficient of friction increases every time the indentation passes. This effect is also observed during the friction test (§ 5.2.5).
- 5 - If the indentation re-enters the concrete, the sign of the frictional component of the interaction force is changed. Figure 5.27 shows equilibrium of forces for loading (5.27a) and reversed loading (5.27b & c).

When elastic behaviour is considered (5.27b), the vertical component of the interaction force (F_{\perp}) for loading and reversed loading is equal. Equilibrium of forces shows that the applied shear force (F_{\parallel}) reduces, and can become negative. If the sheeting is deformed plastically during loading (5.27c), the vertical component of the interaction force for reversed loading reduces ($F_{\perp}^* < F_{\perp}$), which further reduces the applied shear force.

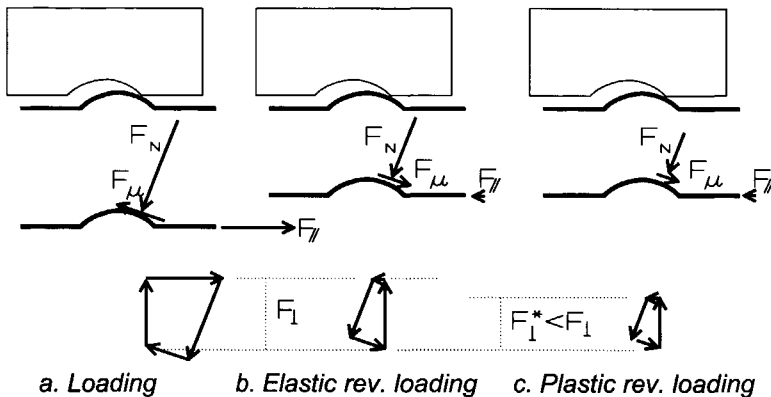
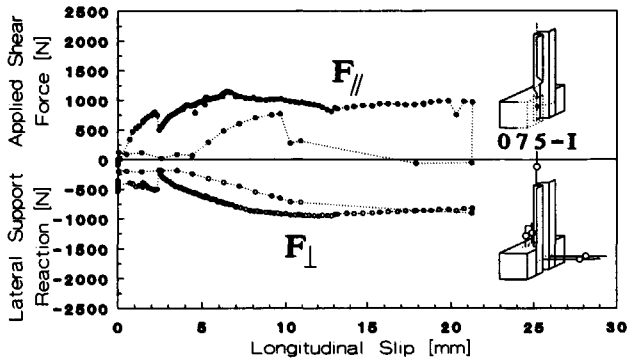


Figure 5.27: Equilibrium of forces for loading & reversed loading

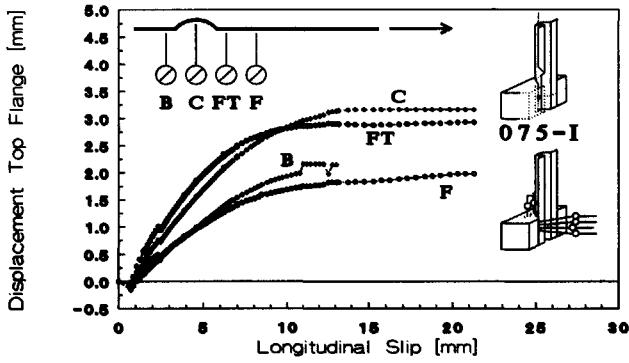
- 6 - Results of 075-I show that relaxation of the lateral support reaction affects the behaviour for reversed loading.

Graphs 5.28b to 5.31b

- 1 - It shows that once the indentation is pushed out of the concrete ($\delta_{\perp} > D/2$), the deformation of the top flange no longer changes.
- 2 - For small values of slip, the indentations rotate ($\delta_{\perp;FT} > \delta_{\perp;C} > \delta_{\perp;B}$). For larger values of slip, the rotation reduces and the displacement $\delta_{\perp;C}$ increases and becomes larger than $\delta_{\perp;FT}$ and $\delta_{\perp;B}$, which implies that plastic deformation of the indentation occurred.
- 3 - For specimen 100-I, the deformation of the top flange is illustrated in Fig. 5.32 for two levels of slip ($\delta_{\perp} = 3.0$ & 15.0 mm). The sections between points F, FT, C and B are assumed to be undeformed. The deformed shape shows the rotation of the indentation and the penetration of the indentation into the concrete. This implies that either the indentation deforms or the concrete is damaged. Both damage to the concrete and plastic deformation of the top flange and the indentation is observed.

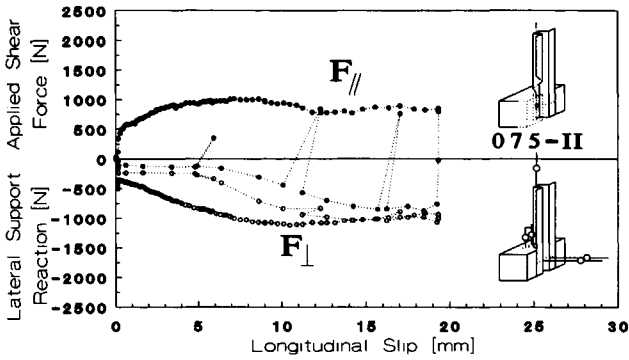


a. Applied shear force and lateral support reaction versus slip

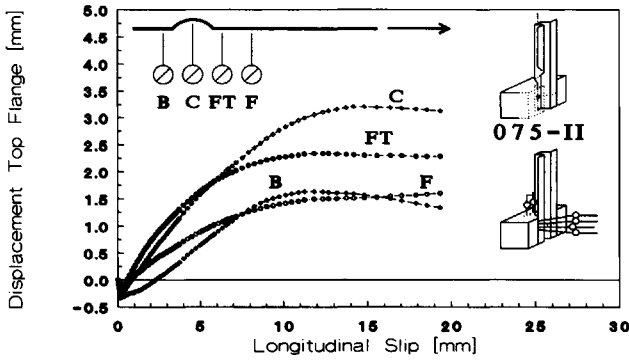


b. Displacement of the top flange versus slip

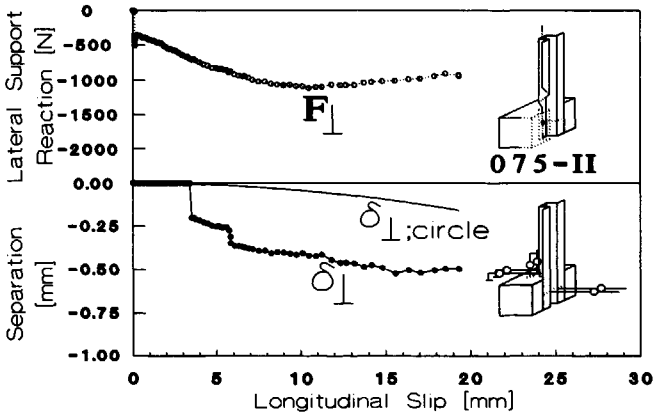
Figure 5.28: Results of Specimen 075-I



a. Applied shear force and lateral support reaction versus slip

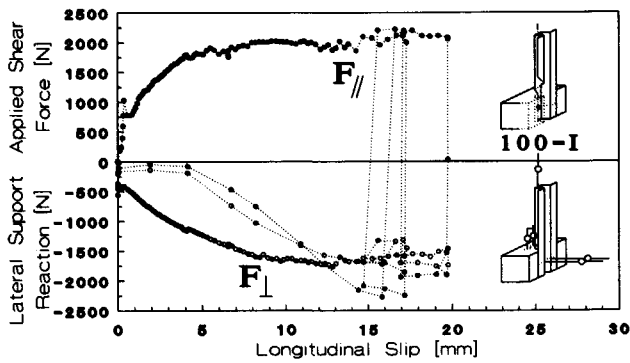


b. Displacement of the top flange versus slip

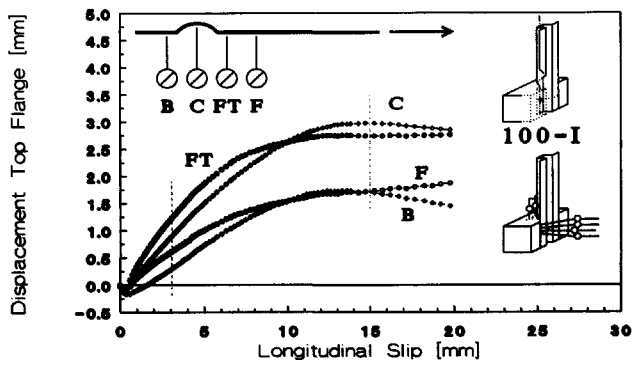


c. Separation and lateral support reaction versus slip

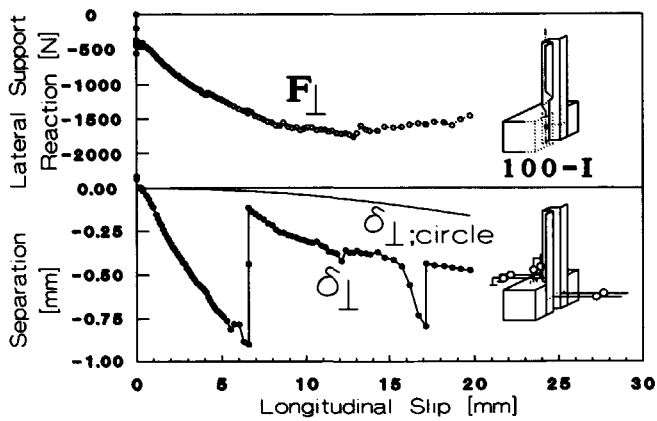
Figure 5.29: Results of specimen 075-II



a. Applied shear force and lateral support reaction versus slip

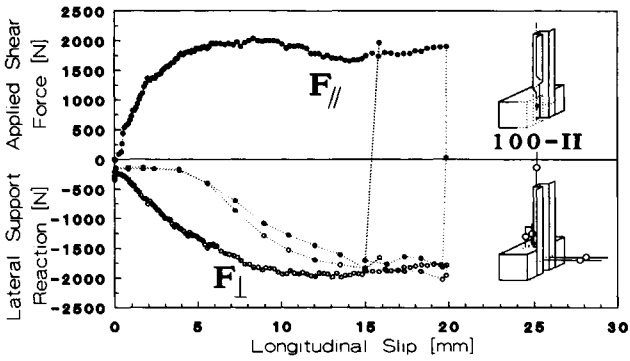


b. Displacement of the top flange versus slip

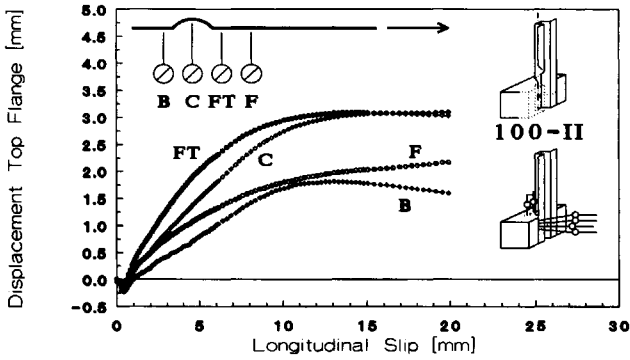


c. Separation and lateral support reaction versus slip

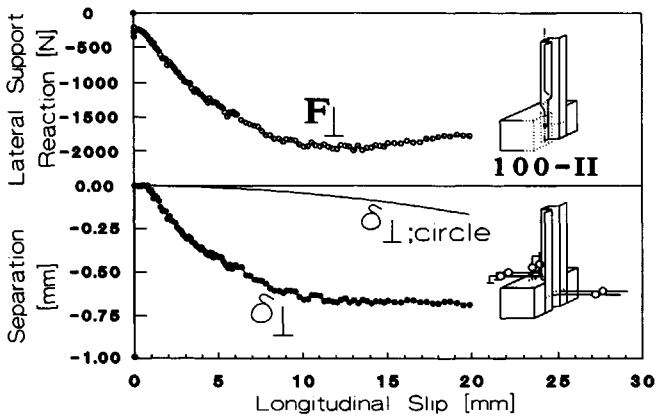
Figure 5.30: Results of specimen 100-I



a. Applied shear force and lateral support reaction versus slip



b. Displacement of the top flange versus slip



c. Separation and lateral support reaction versus slip

Figure 5.31: Results of specimen 100-II

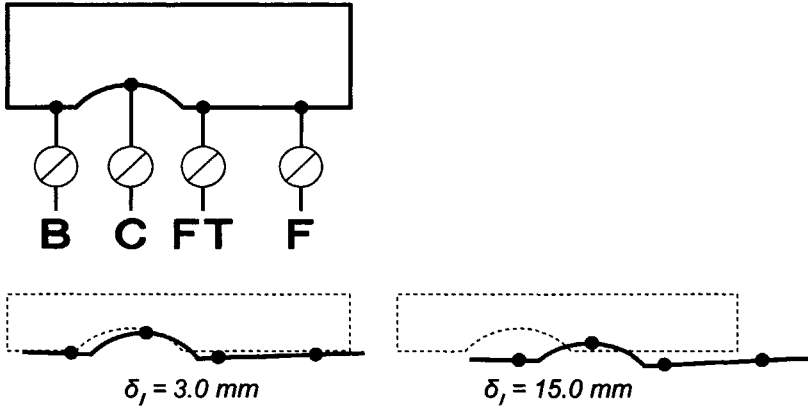


Figure 5.32: Deformation top flange for two levels of slip

- 4 - In all cases, $\delta_{\perp,F}$ is much smaller than $\delta_{\perp,C}$, so deformation of the top flange concentrates at the indentation.
- 5 - Figure 5.33 shows the graph of Fig. 5.30b including reversed loading. When the sheeting is pushed back completely, all points show significant plastic deformation. This confirms that both the indentation and the top flange deform plastically. The plastic deformation of $\delta_{\perp,C}$ remains larger than $\delta_{\perp,FT}$ and $\delta_{\perp,B}$, which proves that the indentation itself deforms plastically.

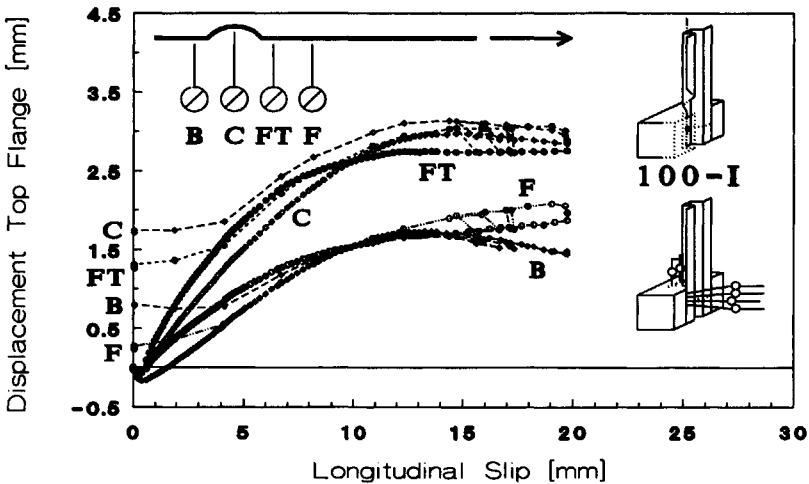


Figure 5.33: Displacement of the top flange including reversed loading

- 6 - Prior to the experiment, the sheeting was taken from the concrete in order to inspect the contact surface. Figure 5.34 shows the graph of Fig. 5.30b for small values of slip. In all cases, the displacements prove that the sheeting was not replaced to its original position. Fig. 5.34 shows that the sheeting was replaced too low. For small values of slip, this results in negative displacements.

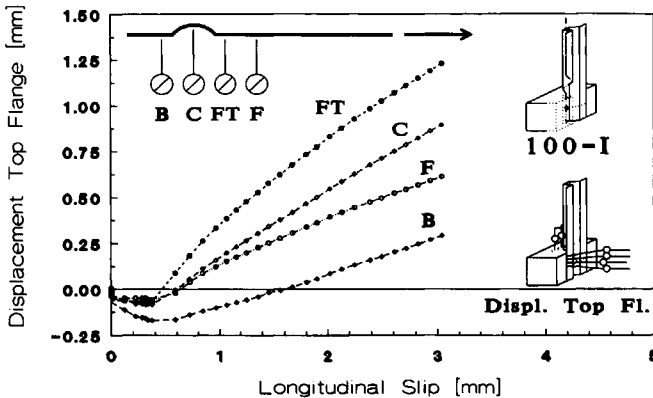


Figure 5.34: Displacement top flange for small values of slip

Graphs 5.29c to 5.31c

- 1 - For specimen 075-I, the separation is not measured.
- 2 - For specimen 100-I, an adjustment of the measurement of the separation was necessary. This did not affect the accuracy of the results.
- 3 - Graphs c show the lateral support reaction F_{\perp} , separation δ_{\perp} and separation caused by the lateral support beam $\delta_{\perp;circle}$. It shows that the separation is almost proportional to the lateral support reaction.
- 4 - Most likely, the separation is caused by the rubber layers between the concrete and the testing frame. The fact that the relation between the lateral support reaction and the separation is almost proportional, supports the assumption that separation is caused by displacement of the concrete with respect to the testing frame. A virtual stiffness of the lateral supports, k_{Sep} , can be calculated by relating the lateral force to the separation, as shown in eq. (5.6).

$$k_{Sep} = \frac{F_{\perp} - F_{\perp;0}}{\delta_{\perp} - \delta_{\perp;circle}} \quad (5.6)$$

In order to determine k_{Sep} , both F_{\perp} and δ_{\perp} are corrected. F_{\perp} is reduced by $F_{\perp,0}$ which is the applied prestress to the lateral supports. The influence of $F_{\perp,0}$ occurs before the actual experiment and therefore does not influence the virtual stiffness k_{Sep} . δ_{\perp} is reduced with $\delta_{\perp,circle}$, which is the separation caused by the lateral support. For 075-II, 100-I and 100-II, k_{Sep} is determined for all measurements. The virtual stiffness is plotted in Fig. 5.35 and presented in Table 5.3.

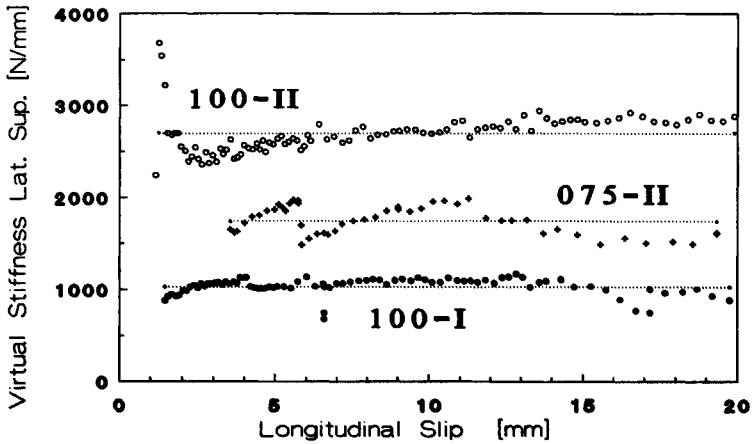


Figure 5.35: Virtual stiffness of the lateral support

k_{Sep} is almost constant for each specimen. The fact that no consistency is found between average values for k_{Sep} supports the idea that k_{Sep} depends on the test arrangement rather than the specimen. The rubber layers and the clamping forces determine the virtual stiffness of the lateral supports, k_{Sep} .

Table 5.3: Virtual stiffness of the lateral support

Specimen	Average value k_{Sep} [N/mm]
075-I	-
075-II	1744
100-I	1029
100-II	2698

5.2.5 Friction Test

After the experiments 075-I to 100-II, a friction test was performed to investigate the coefficient of friction. The test arrangement of Series II was used for a friction test, as shown in Fig. 5.36. The profiled sheeting is replaced by flat sheeting. The lateral force F_{\perp} is applied by the lateral support beams. Longitudinal slip is applied and the shear force F_{\parallel} is measured. The coefficient of friction is calculated from F_{\perp} and F_{\parallel} .

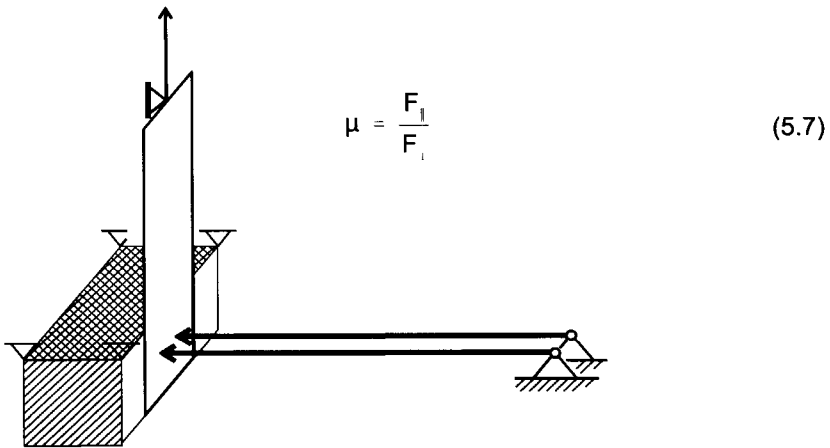


Figure 5.36: Test arrangement friction test

Within the original specimen, apart from a small area around the indentation in the top flange, the sheeting was oiled before the concrete was placed, as shown in Fig. 5.37. Therefore the surface conditions between the flat sheeting and the concrete in the friction test (Area 2) differs from the conditions between the indentation and the concrete in the original experiments (Area 1). Oiling the sheeting was done for two reasons:

- 1 - *Avoiding chemical bond*

The required shear force necessary to break down chemical bond between the sheeting and the concrete is higher than the shear capacity of a connection with only one indentation. The sudden breakdown of chemical bond would influence the conditions of the connection.

- 2 - *Visual inspection of the contact surface*

Inspection of the contact surface was desirable. By oiling the sheeting, the sheeting could be easily taken from the concrete.

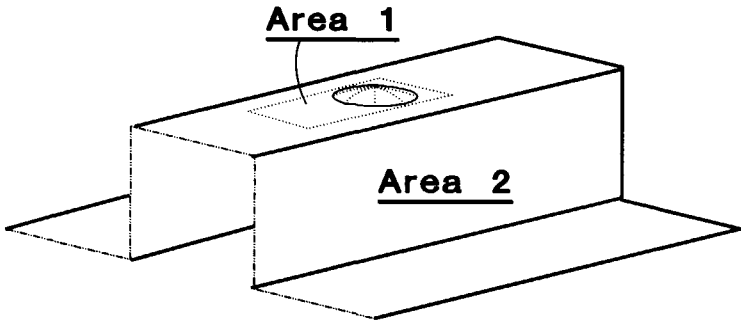


Figure 5.37: Different surface conditions

The visual inspection showed that the oiled areas of the sheeting remained greasy (Area 2). The opposite concrete areas were perfectly flat. At the indentation, some cement paste was stuck to the sheeting (Area 1). The opposite concrete surface was rough due to the absence of the cement paste. Different coefficients of friction can be expected for both surface conditions.

During the test, the flat sheeting was displaced up and down. Two parameters were varied within the test: the lateral force and the range of the applied slip. By increasing the slip range during the experiment, a certain length of the connection was loaded for the first time, whereas other parts were previously loaded. Figure 5.38 shows the results of about 300 measurements. Four levels of lateral force were applied (500, 1000, 1500 & 500 N). Ten cycles of slip were applied, which implies that the contact area passed the origin 20 times. The slip range was increased from ± 2.5 to ± 7.5 mm. The upper part of Fig. 5.38 shows the derived coefficient of friction for each measurement. The lower part shows the corresponding level of slip.

Some observations can be made from Fig. 5.38:

- 1 - The coefficient of friction is different for positive and negative slip rates.
- 2 - The coefficient of friction increases during the experiment, which implies that the number of cycles influences the characteristics of the connection.
- 3 - Within one half cycle the coefficient of friction reaches a maximum when

the origin is passed, which implies that the coefficient of friction is higher if the contact surface is previously loaded.

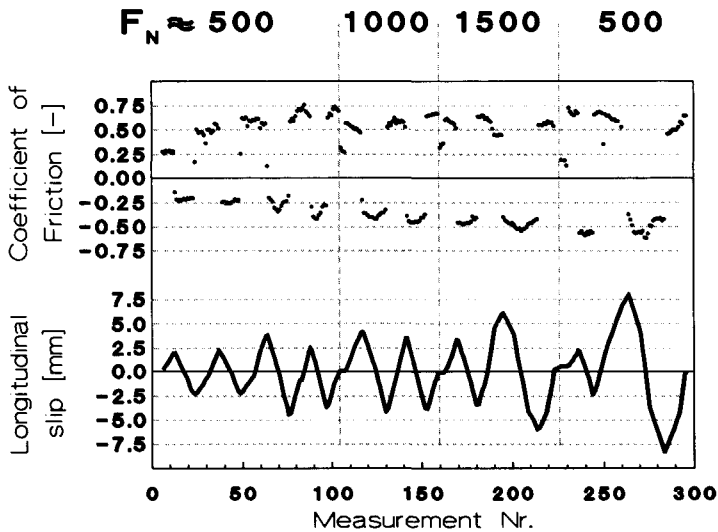


Figure 5.38: Results Friction Test: Slip and Coefficient of Friction

A physical explanation for the different behaviour in different directions can be found in the production method of the sheeting or the difference between pulling and pushing in the test arrangement. The results of this friction test prove that determination of the coefficient of friction is difficult. It also shows that even if surface conditions of a shear connection are identical, different results are obtained with respect to the coefficient of friction. Determination of the coefficient of friction is difficult, and results can only be used as a guidance for similar cases.

5.3 Series III: Realistic Shear Connection (Level 2)

As part of the development of a new type of profiled sheeting, a series of 24 detailed experiments was performed at TNO Building and Construction Research. Apart from the measurements required to determine the shear characteristics of the connection, additional measurements were taken to record the separation and deformation of the sheeting.

5.3.1 Objective of Series III

" Providing experimental data for realistic shear connections, in order to validate the numerical models "

5.3.2 Specimen of Series III

Figure 5.39 shows a typical test specimen. All test specimens were supplied by the manufacturer. One rib of sheeting is tested. Over the length of the concrete block, the sheeting contained 46 indentations. Reinforcement bars were placed in the concrete. The bars were located in the plane of the neutral axis of the sheeting.

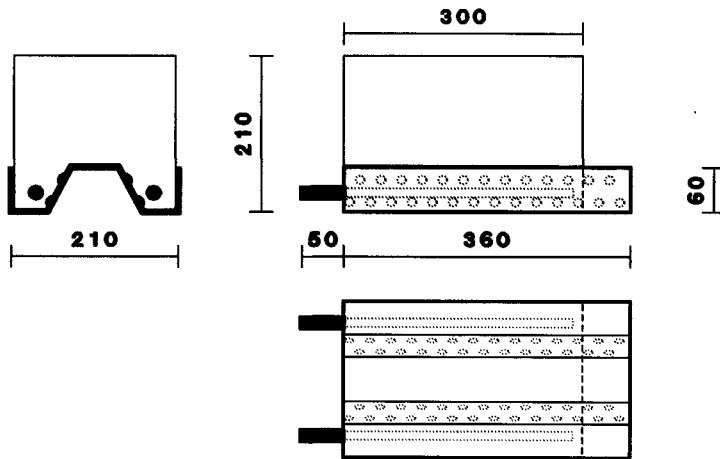


Figure 5.39: Appearance specimen Series III

Four different types of sheeting (I to IV) and two different types of indentations (B(ig) & S(mall)) were tested. For each combination 3 specimens were available. The different types of sheeting are shown in Fig. 5.40. Although not developed for that purpose, the different types of sheeting enable investigation of the ratio between deformation and separation, since the resistance to vertical separation differs significantly.

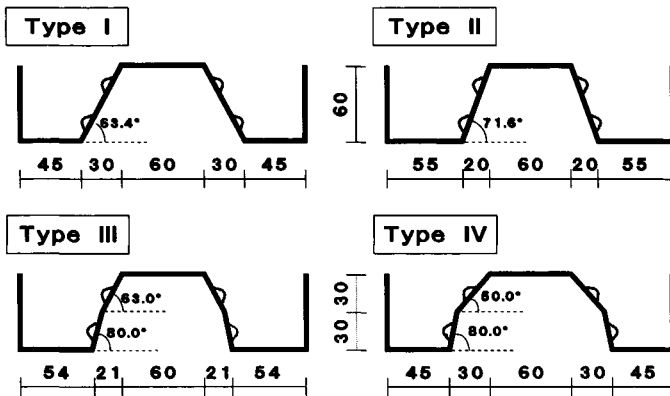


Figure 5.40: Different types of Sheeting

The indentations consisted of a spherical and a conical part. The shape of the indentations was determined by digitalized photographs. The shape of all indentations was remarkably accurate. The location of the indentations in the web varied between different groups of specimen, as illustrated in Fig. 5.41. The lower indentations were located closer to the edge of the web than the upper indentations. In general, the response of the sheeting improves when indentations are located closer to the edges. Especially the location of the lower indentation is important, since it provides resistance to vertical separation.

	IS	IB	IIS	IIB	IIIS	IIIB	IVS	IVB	Average
H_{LOW}	11.3	10.7	13.3	13.6	14.2	14.0	16.5	10.3	13.0
H_{UP}	16.2	16.5	14.5	14.1	14.7	13.8	13.7	15.5	14.9

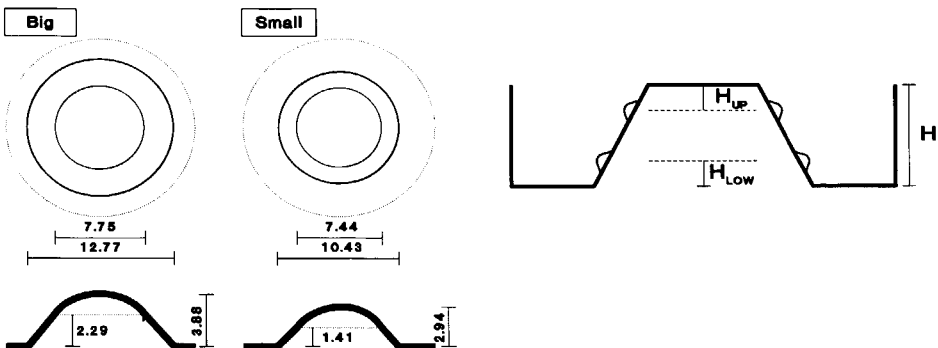


Figure 5.41: Geometry and location of the indentations

Geometrical properties of all specimen were measured. Normal weight concrete was used. Material properties were not supplied. The surface of the sheeting was clean, but not oiled before the concrete was placed.

5.3.3 Test Arrangement of Series III

The test arrangement was developed by TNO. The specimen was placed vertically in the testing frame, as shown in Fig. 5.42. It was standing on the reinforcement bars, which acted as hinges. A solid steel block was placed on top of the sheeting to distribute the load over the cross-section of the sheeting. The bottom flange of the sheeting was supported by vertical sliders, which kept the sheeting in a vertical position. An external lateral force (F_{\perp}) of 500 N was applied to the specimen, and kept constant during the experiments.

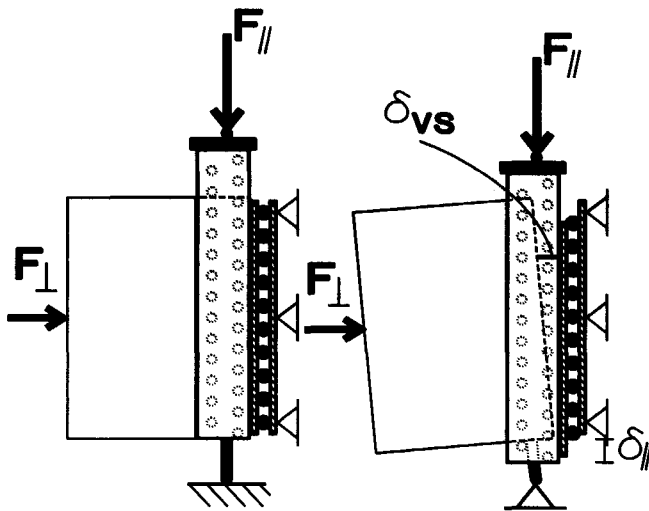


Figure 5.42: Measurements Specimen III

Due to the test arrangement, vertical separation between concrete and sheeting is not constant over the length of the specimen. The concrete block rotates with respect to the sheeting once separation occurs, as shown in Fig. 5.42. Since the separation, and therefore the deformation of the sheeting, varies over the length of the specimen, a cross-sectional analysis is not representative for the deformed shape of the specimen.

To determine the characteristics of the shear connection, the applied shear force F_{\parallel} (①), the longitudinal slip between concrete and sheeting δ_l and the applied lateral force F_{\perp} were measured, as shown in Fig. 5.43. Slip between concrete and sheeting was measured at the loading end of the specimen. The level of slip changes over the specimen, due to axial deformation of both concrete and sheeting. This effect may become important when the resistance of the shear connection is high.

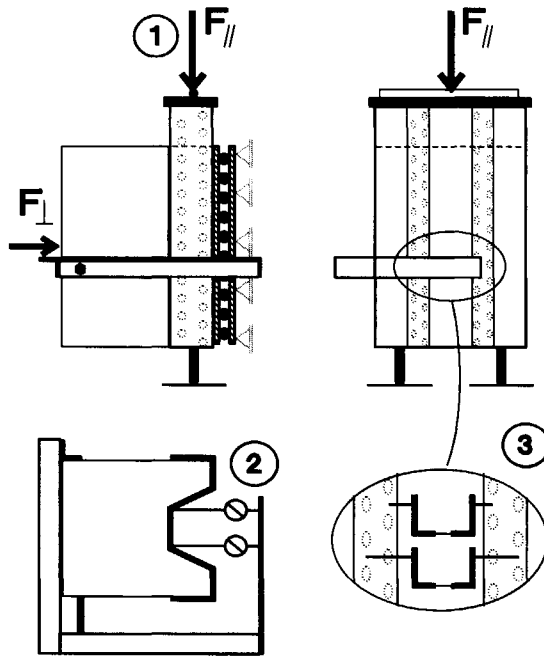


Figure 5.43: Measurements Specimen III

Additional measurements were taken to record the separation (②) and deformation (③) of the sheeting at a certain cross-section, schematically shown in Fig. 5.43. The relative displacement of the edges of the top flange with respect to the concrete were measured. The deformation of the web was measured by recording the shortening of the distance between opposite indentations. For some specimens with sloping webs (III & IV) the shortening between opposite angles was measured.

5.3.4 Results of Series III

Figures 5.44 to 5.47 show results of representative specimen from each group containing big indentations. In the upper part of the graph, the applied shear force (①) is plotted versus longitudinal slip. In the lower part, the vertical separation (②) and the shortening between the webs (③) is plotted versus longitudinal slip. The shortening between the webs equals twice the average horizontal displacement of the webs.

Figures 5.44 to 5.47 show that the strength and stiffness of the connection improve from Type I to IV. Specimen with big indentations behave better than specimens with small indentations. For each type of measurement general remarks are made:

- ① / 1 Chemical bond between the concrete and sheeting results in a shear force for small values of slip. Breakdown of chemical bond leads to a sudden increase of slip.
- ① / 2 The ultimate shear force is reached between a slip of 1.0 and 2.0 mm.
- ① / 3 The maximum slip approximately equals half the diameter of an indentation, which implies that the indentation is pushed out of the concrete completely. The remaining resistance for large values of slip is considerable.

- ② / 1 The recorded separation of the top flange is almost proportional to the slip. The ratio between separation and slip increases slightly, once the ultimate shear force is reached.
- ② / 2 For Type I & II, the separation of the bottom edge of the web is smaller than the recorded separation of the top edge of the web, due to the deformation of the web: $\delta_{vs;bfl} < \delta_{vs;tfl}$. For Type III & IV, the web stretches due to the angle between the separate parts of the web. Therefore, the separation of the bottom edge of the web is larger than the recorded separation at the top: $\delta_{vs;bfl} > \delta_{vs;tfl}$.
- ② / 3 In most cases, the recorded separation at both edges of the top flange is equal, which implies a symmetrical deformation of the cross-section.

- ③ / 1 The shortening between the webs reaches a maximum value. Due to the slope of the web, the appearance of separation and deformation of

concrete the shortening between the webs is smaller than twice the height of one indentation.

- ③ / 2 The shortening between the upper indentations is larger than the shortening between the lower indentations. Partly this can be explained by the shortening of the web, which reduces the effect of the top flange to the deformation of the web (§ 4.5). Secondly, the lower indentations are located closer to the edges of the web. For Type III & IV, the larger span of the upper part of the web leads to larger displacements.

Comparison of Type I & II

Due to the steeper slope of the web, the separation of Type II is smaller than for Type I. Therefore, the deformation of the web is larger for similar values of slip. The ratio between deformation and separation increases, which improves the characteristics of the connection. The more favourable location of the indentations in the Type I specimen reduces the difference between Type I & II.

Comparison of Type II & III

Type III behaves better than Type II, although the average slope of the web is equal. The angle in the web generates arching action and increases the stiffness of the web, which improves the response of the sheeting. Due to the steep lower part of the web, the vertical separation of Type III is smaller than for Type II. Again, the ratio between deformation and separation increases, which explains the improvement of the shear characteristics.

Comparison of Type III & IV

Type IV behaves significantly better than Type III. Apart from the increased stiffness of the web, the web is locked between the lower indentation and the top flange, due to the stretching arch. Interlocking creates contact forces between the top flange and the concrete, which contribute to the shear resistance via friction. Furthermore, caused by the more favourable location of the indentations in the Type IV specimen, the difference between Type III & IV is significant. Type IV exhibits less ductility compared to all other types, since the advantageous effect of interlocking disappears when the level of separation increases. The recorded separation of Type IV remains small until the ultimate shear force is reached. Apparently the top flange is still pushed towards the concrete, while the concrete rotates from the sheeting, as shown in Fig. 5.42. Similar to the comparison between Type II and III, the reduction of the separation from Type

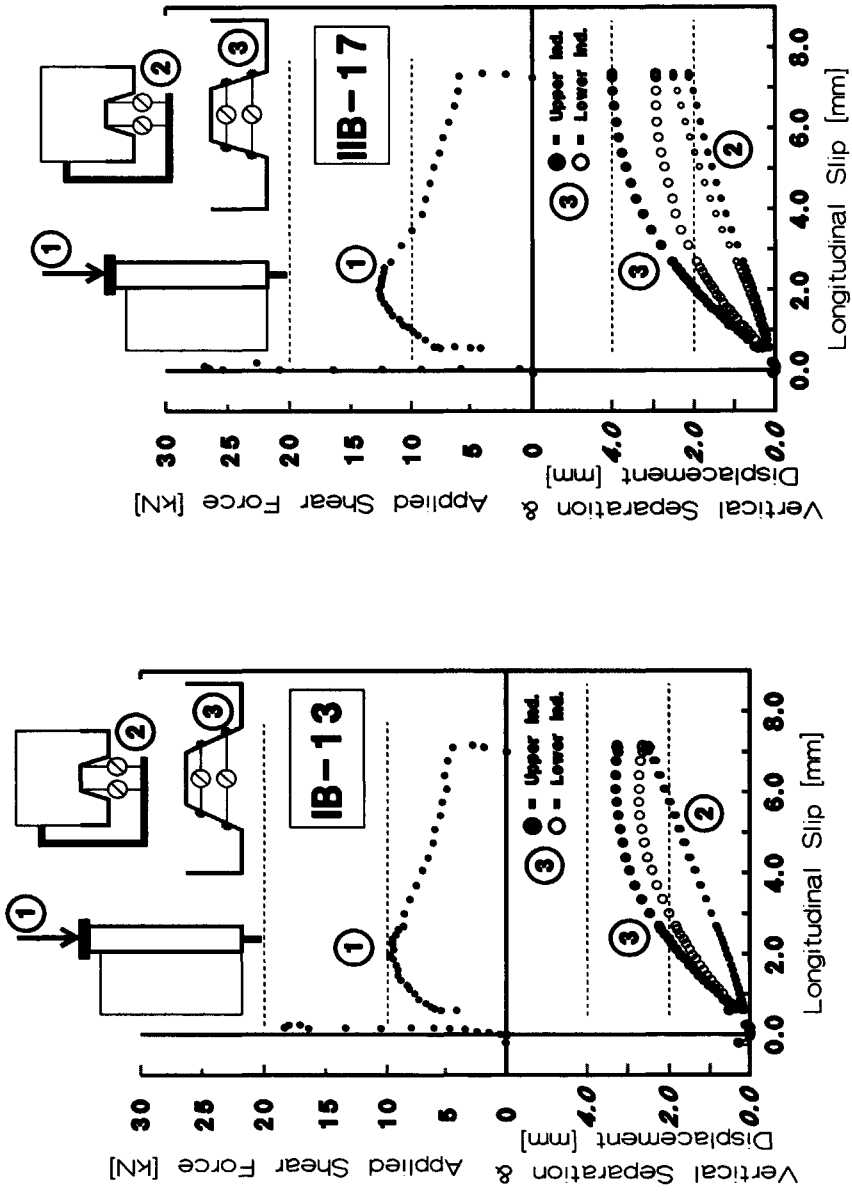


Figure 5.44: Results of IB-13

Figure 5.45: Results of IIB-17

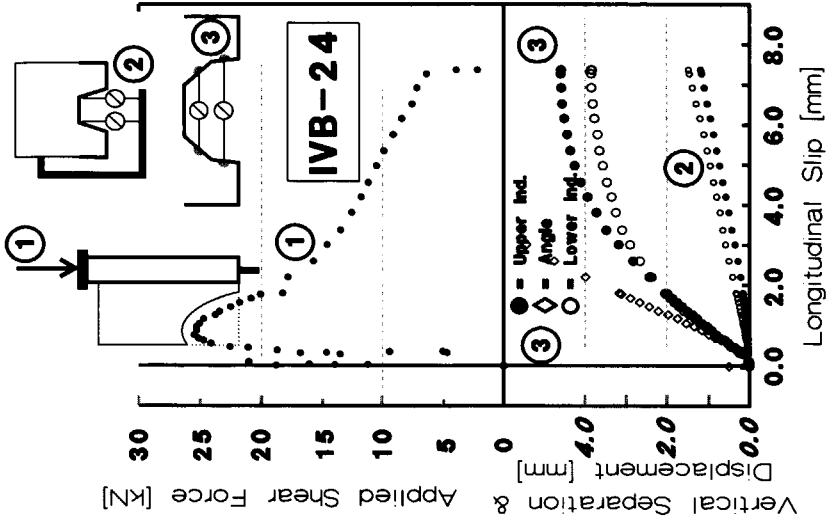


Figure 5.47: Results of IVB-24

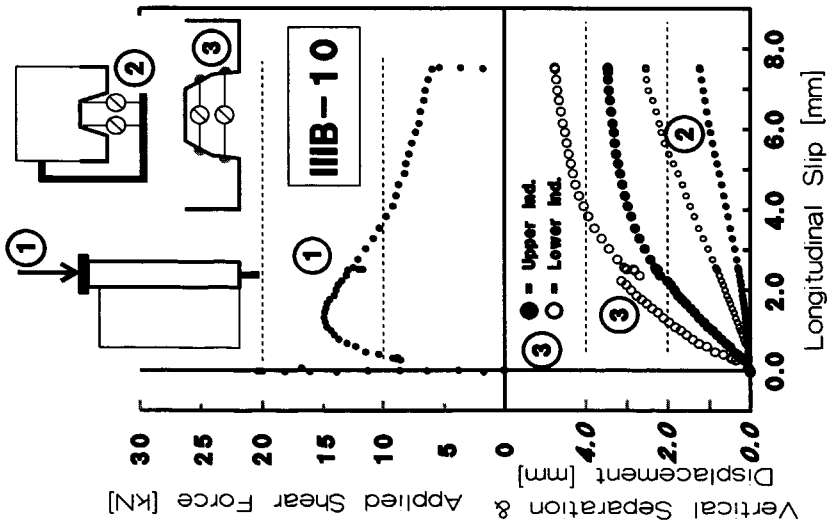


Figure 5.46: Results of IIIB-10

III to IV increases the ratio between deformation and separation, and therefore the characteristics of the connection.

Experimental results show that the angle in the web of Type III & IV improves both the bending resistance of the web and the resistance to vertical separation. Both effects improve the characteristics of a connection. Results of Type IV show that the influence of the angle can be significant. A minimum angle is required to obtain the beneficial effect of contact between the upper edge of the web and concrete.

5.4 Conclusions for Chapter 5

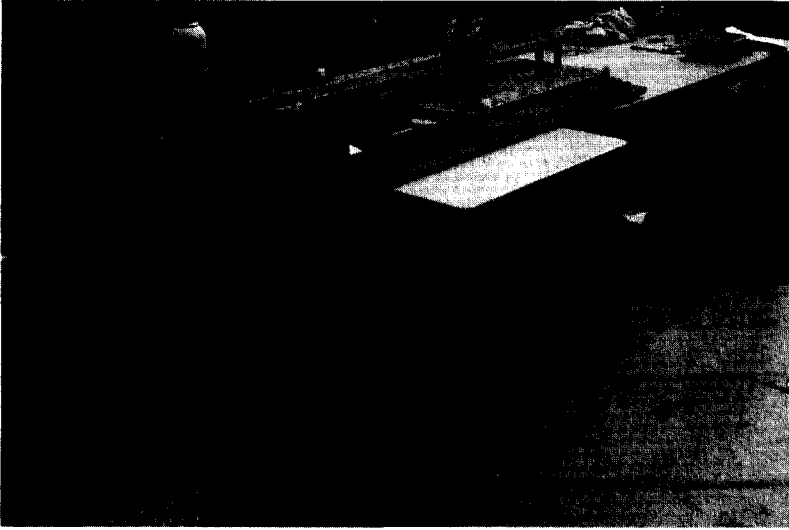
- # The different embossments used in Series I are effective for investigating the direction of interaction forces and the coefficient of friction. (§ 5.1)
- # The test arrangement and specimen of Series II prove that it is possible to perform simple experiments at Level 1. (§ 5.2)
- # The geometry of the sheeting in Series II was chosen to avoid internal balancing of forces, as found in both re-entrant and trapezoidal profiles. However, due to the frictional forces between the webs and the concrete the measured forces are not equal to the interaction force between the indentation and the concrete. (§ 5.2)
- # Visual inspection of the interface between concrete and sheeting before experiments is not recommended, since replacing the sheeting is difficult. (§ 5.2)
- # Determination of the coefficient of friction is difficult, and results can only be used as a guidance for similar cases. The coefficient of friction increases if the contact surface is previously loaded and can be different in different directions. (§ 5.2.5)
- # Since the ratio between the deformation and displacement is different for the considered rib types, Series III provides valuable experimental data. (§ 5.3)

- # Although the location of the indentations varied between specimen, the specimen of Series III prove that specimen can be prepared with a similar accuracy as provided by roll-formers. (§ 5.3)

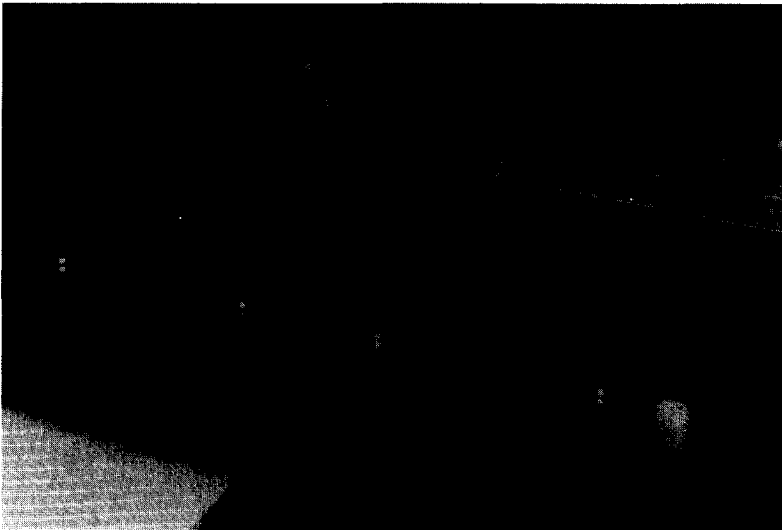
- # The test arrangement of Series III shows that boundary conditions are very important within a small-scale specimen. The fact that the sheeting is pushed down and the concrete block rotates once vertical separation occurs, makes it hard to analyse the experimental results. (§ 5.3)

- # The sloping webs in Type III & IV improve the behaviour of the shear connection. If the angle remains small, the effect is limited (Type III). If the angle is larger (Type IV), the web is locked between the lower indentation and the top flange, which increases the resistance significantly. Since the interlocking effect disappears for larger values of slip, the behaviour is less ductile than established for trapezoidal profiles with steeper webs. (§ 5.3)

5.5 Photographs



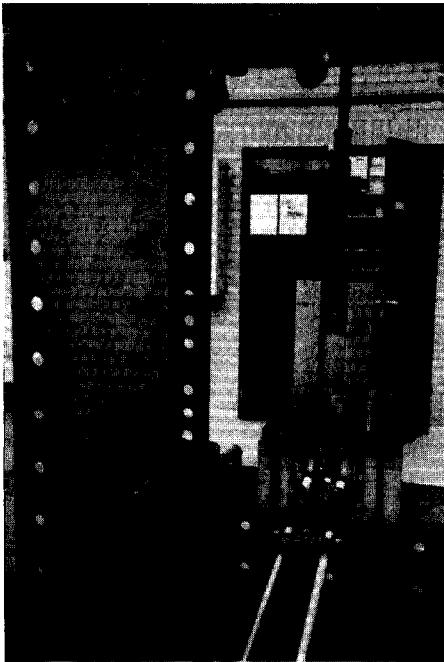
Series 1: Overview test arrangement



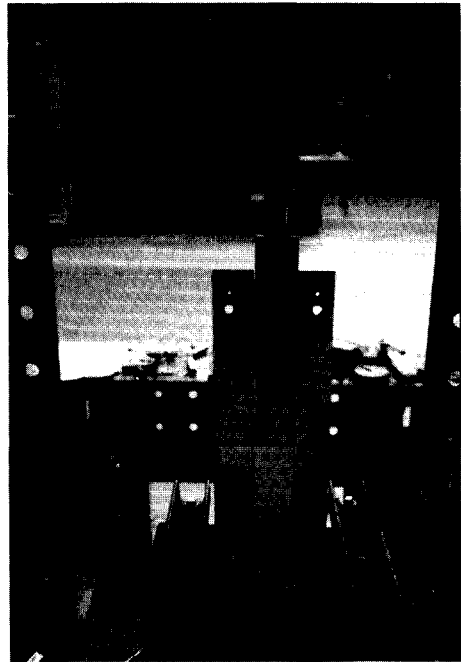
Series 1: Sheeting - circular embossment - measurements of deflection



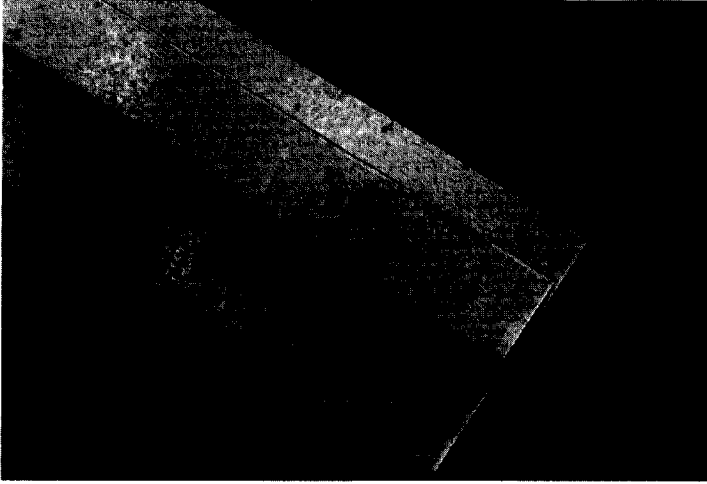
Series 1: Deformed sheeting - pyramid embossment - measurement of slip



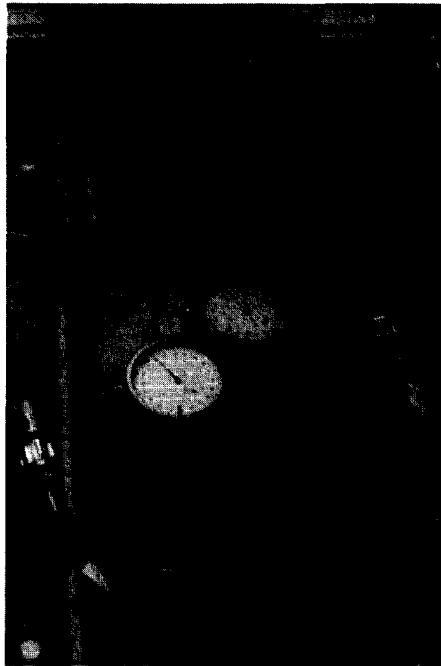
Series 2: Overview test arrangement - lateral support beams



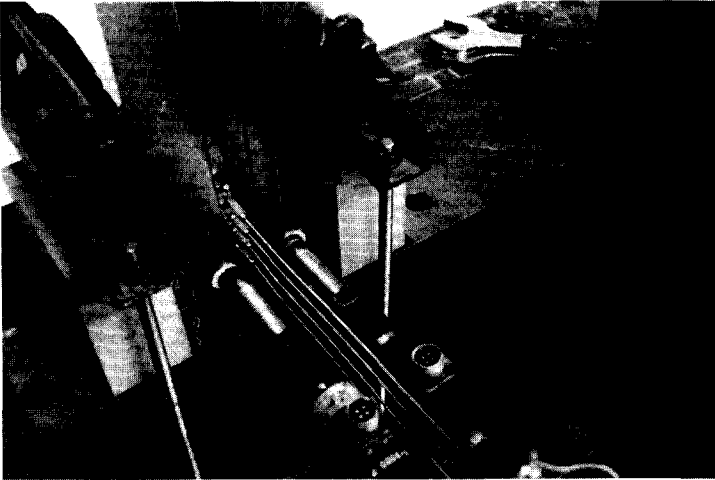
Series 2: Applied shear force - concrete block clamped to testing frame



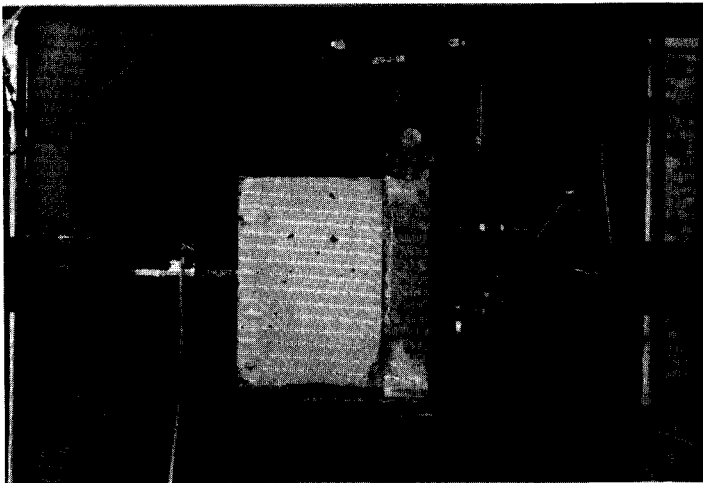
Series 2: Inspection sheeting with indentation before testing



Series 2: Measurement of slip and separation



Series 2: Lateral support bottom flange - measurement of displacement top flange



Series 3: Overview test arrangement

6. VALIDATION

6.0 Introduction

The hypothesis and the numerical models are validated by the experiments, discussed in chapter 5. Figure 6.1 shows a refined version of Fig. 1.5, relating the contents of this chapter to the hypothesis, the experiments and the numerical models. Series I (§ 5.1) is used to validate the assumption concerning the direction of interaction forces between indentations and concrete in the hypothesis (§ 6.1). Series II (§ 5.2) and III (§ 5.3) are used to validate the numerical models. The FE-models are validated by the experiments. Since nonlinear phenomena are not included in SF-models, the experiments can not be used to validate the SF-models. Validated FE-models are used to validate the SF-models (§ 6.2 & 6.3).

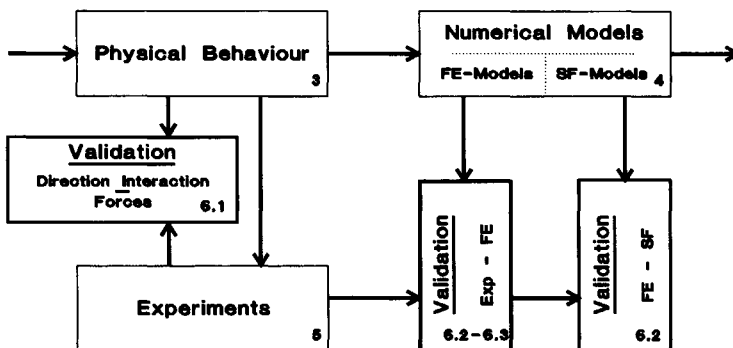


Figure 6.1: Outline validation hypothesis and numerical models

6.1 Series I: Validation Hypothesis

The validation of the assumption concerning the direction of interaction forces between indentations and concrete in composite slabs is based on a similar type of shear connection, for which the assumption holds. This connection is discussed in § 6.1.1. In § 6.1.2, the differences between this connection and shear connections in composite slabs are listed, followed by the actual validation of the assumption in § 6.1.3. In § 6.1.4 theoretical and numerical results are

compared with the experimental results.

6.1.1 Comparable Shear Connection: Concrete Crack subjected to Shear

The behaviour of cracks subject to shear displacements [9], is modelled analogous to the suggested approach for composite slabs. The model consists of spherical aggregate particles and a cement matrix. The model is simplified into a 2-D analysis by considering a representative slice of the volume. The strength and stiffness of the aggregate particles is higher than those of the cement matrix. The bond zone between particles and matrix is the weakest link. Hence, cracks occur through the matrix and along the circumference of the aggregate particles, as shown in Fig. 6.2.

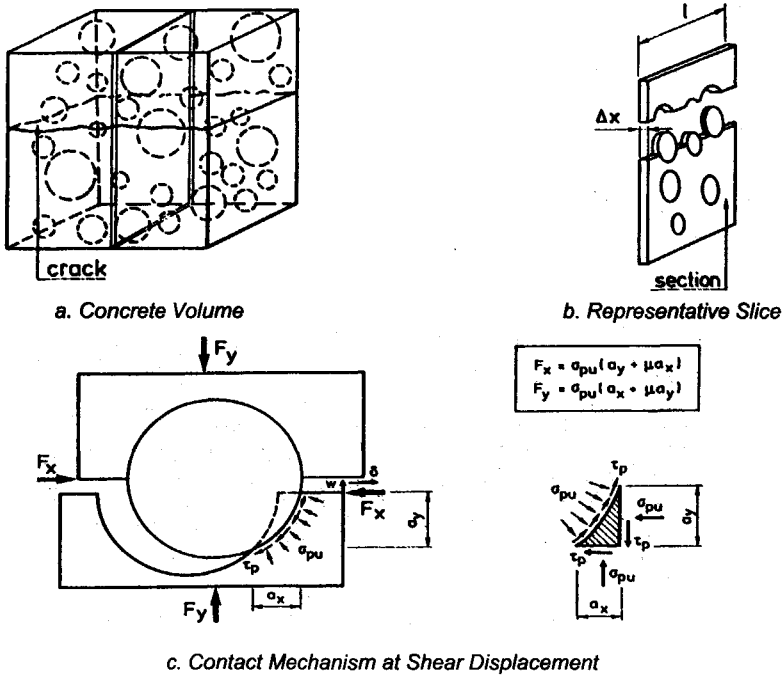


Figure 6.2: Concrete crack subject to shear

The contact mechanism illustrates the behaviour of one particle section. Apart from the shear displacement, separation occurs. The matrix is considered to be perfectly brittle, with a crushing strength σ_{pu} . With penetration of the particle into the matrix, normal and frictional forces occur. The direction of the normal and

frictional forces correspond to the assumption concerning the interaction forces between indentations and concrete in composite slabs.

6.1.2 Comparison Connection Concrete Crack Model versus Composite Slabs

A comparison is made between the characteristics of the shear connection for concrete cracks and composite slabs.

<i>Concrete Crack in Shear</i>	<i>Composite Slab</i>
<p>Model consists of aggregate particles and a cement matrix. Higher strength and stiffness of aggregate particles compared to cement matrix. Interface between particles and matrix weakest link. Cracks through matrix and along circumference of aggregate particles.</p> <p style="padding-left: 40px;">Brittle behaviour cement matrix.</p>	<p>① Model consists of profiled sheeting containing indentations, and concrete. Concrete at interface is cement paste rather than structural concrete. Interface between profiled sheeting and cement paste weakest link. Cracks along surface sheeting.</p>
<p>High resistance to separation results in large interaction forces and considerable penetration of aggregate particles into cement matrix.</p>	<p>② Behaviour cement paste comparable to behaviour cement matrix.</p> <p>③ Due to its limited thickness, sheeting deforms and indentations are pushed out of the concrete. Limited resistance to separation results in smaller interaction forces and reduces the penetration of indentations into paste.</p>
<p>Straight crack is considered: direction forces on each particle coincide. All particles together show equilibrium with external loads.</p>	<p>④ Interaction forces are (partly) balanced internally, due to geometry sheeting and location indentations. External lateral forces are smaller (support reaction) or zero.</p>
<p>Irreversible deformation cement matrix. In case of cyclic loading, the shear resistance becomes path-dependent.</p>	<p>⑤ If cement paste deforms, "channels" appear. Shear resistance becomes path-dependent, since resistance perpendicular and parallel to "channels" is different.</p>

The main difference between both types of shear connections lies in the resistance to separation. Due to the flexible behaviour of the profiled sheeting, interaction forces between the profiled sheeting and the concrete remain smaller, and therefore the tendency of indentations to penetrate into the cement paste is smaller. The shear connection in concrete cracks proves that the assumption concerning the direction of the interaction forces holds if a stiff particle, either aggregate or indentation, penetrates into a weaker, brittle material. The assumption also holds for limited penetration.

In order to prove that the assumption holds for composite slabs it should be validated that the assumption holds for infinite small penetration. The contact area, described by the penetrated cement matrix, reduces to a contact point. In principal, the direction of the interaction force at a contact point is singular. If the assumption is validated for connections with contact points instead of contact areas, the assumption holds for shear connections in composite slabs.

6.1.3 Actual Validation Series I

The validation is based on the derived values for the coefficient of friction μ , as shown in § 5.1, Figs. 5.9 to 5.12 and Table 5.1. Average values of μ are presented again in Table 6.1. μ is almost constant within each experiment, which proves that μ is constant over the considered range of F_N . The fact that μ is almost constant within the P-series does not prove the validity of the assumption. The fact that μ is also constant for the C-series proves that the assumption holds, since the variation of the inclination does not influence the results. Hence, the validation of the assumption is based on the derived coefficients of friction μ , which are almost constant for both pyramid and circular embossments.

No consistency is expected between the results of pyramid and circular embossments, since the embossments are produced in a different manner, resulting in different surface conditions. In both cases, the surface conditions are different in opposite directions, so the positive and negative values found in the P-series are not expected to be equal.

Table 6.1: Evaluation coefficient of friction circular embossments

Experiment	Initial Gap [mm]	Average μ per Experiment [-]	Average μ C-Series [-]	Deviation of results from average %
P075	-	+0.355 / -0.247		-
C075-I	0.500	0.157	0.157	-0.2
C075-II	1.382	0.130	0.157	-17.4
C075-III	2.329	0.185	0.157	+17.6
P100	-	+0.186 / -0.126		
C100-I	0.703	0.137	0.146	-5.9
C100-II	1.710	0.134	0.146	-8.0
C100-III	4.883	0.166	0.146	+14.0

Although a factor of approximately two is found between the average values found for P075 and P100, no systematic error is found in the test arrangement or the derivation of μ . The large difference between the results is probably caused by a different orientation of the embossment in the test arrangement.

Consistency is expected within the C-series, since the embossments were orientated in the same direction. Considering the indirect way the coefficient of friction is determined and the limited number of measurements within each experiment, especially the ones with large initial gaps, the results are reasonably consistent.

6.1.4 Comparison Experimental, Theoretical and Numerical Results Series I

Once a value for the coefficient of friction is available, both theoretical and numerical models can be evaluated. A theoretical model is used in § 3.4 to illustrate the hypothesis. For the considered shear connection the theoretical model corresponds to the SF-model. A simple FE-model is used to obtain FE-results.

The comparison between experimental, theoretical and numerical results is not performed to validate either the hypothesis or the numerical models, but only to illustrate the models. The experiments of Series I are simplified to such an extent

that only the assumption concerning the direction of the interaction forces and the value for the coefficient of friction are unknown. Once the assumption is validated and a value is derived for the coefficient of friction, the experimental, theoretical and numerical SF-results should be consistent.

Since, due to the influence of the initial gap ($\delta_{z,0}$), circular embossments are most interesting, the results of C100 are illustrated. Figs. 6.3 to 6.5 show the experimental, theoretical and numerical FE-results of specimen C100-I to III. The lower parts of each graph shows the coefficient of friction, μ . The dots represent the derived values for each measurement. The straight line represents the average value of the coefficient of friction $\langle\mu\rangle$ for each experiment. $\langle\mu\rangle$ is used within the theoretical and numerical models. The upper part of Figs. 6.3 to 6.5 show the applied shear force. The dots represent the experiments, the continuous line represent the theoretical results and the discontinuous line represent the FE-results. The theoretical and numerical results should be similar. The results may deviate from the experimental results, according to the deviation of the coefficient of friction from the average coefficient of friction.

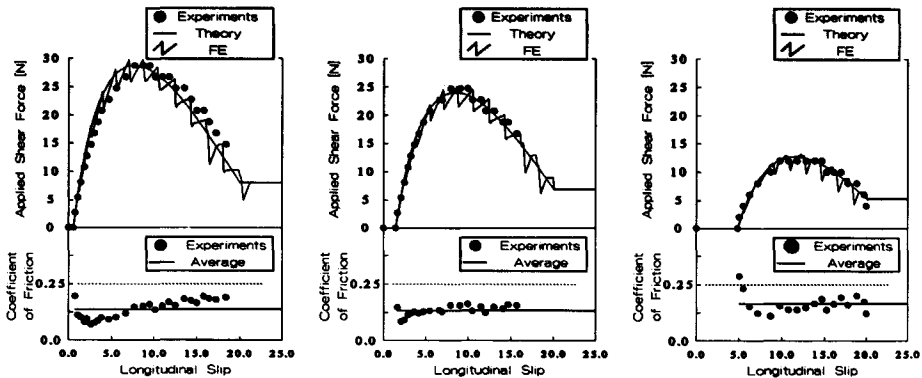


Figure 6.3: Results C100-I Figure 6.4: Results C100-II Figure 6.5: Results C100-III

The discontinuous nature of the FE-results is discussed in § 4.5.2 and illustrated in Fig. 4.14. For more complicated 3-D models, discontinuity occurs in two directions. If the number of elements over the indentations is increased, the effect of the discontinuous nature of the applied shear force is reduced.

6.2 Series II: Validation Simplified Shear Connection (Level 1)

Experimental results of Series II are used to validate the FE-models. The final FE-model contains all relevant phenomena of the specimen. The model is developed in a stepwise manner (§ 6.2.1). Since SF-models contain numerous simplifications, SF-results cannot be compared to experimental results directly. Validated FE-models are used to validate SF-models (§ 6.2.2).

6.2.1 Validation of FE-Models

Within the final FE-model, describing the experiments of Series II, all relevant phenomena are included:

Plasticity of sheeting

Even for small values of slip, plastic deformation of the flange occurs. The material properties presented in Table 5.2 are used.

Crushing of concrete in front of the indentation

Visual inspection of the specimen after testing showed deformation of the concrete, similar to the deformation of the cement matrix of Fig. 6.2. Accurate modelling of the concrete interface is difficult, since distinction should be made between the outer layer of cement paste and the concrete. Description of geometrical and material properties of the outer layer of paste lies outside the scope of the thesis. Therefore, fictitious properties are derived, which lead to in plastic deformation of the concrete, matching the damage found in experiments. The fictitious material properties for concrete used in Series II and III are presented in Table 6.2.

Table 6.2: Fictitious material properties concrete in Series II and III

	Measured Values		Fictitious Values	
	f_{cc} [N/mm ²]	E_c [N/mm ²]	f_{fyld} [N/mm ²]	E_{fc} [N/mm ²]
Series II	74.66	41333	35.00	30000
Series III	41.01	-	7.50	10000

Contact between indentation and concrete, including friction (Area 1)

The tested interface within the friction test (§ 5.2.5) differs from the interface

in Area 1. Figure 5.38 shows that after a number of cycles the coefficient of friction reaches a value of 0.50. The first cycles show values between 0.25 and 0.30. Apparently the contact surface roughens during the first cycles. Inspection of specimen after experiments shows that the cement paste behaves as sand paper when indentations slide along the concrete surface. Small particles are forced through the paste. Since high strength concrete was used in Series II, a value of 0.30 is used for the coefficient of friction, where the concrete crack model uses a value of 0.40.

Contact between web and concrete, including friction (Area 2)

If a slip displacement is applied to the sheeting, the top flange deforms and the web is pushed towards the concrete, contributing to the shear resistance via friction. Since the contact surface is large, no deformation of concrete occurs. The surface of the sheeting in Area 2 was oiled in order to prevent chemical bond. Nevertheless, the same value for the coefficient of friction is used as for Area 1.

Separation between sheeting and concrete

Separation between sheeting and concrete, which occurred during experiments, is taken into account.

The FE-model is built up in a stepwise manner in order to obtain understanding into different aspects of the shear connection. Four different models are developed (M1 to M4), as illustrated in Figs. 6.6 and 6.7.

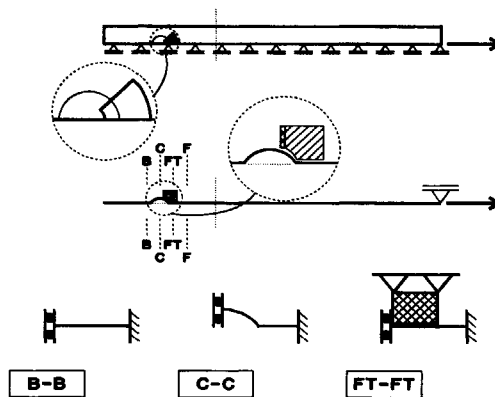


Figure 6.6: Stepwise development FE-models: M1 & M2

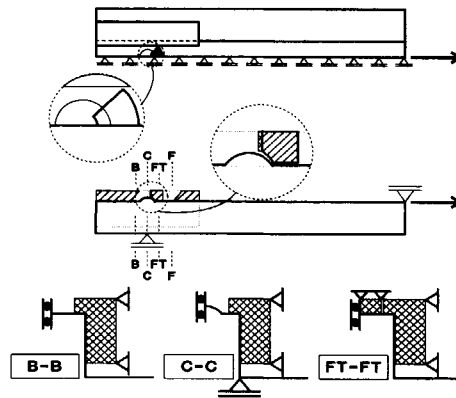


Figure 6.7: Stepwise development FE-models: M3 & M4

M1 & M2 consider only the top flange of the sheeting. M3 & M4 also consider the web and bottom flange. Considering contact and severe plastic deformation of the flange and concrete in combination with geometrical nonlinear behaviour caused numerical instability in the FE-models. Therefore, geometrical linear behaviour is considered for all models.

The edges of the flanges in M1 & M2 are clamped. In front of the indentation, a block of concrete is placed, which has a similar shape as the indentation. Contact elements are present between the indentation and concrete. The top of the concrete block is fully fixed. Within M2, the concrete block is not fixed in the vertical direction. Springs are used to model separation between the sheeting and concrete, as shown in Fig. 6.8. The properties of the springs are based on the virtual stiffness of the lateral supports, as presented in Table 5.3.

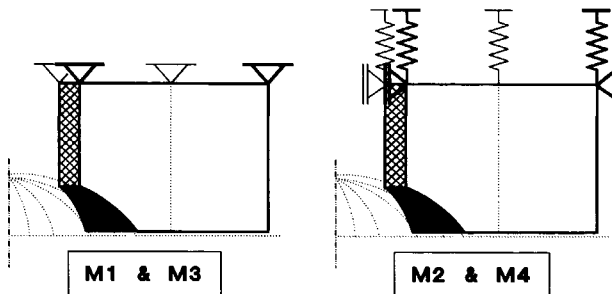


Figure 6.8: Boundary conditions concrete block in Model 1-3 & 2-4

For M1, alternately elastic and plastic material behaviour is considered for sheeting and concrete, in order to illustrate the influence of both materials. Figure 6.9 shows results of all combinations of elastic and plastic material behaviour of both sheeting and concrete: M1EE, M1EP, M1PE & M1PP.

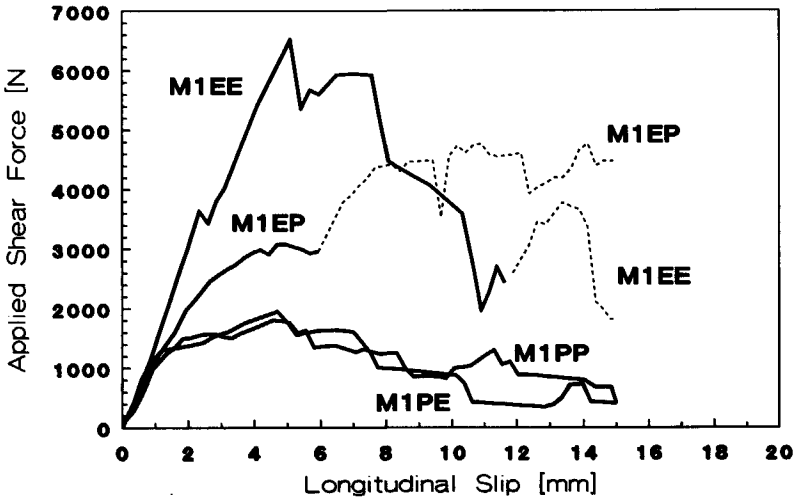


Figure 6.9: Results Model 1: M1EE, M1EP, M1PE & M1PP

If elastic behaviour is considered (M1EE), large interaction forces occur between the indentation and the concrete due to the unlimited bending resistance of the top flange. Even for large interaction forces the deformation of concrete is limited. For large values of slip, the indentation is pushed out of the concrete and the shear resistance reduces significantly. If plasticity of steel is considered (M1PE & M1PP), plastic hinges occur at the toe of the indentation and along the edges of the flange, reducing the lateral support reaction and therefore the shear resistance of the connection. If plasticity of concrete is considered (M1EP & M1PP), the strength and stiffness of the connection reduces. The stiffness reduces since part of the applied slip is taken by the deformation of the concrete. The strength reduces since the deformation of the flange reduces. For large values of slip, the reduction of the shear resistance is smaller. The indentation digs its way through the concrete and is not pushed out of the concrete completely.

Within the FE-models M1EE and M1EP, a phenomenon occurs, which does not

occur during the experiments. During experiments, the cement paste in front of the indentation is crushed, similar to the cement matrix in Fig. 6.2. The volume of the paste reduces, as illustrated in Fig. 6.10a. Within the FE-model, the volume of the concrete remains constant. Material is pushed from the contact area forwards, as illustrated in Fig. 6.10b. Within the FE-model the indentation contacts this material, which increases the shear resistance. Results of M1EE and M1EP which are affected by this material flow are presented as dotted instead of solid lines.

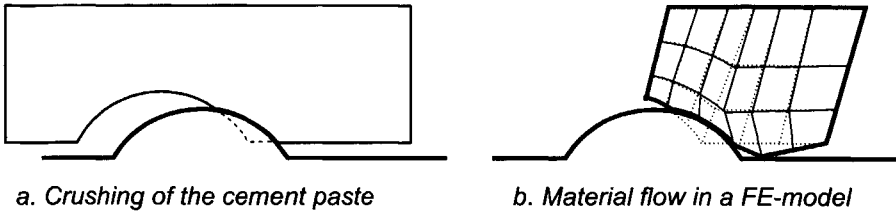


Figure 6.10: Material flow in FE-models M1EE & M1EP

Figure 6.11 shows results for all models with plastic behaviour of both sheeting and concrete (M1PP, M2PP, M3PP & M4PP). M4PP is the final FE-model.

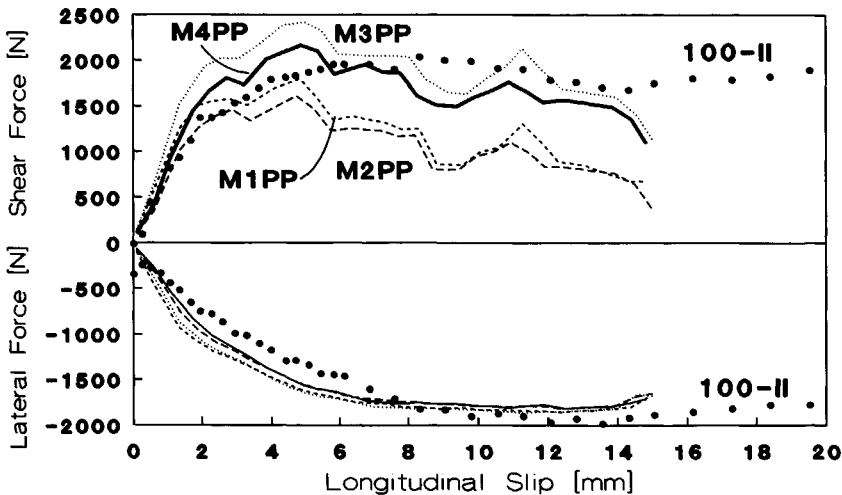


Figure 6.11: Results of 100-II, M1PP, M2PP, M3PP & M4PP

The separation between sheeting and concrete, caused by the described circle

of the support beams, is neglected, since it is small for the considered levels of slip, as shown in eq. (6.1).

$$\delta_{vs;circle} = L_p - \sqrt{L_p^2 - \delta_i^2} \leq 1200 - \sqrt{1200^2 - 15^2} \approx 0.09 \text{ mm} \quad (6.1)$$

Figure 6.12 shows results of M3PP. The web and bottom flange of the sheeting are modelled and contact between web and concrete is included, which contributes to the shear resistance via friction. Once plastic deformation of the edges of the flange occurs, the contribution of friction remains constant. At a slip level of 10-12 mm, an increase of the shear resistance caused by material flow can be recognized again. Figure 6.13 shows results of M4PP including reversed loading.

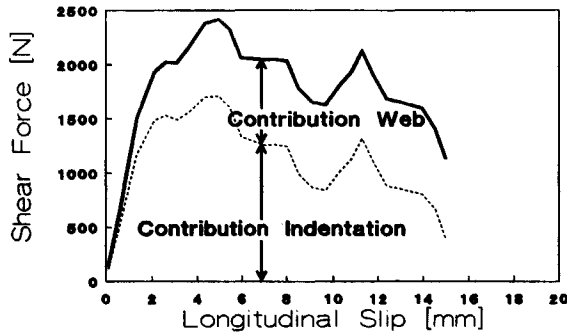


Figure 6.12: Results of M3PP

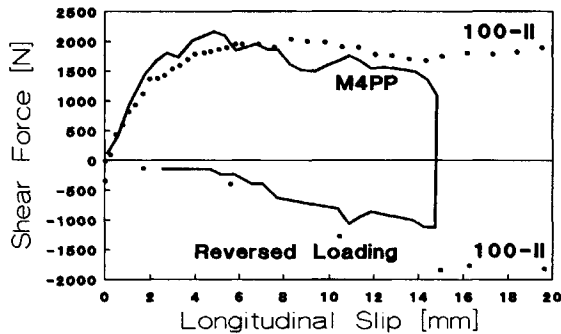


Figure 6.13: Results of M4PP including reversed loading

Figure 6.14 shows the vertical displacement of the top flange. For all models the number of elements, the normalized CPU-time and the ultimate shear and lateral forces are presented in Table 6.3.

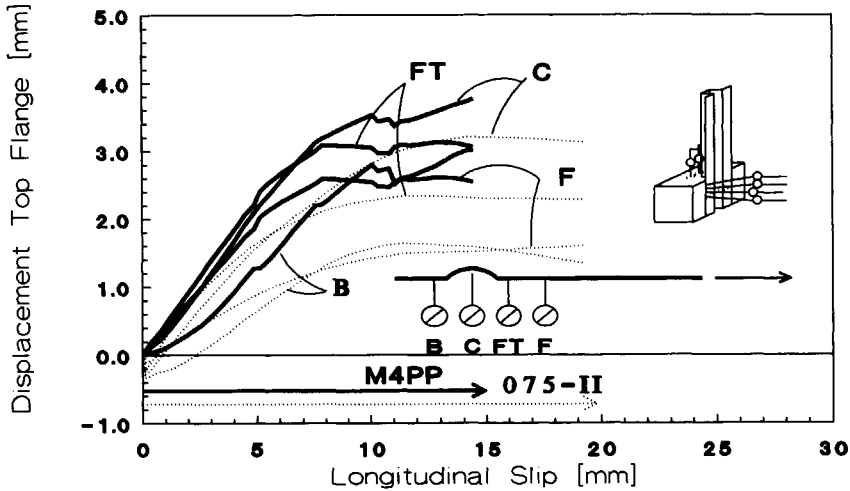


Figure 6.14: Vertical displacement of the top flange of model M4PP

Table 6.3: Results of FE-models

MODEL	Material Behaviour		Number of Elements				Computing Time	Ultimate Forces	
	Sheeting	Concrete	Shells	Solids	Contact	Springs	M3PP = 100 %	Shear	Lateral
M1EE	E	E	62	54	336	-	24	6517	10218
M1EP	E	P	62	54	336	-	36	4762	5910
M1PE	P	E	62	54	336	-	56	1952	1838
M1PP	P	P	62	54	336	-	60	1806	1852
M2PP	P	P	62	54	336	4	60	1610	1818
M3PP	P	P	97	57	366	-	100	2470	1864
M4PP	P	P	97	57	366	4	96	2164	1814

In Fig. 6.11 the results of the FE-models are compared to those of specimen

100-II, using sheeting with a thickness of 1.00 mm. Similar to Fig. 6.11, Fig. 6.15 shows results of all plastic models for specimen 075-II.

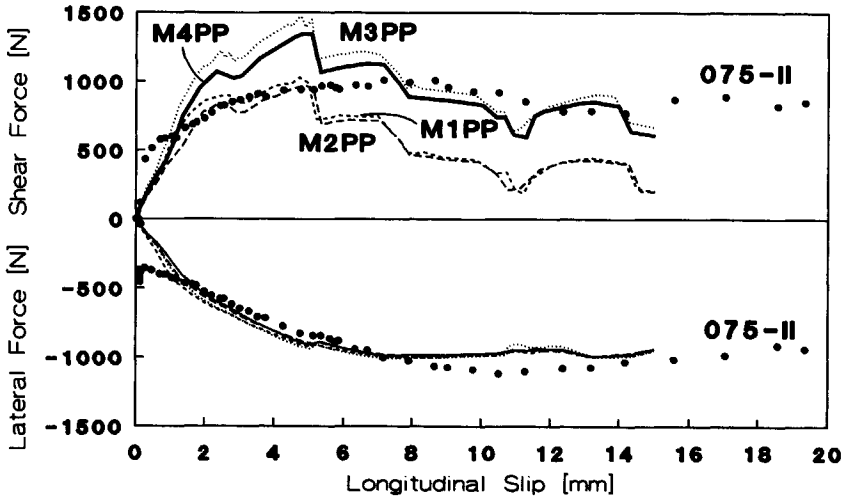


Figure 6.15: Results 075-II, M1PP, M2PP, M3PP & M4PP

6.2.2 Validation of SF-Models

Two series of four SF-models are developed for Series II:

SF-I SF-models evaluated using the visual solution method (§ 3.4)

SF-II SF-models evaluated using the general solution method (§ 4.3.1)

The visual solution method can be used, if apart from the slip, one degree of freedom is considered. In other cases the general solution technique can be used. Four SF-I- and four SF-II-models are evaluated.

6.2.2a SF-I-Models

Within the visual solution method, the ACTION I, ACTION II and REACTION part of the analysis are evaluated separately. If rotation of the indentation is neglected, δ_{\perp} is the only degree of freedom, apart from the applied slip. If deformation of the indentation is neglected, both ACTION parts are evaluated

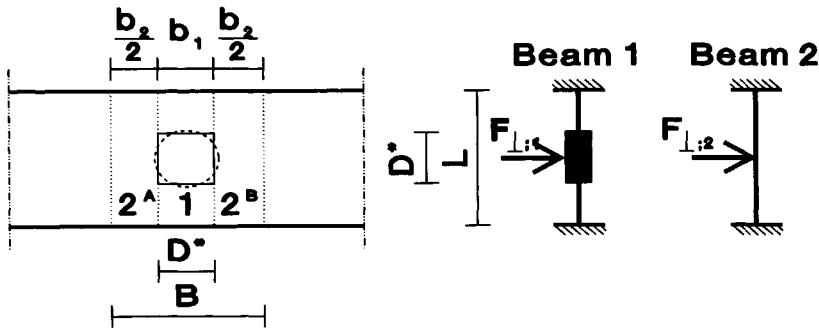


Figure 6.16: Determination of the elastic response (SF-I-1) using a 2-D beam model of the top flange

similar to Fig. 3.12. The difference between the four SF-I models is found in the REACTION part.

SF-I-1: Elastic 2-D beam model of the top flange

As illustrated in Fig. 6.16, a 2-D beam model is used to determine the response of the top flange. Two parallel elements are considered in order to take the influence of the indentation to the stiffness of the flange into account. The spherical indentation is replaced by a square block with an equally projected area and infinite stiffness. Arbitrarily, the total width of the beams equals the span ($B = b_1 + b_2 = L$).

If the deformation pattern is assumed to be cylindrical over the considered width B , the response of the flange results from the separate elements:

$$k_{\perp} = \frac{F_{\perp}}{\delta_{\perp}} = \frac{F_{\perp;1} + F_{\perp;2}}{\delta_{\perp}} = 192 \cdot \left(\frac{EI_1}{L_1^3} + \frac{EI_2}{L_2^3} \right) = 1820 + 784 = 2604 \text{ N/mm} \quad (6.2)$$

$$\text{with: } EI_1 = E \cdot \frac{b_1 \cdot t^3}{12} \quad EI_2 = E \cdot \frac{b_2 \cdot t^3}{12} \quad E = 205.000 \text{ N/mm}^2$$

$$b_1 = D^* \quad b_2 = L - D^* \quad L_1 = L - D^* \quad L_2 = L$$

$$t = 0.982 \text{ mm} \quad B = L = 50.0 \text{ mm} \quad D^* = \sqrt{\pi/4} \cdot D = 18.4 \text{ mm}$$

SF-I-2: Plastic 2-D beam model of the top flange

For the plastic response of the top flange a square part of the flange is considered with yield lines according to Fig. 6.17.

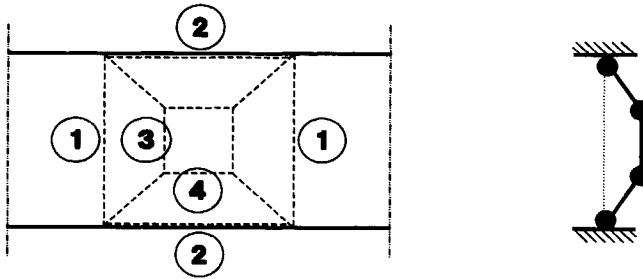


Figure 6.17: Determination of the plastic response (SF-I-2)

The plastic capacity of the top flange is:

$$F_{\perp;P} = \frac{4 \cdot m_p \cdot B + 4 \cdot m_p \cdot L}{\frac{L - D^*}{2}} = \frac{16 \cdot m_p \cdot L}{L - D^*} = 2264 \text{ N} \quad (6.3)$$

$$\text{with: } m_p = f_{yld} \cdot \frac{t^2}{4} \quad f_{yld} = 371 \text{ N/mm}^2$$

SF-I-3/4: Elastic/Plastic 3-D FE-model of the top flange

The elastic and plastic response of the top flange are also determined using an FE-model:

$$k_{\perp;FE-E} = \frac{F_{\perp;FE-E}}{\delta_{\perp}} = 2518 \text{ N} \quad (6.4)$$

$$F_{\perp;FE-P} = 1762 \text{ N} \quad (6.5)$$

Considering the simplicity of 2-D beam model used in SF-I-1, the difference between SF-I-1 and the sophisticated FE-model used in SF-I-3 is small. The difference between SF-I-2 and -4 lies in the development of the yield pattern, shown in Fig. 6.17. Results of the FE-model show that yield lines ① are hardly developed, which reduces the result of eq. (6.3) by 25 %: 75% of 2264 = 1698 N.

The visual solution method is evaluated for SF-I-3 and -4 in Fig. 6.18. Results are compared with SF-II- and FE-results in Figs. 6.19 to 6.21 and 6.23.

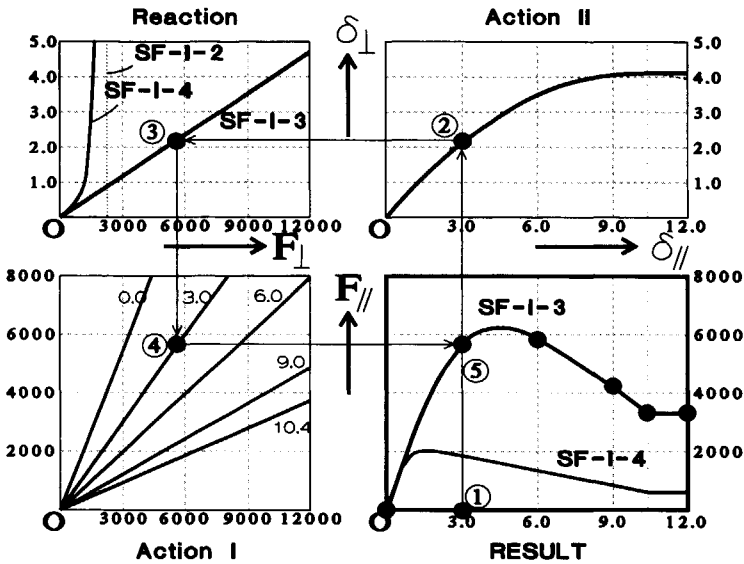


Figure 6.18: Visual solution method: results of SF-I-3 & SF-I-4

6.2.2b SF-II-Models

Four SF-II-models are evaluated and validated using FE-results. Rotation of the indentation is considered in SF-II-1. Deformation of concrete, plasticity of sheeting and contact between web and concrete are considered in SF-II-2 to -4.

SF-II-1: Additional degree of freedom; rotation of the indentation

Eccentricities of the interaction force with respect to the indentation cause rotation of the indentation. Similar to the determination of the response of the sheeting to vertical loading, the rotational stiffness of the indentation in the top flange can be determined using an FE-model. The rotational stiffness is included in the general solution technique. A positive rotation of the indentation reduces the vertical displacement of the indentation δ_{\perp} in the ACTION II part. Figure 6.19 shows results of SF-II-1, SF-I-3 and M1EE. Results of SF-II-1 can be compared to M1EE. The difference between SF-I-3 and SF-II-1 illustrates the influence of the rotation of the indentation. Rotation of the indentation reduces the stiffness. For SF-II-2 to SF-II-4, the rotation of the indentation is neglected.

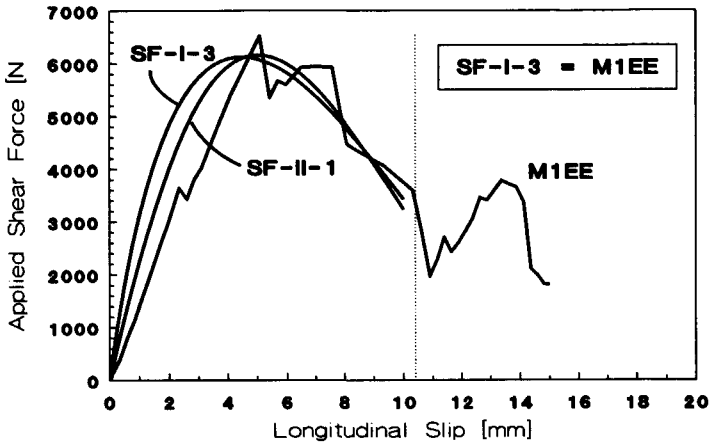


Figure 6.19: Results of SF-I-3, SF-II-1 & M1EE

SF-II-2: Inclusion of deformation of the concrete

Within the ACTION II part of the general solution technique, the deformation of concrete can be included. A 3-D approach of the 2-D concrete crack model, illustrated in Fig. 6.2, is used. A_x is the projected frontal area and A_z is the projected upper area of the crushed concrete.

$$F_1 = F_x = \sigma_{pu} \cdot (A_z + \mu \cdot A_x) \quad (6.6)$$

$$F_{\perp} = F_z = \sigma_{pu} \cdot (A_x - \mu \cdot A_z) \quad (6.7)$$

$$\text{with: } \sigma_{pu} = 8.0 \cdot \sqrt{f_{cc}} \quad \text{for: } 15 < f_{cc} < 60 \text{ N/mm}^2$$

$$\mu = 0.30$$

$$f_{cc} = 74.66 \text{ N/mm}^2$$

Within the concrete crack model, the concrete is considered to behave perfectly brittle with a crushing strength of σ_{pu} , which is related to the crushing strength of 150-mm cubes, f_{cc} . Although the strength of the concrete used in Series II lies outside the given f_{cc} -range, the formula for σ_{pu} is used.

Results of SF-II-2 can be compared to M1EP. Within the concrete crack model and SF-II-2, the volume of the cement matrix reduces, if concrete is crushed. As mentioned in § 6.2.1, the material flow within the FE-model influenced the results of M1EE and M1EP. An additional FE-model, M1EP', is evaluated which

eliminates the influence of material flow, by allowing the indentation to penetrate through the concrete, which does not exist if brittle cement paste is considered. Figure 6.20 shows results of SF-I-3, M1EE, SF-II-2, M1EP & M1EP'. The difference between SF-I-3 and SF-II-2 illustrates the influence of deformation of concrete. Although high strength concrete is used, the influence is considerable, due to the large interaction forces between the indentation and concrete.

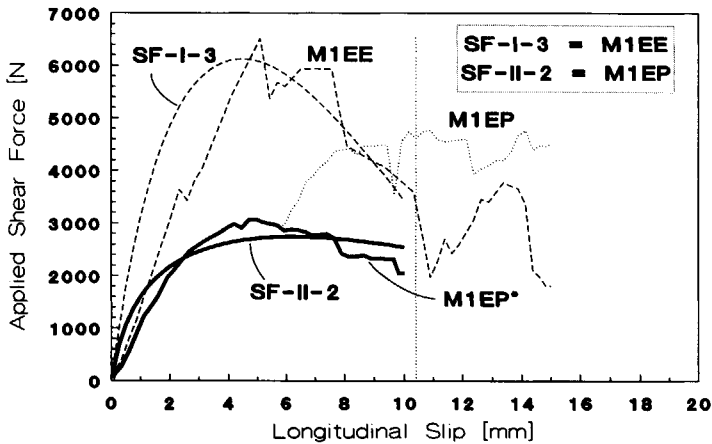


Figure 6.20: Results of SF-I-3, SF-II-2, M1EE, M1EP & M1EP'

SF-II-3: Plasticity of the sheeting

SF-I-4 considers plasticity of the sheeting, and elastic behaviour of the concrete, similar to M1PE. SF-II-3 considers plasticity of sheeting and concrete similar to M1PP. Figure 6.21 shows the results of SF-I-4, M1PE, SF-II-3 & M1PP.

The stiffness of SF-I-4 is higher than for M1PE. This is partly caused by the neglecting of rotation, which improves the stiffness of the connection, as illustrated in Fig. 6.19. If rotation of the indentation is considered, yielding of the top flange occurs earlier at the front toe of the indentation. Therefore the reduction of the stiffness will be larger than shown in Fig. 6.19.

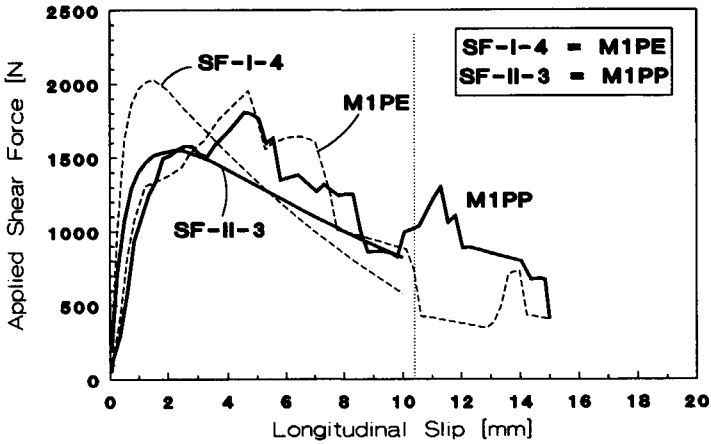


Figure 6.21: Results of SF-I-4, SF-II-3, M1PE & M1PP

SF-II-4: Contact between the webs and the concrete

The influence of contact between the webs and the concrete can be included in the general solution technique, using results of SF-I models. For SF-I-3 and -4 the bending moments at the clamped edges result from the FE-models. For SF-I-1 and -2, the bending moments result from the 2-D beam analysis, where M_1 acts over b_1 and M_2 acts over b_2 .

Elastic: $M_{E;1} = \frac{F_{\perp;1} \cdot L_1}{8}$ $M_{E;2} = \frac{F_{\perp;2} \cdot L_2}{8}$ (6.8)

Plastic: $M_{P;1} = m_p \cdot b_1$ $M_{P;2} = m_p \cdot b_2$ (6.9)

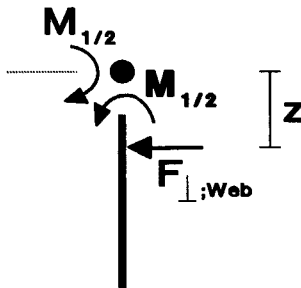


Figure 6.22: Conversion bending moments to contact forces

The conversion of bending moments to contact forces between the webs and

concrete is illustrated in Fig. 6.22. The lever arm z is assumed to be 10.0 mm. The assumption is based on the fact that the edge of the flange moves away from the concrete when the flange deforms. This implies that z is larger than can be expected from the stiffness ratio between the sheeting and the concrete.

$$F_{\perp;Web} = \frac{M_{1/2}}{z} \quad (6.10)$$

$$F_{\parallel;Web} = \mu \cdot F_{\perp;Web} \quad (6.11)$$

The contribution of $F_{\parallel;Web}$ is added to the results of SF-II-3 within the general solution technique. Results can be compared to M3PP. Figure 6.23 shows results of SF-II-3, SF-II-4, M1PP & M3PP.

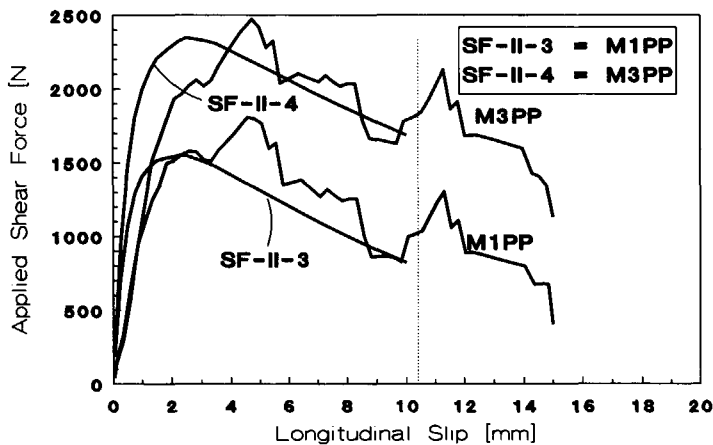


Figure 6.23: Results of SF-II-3, SF-II-4, M1PP & M3PP

All SF-models are evaluated for specimen containing sheeting with a thickness of 1.00 mm. Results for sheeting with a thickness of 0.75 mm are shown in Fig. 6.24.

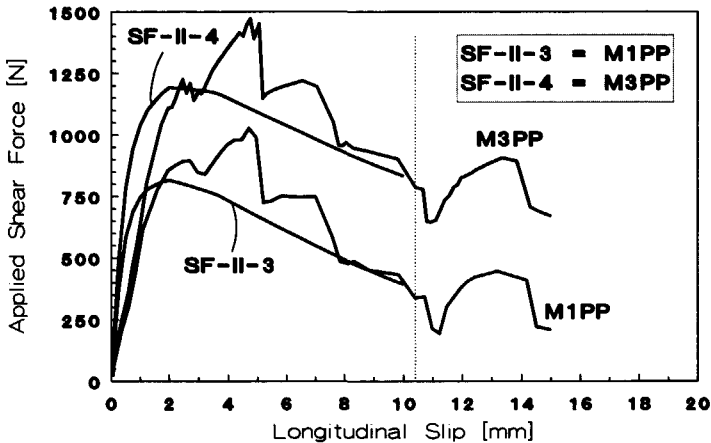


Figure 6.24: Results of SF-II-3, SF-II-4, M1PP & M3PP for 0.75 mm

The stepwise development of the SF-models in this paragraph illustrates the possibilities of the general solution technique. Four different phenomena were described and included in the general solution technique in SF-II-1 to -4. Appropriate tools were used for the description of the different phenomena. Similar to the stepwise development of FE-models, the stepwise development of the SF-models increases understanding of the physical behaviour. The validation of Series II, in which the FE-models are validated by experiments and the SF-models by the validated FE-models illustrates the strength of the two different type of models.

6.3 Series III: Validation Realistic Shear Connections (Level 2)

For Series III, no SF-models are considered. The FE-models are validated by experimental results.

The FE-models of Series III are cross-sectional models, modelling half a web, containing two indentations. Concrete volumes are placed in front of the indentations and at the flanges. The external lateral force, applied to the test specimen, is represented by a proportional lateral force at the bottom flange. All phenomena summarized in § 6.2.1 are included in the FE-models.

Plasticity of Sheeting

Material properties are not supplied by the manufacturer. Therefore the material properties of Series II are used.

Crushing of concrete in front of indentations

Similar to Series II, the fictitious material properties are determined by matching the damage found in experiments to the plastic deformation of FE-models. Series III contains normal strength instead of high strength concrete and interaction forces remain five times smaller. The fictitious material properties are based on properties of the cement paste and the actual concrete. If interaction forces remain small, the properties of cement paste are dominant, where for large interaction forces the paste is crushed and the properties of concrete become more important. The derived properties for Series III are also presented in Table 6.2.

Contact between indentations and concrete

Similar to Series II, concrete volumes are placed in front of the indentations. The coefficient of friction is increased from 0.30 to 0.40. Usage of high strength concrete justifies a reduction of the coefficient of friction in Series II. For normal strength concrete the coefficient of friction used in the concrete crack model is more appropriate.

Contact between flanges and concrete

Similar to contact between the webs and the concrete in Series II, contact occurs between flanges and concrete. No deformation of concrete is considered in these areas.

Separation between sheeting and concrete

Within the cross-sectional FE-models the separation is not restricted.

In Figs. 6.25 to 6.28 experimental and FE-results of representative specimen of Type I and II are shown. Results for big indentations show reasonable agreement with the applied shear force. The deformation and separation is slightly over-estimated. Results for small indentations show reasonable agreement for the deformation and the separation, while the strength and stiffness are under-estimated. This implies that the considered FE-models tend to under-estimate the strength and stiffness of the connection.

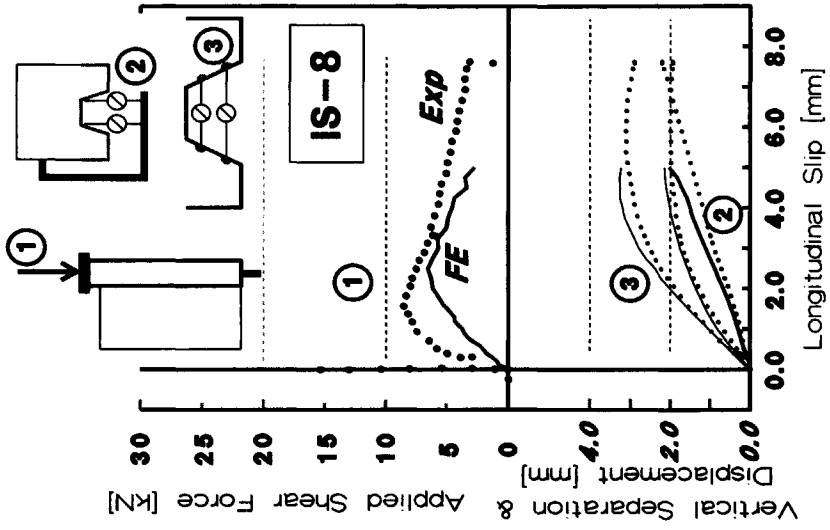


Figure 6.26: Validation for specimen IS-8

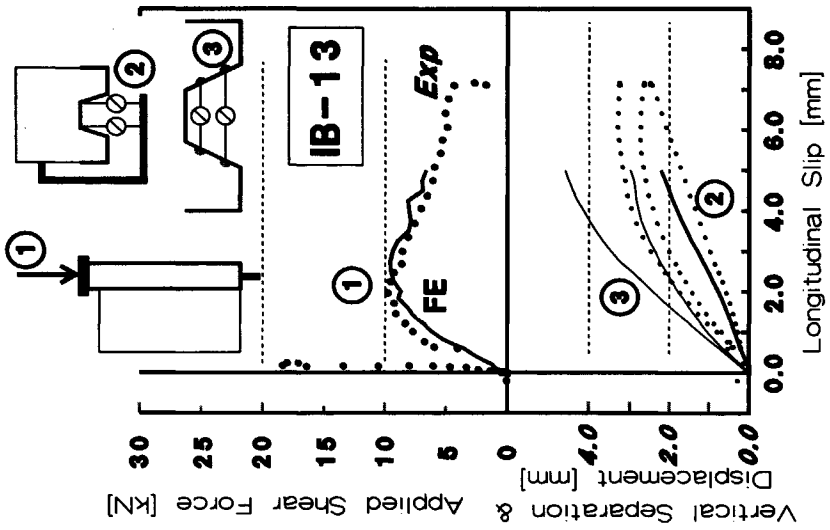


Figure 6.25: Validation for specimen IB-13

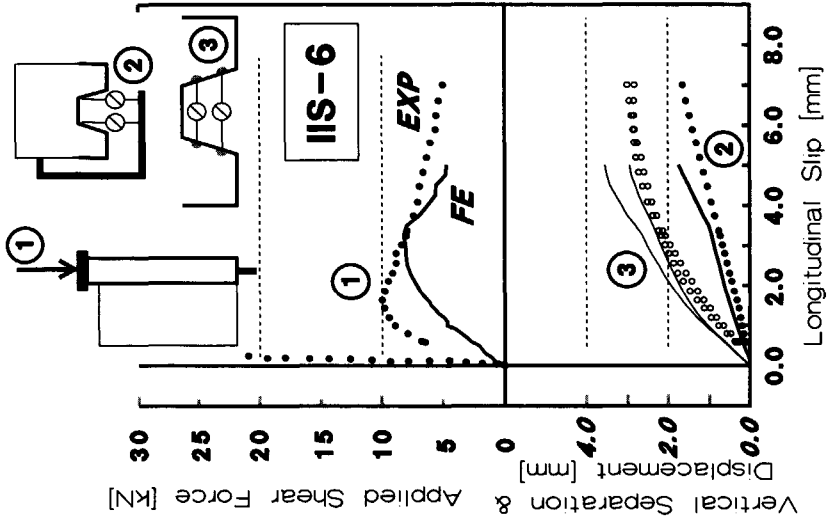


Figure 6.27: Validation for specimen IIB-17

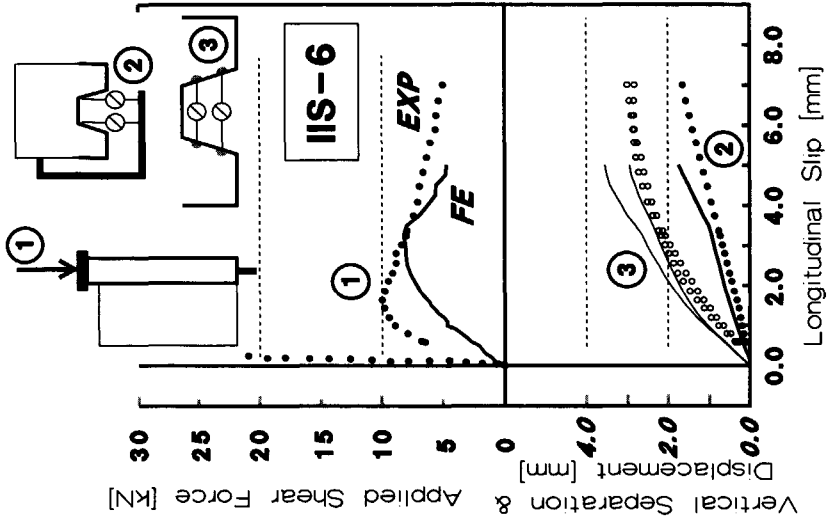


Figure 6.28: Validation for specimen IIS-6

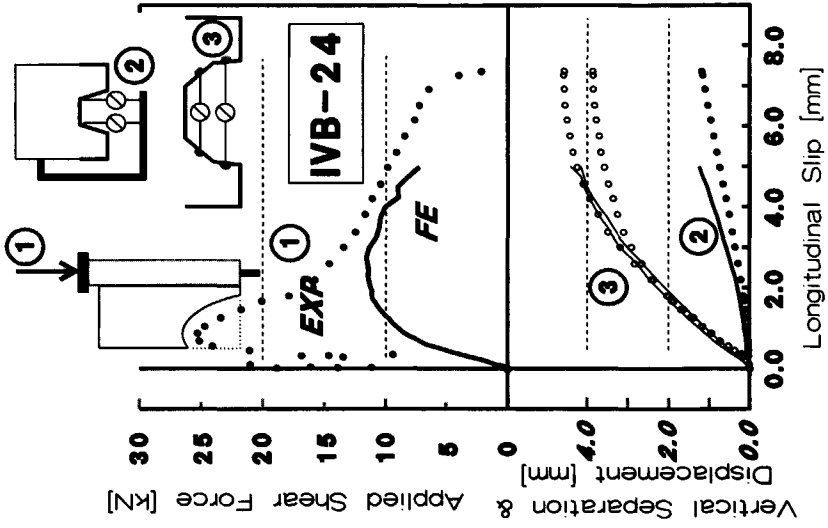


Figure 6.30: Validation for specimen IVB-24

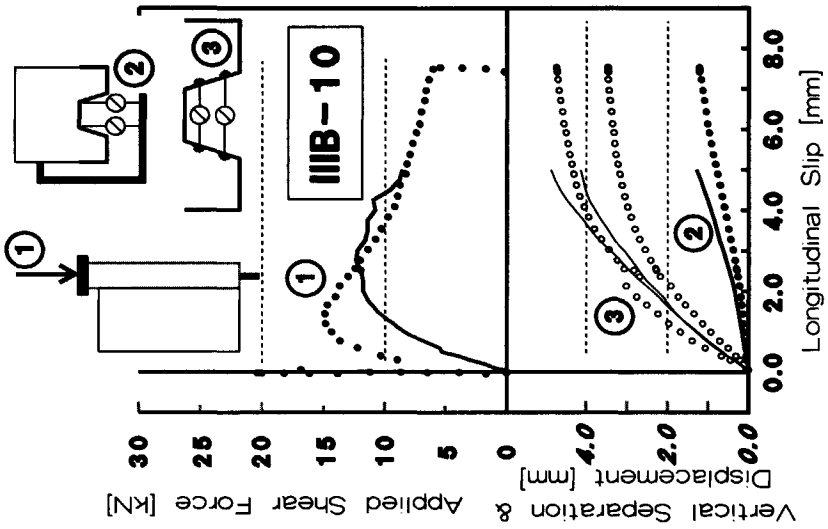


Figure 6.29: Validation for specimen IIIB-10

In Figs. 6.29 to 6.30 a similar comparison is given for representative specimen of Type III and IV, containing only big indentations. The FE-results for these specimen are significantly lower than the experimental results.

The cross-sectional approach of the numerical models does not match the deformed shape of the specimen, as illustrated in Fig. 5.42. The concrete block rotates when separation occurs. The measurements are taken 125 mm from the bottom of the specimen. The vertical separation between the bottom flange and the concrete varies over the specimen from $\bar{\delta}_{VSMmin}$ to $\bar{\delta}_{VSMmax}$:

$$\bar{\delta}_{VSMmin} = \frac{L_0}{L_0 + L_M} \cdot \delta_{VSM} = \frac{50}{175} \cdot \delta_{VSM} = \frac{2}{7} \cdot \delta_{VSM} \quad (6.12)$$

$$\bar{\delta}_{VSMmax} = \frac{L_0 + L}{L_0 + L_M} \cdot \delta_{VSM} = \frac{350}{175} \cdot \delta_{VSM} = 2 \cdot \delta_{VSM} = 7 \cdot \bar{\delta}_{VSMmin} \quad (6.13)$$

with: $\bar{\delta}_{VSM}$ = measured vertical separation bottom flange at L_M
 L_0 = length reinforcement bar underneath specimen = 50 mm
 L_M = location measurements from bottom specimen \approx 125 mm
 L = length specimen = 300 mm

The numerical models represent a cross-section of the specimen. So far, results at cross-section M are considered. If boundary conditions are applied which result in smaller values of $\bar{\delta}_{VS}$, representing the lower part of the specimen, the characteristics of the shear connection improve. The reduction of the separation requires an external compressive lateral force. The reverse, if larger values of $\bar{\delta}_{VS}$ are considered, representing the upper part of the specimen. If the positive effect of restricted separation ($\bar{\delta}_{VSM} - \bar{\delta}_{VSMmin}$) equals the negative effect of increased separation ($\bar{\delta}_{VSM} - \bar{\delta}_{VSMmax}$), the cross-sectional approach is a reasonable representation of the specimen.

For all rib types, shown in Figs. 6.25 to 6.30, the separation of the bottom flange ($\bar{\delta}_{VSM}$) is almost proportional to the longitudinal slip ($\bar{\delta}_l$). In Table 6.4 the ratio between the separation at the bottom flange and the longitudinal slip is presented. It shows that the separation of the bottom flange reduces for steeper webs (Type I-II). The separation of the bottom flange for profiles with sloping webs is larger, due to stretching of the web (Type II-III/IV). Increasing the angle in the web further increases the separation (Type III-IV).

Table 6.4: Results linear regression between δ_{VSM} and δ_l

	IB	IS	IIB	IIS	IIIB	IVB
Ratio δ_{VSM} over δ_l	0.3446	0.3361	0.2751	0.2628	0.3817	0.5563

For all specimen, two additional calculations are performed. The separation between the bottom flange and the concrete was forced to respectively δ_{VSMmin} and δ_{VSMmax} , using eq. (6.12) and the ratios as presented in Table 6.4. Equilibrium of lateral forces for the overall specimen is not checked. In order to satisfy equilibrium within the specimen, the external compressive and tensile lateral forces acting with δ_{VSMmin} and δ_{VSMmax} should be comparable.

For all specimens, the applied shear force of the original and additional calculations are shown in Figs. 6.31 to 6.36. It shows that for regular trapezoidal profiles (Type I & II) the positive and negative effect of variations of separation on the applied shear force are comparable. The same holds for the applied lateral forces, which implies that the cross-sectional approach is a reasonable representation for these configurations.

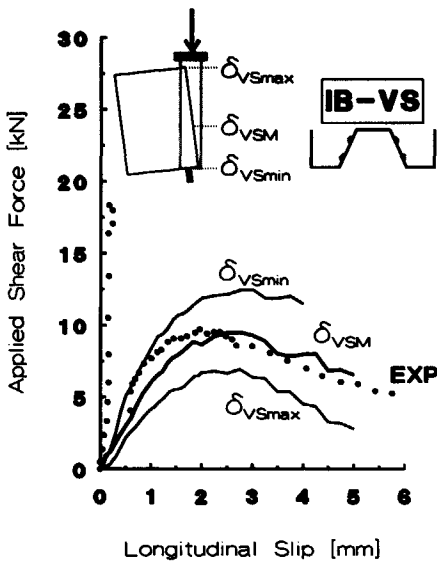


Fig. 6.31: 3 Levels of separation IB-VS

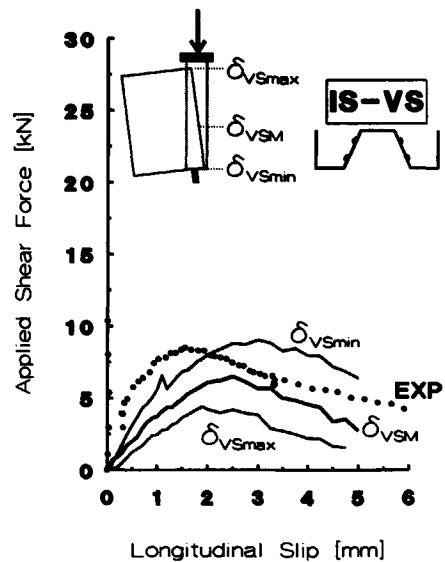


Fig. 6.32: 3 Levels of separation IS-VS

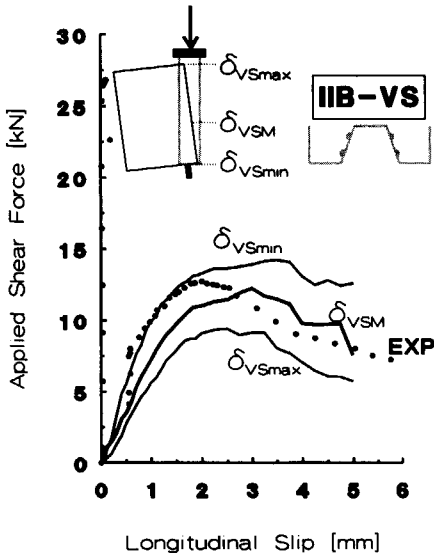


Fig. 6.33: 3 Levels of separation IIB-VS

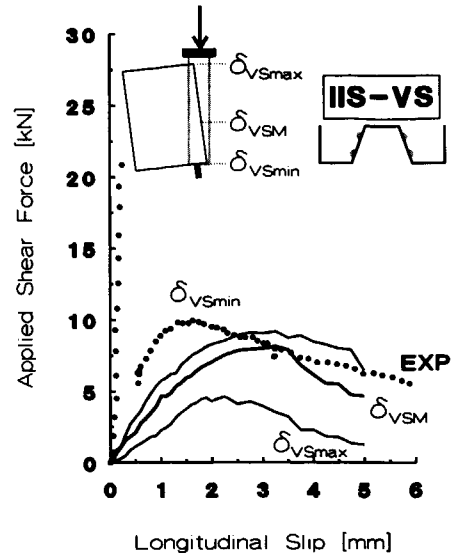


Fig. 6.34: 3 Levels of separation IIS-VS

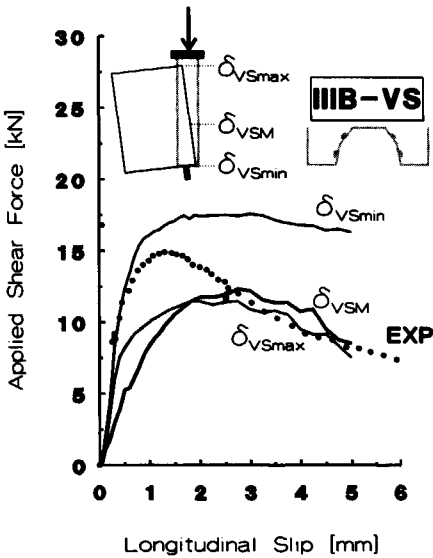


Fig. 6.35: 3 Levels of separation IIIB-VS

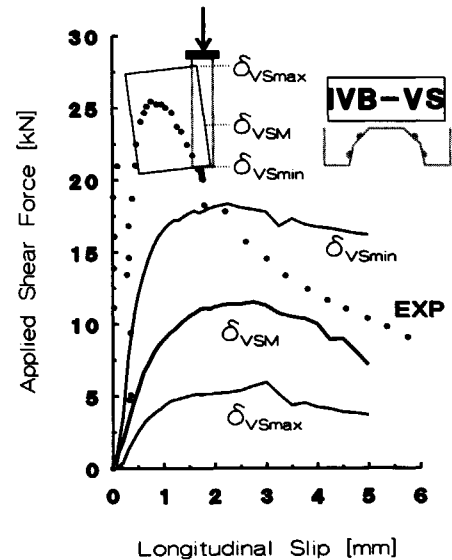


Fig. 6.36: 3 Levels of separation IVB-VS

For specimen with sloping webs (Type III & IV) the effect of the forced separation is larger than the effect found for the trapezoidal profiles (Type I & II). For specimen of Type IV the positive and negative effect on the applied shear force is comparable. For specimen of Type III, the results for $\delta_{V_{Smax}}$ do not meet the pattern as found in all other specimen. It is likely that the FE-results for this calculation are not correct ($\delta_{V_{Smax}}$). Results of the external lateral force are not comparable. It appears that the required compressive lateral force acting with $\delta_{V_{Smin}}$ is larger than the required tensile force for $\delta_{V_{Smax}}$. This implies that the comparison between the experimental and numerical results using different levels of separation is not suitable for specimen with sloping webs.

The large difference between the experimental and FE-results for specimen IVB cannot be explained by the FE-models. The shear strength found in full-scale experiments lies closer to the FE-results [11]. The characteristic shear strength of the developed profile, corresponding to specimen IVB in this chapter, is 0.22 N/mm², which corresponds to an applied shear force of 13.3 kN for the considered specimen. It seems that the form of the test arrangement had a positive effect on the strength of small-scale specimen containing sloping webs. Since the numerical results are supported by the full-scale experimental results, no further development of the FE-models is considered.

Although the overall behaviour of the small-scale specimen containing sloping webs is not validated by the FE-models, the influence of the sloping webs on the shear resistance, as given in § 5.3, is supported by the FE-results. In § 5.3 it is stated that interlocking occurs between the lower indentation and the top flange, which evokes contact forces between the top flange and the concrete. Figure 6.36 shows an angle in the course of the applied shear force at a level of slip of approximately 2 mm. Within the FE-models, this level of slip corresponds to first separation of the edge between the web and the top flange. The FE-results do not show a significant influence on the loss of contact to the applied shear force, similar to the experimental results. However, the fact that the characteristic point in the experimental results coincides with the occurrence of separation at the top flange, supports the idea concerning the interlocking of the web.

6.4 Conclusions for Chapter 6

- # The assumption concerning the direction of interaction forces as given in the hypothesis is valid. For the considered range of interaction forces, a constant value for the coefficient of friction was established. (§ 6.1)
- # Stepwise development of numerical models, both SF- and FE-models, increases understanding into the behaviour of shear connections. (§ 6.2)
- # FE-models can be validated by experiments. SF-models can be validated by validated FE-models. (§ 6.2)
- # The SF-models illustrate the possibilities of the general solution technique. Within the general solution technique, due to the separate analysis, description of phenomena can be performed using the most suitable tools. (§ 6.2)
- # With respect to deformation of concrete, the outer layer of concrete is important. Description of geometrical and material properties of this outer layer of paste is beyond the scope of the thesis. Inspection of connections after experiments is very important. The deformation of the concrete supplies valuable information for the determination of the properties of the cement paste. Fictitious properties are derived, which result in plastic deformation of concrete, matching the damage found in experiments. (§ 6.2/3)
- # Within the numerical models, coefficients of friction of 0.30 and 0.40 are used for respectively high strength and normal strength concrete (Series II/III). Within the concrete crack model a coefficient of friction of 0.40 is used. The reduction of the coefficient to 0.30 for Series II is based on the fact that high strength concrete improves the properties of the cement paste and therefore smoothens the concrete surface. (§ 6.2/3)
- # By using small-scale experiments to determine the behaviour of the shear connection, usually boundary conditions are applied which are not present in full-scale slabs. Together with the fact that by definition not all phenomena can be considered, for instance curvature and cracking of

concrete, it is questionable whether small-scale experiments can be used to determine the behaviour of shear connections in composite slabs.

(§ 6.3)

For common trapezoidal profiles (Type I and II), the results obtained by the cross-sectional approach in the FE-models show reasonable agreement with the small-scale experimental results. (§ 6.3)

Rapid development of FE-tools solves limitations, such as the linear contact elements and the considered geometrical linear behaviour. In general it can be stated that the stepwise development of FE-models, required for the development of accurate models, is more important than practical or technical limitations of current FE-tools. (Chapter 6)

7. PARAMETRIC STUDY

7.0 Introduction

Three parametric studies are performed, based on three types of profiled sheeting, using both SF- and FE-models.

Transparency is the most important feature of SF-models. The visual solution method as presented in § 3.4 leads to ultimate transparency by showing different parts of the connection, the relations between them, and the influence of each part on the overall behaviour of the connection. SF-models should be considered as tools enabling investigation of shear connections, which are too complicated for the visual solution method.

Application of FE-models instead of SF-models is more appropriate if the transparency or the flexibility of SF-models is affected by the configuration of the connection. Furthermore, application of FE-models is required if physical phenomena are to be considered, which can not be included in SF-models.

Similar to the validation procedure presented in chapter 6, FE-models describe the actual behaviour of shear connections provided all relevant phenomena and geometrical data are included in the FE-model. Due the simplifications in SF-models, SF-results can only be compared to FE-results obtained by simplified FE-models. SF-results can be used for qualitative analysis or for analysis of specific phenomena or geometrical properties.

7.1 Parametric Study Example Chapters 3 & 4

Based on the geometry of the example, evaluated in § 3.5 & 4.5, a parametric study is performed using SF-models. Since the ACTION and REACTION modules within the SF-model are described in parameters, determination of the influence of variations is simple and fast. Five parameters are varied. The underlined values correspond to the basic configuration:

Chapter 7

- SF①: Location indentation: $\alpha=1/3$, 1/2 & 2/3
- SF②: Slope web: 0°, 15° & 30°
- SF③: Height indentation: 2.5, 3.0 & 3.5 mm
- SF④: Coefficient of friction: 0.3, 0.4 & 0.5.
- SF⑤: Resultant lateral force: 0, 75 & 150 N

An FE-model is used to vary parameters which are difficult to consider using SF-models:

- FE①: Plasticity: no plasticity & 360 N/mm²
- FE②: Longitudinal prestress in the sheeting: 0 & 95 % f_{yld}

Results are shown in Figs. 7.1 to 7.7. The applied shear force is plotted on the left axis. The vertical separation is plotted on the right axis.

SF①: Location indentation (Fig. 7.1)

When the indentation is moved up ($\alpha=2/3$) or down ($\alpha=1/3$) with respect to the original position ($\alpha=1/2$), the shear resistance increases, due to the more favourable location of the forces acting on the web. Due to rotation of the indentation (φ_x) the resistance to vertical separation increases when the indentation is moved down ($\alpha=1/3$) and decreases when the indentation is moved up ($\alpha=2/3$). Due to the higher resistance to vertical separation, moving down the indentation is more beneficial.

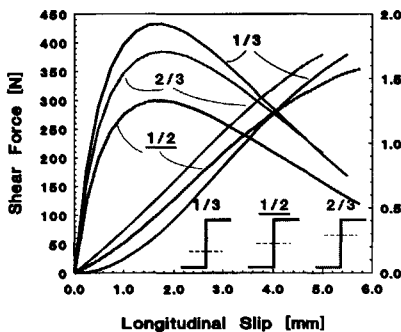


Figure 7.1: SF①: Location indentation

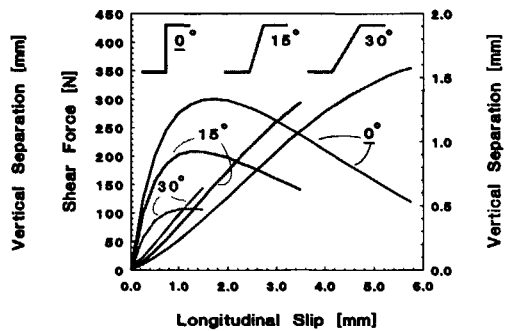


Figure 7.2: SF②: Slope web

SF②: Slope web (Fig. 7.2)

When the slope of the web increases, the resistance to vertical separation

decreases. The sheeting is pushed away from the concrete. Contact is lost between the flanges and concrete. When the slope of the web increases, the strength, stiffness and ductility of the connection decreases.

SF③: Height indentation (Fig. 7.3)

Over-riding of indentations by the concrete is related to the height of indentations. For the considered circular indentation the inclination of the indentation at the toe increases with the height of the indentation. Therefore, both the stiffness and the strength of the connection increase. Due to the increased inclination at the toe, vertical separation remains smaller for small values of slip. For larger values of slip the larger interaction forces for the higher indentations lead to a higher level of separation.

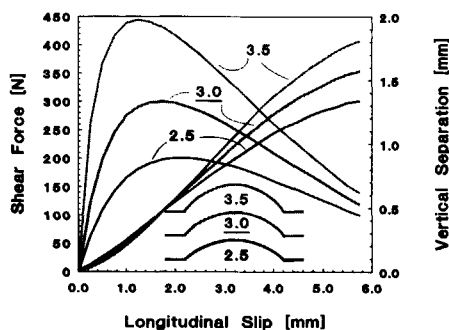


Figure 7.3: *SF③: Height indentation*

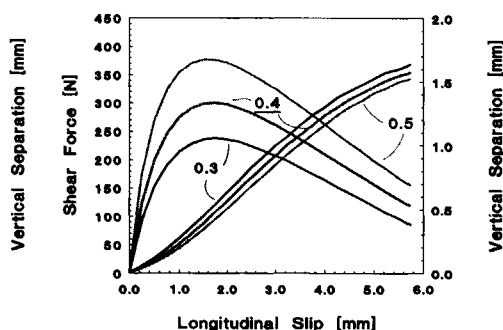


Figure 7.4: *SF④: Coefficient of friction*

SF④: Coefficient of friction (Fig. 7.4)

Similar to the inclination of indentations, the coefficient of friction influences the direction of interaction forces. Increasing the coefficient of friction improves both the shear resistance and the resistance to vertical separation. The improvement of the shear resistance results in higher interaction forces. In spite of the improved shear resistance, vertical separation reduces for higher values for the coefficient of friction.

SF⑤: Resultant lateral force (Figs. 7.5)

In general, external lateral forces reduce vertical separation and improve the shear resistance. Due to the simplicity of the mechanical model used in the REACTION module, vertical separation is negative for small values of slip. Profiles with limited resistance to vertical separation benefit most from the

presence of external lateral forces. Within the basic configuration, the tendency to separate is limited. The contribution of friction is approximately 60% ($0.40 \cdot 75 \text{ N} = 60\% \cdot 50 \text{ N}$). The remaining 40% is caused by the reduced separation.

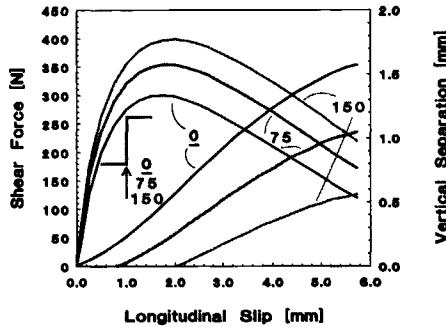


Figure 7.5: SF@0°: Lateral force

FE①: Plasticity

Due to plasticity, the shear resistance of the connection decreases, since the resistance of the web to forces perpendicular to the web is limited. Due to the presence of the indentation, first yielding occurs at the upper and lower toe of the indentation, due to the local stress concentrations. The level of vertical separation is hardly influenced by the occurrence of plastic behaviour.

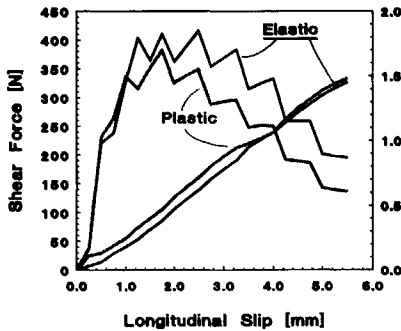


Figure 7.6: FE①: Plasticity

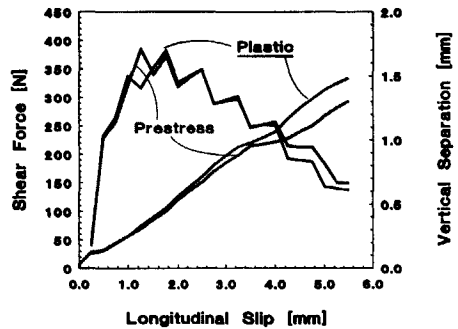


Figure 7.7: FE②: Longitudinal 'prestress'

FE②: Longitudinal prestress in the sheeting

Due to the shear connection, high tensile stresses can be present in the sheeting. Longitudinal tensile stresses reduce the bending capacity of the web and flanges, and therefore reduces the shear resistance. However, it shows that

large longitudinal tensile stresses hardly influence the shear characteristics.

7.2 Parametric Study Series II

Based on the geometry of the experimental Series II (§ 5.2), a parametric study is performed using both SF- and FE-models. Since SF-models contain simplifications, results of the basic configurations of the SF- and FE-models are not identical. Although the SF-models are not able to describe the actual behaviour of the connection, results of both models supply valuable information about the influence of variation of parameters of shear connections to the shear resistance.

Four parameters are varied, using both SF- and FE-models and two using only FE-models. Again the underlined values correspond to the basic configuration of Series II. Results are plotted in Figs. 7.8 to 7.17 and discussed briefly.

- SF①/FE① Thickness sheeting: 0.75, 1.00 & 1.25 mm
- SF②/FE② Plasticity of steel: 240, 360 & 480 N/mm²
- SF③/FE③ Coefficient of friction: 0.2, 0.3 & 0.4
- SF④/FE④ Height indentation: 3.0, 3.6, 4.134 & 4.8 mm
- FE⑤ Strength of concrete: 15, 25, 35 N/mm²
- FE⑥ Longitudinal prestress in the sheeting: 0, 50, 70 & 90 % f_{yd}

SF①/FE①: Thickness sheeting (Figs. 7.8 & 7.9: $0.75 < t < 1.25$ mm)

The bending capacity of the sheeting is quadratically proportional to the thickness. The stiffness is proportional to the third power. All SF-models are based on the procedure as given in § 6.2.2. The visual solution method is used, assuming a bi-linear relation between F_{\perp} and δ_{\perp} based on the models SF-I-1 & SF-I-2 (§ 6.2.2a). For the SF-models the variation of the shear resistance is almost proportional to the variation of the bending capacity of the sheeting. Within FE-models, a higher bending capacity results in larger interaction forces, which increase the deformation of concrete and reduce the effect of the improved capacity and stiffness.

Strength

$$M_p(0.75) : M_p(1.00) : M_p(1.25) = 0.75^2 : 1.00^2 : 1.25^2 = 0.56 : 1.00 : 1.56 \quad (7.1)$$

Chapter 7

SF①: $F_{l,max}(0.75) : F_{l,max}(1.00) : F_{l,max}(1.25) \approx 0.52 : 1.00 : 1.61$ (7.2)

FE①: $F_{l,max}(0.75) : F_{l,max}(1.00) : F_{l,max}(1.25) \approx 0.60 : 1.00 : 1.40$ (7.3)

Stiffness

$EI(0.75) : EI(1.00) : EI(1.25) = 0.75^3 : 1.00^3 : 1.25^3 = 0.42 : 1.00 : 1.95$ (7.4)

SF①: $F_{l,max}(0.75) : F_{l,max}(1.00) : F_{l,max}(1.25) \approx 0.46 : 1.00 : 2.15$ (7.5)

FE①: $F_{l,max}(0.75) : F_{l,max}(1.00) : F_{l,max}(1.25) \approx 0.51 : 1.00 : 1.67$ (7.6)

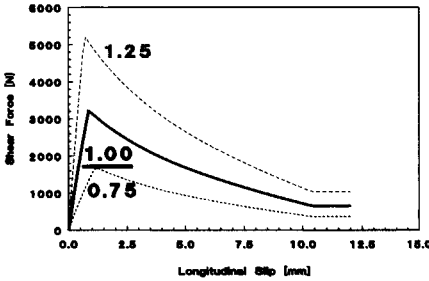


Figure 7.8: SF①: Thickness sheeting

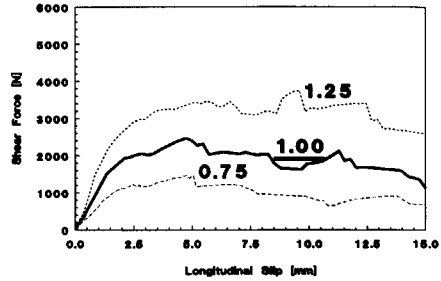


Figure 7.9: FE①: Thickness sheeting

SF②/FE②: Plasticity of steel (Figs. 7.10 & 7.11: $240 < f_{yld} < 480 \text{ N/mm}^2$)

Similar to variation ① the yield stress influences the bending capacity of the sheeting. Only the strength of the shear connection is influenced. Similar to the comments given for variation ① the variation of the shear resistance found with SF-models is almost proportional to the bending capacity, where for the FE-models the effect is reduced by the deformation of concrete.

Strength

$M_p(0.75) : M_p(1.00) : M_p(1.25) = 240 : 360 : 480 = 0.67 : 1.00 : 1.33$ (7.7)

SF②: $F_{l,max}(0.75) : F_{l,max}(1.00) : F_{l,max}(1.25) \approx 0.70 : 1.00 : 1.25$ (7.8)

FE②: $F_{l,max}(0.75) : F_{l,max}(1.00) : F_{l,max}(1.25) \approx 0.80 : 1.00 : 1.20$ (7.9)

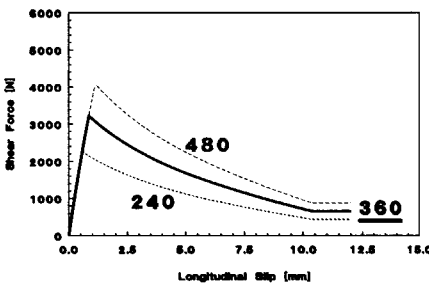


Figure 7.10: SF②: Plasticity of steel

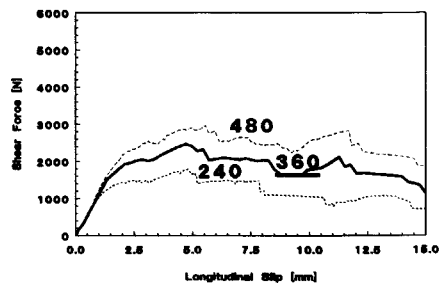


Figure 7.11: FE②: Plasticity of steel

SF③/FE③: Coefficient of friction (Figs. 7.12 & 7.13: $0.2 < \mu < 0.4$)

The variation of the coefficient of friction changes the direction of the interaction force, which means that a similar response of the sheeting leads to different values for the shear resistance.

$$\frac{F_{\parallel}}{F_{\perp}} = \frac{\mu + \tan \varphi}{1 - \mu \cdot \tan \varphi} \tag{7.10}$$

For the circular indentation, $\tan \varphi$ is different for different values of slip. Equation (7.11) shows the ratio between F_{\parallel} and F_{\perp} for a value of $\tan \varphi$ corresponding to a value of slip of 5.0 mm. Since only the direction, but not the size of the interaction force changes, the variation of the strength is almost proportional to the variation of the coefficient of friction in both models. The response of the sheeting and the deformation of concrete is hardly influenced.

Strength ($\delta_f=5.0$ mm)

$$\frac{F_{\parallel}}{F_{\perp}}(0.30) : \frac{F_{\parallel}}{F_{\perp}}(0.40) : \frac{F_{\parallel}}{F_{\perp}}(0.50) = 0.84 : 1.00 : 1.18 \tag{7.11}$$

$$\text{SF③: } F_{\parallel;\text{max}}(0.30) : F_{\parallel;\text{max}}(0.40) : F_{\parallel;\text{max}}(0.50) \approx 0.81 : 1.00 : 1.19 \tag{7.12}$$

$$\text{FE③: } F_{\parallel;\text{max}}(0.30) : F_{\parallel;\text{max}}(0.40) : F_{\parallel;\text{max}}(0.50) \approx 0.78 : 1.00 : 1.20 \tag{7.13}$$

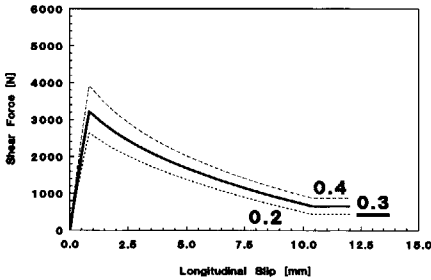


Figure 7.12: SF③: Coefficient of friction

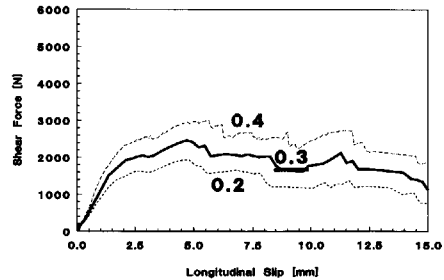


Figure 7.13: FE③: Coefficient of friction

SF④/FE④: Height indentation (Figs. 7.14 & 7.15: $3.0 < H_{ind} < 4.8$ mm)

The height of the circular indentation affects the inclination of the indentation, $\tan \varphi$, which influences the direction of the interaction forces, as shown in eq. (7.11). In this case both the stiffness and the strength are considered. For the stiffness the value of $\tan \varphi$ is based on a value of slip of 1.0 mm, where for the strength again a value of slip of 5.0 mm is considered. Similar to variation ③, the

height of the indentation influences the inclination of the indentation, which effects the direction of interaction forces. The influence to the inclination reduces if the level of slip increases. Due to plastification of the top flange, the actual height of the indentation hardly influences the response of the sheeting, so the variation of the strength of the connection is mainly caused by the direction of the interaction force, $\tan \phi$. Since the stiffness of the connection is considered at a smaller level of slip, the influence to the stiffness is larger as found for the inclination alone.

Stiffness ($\delta_f=1.0 \text{ mm}$)

$$\tan \phi (3.0) : \tan \phi (3.6) : \tan \phi (4.1) : \tan \phi (4.8) = 0.69 : 0.85 : 1.00 : 1.20 \quad (7.14)$$

$$\text{SF}\textcircled{4}: k_f(3.0) : k_f(3.6) : k_f(4.134) : k_f(4.8) \approx 0.70 : 0.84 : 1.00 : 1.23 \quad (7.15)$$

$$\text{FE}\textcircled{4}: k_f(3.0) : k_f(3.6) : k_f(4.134) : k_f(4.8) \approx 0.63 : 0.77 : 1.00 : 1.44 \quad (7.16)$$

Strength ($\delta_f=5.0 \text{ mm}$)

$$\tan \phi (3.0) : \tan \phi (3.6) : \tan \phi (4.1) : \tan \phi (4.8) = 0.76 : 0.89 : 1.00 : 1.13 \quad (7.17)$$

$$\text{SF}\textcircled{4}: F_f(3.0) : F_f(3.6) : F_f(4.134) : F_f(4.8) \approx 0.83 : 0.92 : 1.00 : 1.09 \quad (7.18)$$

$$\text{FE}\textcircled{4}: F_f(3.0) : F_f(3.6) : F_f(4.134) : F_f(4.8) \approx 0.72 : 0.86 : 1.00 : 1.16 \quad (7.19)$$

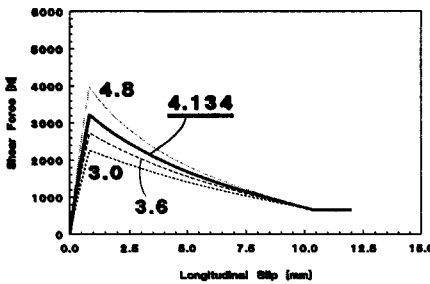


Figure 7.14: SF@: Height indentation

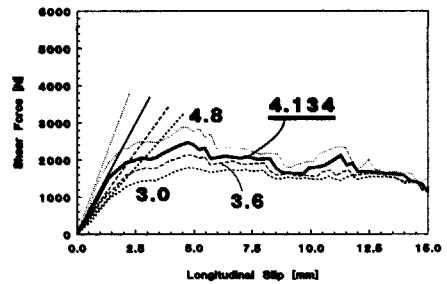


Figure 7.15: FE@: Height indentation

FE@: Strength of concrete (Fig. 7.16: $15 < f_c < 35 \text{ N/mm}^2$)

The behaviour of the concrete is very important for the behaviour of the shear connection. Due to the deformation of concrete, part of the applied slip is taken by the concrete, and the displacements of indentations are reduced, which reduces the stiffness and strength of the connection. If elastic behaviour of the concrete is considered, the indentation is pushed out of the concrete for larger values of slip, which leads to a considerable reduction of the shear resistance, as illustrated by the results of all elastic SF-models. If deformation of concrete occurs, the indentations dig channels in the concrete, and the reduction of the shear resistance for larger values of slip is smaller. This physical phenomenon

causes the differences between the SF- and the FE-models.

The considered strength of concrete corresponds to the strength of the cement paste in high strength concrete ($f_c = 35 \text{ N/mm}^2$ - Table 6.2 - § 6.3) . Reduction of the strength of the cement paste to 25 N/mm^2 hardly affects the strength. Further reduction to 15 N/mm^2 reduces the strength of the connection. In general, the reduction of the strength of the cement paste improves the deformation capacity. The strength of 15 N/mm^2 for the cement paste is still larger than the strength determined for regular concrete in § 6.3.

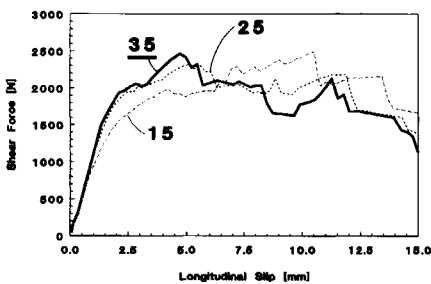


Figure 7.16: FE@: Strength of concrete

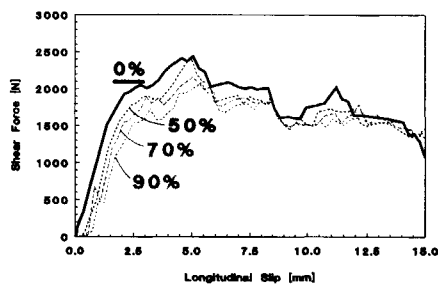


Figure 7.17: FE@: Longitudinal prestress

FE@: Longitudinal prestress in the sheeting (Fig. 7.17: $0 < \% f_{yld} < 90\%$)

If a longitudinal prestress is present in a reduction of the shear resistance can be expected, since longitudinal stresses reduce the bending capacity of the cross-section. If a prestress of 90% of the yield strength is applied the reduction of the strength is only 15 %. Apparently redistribution of stresses reduces the effect of the prestress to the yield pattern of the cross-section. Part of the reduction of the strength is a result of the displacement and deformation of the indentation caused by the applied prestress, which reduces the effectiveness of the indentations.

From Fig. 7.17 it seems that the stiffness of the connection is affected. However, since the prestress is applied to the rear of the model, before slip is applied at the front, elongation of the sheeting occurs and the indentation moves backwards, resulting in a zero stiffness for small values of slip.

7.3 Parametric Study Series III

Based on the geometry of the experimental Series III (§ 5.3), a parametric study is performed, similar to § 7.2. The most important difference between Series II and III is the response of the sheeting. According to the hypothesis, the response of the sheeting is a combination of displacement (separation) and deformation of the sheeting, whereas the ratio between deformation and displacement is a measure for the shear resistance. Within Series II, vertical separation is prevented, which increases the level of deformation. The sheeting in Series III behaves more flexibly due to the presence of separation.

Similar to § 7.2 both SF- and FE-models are used for the parametric study. Again results of the basic configuration for both models are not identical, since the SF-models contain simplifications which affect the behaviour of the shear connection. Within the SF-models, the material behaviour is linear elastic, since inclusion of nonlinear behaviour reduces the transparency of the models and therefore violates the basic principles of SF-models.

Four parameters are varied, using both SF- and FE-models. Three parameters are varied using only FE-models. The underlined values correspond to the basic configuration of Series III:

- SF①/FE① Location indentation: 0.150, 0.175, 0.200, 0.225, 0.250 & 0.275
- SF②/FE② Slope web: -9.5°, 0°, 9.5°, 18.4°, 26.6° & 33.7°
- SF③/FE③ Lateral Force: 0, 21.4, 150, 300 & 450 N
- SF④/FE④ Thickness sheeting: 0.70, 0.80, 0.90, 1.00, 1.10 & 1.20 mm
- FE⑤ Plasticity of sheeting: 240, 360 & 480 N/mm²
- FE⑥ Strength of concrete: 7.5, 15, 30 N/mm²
- FE⑦ Longitudinal prestress in the sheeting: 0, 70 & 90 % f_{yd}

SF①/FE①: Location indentation (Figs. 7.18 & 7.19: $0.150 < \alpha < 0.275$)

The location of the indentation is very important for the behaviour of trapezoidal profiles. Firstly, indentations within trapezoidal profiles resist both longitudinal slip and vertical separation. Located closer to the edges of the web, the resistance to vertical separation increases significantly. Secondly, the location of the indentation in the web influences the deformation of the sheeting. Both effects are also mentioned in § 7.1 for SF①.

The SF-models consider linear elastic behaviour for both the sheeting and the concrete, which leads to a significant reduction of the shear resistance for larger values of slip, since the indentations are pushed out of the concrete. Figure 7.18 shows that the ultimate shear resistance increases significantly if α decreases, due to the more favourable location of interaction forces acting on the web, which improves the response of the sheeting. It also shows that until the ultimate shear stress is reached, the level of separation for all configurations is almost equal. Since interaction forces are larger for smaller values of α , the resistance to vertical separation is larger.

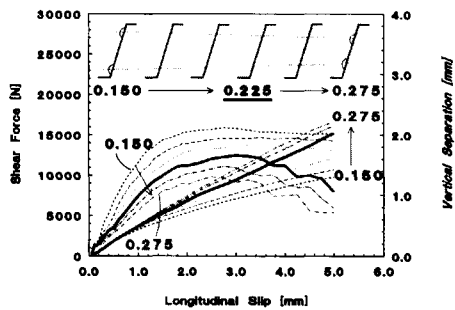
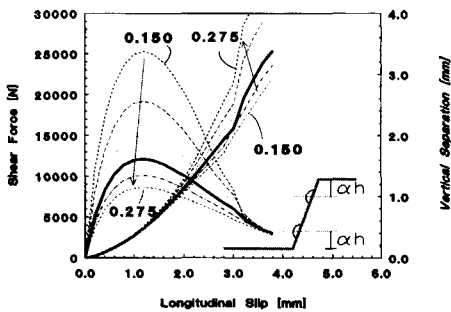


Figure 7.18: SF@: Location indentation Figure 7.19: FE@: Location indentation

Within the FE-models, deformation of concrete improves the resistance for larger values of slip. Since the indentations are not pushed out of the concrete completely, vertical separation remains smaller than found within the SF-models. For $\alpha \geq 0.225$, the deformation of concrete is limited, which leads to a reduction of the strength similar to the reduction found within SF-models. For $\alpha < 0.225$ interaction forces become larger, which increases the deformation of concrete. The reduction of the strength for large values of slip is limited. The stiffness of the shear connection increases if α reduces.

SF@/FE@: Slope web (Figs. 7.20 & 7.21: $-9.5^\circ < \beta < 33.7^\circ$)

In general, a steeper web increases the resistance to vertical separation and reduces the 'span' of the web, which improves the response of the sheeting.

Within the SF-models, the slope of the web is varied between -9.5° and 33.7° . A negative slope corresponds to a re-entrant shape. Figure 7.20 shows that the shear resistance of the re-entrant configuration equals the resistance of the configuration with a vertical web. Apparently the resistance to separation

obtained by the vertical web is enough to ensure maximum shear resistance. Decreasing the slope of the web reduces the strength and stiffness, and increases the vertical separation.

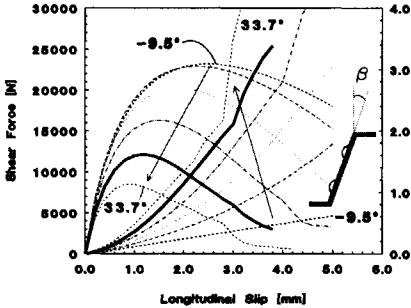


Figure 7.20: SF@: Slope web

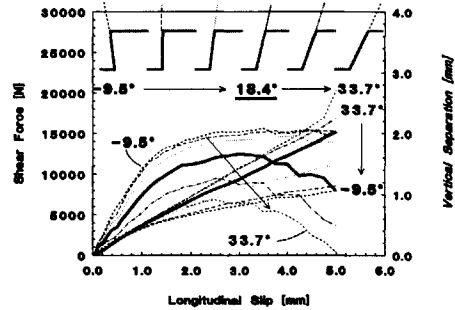


Figure 7.21: FE@: Slope web

Within the FE-models, the slope of the web has a significant influence to the stiffness of the connection. It shows that for $\beta \leq 9.5^\circ$ limited vertical separation occurs and the strength reduction for large values of slip is limited. Profiles with $\beta \geq 18.4^\circ$ show a significant strength reduction over the full range of slip. For larger values of slip, the reduction of the shear resistance implies that the level of deformation of concrete is small. The results for $\beta \geq 26.6^\circ$ show reasonable agreement with the SF-results, which can be explained by the flexible behaviour of the sheeting, resulting in a lower level of plasticity of steel and deformation of concrete. Apparently, the physical behaviour of trapezoidal profiles with a steep web is similar to the behaviour of re-entrant profiles. For the given configuration, the transition between re-entrant and trapezoidal behaviour of a connection corresponds to a slope of the web of approximately 10° .

SF@/FE@: Lateral Force (Figs. 7.22 & 7.23: $0 < F_{LAT} < 450 N$)

In general, the presence of lateral forces improves the shear resistance of a connection. The improvement depends on the internal resistance to vertical separation. A profile with a high resistance to vertical separation benefits from the lateral force by friction. A profile with limited resistance to vertical separation benefits from lateral forces, since the level of separation reduces and the level of deformation increases, which has a more significant influence to the shear resistance as the contribution of friction alone.

The maximum applied lateral force is derived from the support reaction

corresponding to a slab configuration with a span of 4.0 m. The support reaction can be transferred to a lateral force, for the considered width and length of the shear connection.

Within the SF-models, the lateral force varied between -150 and 450 N. It shows that a small or negative lateral force reduces the deformation capacity. The strength increases significantly if the lateral force increases. Approximately 45% of the improvement is caused by a friction. The stiffness increases up to a lateral force of 150 N and does not increase for larger lateral forces. For large lateral forces, the vertical separation remains small, which reduces the effect of further increasing the lateral force. For the SF-models, which assume contact between flanges and concrete in the centre of the flange, negative values for the separation can occur for positive lateral forces.

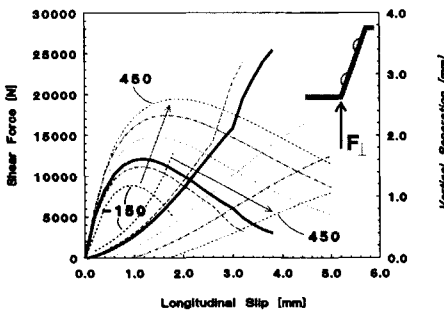


Figure 7.22: SF@: Lateral force

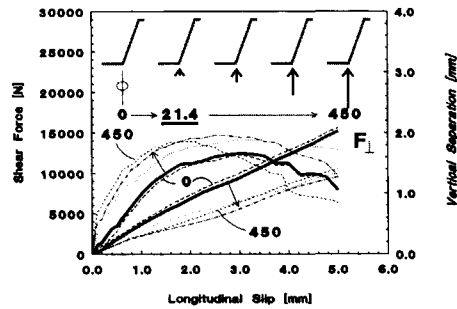


Figure 7.23: FE@: Lateral force

Within the FE-models, the lateral force is varied between 0 and 450 N. The presence of the lateral force ($F_{\perp}=150$ N) improves the strength and stiffness of the connection significantly and reduces the vertical separation. Further increasing of the lateral force ($F_{\perp} \geq 300$ N) improves the stiffness but hardly improves the strength of the connection. For large lateral forces ($F_{\perp} > 300$ N), the strength for large values of slip reduces.

SF@/FE@: Thickness of sheeting (Figs. 7.24 & 7.25: $0.70 < t < 1.20$ mm)

The thickness of the sheeting effects both the bending capacity as the stiffness of the sheeting, which improves the response of the sheeting.

The SF-models do not consider deformation of concrete and plasticity of the sheeting. Figure 7.24 shows that the vertical separation is almost equal for all

thicknesses, which implies that the deformed shape of the sheeting is equal for all configurations. The increase of the strength is proportional to the bending stiffness of the sheeting.

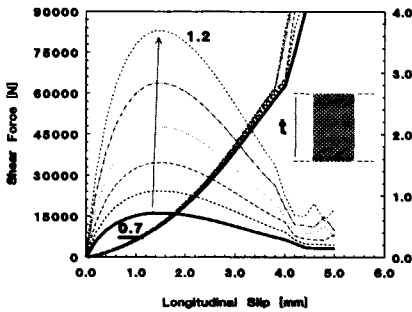


Figure 7.24: SF@: Thickness sheeting

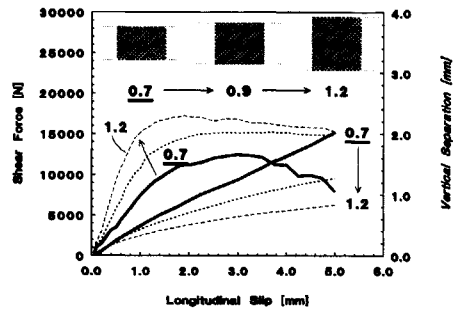


Figure 7.25: FE@: Thickness sheeting

The influence of the thickness is smaller within the FE-models. Apparently the interaction forces corresponding to the large shear resistance found within the SF-models lead to significant deformation of concrete and plastic deformation of the sheeting. Increasing the thickness increases the stiffness of the connection. The influence to the strength is smaller for the larger thicknesses. Due to the deformation of concrete, configurations with larger thicknesses behave more ductile. The level of vertical separation is smaller for larger thicknesses.

FE@: Plasticity of sheeting (Fig. 7.26: $240 < f_{yd} < 480 \text{ N/mm}^2$)

Due to the relative flexible response of the sheeting, the influence of the yield strength is small compared to the re-entrant configuration as discussed in § 7.2. Figure 7.26 shows that first yielding occurs at a slip level of 1.2 mm. Reducing the yield strength, reduces the bending capacity and interaction forces. Similar to earlier comments, smaller interaction forces result in less deformation of concrete, which causes the indentations to be pushed out of the concrete and leads to a strength reduction for large values of slip. Over-riding of the concrete by the indentations increases the level of separation. Increasing the yield strength hardly increases the strength and level of separation, but leads to more ductile behaviour.

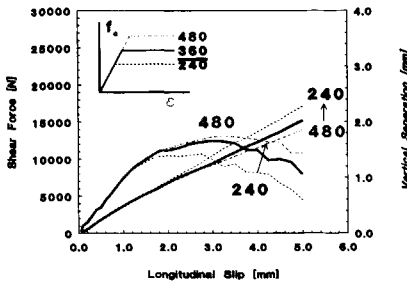


Figure 7.26: FE@: Plasticity sheeting

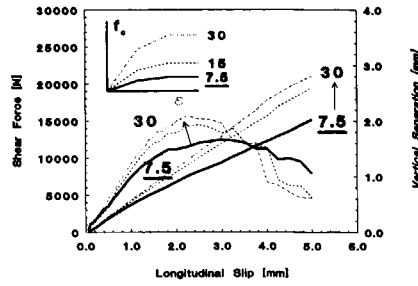


Figure 7.27: FE@: Strength of concrete

FE@: Strength of concrete (Fig. 7.27: $7.5 < f_c < 30 \text{ N/mm}^2$)

As mentioned in § 6.2.1 and 6.3.1 the strength of concrete is a fictitious material parameter, describing the behaviour of the cement paste rather than the actual concrete. As given in § 6.3.1 the strength of the paste varies between 7.5 and 35.0 N/mm² if regular and high strength concrete are considered. In Fig. 7.27 the strength of the paste is varied between 7.5 and 30.0 N/mm².

As illustrated in most FE-results, the influence of the deformation of concrete is important. The influence of the concrete strength and stiffness, as shown in Fig. 7.27 is in accordance with earlier reflections. Increasing the strength of the cement paste from 7.5 to 15.0 N/mm² reduces the level of deformation of the paste, resulting in over-riding of the concrete by the indentation, which explains the significant reduction of the strength for large values of slip and the corresponding higher level of separation. Further increasing the strength to 30 N/mm² has limited effect. Increasing the strength and stiffness of the cement paste

Table 6.2 relates the properties of the cement paste to the properties of concrete. The concrete used in experimental Series III, referred to as regular concrete, can be classified as C30/37. In practice concrete classified as C20/25 and C30/37 behaves similar to the corresponding strength of the cement paste of 7.5 and 15.0 N/mm² in Fig. 7.27.

FE@: Longitudinal prestress in the sheeting: (Fig. 7.28: $0 < \% f_{yld} < 90 \%$)

The influence of variation of the yield strength to the shear resistance is limited due to the flexible response of the sheeting, similar to variation FE@. Therefore the influence of the longitudinal prestresses is also limited. Apparently, the yield

pattern, consisting of yield lines at the edges of the web and at the toe of indentations, is hardly influenced by the applied prestress. Redistribution of stresses over the cross-section allows the prestressed configurations to develop almost the same ultimate strength as the basic configuration.

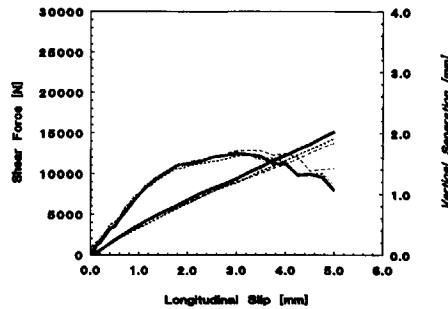


Figure 7.28: FEØ: Longitudinal prestress

Results and conclusions of all parametric studies in this chapter are related to the considered configuration. The configuration of § 7.2 is a representative re-entrant type of sheeting, whereas the configuration of § 7.3 is a representative trapezoidal type of sheeting. The tested Types III & IV (§ 6.3), containing the sloping webs, can also be classified as trapezoidal profiles.

As mentioned in chapter 1 recent profiles often combine re-entrant and trapezoidal portions. Depending on the location and geometry of the re-entrant portions the behaviour of these profiles can be classified as re-entrant or trapezoidal. Most important for the classification of these profiles is the expected level of vertical separation. The re-entrant portion in the upper profile in Fig. 1.3 effectively reduces the level of vertical separation of the sheeting. Therefore the profile can be classified as re-entrant. The re-entrant portion in the centre of the top flange of the lower profile is less effective and therefore hardly affects the level of separation of the sheeting. Therefore the profile can be classified as trapezoidal. If indentations are present in the re-entrant portions, these indentations are more effective than the indentations in the trapezoidal portions. In that case the complete profile can be classified as re-entrant.

7.4 Conclusions Chapter 7

- # The slope of the web can be used to classify profiles. Profiles with steep webs (slope $< 10^\circ$) show a large ratio between deformation and displacement of the sheeting, resulting in plastification of sheeting and deformation of concrete. This is referred to as 're-entrant' behaviour as it is similar to the behaviour found for re-entrant profiles. The remaining profiles show a smaller ratio between deformation and displacement and limited plastification of sheeting and deformation of concrete. This is referred to as 'trapezoidal' behaviour to distinguish it from the previous type of profiles.
- # In Table 7.1 the results of all parameters investigated are presented. Distinction is made between 're-entrant' and 'trapezoidal' types of sheeting.

Table 7.1: Influence of parameters on the behaviour of shear connections

Shape of the profiles	'Re-entrant'			'Trapezoidal'		
Ratio deformation / displacement	<i>large</i>			<i>small</i>		
Slope web	$< 10^\circ$			$> 10^\circ$		
Effect increasing parameter to: +/- = positive/negative effect 0 = no effect	Strength	Stiffness	Ductility	Strength	Stiffness	Ductility
<i>Slope web</i>	0	0	0	-	-	-
<i>Lateral force</i>	+	0	0	+	+	+
<i>Location indentation</i>	+	+	0	+	+	0
<i>Height indentation</i>	+	+	0	+	+	0
<i>Coefficient of friction</i>	+	+	0	+	+	0
<i>Yield strength sheeting</i>	+	0	0	0	0	0
<i>Thickness sheeting</i>	+	+	+	+	+	0
<i>Strength concrete</i>	+	0	-	+	0	-
<i>Longitudinal prestress</i>	0	0	0	0	0	0

- # The properties of the concrete and the cement paste have a significant influence on the physical behaviour of the connection. If the indentations 'dig' channels in the cement paste, the behaviour of the connection is more ductile. The deformation of concrete depends on the properties of concrete and level of the interaction forces. Limited deformation of concrete leads to more brittle behaviour. The deformation of concrete implies that for ductile shear connections, the behaviour is path-dependent.

- # The configurations of § 7.2 and 7.3 can be considered as representative re-entrant and trapezoidal types of sheeting. Most recent profiles combine re-entrant and trapezoidal portions. Depending on the location and geometry of the re-entrant portions the behaviour of these profiles can be classified as re-entrant or trapezoidal.

- # Although only circular indentations are considered in this chapter, the reflections hold for all types of indentations. In general circular or curved indentations behave better than sloping indentations consisting of multiple flat parts, since the maximum inclination is larger.

8. FULL-SCALE SLAB ANALYSIS

8.0 Introduction

According to the three levels of research, illustrated in Fig. 2.30, the work presented in this thesis is based on cross-sectional Level 1 analysis. The accuracy of current full-scale Level 3 models depends mainly on the description of the physical behaviour of the shear connection. Greater understanding of the behaviour of shear connections can lead to improved models.

In § 8.1, a general full-scale model (Level 3) is presented. In § 8.2, a general cross-sectional model for shear connections in composite slabs is presented which relates the Level 1 and 2 analysis of shear connections to the Level 3 full-scale slab analysis. Comments on the Partial Shear Connection method and small-scale experiments are made in § 8.3 and 8.4. Finally, comments on product development are made in § 8.5.

8.1 General Model Full-scale Composite Slab - Level 3

A general full-scale slab model is shown in Fig. 8.1.

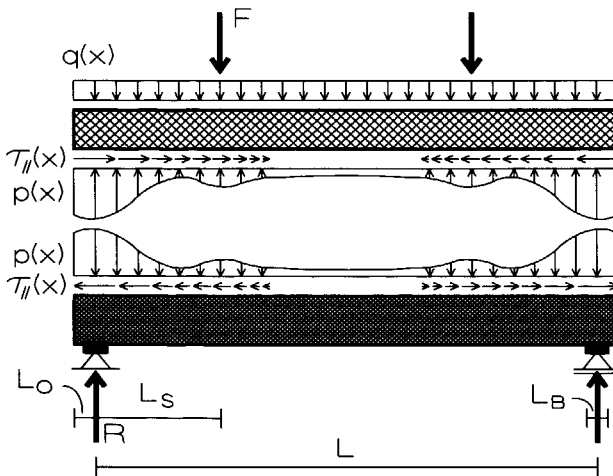


Figure 8.1: General full-scale model for composite slabs

The lateral stress in the connection $p(x)$ distributes the applied load over the concrete and the sheeting. Over the span, the total applied load is transferred from the concrete to the supports via the connection and the sheeting. The nonlinear behaviour of concrete and the presence of concentrated lateral forces, lead to a non-uniform lateral stress distribution $p(x)$. Since the presence of lateral stresses influences the longitudinal shear resistance, the longitudinal shear stress distribution over the span is also non-uniform. Due to the stiffness of the sheeting, the effect of concentrated lateral forces is spread over a length larger than the length over which the forces are applied.

Current full-scale models take into account the shear resistance over the span due to mechanical interlock and a contribution of friction. The Partial Shear Connection method as presented in the Eurocode considers a constant ultimate shear stress $\tau_{U\mu}$ over the shear span L_S+L_O and a concentrated frictional force $T_{U\mu}$ at the supports. The longitudinal shear force T in the critical cross-section $L_x=L_S$ is a summation of the two contributions.

$$T = \int_{-L_O}^{L_S} \tau_{U\mu} dx + T_{\mu} = \tau_{U\mu} \cdot (L_S + L_O) + \mu R \quad [\text{N/mm}] \quad (8.1)$$

The general model considers a non-uniform distribution of lateral stresses over the span instead of a concentrated force at the supports. Therefore also frictional shear stresses instead of a concentrated frictional force are considered.

Two phenomena can be recognized which influence the longitudinal shear stress distribution over the shear span. The cross-sectional analysis presented in this thesis recognizes the influence of vertical separation on the characteristics of the shear connection. The vertical separation is a function of the longitudinal slip and the lateral stress. Since both the level of slip and the lateral stress vary over the shear span, the longitudinal shear stress is not uniformly distributed over the shear span.

A second phenomenon is the shear stress development over the shear span. The slip distribution over the span of a slab consists of a continuous and a discontinuous function. As long as elastic or smeared crack behaviour is considered, the slip distribution over the full span remains continuous [12]. A typical slip distribution for 4-point loading is shown in Fig. 8.2. If connections with

a finite stiffness are considered, slip occurs over the full span, since no discontinuity occurs beneath the applied load.

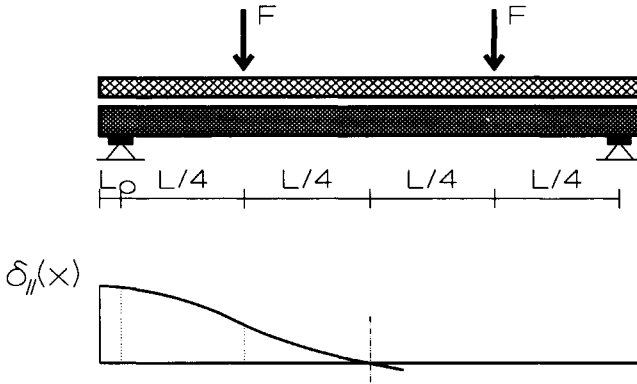


Figure 8.2: Typical elastic slip distribution for 4-point loading

If cracks are considered, a local slip distribution is added to the distribution as shown in Fig. 8.2. Depending on the characteristics of the connection, a limited number of large or a number of smaller cracks arise. Figure 8.3 shows the slip distribution over half a span with only one dominant crack. Due to the cracks the level of slip between the applied loads remains small. The discontinuity underneath the applied load leads to larger values of slip between the applied loads and the supports.

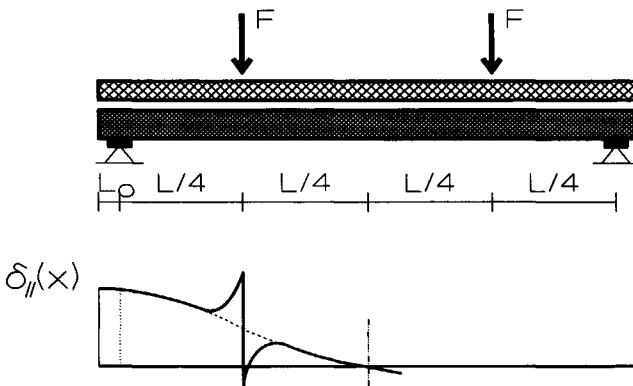


Figure 8.3: Superposition of slip due to cracking of concrete

The ultimate shear force over the shear span is reached when all cross-sections in the shear span reach the ultimate cross-sectional shear stress. For the slip distribution shown in Fig. 8.3, this requires that the ultimate shear stress is available for slip levels between approximately 60 to 120 % of the level of end-slip. For all stress-slip diagrams which do not meet this requirement, a non-uniform distribution of shear stresses is obtained.

Equation (8.2) shows a general formula for the longitudinal shear force in the shear connection. Similar to eq. (8.1), distinction can be made between the shear resistance provided by mechanical interlock ($\tau(x)$) and the resistance provided by friction ($\tau_{\mu}(x)$). $\tau(x)$ is a function of the vertical separation ($\delta_{VS}(x)$) and the longitudinal slip ($\delta_1(x)$). $\delta_{VS}(x)$ is a function of the lateral stress $p(x)$ and $\delta_1(x)$. The frictional stress $\tau_{\mu}(x)$ is related to the lateral stress $p(x)$ via the coefficient of friction μ .

$$T = \int_{-L_0}^{L_s} \tau(x) dx + \int_{-L_0}^{L_s} \tau_{\mu}(x) dx = \int_{-L_0}^{L_s} \tau(x) dx + \mu \cdot \int_{-L_0}^{L_s} p(x) dx \quad (8.2)$$

$$\text{with: } \tau(x) = f(\delta_{VS}(x); \delta_1(x)) \quad (8.3)$$

$$\delta_{VS}(x) = f(p(x); \delta_1(x)) \quad (8.4)$$

Since lateral stresses between the applied point loads remain small, the contribution of friction in eqs. (8.1) and (8.2) are almost equal if the critical cross-section is considered.

$$T = \int_{L_0}^{L_s} \tau(x) dx + \mu \cdot R \quad (8.5)$$

$$\text{with: } R = \int_{L_0}^{L/2} p(x) dx \approx \int_{L_0}^{L_s} p(x) dx \quad (8.6)$$

For profiles with a large resistance to vertical separation and ductile behaviour of the shear connection, the cross-sectional ultimate shear stress is constant over the shear span and can be developed in all cross-sections, which implies that eq. (8.5) equals eq. (8.1). For most re-entrant profiles this is the case. For trapezoidal profiles, vertical separation is more important and the behaviour of

the connection is usually less ductile, which leads to non-uniform shear stress distributions over the shear span.

8.2 General Model Shear Connection - Level 1

Based on the understanding obtained in this thesis, a general cross-sectional model for shear connections in composite slabs is shown in Fig. 8.4. Three degrees of freedom are considered. Apart from the deflection $\delta(x)$ and the longitudinal slip $\delta_l(x)$, the vertical separation between the concrete and the sheeting $\delta_{vs}(x)$ is considered.

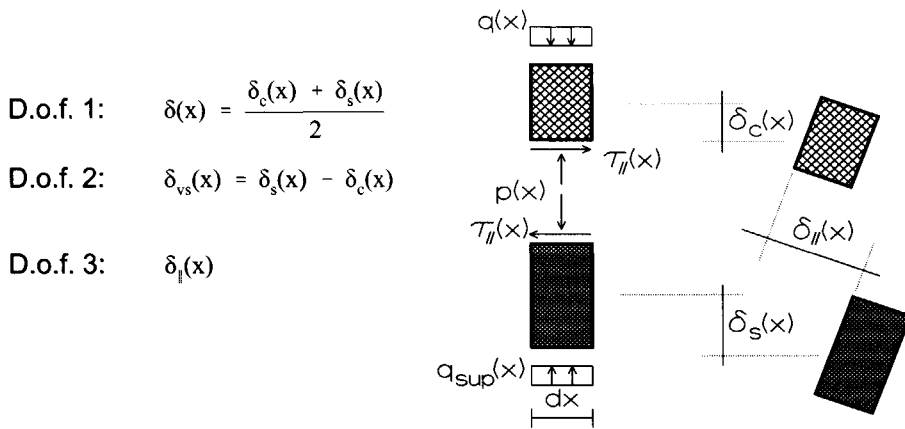


Figure 8.4: General cross-sectional model for composite slabs

Existing methods do not take vertical separation into account. Since the separation is small compared to the deflection, the behaviour of the concrete and the sheeting is hardly influenced by the separation. However, the influence of the separation on the behaviour of the shear connection can be significant. With the vertical separation, also a lateral stress in the connection is introduced ($p(x)$). The shear resistance of the connection is a function of the longitudinal slip and the lateral stress in the connection, as shown in eq. (8.3).

If no lateral stress is present ($p(x)=0$), no external lateral restraints act on the connection. This is referred to as unrestrained separation. As discussed in § 3.2 and 3.3, the behaviour of the shear connection is based on the deformation of the sheeting and the separation between the concrete and the sheeting.

Resistance to separation is required for the development of shear resistance. This implies that for unrestrained separation, apart from a relation between the longitudinal slip and the shear stress, a relation between the slip and the separation exists, as illustrated in Fig. 8.5.

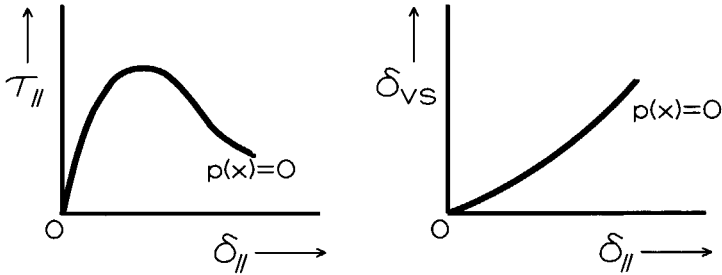


Figure 8.5: Shear stress and vertical separation versus longitudinal slip for unrestrained separation

If lateral stresses are present ($p(x) > 0$), the ratio between the deformation and displacement of the sheeting increases, which improves the shear resistance and reduces the separation, referred to as restrained separation. Restrained separation affects the strength, stiffness and ductility of the connection. Similar to the diagrams shown in Fig. 8.5, diagrams can be determined for different levels of lateral stresses, as shown in Fig. 8.6.

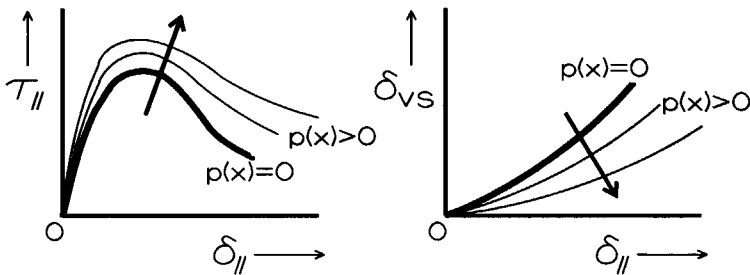


Figure 8.6: Shear stress and vertical separation versus longitudinal slip for restrained separation

The shear resistance for unrestrained separation can be referred to as the pure shear resistance of the connection, where the resistance for restrained separation can be referred to as improved shear resistance. The lateral stress

$p(x)$ in the cross-section contributes directly to the shear resistance by friction. Indirectly it improves the contribution of mechanical interlock by reducing the vertical separation.

The general formula for the longitudinal shear stress in a connection ($\tau_l(x)$) can be derived from eq. (8.2).

$$\tau_l(x) = \tau(x) + \tau_\mu(x) = \tau(x) + \mu \cdot p(x) \quad (8.7)$$

The general cross-sectional model, as illustrated in Fig. 8.4, is generally used for sandwich panels, composite structures or adhesive bonded joints [12,13]. For implementation of the cross-sectional model into a full-scale model as illustrated in Fig. 8.1, it is not required to consider all degrees of freedom in multi-layer structures. By obtaining understanding of the physical behaviour of the connections, the properties of the shear connection should be related to considered degrees of freedom and/or stresses in the connection. The properties and relations can be essentially different for different types of profiles.

The general full-scale model as shown in Fig. 8.1 enables the determination of the behaviour of the composite slab based on the cross-sectional model, as shown in Fig. 8.4. Using either the *General Solution Technique* as illustrated in § 4.3.1 or Finite Element analysis, the behaviour of the slab can be determined for applied loads from zero up to failure.

Determination of the capacity of a slab based only on the cross-sectional model, as shown in Fig. 8.4, is not possible, as mentioned in § 8.1. The ultimate shear stress of each cross-section depends on the level of separation and the lateral stress in the cross-section. Furthermore, the slab configuration and the characteristics of the shear connection determine whether the ultimate shear stress is reached in each cross-section. The ultimate shear force in the connection is not necessarily the summation of the ultimate shear stresses in all cross-sections.

8.3 Partial Shear Connection method

The ultimate shear resistance $\tau_{U\mu}$ used in the PSC method is based on full-scale experimental results. $\tau_{U\mu}$ is not a cross-sectional parameter, but the average shear stress over the considered shear span. For each experiment, the value of $\tau_{U\mu}$ is calculated based on the determined total shear force N_{cf} and the contribution of friction at the supports as illustrated in Fig. 2.27.

$$\tau_{U\mu} = \frac{\eta \cdot N_{cf} - \mu \cdot R}{b \cdot (L_S + L_O)} \quad (8.8)$$

Similar to full-scale experiments used for the determination of values for m and k within the 'm-k' method, two series of experiments are performed for the determination of values for $\tau_{U\mu}$. For the longer spans (Series A), three experiments are required, whereas for the shorter spans (Series B), only one experiment is required. The lowest value of $\tau_{U\mu}$ is used as a basis for the design value τ_{URd} . For all existing profiles, the longer specimens lead to lower values for $\tau_{U\mu}$ than the shorter specimen ($\tau_{U\mu A} < \tau_{U\mu B}$ for $L_{SA} > L_{SB}$) as illustrated in Fig. 8.7.

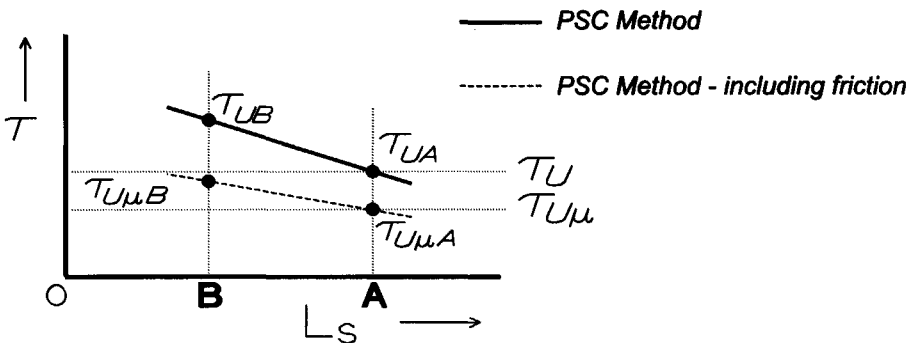


Figure 8.7: General results PSC method including friction at supports

Taking friction at the supports into account leads to a lower value for the ultimate shear stress over the shear span ($\tau_{U\mu} < \tau_u$). In general, the difference between the results for the two series of experiments reduces, but does not disappear by taking friction at the supports into account. The fact that the design value is based on the lowest values for τ_u implies that the design is by definition conservative for shorter spans. The fact that for all tested profiles, the results for longer spans are lower than for shorter spans, implies that the assumed uniform

shear stress distribution over the shear span is not correct.

The two phenomena described in § 8.1, causing non-uniform longitudinal stress distribution over the shear span, explain (part of) the difference between the average values for the shear stress for the longer and shorter spans. The improvement of the shear resistance at the supports, caused by the restricted vertical separation, can be compared to the contribution of friction at the supports. Similar to the effect shown in Fig. 8.7, an extra contribution to the shear force at the supports would further reduce values for series A and B and would also reduce the difference between them.

The second phenomenon deals with the development of the shear stresses over the shear span. For the longer spans, the required level of ductility of the shear connection is higher. Veljkovic introduced a correction factor c_m to take the development of shear stresses over the shear span into account [14]. The correction factor relates the area beneath the stress diagram to the maximum area.

$$c_m = \frac{\int_{-L_o}^{L_x} \tau(x) dx}{L_x} = \frac{\int_{-L_o}^{L_x} \tau(x) dx}{(L_S + L_O) \cdot \tau_u} \quad (8.9)$$

A value of c_m close to 1.0 is found for extremely ductile shear connections as in some re-entrant profiles. Generally, trapezoidal profiles lead to more brittle behaviour, such as the behaviour found for a simple elastic shear connection, as illustrated in § 3.4 and 4.5. Over-riding of indentations by the concrete and vertical separation cause a reduction of the shear resistance for larger values of slip. For these profiles, smaller values for c_m are found, which implies that the difference between the cross-sectional resistance and the average shear resistance found in full-scale experiments is larger. The average shear stress over a shear span as derived with the procedure used in the PSC method underestimates the cross-sectional resistance, especially for the longer shear spans.

The difference between the derived average shear stresses, as presented in Fig. 8.7 can be explained by the phenomena discussed above. Taking into account

friction and the improved behaviour at the supports reduces the average shear stress found in the shorter spans. Taking into account the development of shear stresses over the shear span leads to higher values for the cross-sectional shear resistance for the longer spans. By reducing the difference between the longer and shorter specimen, the conservatism currently introduced by the PSC method for the shorter spans can be reduced.

8.4 Small-scale Experiments

Ever since the PSC method was adopted in the Eurocode small-scale test arrangements are developed to determine values for τ_v with small-scale instead of full-scale experiments. Similar to the cross-sectional analysis as presented in this thesis (Level 1), small-scale experiments (Level 2) provide information about the shear resistance of a shear connection. However, before these small-scale test results can be used within full-scale slab analysis, understanding into the shear stress development over the shear span for different types of profiles, connections and slab configurations is required.

It is recommended that a series of full-scale experiments is performed with at least three different types of representative profiles. The most important parameter should be the shear span. It is recommended to test 5 different shear spans.

Provided that understanding into the development of the shear stresses over the shear span is obtained, small-scale experiments can be effectively used for the determination of the shear resistance corresponding to unrestrained and restrained separation as discussed in § 8.2. Based on the information obtained from the small-scale experiments as presented in § 5.2 and the required experimental data with respect to unrestrained and restrained separation, the following aspects of small-scale test arrangements are discussed:

- A. Lateral forces
- B. Applying shear force via tension in the sheeting
- C. Boundary conditions
- D. Number of indentations - length of considered shear connection
- E. Variation vertical separation over the connection

- F. Orientation of the specimen
- G. Required measurements
- H. Simplicity specimen and test arrangement

A. Lateral forces

In order to obtain values for the pure and improved shear resistance, the test arrangement should allow for testing with and without external lateral forces. If a profile has no internal resistance to vertical separation, the pure shear is limited. Slabs containing such profiles exhibit brittle behaviour. In order to prevent interlocking, it is desirable to apply the external lateral force force controlled, which makes recording of the lateral force easier.

B. Applying shear force via tension in the sheeting

Applying the external shear force to the sheeting in tension instead of compression has three advantages. Firstly, tension represents the actual behaviour of the sheeting in a slab. Secondly, compression in the sheeting might lead to contact stresses which contributes to the shear resistance, which does not occur in practical situations. Finally, by applying the shear force in tension, no risk of instability of the profile occurs.

C. Boundary conditions considered shear connection

By allowing a certain distance between the applied shear force and the actual connection, no effect of the stress distribution in the shear connection occurs. By fixing the concrete to the testing frame, no eccentricities of forces occur. By applying boundary conditions similar to Fig. 5.20, with or without the lateral supports, no unrealistic boundary conditions are applied to the specimen.

D. Number of indentations - length considered shear connection

By reducing the number of active indentations, the length of the considered shear remains small. A limited number of indentations produces a more transparent distribution of forces over the considered connection, and the variation of the slip over the specimen remains small. Reducing the number of active indentations in existing profiles is possible by applying flexible material at the sheeting outside the considered connection during concreting. It is recommended to reduce the considered connection to the smallest repeating section of the profile.

Existing small-scale specimen have a length of approximately 300 mm, which is relatively large compared to shear spans of slabs with short spans. Profiles that perform well are able to reach up to 40 % of the yield strength of the sheeting over 300 mm, which results in an elongation of the sheeting over the considered connection of up to 0.15 mm. The corresponding stress level does not influence the shear resistance.

E. Variation vertical separation over the connection

The variation of the vertical separation should be limited over the considered connection, unlike the specimen shown in Fig. 5.42. By applying the shear force in tension, reducing the length of the considered connection and increasing the distance between the applied shear force and the connection rotation of the specimen, and therefore the variation of separation over the connection is limited. That way, the cross-sectional behaviour of the connection is obtained. The cross-sectional behaviour can be validated more easily by numerical models than the more complex behaviour as shown in Fig. 5.42.

F. Orientation of the specimen

Since the deformation and displacement of the sheeting is important for small-scale specimen, visual inspection of the sheeting is important. Due to the reduced length of the shear connection, not only the displacements, but also the forces remain small. This requires good accessibility of the specimen and the loading and measurement equipment. Placing the specimen in a vertical position, like the specimen discussed in § 5.2, was very convenient.

G. Required measurements

The applied load, the longitudinal slip and the vertical separation should be measured. In order to record the deformation of the sheeting multiple measurements are required. The number of cross-sections in which the slip and separation is measured and the number of measurements per cross-section depends on the geometry of the sheeting. If rotation of the sheeting is possible, if displacement perpendicular to the slip and separation is possible or if the slip or separation varies over the shear connection the number of required measurements increases.

H. Simplicity specimen and test arrangement

The form of the specimen and the test arrangement should remain simple.

Measuring small forces and displacements does not necessarily require complex measuring equipment. The phenomena which are essential for the analysis of the shear connection, based on the hypothesis as discussed in chapter 3, can be recorded and observed in a simple, inexpensive, flexible and fast way, as discussed in § 5.2.

In general it is stated that a small-scale experiment should focus on the cross-sectional behaviour rather than on the behaviour of a small slab. The size of existing small-scale specimen seems to be a result of a minimum specimen size required to apply the forces and (control) boundary conditions. The test arrangement discussed in § 5.2 shows that with a similar specimen size, the cross-sectional behaviour can be obtained from small-scale experiments.

8.5 Product development

Longitudinal shear resistance is only one criteria during the development of profiles for composite slabs. Depending on the field of application, the production (material efficiency, transport,), the construction stage (properties of sheeting, required maximum unpropped span, fixing,) and the normal stage (efficiency material, efficiency of shear studs, fixing of ceilings, services and installations,) lead to practical, technical and commercial criteria.

As illustrated in chapter 7, the developed tools are very useful for product development. The influence of variations of parameters on the shear resistance can be investigated without considering the overall behaviour of the connection. For instance, the optimum location or geometry of indentations can be investigated without considering the complete connection or slab.

During product development, the longitudinal shear connection is approached differently from the approach used during design. During design, the characteristics of the connection are known. The design procedure is a tool to determine the load capacity of a slab. During the development of profiles, the required capacity of the shear connection should be known. In order to illustrate the various requirements for different types of sheeting, the three different fields of application, presented in Table 1.1, are considered. In Table 8.1, the required level of shear resistance for full interaction is calculated.

Table 8.1: Required level of shear resistance for full interaction

	Span		Short	Regular	Long
Height sheeting	H_s	[mm]	15-35	40-80	200-225
Slab depth	H_t	[mm]	40-100	100-200	280-340
Span range	L	[m]	0.6-1.5	2.0-6.0	4.0-9.0
Considered shear span	L_s	[mm]	250	900	1.800
Effective area of steel	A_s	[mm ² /m]	≈600	≈1.000	≈1.000
Required shear resistance for full interaction	$\langle \tau_{Ud} \rangle$	[N/mm ²]	≈0.72	≈ 0.33	≈ 0.16

For profiles used for short and long spans, longitudinal shear resistance is less critical than for profiles for regular spans. For short spans, the available types of sheeting do not reach the level of shear resistance as given in Table 8.1. However, the obtained level is sufficient to prevent longitudinal shear failure for common applications. For long spans, for example for sheeting referred to as deep decking, the required level of shear resistance is low due to the longer shear spans. Additional bottom reinforcement is always required which makes longitudinal shear resistance less critical. For profiles used for regular spans, additional bottom reinforcement should be minimized to meet the required simplicity and speed in construction.

Currently the most important design criteria for new profiles in Europe are material efficiency of both steel and concrete and achieving long unpropped spans during construction. Both steel and concrete are most efficiently used with trapezoidal profiles which do not have steep webs. For these profiles, longitudinal shear resistance is very important. Limited internal resistance to vertical separation is provided, which implies that the distinction between pure and improved shear resistance is more pronounced. During the development of new trapezoidal profiles, the main challenge is to obtain sufficient resistance to both longitudinal shear and vertical separation. An understanding of the cross-sectional behaviour and the shear stress development over the shear span becomes more and more important.

8.6 Conclusions for Chapter 8

- # A general full-scale model and a general cross-sectional model for composite slabs is presented. The models take vertical separation and non-uniform distributed lateral and longitudinal shear stresses over the shear span into account. (§ 8.1-2)
- # Similar to existing models, the general full-scale model distinguishes a contribution of mechanical interlock and a contribution of friction. Both effects are non-uniformly distributed over the shear span. (§ 8.1)
- # The non-uniform distribution of longitudinal shear stresses over the shear span is a result of both cross-sectional and full-scale phenomena. Vertical separation and lateral stresses lead to different shear characteristics for different cross-sections in the shear span. The ductility of each cross-section determines whether the ultimate shear stress is reached in all cross-sections, referred to as the development of shear stresses over the shear span. (§ 8.1)
- # For trapezoidal profiles with limited internal resistance to vertical separation and limited ductility of the shear connection, the difference between the general full-scale model and existing full-scale models is considerable. For re-entrant profiles, the difference is limited. (§ 8.3)
- # The capacity of a full-scale slab can not be determined by using only the cross-sectional properties of the shear connection. (§ 8.2)
- # Different values for the average longitudinal shear stress found for different spans in full-scale experiments prove that the longitudinal shear stress distribution is not uniformly distributed over the shear span. Using the average stress as a basis for design introduces conservatism for shorter spans. (§ 8.3)
- # In order to apply results of cross-sectional analysis and small-scale experiments in full-scale analysis, understanding of the development of longitudinal shear stresses over the shear span for different types of profiles is required. (§ 8.4)

- # Requirements for small-scale test arrangements which provide relevant data for the general cross-sectional and full-scale models are based on unrestrained and restrained separation in shear connections. (§ 8.4)

- # Cross-sectional analysis and small-scale experiments can be very useful for product development. (§ 8.5)

- # The considered non-uniform distribution of stresses in the general full-scale model are most important for trapezoidal profiles used for regular spans (2.0-6.0 m). Since these profiles combine material efficiency for both steel and concrete these profiles are currently very important in Europe. (§ 8.5)

9. CONCLUSIONS AND RECOMMENDATIONS

Greater Understanding

The aim of this thesis was to obtain insight into the behaviour of connections in composite slabs. In this thesis, the physical behaviour of shear connections in composite slabs is investigated by analysing the mechanisms which determine the behaviour of the connection. A hypothesis concerning the behaviour of connections is presented which is based on ACTION, the over-riding of indentations by the concrete after longitudinal slip has occurred, and REACTION, the response of the sheeting to the over-riding of indentations. It is stated that the response of the sheeting is a combination of deformation and displacement and that the ratio between the deformation and displacement, determines the characteristics of the shear connection.

Based on the distinction between *Action* and *Reaction*, a method for analysing shear connections is developed. Based on the strict distinction between ACTION and REACTION, three different parts of the analysis are distinguished. These parts are analysed separately, using the most suitable tool for the specific configuration. The determination of the behaviour of the connection consists of combining the results of the separate parts. The strength of the method is illustrated by the *Visual Solution Method*, which supplies the ultimate level of transparency in both the method itself and the behaviour of simple shear connections.

Models

It is stated that due to the diversity of existing and possible new profiles a general model is not feasible nor desirable. A general model does not provide the required level of flexibility to approach new types of connections. In order to obtain greater understanding and establish flexible tools, a procedure for analysing rather than a general model is developed.

S(implified)F(rame)-models are developed to apply the procedure of the Visual Solution method for more complicated connections. SF-models are also based on the strict distinction between the separate parts of the analysis. Similar to the Visual Solution Method transparency is an important feature for obtaining greater understanding.

All nonlinear phenomena of shear connections can be implemented in F(inite)-E(lement)-models. Although not always obvious, the principles of the hypothesis are also present in the FE-models.

With both the SF- and FE-models cross-sectional analysis are performed. Results of cross-sectional analysis cannot be used directly for comparison with small- or full-scale analysis. Based on understanding of the cross-sectional and the behaviour of composite slabs both small- and full-scale analysis can be performed.

The considered examples and parametric studies prove that the combination of SF- and FE-models supplies a powerful tool for investigating shear connections. FE-models can be used to determine the actual behaviour of shear connections. SF-models can be used to investigate specific elements of the connection qualitatively. Results of SF-models can be validated by simplified FE-models. Although constant developments of FE-analysis allow for sophisticated parametric investigation, simple and transparent models like SF-models are important for obtaining greater understanding.

Observations from experiments and analysis

Important observations concerning the behaviour of shear connections in composite slabs are the difference between restrained and unrestrained vertical separation, the difference between re-entrant and trapezoidal profiles and the influence of the concrete properties to the ductility of the connection.

Between the supports, no external lateral stresses are present in the connection. Internal resistance to vertical separation between the sheeting and the concrete is required for the development of shear resistance. This referred to as unrestrained vertical separation and pure shear resistance. A greater understanding of the pure shear resistance of connections is very important. A limited level of pure shear resistance leads to brittle behaviour of slabs, due to end anchorage failure at the supports, and leads to a non-uniform stress distribution in the connection, which makes application of the Partial Shear Connection method less accurate.

At the supports, a lateral force is present in the connection. Apart from a contribution of friction, the lateral force reduces the level of separation, which

improves the behaviour of the connection at the supports. This is referred to as restrained separation and improved shear resistance. Restrained separation affects the strength, stiffness and ductility of the connection. If, for different levels of slip, the shape of the stress-slip diagrams for restrained separation is similar to the shape found for unrestrained separation the improvement of the behaviour can be modelled as a concentrated force at the supports similar to the approach used for friction at the supports. However, usually the shape is different and the non-uniform shear stress distribution over the shear span needs to be considered to determine the behaviour of a composite slab.

Based on the geometry of the profiled sheeting, distinction can be made between re-entrant and trapezoidal profiles. Re-entrant profiles usually supply internal resistance to vertical separation, which reduces the difference between restrained and unrestrained separation. Re-entrant profiles usually provide high shear resistance and ductile behaviour, since the ratio between deformation and displacement is large and the level of deformation of concrete is large due to the high level of interaction forces.

The internal resistance to vertical separation in trapezoidal profiles is supplied by the indentations. The indentations provide resistance to both longitudinal shear and vertical separation, which implies that the geometry of the sheeting and the geometry and location of the indentations is more important than for re-entrant profiles. Trapezoidal profiles with steep webs ($<10^\circ$) lead to similar behaviour as found for re-entrant profiles. Regular trapezoidal profiles exhibit more brittle behaviour than re-entrant profiles due to the larger level of vertical separation and smaller level of deformation of concrete. Due to the more brittle cross-sectional behaviour the ultimate cross-sectional shear stress is usually not fully developed over the shear span of a composite slab. Trapezoidal profiles return non-uniform distributed shear stresses over the shear span, due to the difference between restrained and unrestrained separation and the development of shear stresses over the shear span.

The parametric studies and the experimental results show that the concrete properties are very important if ductility of the connection is considered. With respect to the concrete the properties of the cement paste between the sheeting and the concrete are important. Properties of the paste differ from the properties of concrete. When interaction forces between the sheeting and the paste remain

small, the properties of the paste are dominant over the concrete properties. Without deformation of the paste/concrete the indentations are pushed out of the concrete. Similar to elastic behaviour, the shear strength reduces significantly and brittle behaviour is obtained. If larger interaction forces occur, the indentations "dig" channels in the paste/concrete. That way the indentations are never pushed out completely, and a certain level of resistance is available for all levels of slip. Therefore ductile behaviour is obtained.

Full-scale slab analysis

In order to determine the behaviour of full-scale composite slabs implementation of the cross-sectional analysis is required. For re-entrant profiles the shear stress distribution over the shear span is almost uniformly distributed due to the ductile cross-sectional behaviour and limited difference between restrained and unrestrained behaviour. This implies that results of cross-sectional analysis can be used for full-scale analysis, and that the PSC method is accurate.

For trapezoidal profiles, the shear stress distribution over the shear span is not uniformly distributed. Cross-sectional analysis can be performed. Translation of cross-sectional analysis to full-scale analysis is required, since, due to the more brittle behaviour, the ultimate cross-sectional resistance will not be reached over the full shear span.

In order to investigate the non-uniform distribution of shear stresses, it is recommended to perform a series of full-scale experiments containing at least 3 representative types of sheeting. For each type of sheeting, only the shear span should be varied. In order to investigate the development of shear stresses over the shear span it is recommended to test 5 different shear spans. As a minimum, the deflections and endslip should be measured. All information about the vertical separation and the longitudinal slip over the span is useful. After the experiments, the local deformation of concrete and possible deformation of indentations should be recorded accurately.

Application

Similar to cross-sectional analysis, small-scale experiments can be used for the determination of the behaviour of shear connections. It is important that small-scale experiments take into account the issues of unrestrained and restrained separation. Simple test arrangements can be used which supply all required

information. Application of results of small-scale experiments in full-scale analysis requires understanding of the distribution of shear stresses over the shear span, which points out the importance of the recommended series of experiments.

Application of the hypothesis, the Visual Solution method and the SF- and FE-models during product development already proved to be very effective. All information obtained from the available cross-sectional analysis can be applied to optimize the geometry of the sheeting and indentations before a roll-former is made.

Although longitudinal shear is only one criteria during product development, it becomes more important, since the demand for trapezoidal profiles increases, due to their overall efficiency in material use. Obtaining the required level of internal resistance to vertical separation in order to obtain the required level of shear resistance is an important technical challenge during the development of new types of profiled sheeting.

REFERENCES AND BIBLIOGRAPHY

With respect to references, distinction is made between references which are mentioned in the text [1-14] and a bibliography [-]. Although the references in the bibliography were not directly related to the fundamental approach as presented in this thesis, they are valuable for obtaining a greater understanding into the behaviour of shear connections or the behaviour of composite slabs.

REFERENCES

- [1] Eurocode 4, *Design of Composite Steel and Concrete Structures - Part 1.1: General rules and rules for building*, prEN 1994-1-1:1992, CEN, Brussels, 1999
- [2] Minas F., *Beitrag zur Versuchsgestützten Bemessung von Profilblechverbunddecken mit nachgiebiger Verdübelung*, Doctoral Thesis Universität Kaiserslautern - 1999
- [3] Eurocode 4, *Design of Composite Steel and Concrete Structures - Part 1.1: General rules and rules for building*, ENV 1994-1-1:1992, CEN, Brussels, 1992
- [4] Patrick, M., *A New Partial Shear Connection Strength Model for Composite Slabs*, Journal of Steel Construction, Australian Institute of Steel Construction, Vol.24, No.3, pp. 2-17, 1990, Australia
- [5] Patrick, M., Bridge, R.Q., *Partial Shear Connection Design of Composite Slabs*, Engng. Strct., Vol.16, No.5, pp. 348-362, 1994, Australia
- [6] Veljkovic, M., *An improved Partial Shear Connection Method for Composite Slab Design*, Engineering Foundation Conferences, Composite Construction III, Composite Slab Session, Preliminary Proceedings pp. 100-115, 1995, Irsee, Germany
- [7] Daniels, B.J., *Shear Bond Pull-Out Tests for Cold-formed steel Composite Slabs*, Publication ICOM 194, 1988
- [8] Patrick, M., Bridge, R.Q., *The Slip-Block test for Composite Slab Shear Connection Performances*, International Workshop on Cold-Formed Steel Structures, 1993
- [9] Walraven, J., *Rough Cracks Subjected to Earthquake Loading*, Journal of Structural Engineering, Vol. 120, No.5, pp 1510-1524, 1994
- [10] Stark, J.W.B., *Koud Gevormde Profielen*, Staalcentrum Nederland en Staalbouwkundig genootschap, november 1976

References and Bibliography

- [11] *Longitudinal Shear Resistance of Composite slabs: Evaluation of Existing Tests*, ECCS - TC 7 - WG 7.6: Composite Slabs, 1998 No. 106
- [12] Schuurman, R.G., *Een niet-lineair rekenmodel voor Staalplaatbetonvloeren*, Delft University of Technology Rapport nr. 25-06-91-03/A2, TNO-IBBC Rapport nr. BI-91-031, 1991
- [13] Straten, I.J.J. van, *Development of Design Rules for Structural Adhesive Bonded Joints - A Systematic Approach*, Dissertation Delft University of Technology, 2000
- [14] Veljkovic, M., *Behaviour and Design of Shallow Composite Slabs*, Engineering Foundation Conferences, Composite Construction IV, Preliminary Proceedings, Session M3: Composite Slabs, June 2000, Banff, Alberta, Canada

BIBLIOGRAPHY

- [-] Bode, H., Sauerborn, I., *Modern Design Concept for Composite Slabs with Ductile Behaviour*, Engineering Foundation Conferences, Composite Construction II, pp. 125-141, 1992, Irsee, Germany
- [-] Bode, H., *Theorie un Praxis im Konstruktiven Ingenieurbau - Festschrift zu Ehren von Prof.Dr.-Ing. Helmut Bode*, Kaiserslautern, August 2000
- [-] Bode, H., Minas, F., Sauerborn, I., *Partial Connection Design of Composite Slabs*, Structural Engineering International 1/96, pp. 53-56, 1996
- [-] Brekelmans, J.W.P.M., *Cross-sectional experimental investigation on shear bond failure of a composite slab as part of SPRINT-project RA31 and in connection with Super-Holorib 51/0.9 from Richard Less (Eng)*, TNO Report B-88-148, 1988, The Netherlands
- [-] Brekelmans, J.W.P.M., Daniels B.J., Schuurman, R.G., *Analysis of the vertical load tests on deep composite slabs. Part of ECSC project "Steel intensive systems for shallow floor constructions"*, TNO-Report 96-Con-R1147, 1996
- [-] Crisinel, M., O'Leary, D., *Composite Floor Slab Design and Construction*, Structural Engineering International SEI, Journal of the IABSE 1/96
- [-] Daniels, B.J., Crisinel, M., *Composite Slab Behaviour and strength Analysis - Part I: Calculation Procedure - Part II: Comparisons with Test Results and Parametric Analysis*, Journal of Structural Engineering, Vol.119, No.1, 1993
- [-] Daniels, B.J., *Shear Bond Pull-Out Tests for Cold-formed steel Composite Slabs*, Publication ICOM 194, 1988
- [-] Daniels, B.J., *Comportement et Capacite Portante des Mixtes - Modelisation Mathematique et Etude Experimentale*, These No. 895, 1990, EPFL Lausanne, Switzerland
- [-] Duffy, C.T., O'Leary, D., *Shear Bond Capacity Tests on Composite Slabs with Combideck*, Report SJ579A, Salford University, 1994, United Kingdom
- [-] Eurocode 2, *Design of Concrete Structures - Part 1: General rules and rules for buildings*, prEN 1992-1:2001 - December 1999
- [-] Eurocode 3, *Design of Steel Structures - Part 1.1: General rules and rules for buildings*, ENV 1993-1-1:1993, CEN, Brussels, 1992

- [-] Eurocode 3, *Design of Steel Structures - Part 1.3: General rules: Supplementary rules for cold formed thin gauge members and sheeting* - ENV 1993-1-3: 1993, CEN, Brussels, 1992
- [-] Jolly, K.C., Zubair, A.K.M., *The efficiency of Shear Bond Interlock Between Profiled Steel Sheeting and Concrete*, International Conference on Steel and Aluminium Structures, Composite Steel Structures-Advance, Design and Construction, Cardiff, 1987, United Kingdom
- [-] Johnson, R., *Composite Structures of Steel and Concrete - Vol.1 Beams-Slabs-Columns and Frames for Building*, Blackwell Scientific Publications, 1994, United Kingdom
- [-] Koning, C.M. de, *Beproeving Staalplaat-betonvloeren*, TNO-IBBC Rapport Nr. B-72-7, 1972
- [-] Koning, C.M. de, Stark, J.W.B., *Bepaling van de Opneembare Schuifkracht bij Staalplaat-betonvloeren*, TNO-IBBC Rapport Nr. B-75-356, 1972
- [-] Li, A., *Load Bearing Capacity and Behaviour of Composite Slabs with Profiled Steel Sheet*, Doctoral thesis, Chalmers University of Technology, Göteborg, 1993, Sweden
- [-] Li, A., Cederwall, K., *Slip and Separation at the Interface of Composite Slabs*, Twelfth International Specialty Conference on Cold formed Steel Structures, pp. 385-397, University of Missouri-Rolla, 1994, St. Louis, U.S.A.
- [-] Patrick, M., Bridge, R.Q., *Parameters Affecting the Design and Behaviour of Composite Slabs*, International Symposium on Mixed Structures, IABSE, Vol.60, pp. 221-225, Brussels, Belgium
- [-] Patrick, M., Bridge, R.Q., *The Slip-Block test for Composite Slab Shear Connection Performances*, International Workshop on Cold-Formed Steel Structures, 1993
- [-] Patrick, M., Bridge, R.Q., *Partial Shear Connection Design of Composite Slabs*, Engng. Strct., Vol.16, No.5, pp. 348-362, 1994, Australia
- [-] Patrick, M., Poh, W.K., *Controlled Test for Composite Slab Design Parameters*, IABSE Symposium on Mixed Structures Including New Materials, Brussels, Belgium
- [-] Patrick, M., *Shear Connection Performances of Profiled Steel Sheeting in Composite Slabs*, Doctoral Thesis University of Sydney, 1994, Australia
- [-] Porter, M.L., Ekberg Jr., C.E., *Investigation of cold-formed steel-deck-reinforced concrete floor slabs*, First Specialty Conference on Cold formed Steel Structures, University of Missouri-Rolla, pp. 179-185, 1971, St. Louis, U.S.A.
- [-] Sauerborn, I., *Zum grenztragfähigkeit von durchlaufenden Verbunddecken*, Disertation Universität Kaiserslautern, 1995, Germany
- [-] Schanzenbach, J., *Zum Einfluß von Dübelnachgiebigkeit und Unterverdübelung auf das Tragverhalten von Verbunddurchlaufträgern im Hoch- und Industriebau*, Disertation Universität Kaiserslautern, 1988, Germany
- [-] Schumacher, A, Crisinel, M., *Development of a New Design Approach for Composite Slabs*, Engineering Foundation Conferences, Composite Construction IV, Preliminary Proceedings, Session M3: Composite Slabs, June 2000, Banff, Alberta, Canada
- [-] Schuster, R.M., *Composite Steel-deck-reinforced Concrete Systems Failing in Shear-bond*, Preliminary Report Ninth Congress IABSE Amsterdam, 1972, pp 185-191, Ed. IABSE, Zürich
- [-] Schuurman, R.G., Stark, J.W.B., *Behaviour of Longitudinal Shear Connection in Composite Slabs*, Fourth Pacific Structural Steel Conference 1995, Vol.3, pp. 161-169, Singapore

References and Bibliography

- [-] Schuurman, R.G., Stark, J.W.B., *Behaviour of Connection between Concrete and Decking in Composite Slabs*, Engineering Foundation Conferences, Composite Construction III, June 1996, Irsee, Germany
- [-] Schuurman, R.G., Stark, J.W.B., *Longitudinal Shear Resistance of Composite slabs - To a better understanding of the physical behaviour*, Engineering Foundation Conferences, Composite Construction IV, Preliminary Proceedings, Session M3: Composite Slabs, June 2000, Banff, Alberta, Canada
- [-] *Staalplaat-betonvloeren - deel 1: Richtlijnen en rekenvoorbeelden - RSBV1990 Richtlijnen voor het ontwerp en de vervaardiging van staalplaat-betonvloeren*, SG/CS/CUR-Rapport 7 - Centrum Staal, Staalbouwkundig Genootschap, Civieltechnisch Centrum Uitvoering Research en Regelgeving, 1991
- [-] *Staalplaat-betonvloeren - deel 2: Theorie*, SG/CS/CUR-Rapport 8 - 1991
- [-] Stark, J.W.B., *Design of composite Floors with Profiled Steel Sheet*, Fourth Specialty Conference on Cold formed Steel Structures, pp. 893-922, University of Missouri-Rolla, 1978, St. Louis, U.S.A.
- [-] Stark, J.W.B., Schuurman, R.G., Brekelmans, J.W.P.M., *Longitudinal Shear Resistance of Composite Slabs - Parameters affecting Physical Behaviour*, Theorie un Praxis im Konstruktiven Ingenieurbau - Festschrift zu Ehren von Prof.Dr.-Ing. Helmut Bode, Kaiserslautern, August 2000
- [-] Veljkovic, M., *Development of a new sheeting profile for composite floors- Experimental study and interpretation*, Tulea 1993:47, Luleå University of Technology, 1993, Sweden
- [-] Veljkovic, M., Kusters, G.M.A., Hendriks, M.A.N., *3-D Nonlinear Analysis of Composite Slabs*, DIANA Computational Mechanics 1994, pp. 395-404, Kluwer Publisher, 1994, The Netherlands
- [-] Veljkovic, M., *Interaction Between Concrete and Sheeting in Composite Slabs*, Nordic Concrete Research, Publication No.17, 2/1995, pp. 93-108, 1995, Oslo, Norway
- [-] Veljkovic, M., *Longitudinal Shear Capacity of Composite Slabs*, Nordic Steel Construction Conference 1995, Swedish Institute of Steel Construction & Division of Steel Structures, pp.547-554, 1995, Malmö, Sweden
- [-] Veljkovic, M., *An improved Partial Shear Connection Method for Composite Slab Design*, Engineering Foundation Conferences, Composite Construction III, Composite Slab Session, Preliminary Proceedings pp. 100-115, 1995, Irsee, Germany
- [-] Veljkovic, M., *Behaviour and Resistance of Composite Slabs - Experiments and Finite Element Analysis*, Dissertation Luleå University of Technology, 1996, Sweden
- [-] Veljkovic, M., *Influence of Load Arrangement on Composite Slab Behaviour and Recommendations for Design*, Journal of Constructional Steel Research, Vol.45, No.2, pp149-178
- [-] Walraven, J.C., *Aggregate Interlock: A Theoretical and Experimental Analysis*, Dissertation Delft University of technology, 1980
- [-] Wright, H., Essawy, M.I., *Bond in Thin Gauge Steel Concrete Composite Structures*, Engineering Foundation Conferences, Composite Construction III, Composite Slab Session, Preliminary Proceedings pp. 86-99, June 1995, Irsee, Germany
- [-] Wright, H., Veljkovic, M., *Towards a numerical procedure for composite slab assessment*, Thirteenth International Specialty Conference on Cold-formed Steel Structures, pp. 415-435, 1996, St. Louis, Missouri, U.S.A.

NOTATIONS

Upper case

b	[m]	width
f	[N/m ²]	stress
h	[m]	overall slab depth - height - height indentation
m	[Nm/m]	bending moment
p	[N/m ²]	lateral stress
q	[N/m]	applied distributed load
t	[m]	thickness
z	[m]	lever arm
A	[m ²]	area
D	[m]	diameter indentation
E	[N/m ²]	Young's modulus
F	[N]	applied concentrated force (see P)
G	[N]	self weight
H	[m]	height indentation
I	[m ⁴]	second moment of area
L	[m]	span - length
M	[Nm]	internal/external bending moment
N	[N]	normal force - normal direction
P	[N]	applied concentrated load (see F)
Q	[N]	internal shear force (ch. 2)
R	[N]	support reaction - radius indentation
S	[m ³]	elastic modulus
T	[N]	total shear force
V	[N]	support reaction - internal shear force
W	[m ³]	section modulus

Greek notations

γ	[-]	safety factor
δ	[m]	displacement - deflection and slip
η	[-]	degree of interaction
κ	[1/m]	curvature
μ	[-]	(coefficient of) friction
σ	[N/m ²]	normal stress
τ	[N/m ²]	shear stress
φ	[rad]	angle relating the normal direction in a point of contact to the normal direction of the contact area - rotation

Notations and Terminology

Lower case

a	steel/reinforcement
c	concrete
d	distance centroid steel area to top of slab
e	elastic
ext	external
fi	full interaction
fl	flange
fp	fictitious penetration
ind	indentation
k	stiffness
ni	no interaction
p	plastic
s	sheeting
u	ultimate
vs	vertical separation
y	yield
yld	yield
Rd	design resistance
Sd	design strength
	parallel
⊥	perpendicular

Steel-concrete composite slab notations

F_i	[N]	interaction force between concrete and sheeting/indentation
F_N	[N]	normal force in point of contact
F_l	[N]	(longitudinal) shear force
F_{\perp}	[N]	force perpendicular to area of contact or composite slab
F_{μ}	[N]	frictional force in point of contact
L_o	[m]	overhang
L_s	[m]	shear span
L_{sf}	[m]	required shear span for flexural failure
δ_i	[m]	vertical separation
δ_l	[m]	(longitudinal) slip
δ_{\perp}	[m]	displacement perpendicular to area of contact or composite slab
τ_l	[N/m ²]	(longitudinal) shear stress
τ_o	[N/m ²]	(longitudinal) shear stress in shear connection (ch. 2)

TERMINOLOGY

<i>Chemical bond</i>	Shear connection between concrete and steel arising during hardening of concrete
<i>Composite action</i>	Phenomenon that properties of a composite cross-section benefit from the connection between the separate elements (see also <i>no- and full interaction</i>)
<i>Composite slab</i>	Steel-concrete composite slab consisting of concrete and <i>profiled sheeting</i>
<i>Embossments</i>	see <i>indentations</i>
<i>Flexural failure</i>	Failure with ultimate capacity in critical cross-section
<i>Frictional interlock</i>	Shear resistance provided by contact forces between concrete and sheeting (see also <i>mechanical interlock</i>)
<i>Full interaction</i>	Infinite strength and stiffness of shear connection between separate elements in composite cross-section
<i>Indentations</i>	Deformations in profiled sheeting in order to achieve shear resistance by <i>mechanical interlock</i>
<i>Improved shear resistance</i>	Improvement of the <i>pure shear resistance</i> due to <i>restrained separation</i> at the supports
<i>Lateral force</i>	Force acting perpendicular to a slab pushing the sheeting towards the concrete, f.i. support reactions
<i>(Longitudinal) slip</i>	Relative displacement between concrete and sheeting in connection
<i>(Longitudinal) shear connection</i>	Connection between concrete and sheeting providing (longitudinal) shear stresses
<i>Longitudinal shear failure</i>	Failure of the <i>shear connection</i> prior to <i>flexural failure</i>
<i>(Longitudinal) shear resistance</i>	Ability of a <i>shear connection</i> to develop (longitudinal) shear stresses in a connection
<i>Mechanical interlock</i>	Shear resistance provided by indentations or friction
<i>No interaction</i>	No strength and stiffness of shear connection between separate elements in composite cross-

Notations and Terminology

	section - properties equals summation of properties of separate elements
<i>Partial interaction diagram</i>	Diagram relating the bending resistance of a slab to the applied bending moments
<i>Profiled sheeting</i>	Sheeting produced by a cold roll-forming process
<i>Props</i>	Temporary supports during casting of concrete
<i>Pure bond</i>	see <i>chemical bond</i>
<i>Pure shear resistance</i>	Shear resistance of a connection without external lateral forces (see <i>unrestrained separation</i>)
<i>Re-entrant profiles</i>	Sheeting with 'closed' wedge shaped ribs
<i>Restrained separation</i>	External restraints to the vertical separation in a cross-section - separation smaller than free separation (see also <i>unrestraint separation</i>)
<i>Roll-former</i>	Machine transferring flat to profiled sheeting
<i>Shear connection</i>	Physical connection between concrete and sheeting
<i>Shear span</i>	Length <i>shear connection</i> between support and critical cross-section
<i>Shear tension failure</i>	see <i>vertical shear failure</i>
<i>Trapezoidal profiles</i>	Sheeting with open ribs
<i>Unrestrained separation</i>	No external restraints to the vertical separation in a cross-section - free separation
<i>Vertical shear failure</i>	Failure of a cross-section in shear

SAMENVATTING

In dit proefschrift wordt de schuifverbinding tussen de staalplaat en het beton in staalplaat-betonvloeren beschouwd, waarbij de schuifweerstand wordt verzorgd door in de staalplaat aangebrachte indeukingen. Het doel van het onderzoek was het verkrijgen van inzicht in het fysisch gedrag van de schuifverbinding. Bestaande ontwerpmethoden voor staalplaat-betonvloeren zijn empirisch, waardoor toepassing van bestaande staalplaten en de ontwikkeling van nieuwe staalplaten wordt belemmerd. Beide aspecten zijn belangrijk in de huidige Europese markt.

Door de mechanismen te beschrijven die de schuifweerstand verzorgen is inzicht verkregen in het fysisch gedrag van de schuifverbinding. Onderscheid wordt hierbij gemaakt tussen het vervormen en verplaatsen van de staalplaat. De verplaatsing bestaat uit verticale separatie tussen de staalplaat en het beton. Verticale separatie reduceert de vervorming van de staalplaat, en daarmee de schuifweerstand van de verbinding.

Een methode voor de analyse van schuifverbindingen is ontwikkeld. De aanpak is ook toepasbaar voor andere schuifverbindingen, zolang de mechanismen die de schuifweerstand verzorgen beschreven kunnen worden. Voor eenvoudige verbindingen is een *Visuele Oplossingsmethode* ontwikkeld, waarmee een optimaal inzicht in verschillende aspecten en parameters van verbindingen kan worden verkregen. Voor meer complexe verbindingen zijn Vereenvoudigde Raamwerkmodellen (*SF- = Simplified Frame models*) ontwikkeld. Met behulp van Eindige Elementen modellen (*FE- = Finite Element models*) zijn alle niet-lineaire eigenschappen van de verbinding beschouwd. Omdat de FE-modellen minder transparant zijn is het herkennen van mechanismen moeilijker. De combinatie van de eenvoudige, transparante modellen en de nauwkeurigere, maar complexere modellen levert een stuk gereedschap voor het uitvoeren van parameterstudies en een hulpmiddel tijdens produktontwikkeling.

Gebaseerd op de uitgevoerde experimenten en het verkregen inzicht zijn randvoorwaarden gegeven voor het uitvoeren van detailproeven. Het blijkt dat

Samenvatting

de bestaande detailproeven vereenvoudigd kunnen worden, ondanks het feit dat voor een goede beschrijving van het gedrag meer meetgegevens nodig zijn.

Verticale separatie is het belangrijkste voor trapeziumvormige staalplaten. De vorm van zwaluwstaartvormige staalplaten biedt weerstand tegen verticale separatie aanwezig. In Europa is optimaal materiaalgebruik van zowel staal als beton noodzakelijk voor de ontwikkeling van een concurrerend vloersysteem. Hierdoor worden en zijn trapeziumvormige staalplaten ontwikkeld, die een beperkte weerstand tegen verticaal separatie hebben. Voor deze profielen is de schuifverbinding tussen de staalplaat en het beton, inzicht in het fysisch gedrag van de verbinding en de invloed van het gedrag van de verbinding op het gedrag van de vloer erg belangrijk.

ACKNOWLEDGMENTS

The research described in this thesis was started in at the Eindhoven University of Technology and continued at the Delft University of Technology.

Dutch Engineering is gratefully acknowledged for creating a situation which made it possible to combine a job with finishing this thesis, even when the finishing lasted almost 4 years.

I like to thank TNO Building and Construction Research for their financial, technical and practical support over the years. I would like to thank Mr. Velthorst (Hody B.V.) for allowing me to take part in the experiments performed at TNO during the development of their new type of profiled sheeting.

I would like to thank the *Commissie Beek* for the financial support given in the framework of Project 91-CT-1-C: "Constructieve vaardigheden bij het detailleren van staal-betonverbindingen voor civiele bouwconstructies en gebouwen".

For all different reasons I would like to thank (in alphabetical order) Kees Both, Jan Brekelmans, Mario van der Linden, Hendrik Jan Prins, Arie Romeijn, Jan Stark, Wiebren Wind and Gerben de Winkel. If they do not realise they played an important role over the last 10 years, I will definitely explain it when I finally hand them this piece of work.

Last but not least, I like to thank Mariëlle for the support, confidence and especially patience during the writing of this thesis.

CURRICULUM VITAE

Name: Remco Gerben Schuurman
Born: May 3rd, 1967 - Utrecht, The Netherlands

Education

1979-1985 Atheneum B, "Oosterlicht College" Nieuwegein
1985-1991 Doctoral Civil Engineering, Delft University of Technology
Faculty of Civil Engineering
1991-1991 Start Doctorate (Ph D), Eindhoven University of Technology,
Department of Building and Architecture
1992-1997 Completion Doctorate (Ph D), Delft University of Technology
Faculty of Civil Engineering,
Division Mechanics and Constructions,
Section Steel and Timber Structures

Practical experience:

1988-1991 Part-time assistant education, Delft University of Technology
Faculty of Civil Engineering, Division
Mechanics and Constructions, Section Applied
Mechanics
1997- Structural Engineer at Dutch Engineering raadgevend
ingenieursbureau, Zoeterwoude



SBN: 90-407-2199-8

DUP Science